Wireless Power Transmission Utilizing A Phased Array Of Tesla Coils

by

Joseph C. Stark III

Submitted to the Department of Electrical Engineering and Computer Science
in partial fulfillment of the requirements for the degree of

Masters of Engineering in Electrical Engineering

at the

MASSACHUSETTS INSTITUTE OF TECHNOLOGY

May 2004 [June 2004]

Author ....
Department of Electrical Engineering and Computer Science
May 13, 2004

Certified by .....
Chathan M. Cooke
Lecturer and Principal Research Engineer
Thesis Supervisor

Accepted by .....
Arthur C. Smith
Chairman, Department Committee on Graduate Students

BARKER

Wireless Power Transmission Utilizing A Phased Array Of Tesla Coils

by

Joseph C. Stark III

Submitted to the Department of Electrical Engineering and Computer Science
on May 13, 2004, in partial fulfillment of the
requirements for the degree of
Masters of Engineering in Electrical Engineering

Abstract

This thesis discusses the theory and design of coupled resonant systems and how they can be linked in a phased array for the wireless transmission of electrical power. A detailed derivation of their operational theory is presented with a strong emphasis on the current and voltage waveforms produced. Formulas are presented relating the features of the waveforms to specific parameters of the system. They provide a theoretical basis for the design of the Tesla coil systems. Unloaded and loaded operating efficiency is considered from both a power and energy perspective with emphasis on maximizing the two quantities. With these design formulas, a working set of two distinct coupled resonant systems were locked in frequency and controllable in phase to produce a phased array capable of wireless power transmission. The operational details and practical design considerations are presented and explained. The measured output waveforms were found to closely agree with the predicted models.

Thesis Supervisor: Chathan M. Cooke
Title: Lecturer and Principal Research Engineer

Acknowledgments

First and foremost, I would like to thank my parents for all their support and encouragement. Without their help, I would not be who I am today. To Tetazoo, much thanks for providing the necessary distractions. And finally, to my advisor, Dr. Chathan Cooke who took me in as a wet-behind-the-ears college grad and showed me the real world of electrical engineering.

Contents

Chapter 1

Introduction

1.1 Overview

Power is important to modern systems. From the smallest MEMS sensors and bionic implants to satellites and oil platforms, it is important to be able to deliver power by means other than wires or transmission lines. In the case of biological implants, there must be a battery or energy storage element present that can receive and hold energy. This element takes up valuable space inside a person. In the case of satellites and oil platforms, either solar panels, fuel cells, or combustion engines are currently used to supply power. Solar panels take up a great deal of weight and bulk in terms of energy density and must be constantly repositioned to maximize exposure to the sun. Fuel cells and combustion engines require fuel and maintenance to be delivered on-site. The use of wireless power transmission, on a scale much larger than used by magnetic induction devices, would allow for systems to operate remotely without the need for relatively large energy storage devices or routine maintenance.

This thesis will explore the theory, design, and construction of a method to transmit wireless electrical power through space. To this end, the Tesla coil configuration is used as the basis to generate high voltage, high frequency electrical power. Multiple Tesla coils, synchronized in frequency, are considered to increase delivered power and provide directionality. The generated power can be radiated to a receiver through an antenna array whose design will vary depending on the needs of the application. For some applications, a focused radiation pattern would be optimal, while for others, such as nanosensors spaced about a wide area, an omnidirectional radiation pattern would be appropriate. The receiver is itself

a resonant system tuned to the high frequency of the radiated power for maximum power transfer, much as a radio receiver must be tuned to a given frequency for higher reception gain.

One of the core requirements of this project is to completely characterize the output waveforms of a Tesla coil. With a complete characterization, designers can tailor the output to meet specifications for power supply and other requirements. Another goal is to characterize the energy and power efficiency of the Tesla coil such that the tradeoffs between efficiency and component size, coupling coefficient, and other parameters is known. Finally, and most importantly, this project considers a new topology of multiple, separate Tesla coils operated in synchronization so as to create an array with directional attributes.

Besides theoretical design considerations, this thesis aims to construct a working phased array. To this end, a method of driving and controlling the two coupled resonant systems is explored and designed. Considerations such as switching frequencies, types of switches, the uses of MOSFETs versus IGBTs, and feedback methods for controlling the system are examined. Ancillary issues such as parasitic losses and inductor coil construction are also considered. Essentially, this thesis aims to demonstrate and explain key elements of the design and construction process.

This thesis is broken down into eight subsequent chapters. The first starts with the lumped parameters, second order circuits that comprise half of the Tesla coil structure and their theory of operation. The operation of capacitors and inductors is explored as well as their properties and physical limits. The Tesla coil itself is represented by two coupled series circuits. Two different modeling approaches are presented allowing a thorough analysis of performance criteria as well as frequency and time domain solutions.

The second chapter discusses how two second order systems can be coupled to yield a single fourth order circuit with a mutual inductance coupling the inductors of the two circuits. These two second order circuits are known as the primary and secondary of the Tesla coil. As the traditional Tesla coil is comprised of two coupled second order systems sharing a resonant frequency, the Tesla coil is also referred to as a coupled resonant system throughout this thesis. The issues of matched resonant frequencies and the interaction of quality factors are presented. The frequency and time domain current and voltage waveforms are heavily discussed and characterized.

The third chapter discusses the operating efficiency of the coupled resonant system.

Concepts such as energy and power efficiency are distinguished and explored. Furthermore, the concept of matched output resistors and their effect on the operational efficiency is shown. Various phenomenon for energy and power losses are characterized.

The fourth chapter discusses the some practical design issues when constructing resonant systems. The chapter emphasizes the characterization of inductors and capacitors and the losses associated with them due to their electrical operation and geometry. Design procedures for optimizing the voltage on the secondary coil are shown as well as procedures for designing other optimizations. The chapter is concluded with a design scenario showing the practical limitations of physical components.

The fifth chapter discusses methods of driving the coupled resonant system. The pulsed system for driving the coils is explored and the theory behind its operation is shown. Methods of synchronizing the resonant frequency between the primary and secondary coils of each resonant system are shown. The theory listed here leads directly to the circuit built in the following chapter.

The sixth chapter shows the building of a phased array, pulse driven, coupled resonant system. Two separate, but nearly identical, systems are built and coupled via frequency and phase control. Various methods are used to control the operation of the coils. Experimental measurements and waveforms are shown.

The seventh chapter gives a comparison between the waveforms measured from the constructed system and the theoretical waveforms predicted. The sensitivity of the system to the coupling coefficient is shown. The accuracy of the theoretical model is shown when their network parameters are correctly chosen.

The eighth chapter is the culmination of the thesis tying together the results of the theoretical design with the constructed system. The benefits of the pulsed, coupled resonant system are weighed against the traditional methods of transmitting electromagnetic energy. Recommendations for future system designs and more generalized resonators are given. Several concerns involving large scale operation are addressed.

1.2 Motivation

When Nikola Tesla began his Colorado Springs experiments, the concept of the Tesla coil was unveiled to the scientific world. Yet, over fifty years later, these remarkable devices are

no more a part of modern equipment than Tesla's infamous death rays. The issue is not a lack of utility, since the Tesla coil is a remarkable device able to generate high voltage, high frequency waveforms with little control circuitry.[34] Instead, one might reason that its lack of use is due to the ill-understood nature of its operation. There are presently very few references that approach the design of the Tesla coil and its method of operation from an engineering standpoint. While there are many builders of Tesla coils that give step by step instructions on how to build a working coil, there is little design theory present in their explanations. Furthermore, these builders are interested in producing electric arcs and visible effects suitable for displays and general amusement, not in producing power supplies and power transmission units which may have significant practical importance.

The primary goal of this thesis is to introduce the theory behind the operation of Tesla coils as well as all coupled resonant systems. Combined with methods of driving the resonant systems and practical issues associated with their construction, it is hoped that future work on this fascinating topic will be encouraged.

Chapter 2

RLC Circuit Analysis

A coupled resonant circuit is a collection of circuits, each oscillating or resonating at one or more frequencies, mutually coupled by electromagnetic influences. These influences can be either electromagnetic, as observed in a transmitting antennae, inductive (magnetostatic), as seen between the two coils of a transformer, or capacitative (electrostatic). This thesis deals primarily with two inductively coupled second order circuits with one natural resonant frequency.

With this restriction, the operational theory of coupled resonant circuits lies in the analysis of second order RLC circuits and their mutual coupling to one another. A straightforward method of analysis is to decompose the resonant system via an electrodynamic lumped-parameter model into three generic electrical elements: resistances, inductances, and capacitances. One elementary yet fundamental model of a coupled resonant system is shown in Figure 2-1 below:

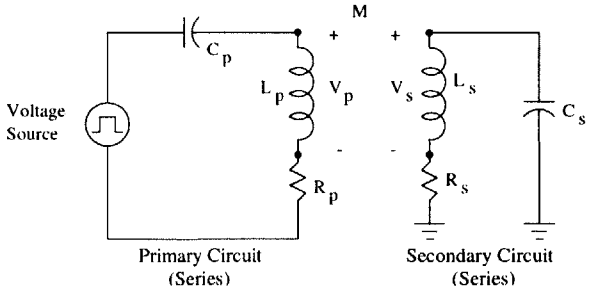

Figure 2-1: A lumped parameter model of a coupled resonant system showing resistances, inductances, and capacitances. Both circuits show a series RLC topology.

This model shows two series circuits, comprised of a resistor, inductor, and capacitor (RLC), magnetostatically coupled by the mutual flux connecting their two inductors. The designation of series versus parallel topology comes from the location of the loss mechanism in the circuit diagram relative to the energy storage elements. In the coupled circuit of Figure 2-1, the loss elements, the resistors, are in series with the energy storage elements, the inductors and capacitors.

By convention, the leftmost circuit will be called the primary, the rightmost circuit the secondary. These designations follow from conventions established in power electronics terminology. These designations make this modelled system identical to that of a Tesla coil. A Tesla coil almost always is comprised of two second order systems coupled through the flux of the inductors. In the case of the Tesla coil, the secondary circuit is often a physically large inductive coil with a parasitic resistance and capacitance modelled as shown above. Regardless of the physical realization of the components, if the models are identical, the the mathematics used to describe their behavior is also identical. To understand both the steady state and transient operation of coupled resonant circuits, it is first necessary to understand the constituent nature of their parts.

2.1 History of the Coupled Resonant System

Magnetic fields and inductive coupling have been studied extensively since the discovery of the transformer by Hans Oersted and Michael Faraday. In 1886, William Stanley, working for Westinghouse, developed the first commercial AC transformer. It was not until the invention of radio by Nikola Tesla in 1891 and its commercial utilization in the early 1900's that the theory of coupled, second order systems assumed the form it has today[10], as will be explored in this and the following chapters.

While Tesla invented and patented the schematic for a coupled resonant radio transmitter system in 1891, he did not publish the mathematical details of its workings.[35] The early years of the twentieth century saw great excitement as Guglielmo Marconi transmitted radio signals across the Atlantic in 1901. A number of radio transmitters were established for communication during World War I, but a complete mathematical understanding of the coupled circuits used to make the transmitter and receiver were not published until the beginning of the 1930's.[2][28] Frederick Terman, in 1935, published his first of a series of

handbooks that described the mathematics behind the operation of coupled second order systems utilizing frequency domain analysis.[32][33]

By the end of the 1930's, commercial radio and communication systems appeared rapidly across the United States and Europe, making use of the now understood coupled systems. With the mathematics of the circuits understood, engineers utilized this powerful theory when designing radar transmitters and modelling power transmission systems.[11]

2.2 Lumped Parameter Analysis

2.2.1 The Capacitor

The capacitors in this project take on two forms. One is a physical device with two terminals and a designated capacitance. The other is a distributed capacitance that exists between a two surfaces of different electrical potentials. A prominent example of distributed capacitance is found between the windings of a large inductor coil and ground. The ground could be an electrical ground or even the floor, the walls, or anything that happens to be around the coil including a person.

Capacitance is a definition of charge storage per unit voltage. All capacitors, by definition, obey the following constitutive relation:

$$Q = C \cdot V \tag{2.1}$$

For a fixed value capacitor whose charge storage follows a linear relationship relative to the applied voltage, the following time domain and frequency domain relations holds:

$$I(t) = \frac{dQ(t)}{dt} = C \cdot \frac{dv(t)}{dt} \tag{2.2}$$

$$I(s) = V(s) \cdot Cs \tag{2.3}$$

where 's' is the Laplace complex frequency operator expressible as $s = \sigma + j\omega$. By Ohm's law, he impedance of a capacitor is given by:

$$Z_c = \frac{1}{Cs} \tag{2.4}$$

The capacitor is considered a passive, energy-storage element that fixes the relationship

between the voltage and current waveforms passing through it. At steady state, the voltage waveform lags the current waveform by 90 electrical degrees.

The energy stored by a capacitor is given by:

$$E_{cap} = \frac{1}{2}CV^2 \tag{2.5}$$

When the voltage is increasing across a capacitor, it is absorbing current over time and charging, thus increasing its stored energy. When the voltage across the capacitor terminals drops, the capacitor will discharge (i.e. release current) and attempt to raise the voltage across its terminals to maintain electrical equilibrium.

All linear circuits can be described with a differential equation whose order is equal to the number of inductors and capacitors in the circuit. In order to fully solve the differential equation and find a dynamic model of a circuit, it is necessary to identify the boundary condition(s) associated with the capacitor. One boundary condition is that for finite currents, the voltage across a capacitor cannot change instantaneously. The current passing through it, however, as well as the time derivative of the voltage, $\frac{dv(t)}{dt}$, can instantaneously change.

The physical limitations of a capacitor are found in both its physical size and the materials used to construct it. The smaller a capacitor is, the more likely it is for high voltage to cause an electrical arc across its terminals. This arc can happen through the air surrounding the capacitor or directly through the dielectric inside a capacitor. When such an arc occurs inside a capacitor, it is said to have reached breakdown voltage. The breakdown potential of still, dry air at STP is approximately 28kV/cm.

Another form of capacitor failure is caused by driving excessive current through it. Excessive current through the dielectric causes heating, changing the electrical properties of the capacitor. In extreme cases, this heating will melt or vaporize the dielectric. The failure mode will vary from capacitor to capacitor depending on physical dimensions, construction techniques, and, most importantly, the type of dielectric used. A subtle but important effect is the stress of electric fields on the dielectric.[18][27] Effects known as dielectric absorption and polarization are the result of some nonlinearities in the charging and discharging cycle of a capacitor. The amount of nonlinearity in the charge and discharge cycle is a direct result of the dielectric used and varies considerably with construction, temperature, and

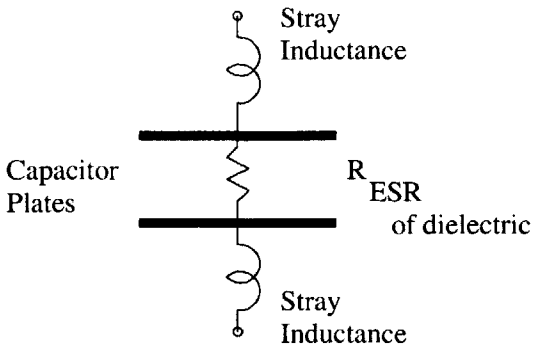

Figure 2-2: Model of a capacitor, with dielectric parasitics and stray inductance from terminal leads.

other environmental factors. Another important caveat with capacitors is their equivalent series resistance, known as ESR which is also directly related to the bulk material properties of the dielectric. Figure 2-2 illustrates how this effect is modelled.

2.2.2 The Inductor

The inductor is the workhorse of the Tesla coil, providing both a means of energy storage, voltage transformation, and a means of coupling two resonant circuits. Inductance is a magnetic effect that is self induced over a given geometry of current flow. For instance, a single current carrying wire in the vacuo of space has a self-inductance. Thus, every length of wire in the final design of the coupled resonant system contributes to the total inductance of the system. However, to keep the mathematics tractable, current carrying wires are bent into highly symmetric cylindrical coils or other geometric objects so that the inductance of the structure dominates over the parasitics in wire lengths joining elements of the circuit.

The time and frequency domain relations quantifying inductance are given below:

$$v(t) = L \cdot \frac{di(t)}{dt} \tag{2.6}$$

$$V(s) = I(s) \cdot Ls \tag{2.7}$$

The expression for inductive impedance is given by dividing the voltage by the current:

$$Z_L = L \cdot s \tag{2.8}$$

Notice the symmetry between the relations for an inductor and capacitor. This symmetry

follows from the symmetry of Maxwell's equations and the creative assignment of electromagnetic definitions. Also, the inductor causes the phase of the current and voltage waveforms passing through it to shift in a similar fashion to a capacitor. The inductor in AC steady state fixes the waveforms such that the voltage leads the current by 90 electrical degrees.

The energy stored by an inductor is given by:

$$E_{inductor} = \frac{1}{2}LI^2 \tag{2.9}$$

As the current passing through an inductor increases, the magnetic field induced by the inductor will increase in magnitude and store energy. Since the energy in an inductor cannot change instantaneously, the current flowing from its terminals must be continuous, i.e. it cannot change magnitude instantaneously. This inability to instantly change is seen often in switched mode power supplies. When inductors are in series with switching transistors, as soon as the transistors attempt to switch the current on or off, thus changing the current flow "instantaneously", the inductors will induce a voltage to maintain the continuity in current. This voltage transient is responsible for destroying many transistor switches.

An inductor adds another order to the differential equation describing the dynamics of the circuit. Again, a boundary condition is needed to fully solve the circuit's dynamics. A boundary condition associated with an inductor is that the current passing through it at any point in time (i.e. $i(t = 0^+)$) cannot change instantly. As is evident from equation 2.6, the voltage across an inductor as well as the current's rate of change, di/dt can change instantly, but the current itself cannot.

The inductor has performance limitations due to both the fundamental device physics of its operation as well as the physical materials used in its construction. As seen from equation 2.8, at low frequencies, the inductor behaves as a short circuit, i.e. as a straight wire. Note that the wire itself will still have its characteristic resistance per unit length, so the voltage across the inductor will not be exactly 0V, even at DC. As the frequency increases, the inductor behaves more like an open circuit. Most inductors are built by wrapping wires around a structure, sometimes magnetic, in order to concentrate the magnetic flux and the energy inside the physical dimensions of the inductor. These wires, however, at higher frequencies will begin to behave as capacitors with charge being stored between adjacent

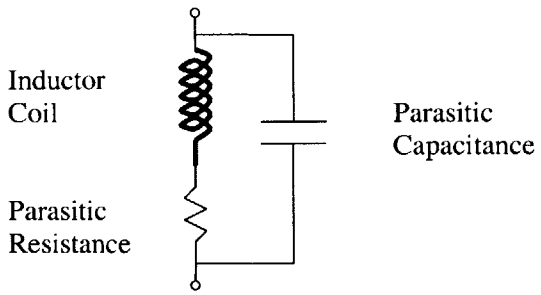

Figure 2-3: Model of an Inductor Coil, with Parasitics

windings. This situation is compounded because as the frequency increases, the currents travelling through the wire tend to stay closer to the wire's surface, a phenomenon known as the skin effect.[31, page 91] This increases both the capacitance and the effective resistance of the inductor. As the capacitance increases, the voltage between subsequent turns increases. If the insulation between the turns is not strong enough, an arc will jump from turn to turn shorting out sections of the coil. Thus, it is important before making an inductor that not only are the wires thick enough to handle short-circuit current levels, but that the insulation is sufficient to handle the voltage levels the coil will be encountering. A lumped parameter model of a typical inductor is shown in Figure 2-3.

2.3 Second Order RLC Circuits

By arranging capacitors, inductors, and resistors in circuits, it is possible to tailor the dynamics of the system to meet certain design specifications. This section consists of an analysis of the frequency and time domain responses of second order RLC circuits and expressions for evaluating their performance.

In all second order systems, whether they model physical interactions or electrical circuits, there are two energy storage devices that dynamically alter the quantity being measured. In the case of an electrical circuit, a second order system implies that there is both a capacitance and an inductance. There are general methods of analyzing second order circuits that allow tailored system responses to fit design criteria. One method is to introduce a generic frequency representation that can be adapted to fit both the series and parallel RLC cases, the Laplace transform. Most references on linear systems include a derivation of the Laplace transform and the mathematical nuances associated with its use.[39] Note

that for this discussion, the complex frequency operator 's' will always represent '$j\omega$' in electrical steady state unless otherwise specified. The derivation of each topology specific transfer function follows in the next two sections.

The Damping Coefficient, ξ, Representation

The damping coefficient representation is one of the most common methods used to represent second order response formulations, certainly the most often used in textbooks. The representation comes from the second order differential equation shown in equation 2.10.

$$\frac{d^2f}{dt^2} + 2\xi\omega_n\frac{df}{dt} + \omega_n^2 f = D(t) \tag{2.10}$$

The variables and parameters used in equation 2.10 are as follows: f is the function that describes a waveform in the second order system. It could represent a voltage or current as a function of time. The parameter ξ [unitless] is the damping coefficient. Its value is an indication of the energy lost in the system per cycle of oscillation. It is used to calculate other parameters that describe features of the second order response. The frequency ω_n [rad/sec] is the characteristic resonant frequency of the system, the frequency at which the system would oscillate if uncoupled or undisturbed from any external influences. The term $D(t)$ is the driving force that couples the system to an external influence. This force can take the form of an input voltage or current.

Solving this differential equation for $D(t) = \delta(t)$ or $D(t) = u(t)$ gives the impulse and step response, respectively. In order to facilitate solving this differential equation, the driving term, $D(t)$ is often set to zero. The solution to the differential equation in this case is called the homogeneous response. The solution for $D(t) \neq 0$ is called the particular solution. If the second order system is linear, these solutions can be added together using superposition.[39] The homogeneous response for the second order formulation given by equation 2.10 is given by equation 2.11. The coefficients A_1 and A_2 are coefficients determined by the boundary conditions of the second order system itself.

$$f(t) = A_1 e^{(-\xi\omega_n + \sqrt{\xi^2-1})t} + A_2 e^{(-\xi\omega_n - \sqrt{\xi^2-1})t} \tag{2.11}$$

Breaking up the time domain solution into particular and homogeneous solutions gives the steady-state and transient behavior, respectively. The particular solution is easily iden-

tified as any behavior in the time domain expression that does not decay away to zero as time goes to infinity. It will usually present itself as a constant or sinusoidal term. The transient response is characterized by its decaying nature. The transient response is usually found as a decaying exponential term that tends to zero as time advances. While the time domain response makes identification of these two terms rather easy, certain patterns in the frequency domain will lend themselves to similar identification. The presence of an $(s+\alpha)$ term in the denominator signals a decaying exponential of magnitude $\exp -\alpha t$. The presence of constant terms is revealed when the highest degree of the operator 's' in the numerator is the same as that in denominator. In mathematical terms, if $\frac{V_{out}(s)}{V_{in}(s)} \rightarrow 0$ as $s \rightarrow \infty$, then there is a constant term in the time domain solution. The mathematically astute, however, will also recognize that equation 2.11 decomposes for $\xi = 1$. In fact, for $\xi < 1$, the exponential terms of the equation become complex while for $\xi > 1$, the solution is just the sum of two decaying exponentials. This characteristic leads to the overdamped, underdamped, and critically damped solutions shown earlier. In each regime, the time domain solution takes on the following forms:

For $\xi < 1$, Underdamped:

$$y(t) = \frac{e^{-\xi\omega_n t}}{\sqrt{1-\xi^2}} \cdot (A_1 \sin(\omega_d t) + \cos(\omega_d t)) \tag{2.12}$$

For $\xi = 1$, Critically Damped:

$$y(t) = (A_1 + A_2 t)e^{-\omega_n t} \tag{2.13}$$

For $\xi > 1$, Overdamped:

$$y(t) = e^{-\xi\omega_n t}(A_1 e^{\sqrt{\xi^2-1}} + A_2 \exp\sqrt{\xi^2-1}) \tag{2.14}$$

The time domain, however, does not hold a monopoly on determining the nature of the time domain response. The frequency domain transfer function, $\frac{V_{out}(s)}{V_{in}(s)}$ predicts the three forms of the time domain solution above. When calculating values for the transfer function, if the response is critically damped, then the frequency domain relation itself will

decompose into the form:

$$(A_1 + A_2 t)e^{-\xi\omega_n t} \Rightarrow \frac{A_1}{s + \omega_n\xi} + \frac{A_2}{(s + \omega_n\xi)^2} \tag{2.15}$$

Another method of solving for the response of a second order system is to determine its frequency response. Equation 2.16 shows the ξ representation of a second order system in the frequency domain. While the model is equated to the ratio of output to input voltage in most texts, it could also be equated to the ratio of currents.

$$H(s) = \frac{V_{out}(s)}{V_{in}(s)} = \frac{\omega_n^2}{s^2 + 2\xi\omega_n s + \omega_n^2} \tag{2.16}$$

Both the series and parallel topologies can be expressed with this transfer function, although the parameters assumes different values for each topology. The parameters include ω_n [rad/sec] and ξ [unitless] as previously discussed. The parameter ω_n represents the natural oscillation frequency of the system; the frequency at which the capacitor and inductor exchange energy in the circuit. In one complete cycle, $2\pi/\omega_n$, all of the capacitor's stored energy has been shunted to the inductor and then returned or vice versa. In the absence of any internal resistances or outside influences, this is the resonant frequency that the circuit would sustain indefinitely. However, the circuits discussed here both include a resistor and a voltage source to introduce external stimuli such that the system will often resonate at a slightly different frequency. A plot of the frequency response of equation 2.16 for a series second order circuit is shown in Figure 2-4. The circuit is that of the primary in Figure 2-1, a series RLC circuit. Notice that frequency response has both a magnitude and phase plot. This is due to the complex frequency operator s used in the Laplace transform. Because $\frac{V_{out}(s)}{V_{in}(s)}$ is a complex function, with both magnitude and phase information, it is useful to employ both plots to gather complete system information.

The amount of output magnitude peaking, M_{peak} and the frequency of the magnitude peak, ω_{peak} can be calculated from ω_n and ξ. Their relations are given as:

$$M_{peak} = \frac{1}{2\xi\sqrt{1-\xi^2}} \tag{2.17}$$

$$\omega_{peak} = \omega_n\sqrt{1-2\xi^2} \tag{2.18}$$

The magnitude of M_{peak} represents the relative height or peaking that occurs in the

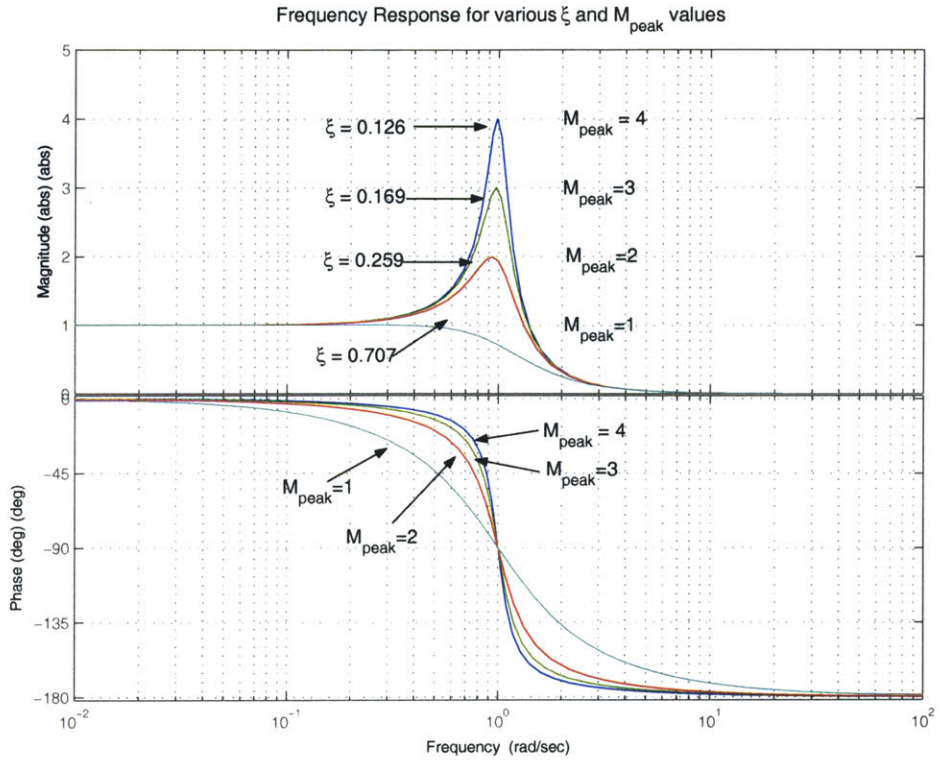

Figure 2-4: Normalized frequency response across a capacitor of the generic 2nd order system. $\omega_n = 1$

frequency domain response. This is best observed in the magnitude portion of Figure 2-4. The frequency at which the frequency response peaks is called the peak frequency, ω_{peak}. When the system is driven at this peak frequency, by the input, $D(t)$, the system output is very sensitive to the magnitude peaking, M_{peak}. When the system is driven at a frequency ω that is a factor of 10 off of ω_{peak}, the response is quite insensitive to changes in M_{peak}. Typically, as the parameter ξ is much less than unity, the peak frequency ω_{peak} is very close to ω_n, the natural resonant frequency of the circuit.

Figure 2-4 represents the voltage across the capacitor versus the voltage applied to the series RLC combination. This can be deduced from the plot because the voltage gain goes to zero at infinite frequency, when the capacitor becomes a short and the voltage across it is zero. The response also goes to unity at DC, when the capacitor acts like an open circuit and passes the input voltage to the output. If the voltage were measured across the inductor, the plot would be flipped left to right.

In the presence of energy losses, i.e. resistive losses, the system naturally oscillates at a slightly lower frequency from ω_n called the damped frequency defined by: $\omega_d = \omega_n\sqrt{1-\xi^2}$. This frequency, ω_d is the actual frequency at which the circuit resonates when there are losses in the system. The value of ω_d is typically so close to ω_n that the latter is almost exclusively used when discussing the dynamics of the system. However, in systems with relatively large losses or large ξ, the damped resonant frequency ω_d should be used when discussing the system response.

Because of the influence of ξ on the system, knowing ξ tells what type of response the system will have to an arbitrary input. For $\xi > 1$, the system is overdamped, for $\xi = 1$, the system is critically damped, and for $\xi < 1$, the system is underdamped. The meaning of this damped frequency, ω_d and its effects are best seen in the time domain graphs of Figure 2-5.

Once a peaking magnitude, M_{peak}, and resonant frequency, ω_n, are known for a circuit, it is often necessary to convert the frequency domain equation into a time dependent equation to observe the transient effects in the time domain. To convert a function from the frequency domain to the time domain requires use of the inverse Laplace transform. For convenience, the following relations are shown below[39, chapter 9]:

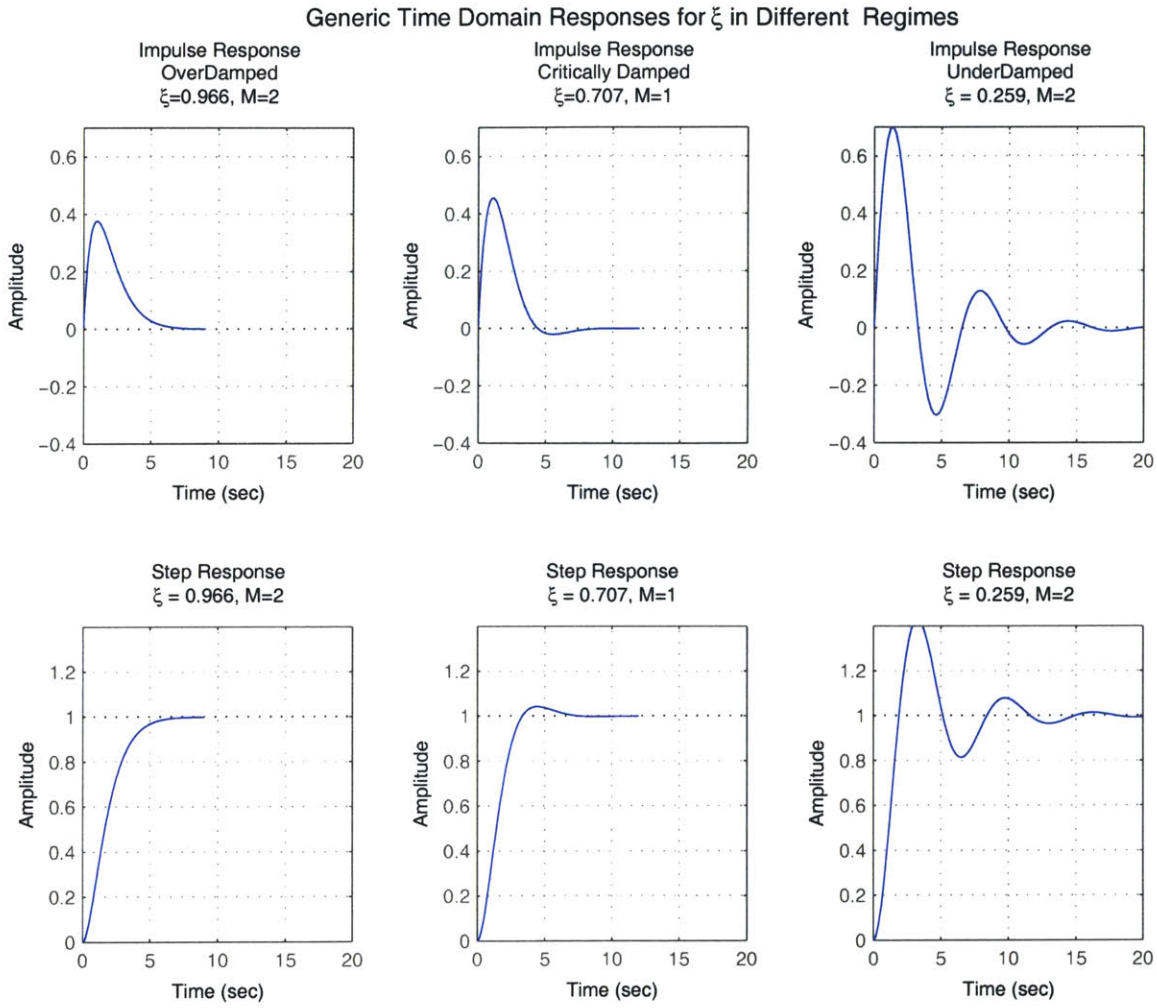

Figure 2-5: Impulse and step responses of a ξ-based model. Leftmost plot represents an overdamped response, the middle plot a critically damped response, the rightmost plot an underdamped response.

$$\begin{array}{lcl} \frac{\beta}{(s+\alpha)^2+\beta^2} & \Rightarrow & e^{-\alpha t} \\ \frac{s+\lambda}{(s+\alpha)^2+\beta^2} & \Rightarrow & e^{-\alpha t}(\cos(\beta t) + \frac{\lambda-\alpha}{\beta}\sin(\beta t)) \\ \frac{\omega_n^2}{s^2+2\xi\omega_n s+\omega_n^2} & \Rightarrow & \frac{e^{-\xi\omega_n t}}{\sqrt{1-\xi^2}}\sin(\omega_d t + \arctan\frac{\sqrt{1-\xi^2}}{\xi}) \end{array}$$

Referring to Figure 2-5, notice the effect of ξ on the oscillation magnitude and frequency. The two types of responses shown are called the step response (bottom) and the impulse response (top). The step response is the reaction of the system to a unit, step input. The impulse response of the system is also the derivative of the step response. It is the response of the system to an input that is infinite in magnitude but lasts for an infinitesimal amount of time. A common analogy is an input spike. One essential requirement for the input impulse is that it have unit area. Because of this, an impulse will always have units of Volt-seconds, Ampere-seconds, etc.

As shown, both the frequency domain and time domain responses are capable of showing how a given second order system behaves. However, each domain offers a view of the system that may be better suited to design for a given application. But just as each domain better lends itself to certain applications, the model used to describe the second order system may not be optimal for a given purpose. While the damping ratio model is common throughout the literature, especially in nonelectrical fields, there is another model that is commonly employed when dealing with radiating and power handling circuits: the Q representation.

The Quality Factor, Q, Representation

The Q or Quality factor representation more directly relates to Tesla coil design requirements and is considered more useful in describing its behavior. Q represents many things to many different types of systems but from a physical point of view it is the ratio of the energy stored in the system divided by the energy lost per cycle. For a second order series RLC circuit, Q can be related to the ratio of circuit impedances: Z_L/R_{total}, the ratio of inductive impedance relative to total resistive loss, at the system resonant frequency, ω_n. The manner in which Q manifests itself in frequency and time domain plots is shown below.

In the frequency domain, the generic Q-based second order response assumes the form:

$$\frac{V_{out}(s)}{V_{in}(s)} = \frac{\omega_n^2}{s^2 + \frac{\omega_n}{Q}s + \omega_n^2} \tag{2.19}$$

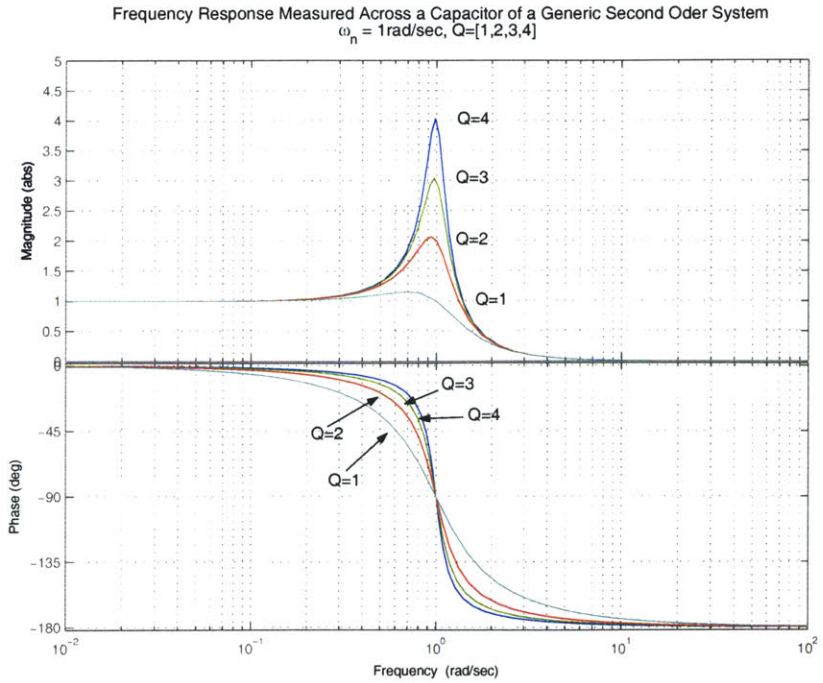

Figure 2-6: Generic 2nd order frequency response of a Q-based representation. The response is measured across a series connected capacitance.

where the natural frequency, ω_n is identical to the natural frequency of the previous model. The difference is that the damping ratio, ξ has been replaced by $\frac{1}{2Q}$. In this representation, Q serves as both the magnitude peaking factor, like M_{peak}, and as a shaping factor that gives information about the response waveform in both time and frequency domains. The conversion between Q and ξ is $Q = \frac{1}{2\xi}$. Figure 2-6 shows the frequency response of a system with resonant frequency $\omega_n = 1$ [rad/sec] at different Q values.

Notice here that the value of Q parallels that of M_{peak} although the two are *not* identical. The value of Q tells the approximate voltage gain factor of the peak value at the system's resonant frequency.

The plots in Figure 2-7 show the step and impulse responses for various values of Q. In the time domain, Q serves as a damping ratio parameter bounding the types of responses. For $Q > 1/2$, the system response is under damped. This allows for high peak magnitudes but at the price of oscillations or "ringing" when the system is excited. For $Q < 1/2$, the system is over damped and does not ring. When the system is driven by an external source, it transitions from its previous state to the new state without any overshoot or oscillations.

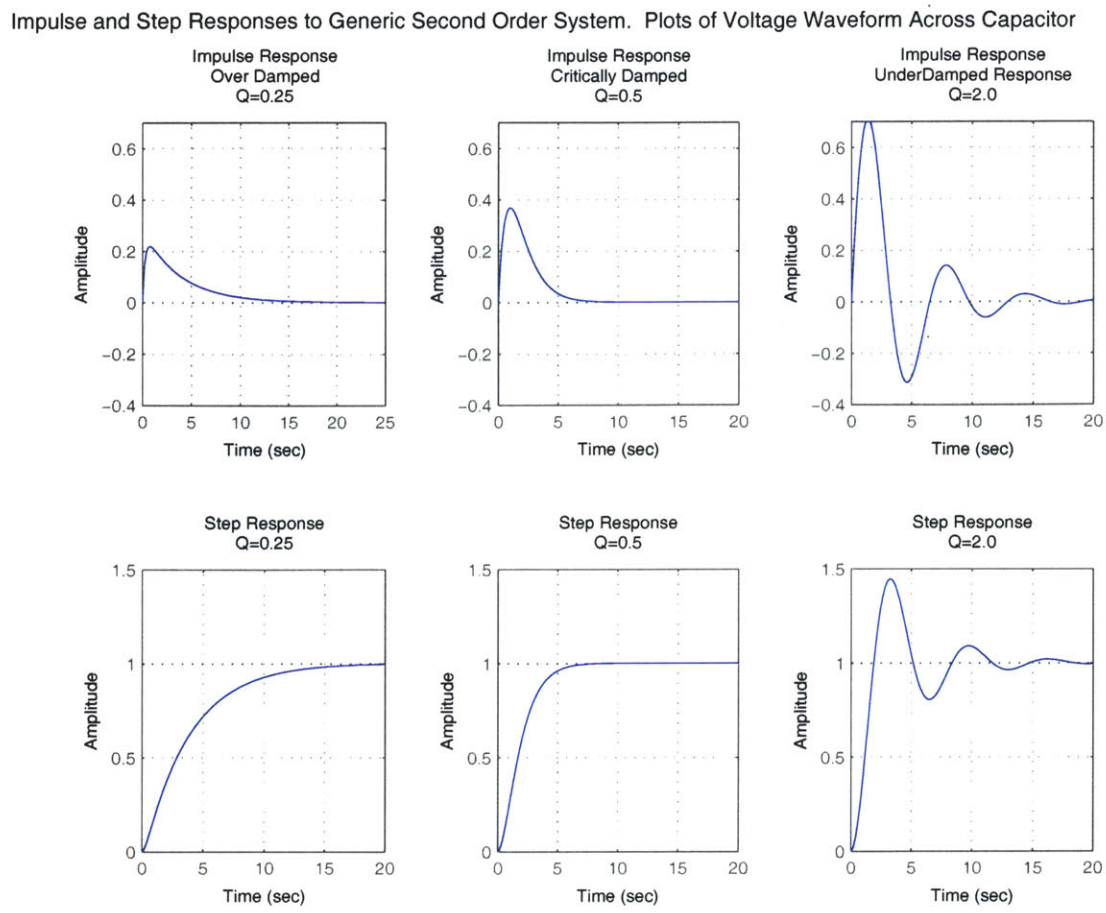

Figure 2-7: Impulse (top) and step (bottom) responses of a Q-based model. Note the time axis scale change in the underdamped response.

When $Q = 1/2$, the system is critically damped and hangs between the two response regimes. Many control engineers design their systems to operate as close to critically damped as possible. This is because a system that is critically damped will take the least amount of time to transition from one state to another and will not overshoot or oscillate. While this response is desirable, keeping the Q of the system *exactly* at $1/2$ is difficult, especially when the circuit is operating with influences from outside sources.

To illustrate the above point, notice the impulse and step responses in Figure 2-7. The impulse response for an underdamped system ($Q = 4$) shows a higher peak than the critically damped ($Q = .5$) or the overdamped system ($Q = .25$). However, it takes slightly longer than 30 seconds to settle to its final value and also overshoots it after 2.5 seconds

of rising. The critically damped system takes 7.5 seconds to find its final value and never overshoots its final value. The equations for the time domain relations take on the same form as those for the ξ system. As Q, however, more directly corresponds to an easily identifiable graph measurement in both the frequency and time domains than does the damping ratio ξ, it makes sense to find expressions that can be normalized to Q instead of ξ. Explicitly, normalizing the time, t, of the system's evolution by the natural frequency of the system, ω_n, better shows how Q affects the system response in the time domain. With the substitution $t = \frac{2\pi}{\omega_n}x$, the time domain solutions become as follows:

The Differential Equation:

$$\frac{d^2y}{dt^2} + \frac{\omega_n}{Q}\frac{dy}{dt} + \omega_n^2 y = D(t) \tag{2.20}$$

The General Solution:

$$y(t) = A_1 e^{-\frac{\omega_n t}{2Q}(1-\sqrt{1-4Q^2})} + A_2 e^{-\frac{\omega_n t}{2Q}(1+\sqrt{1-4Q^2})} \tag{2.21}$$

Normalized Underdamped ($Q > 0.5$):

$$y(x) = e^{-\frac{\pi x}{Q}}(A_1 \cos(\frac{\pi x}{Q}\sqrt{4Q^2-1}) + A_2 \sin(\frac{\pi x}{Q}\sqrt{4Q^2-1})) \tag{2.22}$$

Normalized Critically Damped ($Q = 0.5$):

$$y(x) = (A_1 + A_2 x)e^{-2\pi x} \tag{2.23}$$

Normalized Overdamped ($Q < 0.5$):

$$y(x) = A_1 e^{-\frac{\pi x}{Q}(1-\sqrt{1-4Q^2})} + A_2 e^{-\frac{\pi x}{Q}(1+\sqrt{1-4Q^2})} \tag{2.24}$$

A plot of these normalized equations is shown in Figure 2-8. In the case of the underdamped response, notice how the value of Q determines both the amplitude of the oscillation and how many cycles it undergoes before it essentially settles. With the initial conditions $A_1 = 0, A_2 = 1$, the system completes one cycle every value of x. Notice however, from equation 2.22, the frequency of oscillation is actually $\omega_d = \frac{\omega_n}{2Q}\sqrt{4Q^2-1}$. As Q goes to infinity, the damped oscillation frequency, ω_d approaches the ideal resonant frequency, ω_n.

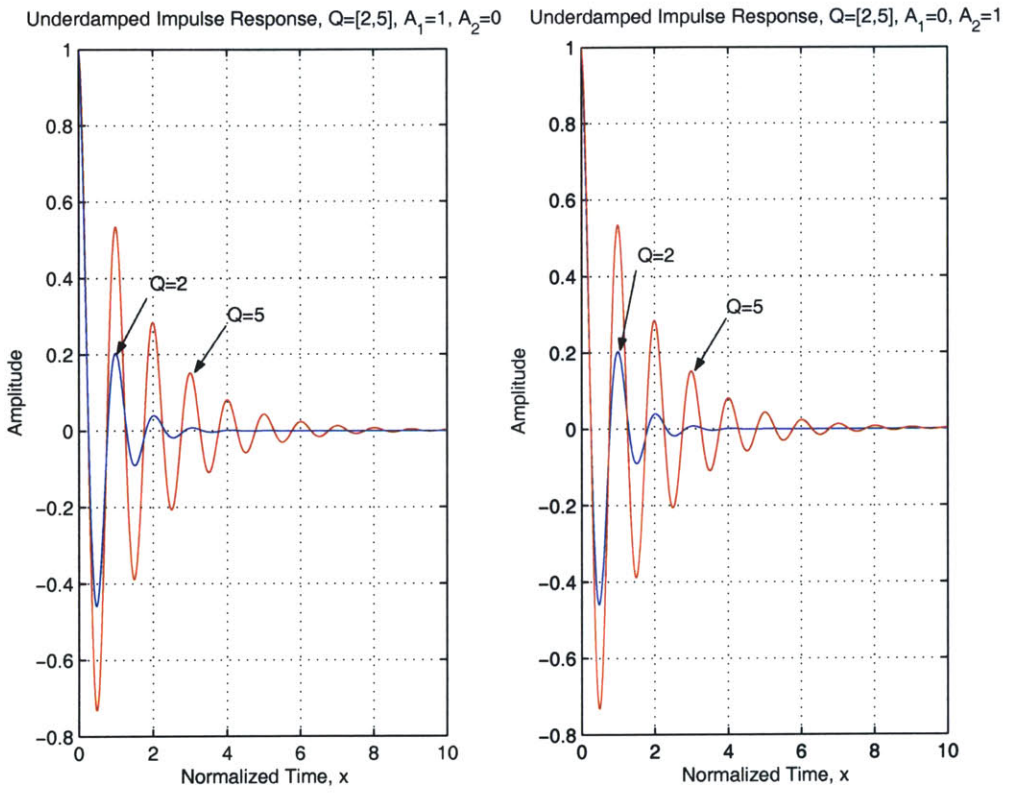

Figure 2-8: A normalized time domain plot for the underdamped impulse response. $A_1 = 1, A_2 = 0$ (left), $A_1 = 0, A_2 = 1$ (right).

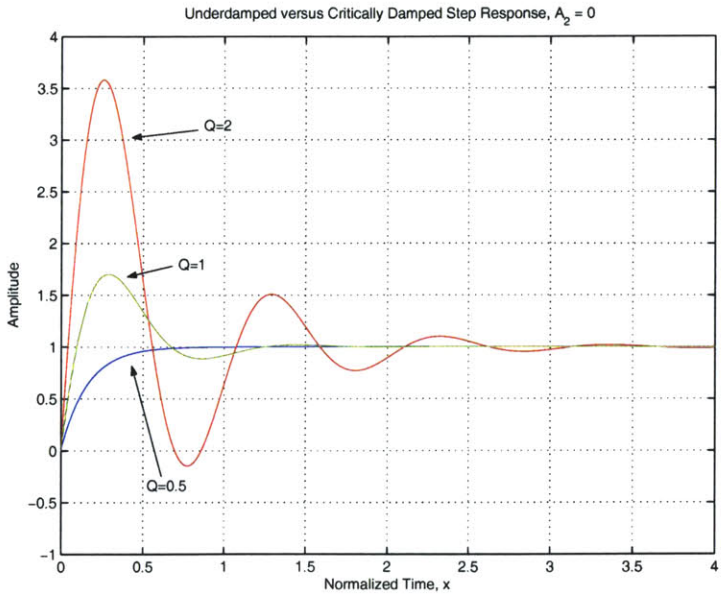

Figure 2-9: A normalized time domain plot of the under and critically damped step response. $A_2 = 0$, A_1 set to keep $y(0) = 0$ and $y(\infty) = 1$

The normalized step response is shown in Figure 2-9. Here the attractiveness of the critically damped response is apparent. It settles to its final value in approximately one half of a cycle versus the other underdamped responses. The critically damped response sets the performance limit on how fast the system can reach steady state. As the operating frequency of a circuit increases, this manner of response is critical. If the circuit's response cannot keep with the frequency of the source drive, its output is useless. For example, if the system had a Q of 2 and the source had a normalized switching period of 2, then the circuit output would still be oscillating when the next switch arrived. This represents a limitation to the speed of the circuit. If the circuit was critically damped with a $Q = 0.5$, then a switching period of 2 is more than enough time for the circuit to settle to its final value.

The overdamped response, shown in Figure 2-10 represents a cautious approach to circuit design. It is used whenever stability is more important than settling time. The system transitions smoothly towards its final value taking an arbitrarily long amount of time to do so as Q tends towards zero.

The power of these generic methods is that they allow the circuit's characteristics to be

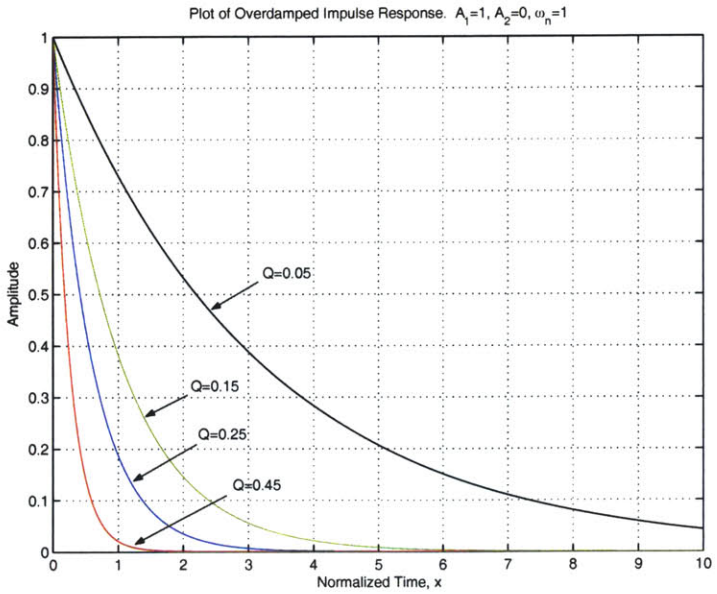

Figure 2-10: A normalized time domain plot of the overdamped impulse response

optimally tailored to a given application before any component values are decided upon. The components can be chosen to meet a performance specification. Specifications such as energy efficiency, output voltages, and step responses can be easily determined to within a few percent accuracy. In the next two sections, the frequency and time domain expressions for various circuit quantities in the series and parallel topologies are derived.

2.4 Series RLC Circuits

In a series RLC circuit, a voltage or current source is connected in series with a resistor, capacitor, and inductor. While the ordering of the components does not affect the operation of the system as a whole, the component placement in Figure 2-11 represents the primary of Figure 2-1. The resistor placed next to the inductor represents both the equivalent series resistance of the capacitor as well as the resistance of the wire used to wind the inductor. Depending on the specifications, one resistance may dominate over another. Of course, the resistor could actually be a physical component placed in the circuit to measure current, draw voltage away from a component, or to simplify analysis by masking parasitic resistances with a single dominant resistance.

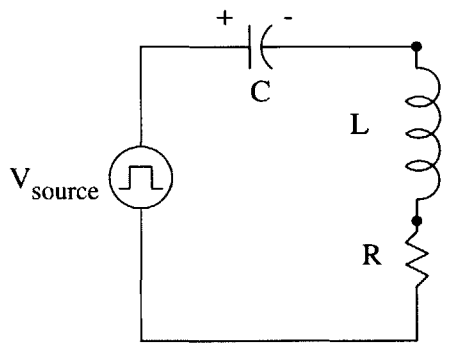

Figure 2-11: Schematic of a series RLC circuit

In order to solve a series RLC circuit in the frequency domain, it is imperative to recognize that the current through all the components is equal, by Kirchhoff's current law (KCL), and that any component voltages can be easily solved from knowing the current. It is simply a matter of writing Ohm's Law:

$$Z(s) = R + Ls + \frac{1}{Cs} \tag{2.25}$$

$$I(s)Z(s) = V_{in}(s) = I(s)(R + Ls + \frac{1}{Cs}) \tag{2.26}$$

$$I(s) = V_{in}/Z(s) = V_{in}C\frac{s}{LCs^2 + RCs + 1} \tag{2.27}$$

Now, we multiply the top and bottom of the second part by $\frac{1}{LC}$ to get:

$$I(s) = V_{in}\frac{\frac{s}{L}}{s^2 + \frac{R}{L}s + \frac{1}{LC}} \tag{2.28}$$

which can be expressed in terms of the circuit network parameters:

$$I(s) = V_{in}Cs\frac{\omega_n^2}{s^2 + \frac{\omega_n}{Q}s + \omega_n^2} \tag{2.29}$$

where $\omega_n = \frac{1}{\sqrt{LC}}$ [rad/sec] is the natural frequency of the system and $Q = \omega_n\frac{L}{R}$ or $Q = \frac{1}{R}\sqrt{\frac{L}{C}}$ is the quality factor. Other quantities in the circuit are easily obtainable from these relations. The voltage across the ideal inductor is given:

$$V_{inductor} = Z_L(s)I(s) = (V_{in}LCs^2)\frac{\omega_n^2}{s^2 + \frac{\omega_n}{Q}s + \omega_n^2} \tag{2.30}$$

$$V_{inductor} = V_{in}\frac{s^2}{s^2 + \frac{\omega_n}{Q}s + \omega_n^2} \tag{2.31}$$

The voltage across the capacitor and resistor are given as:

$$V_{capacitor} = Z_C(s)I(s) = V_{in}\frac{\omega_n^2}{s^2 + \frac{\omega_n}{Q}s + \omega_n^2} \tag{2.32}$$

$$V_{resistor} = V_{in}\frac{RCs\omega_n^2}{s^2 + \frac{\omega_n}{Q}s + \omega_n^2} \tag{2.33}$$

The presence of the squared 's' term in equation 2.30 makes the order of the numerator of the transfer function equal to the denominator. Thus, as the operating frequency goes to infinity, the final value of the transfer function goes to the magnitude of V, as seen in the previous section's example. This makes physical sense; as the operating frequency goes to infinity, the impedance of the capacitor goes to zero and acts like a short while the impedance of the inductor goes to infinity and acts like an open.

Time domain equivalent equations cannot be uniquely determined without knowing the voltage input to the system. However, once a circuit is known, its impulse response form $H(s) = \frac{\omega_n^2}{s^2+\frac{\omega_n}{Q}s+\omega_n^2}$ can be converted into the time domain using equation 2.21. Each multiple of 's' in the numerator of $H(s)$ requires a derivative be taken of the resulting time domain expression.

2.5 Parallel RLC Circuits

The parallel RLC circuit discussed in this section is not shown in the coupled second order systems of Figure 2-1. A parallel RLC topology in one in which the circuit elements share a common voltage whereas the series RLC topology share a common current. Stated in terms of the quality factor, Q, a series circuit is one where the greater the resistance, the lower the value of Q. In a parallel circuit, the larger the resistance, the greater the value of Q. Some second order circuits share characteristics of both series and parallel topologies. The topology of a typical parallel circuit is shown in Figure 2-12.

The procedure used to solve the dynamics of this circuit is identical to solve any parallel RLC circuit. In analyzing parallel circuits, it is important to note voltage relationships. In this circuit, the voltage across the capacitor leg is identical to that of the inductor and resistor leg. This voltage is equal to the source voltage, V_{in}. The impedances on the

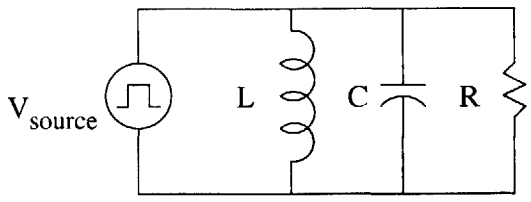

Figure 2-12: Schematic of a parallel RLC circuit

capacitor, inductor, and resistor leg are respectively:

$$Z_C = \frac{1}{Cs} \tag{2.34}$$

$$Z_L = Ls \tag{2.35}$$

$$Z_R = R \tag{2.36}$$

This makes the currents down each of the legs and the total current supplied by the voltage source, V_{in}, equal to:

$$I_C = V_{in}Cs \tag{2.37}$$

$$I_L = \frac{V_{in}}{Ls} \tag{2.38}$$

$$I_R = \frac{V_{in}}{R} \tag{2.39}$$

$$I_{total} = V_{in}\frac{LCs^2 + \frac{L}{R}s + 1}{Ls} \tag{2.40}$$

The total impedance seen by the voltage source is the parallel combination of the three impedances or found by dividing the voltage, $V_{in}(s)$ by the total current, $I_{total}(s)$. This expression can be reduced to:

$$Z_{thevenin} = \frac{Ls}{LCs^2 + \frac{L}{R}s + 1} = \frac{\frac{s}{C}}{s^2 + \frac{1}{RC}s + \frac{1}{LC}} \tag{2.41}$$

In case the expression for the total and capacitor current is unsettling as their numerators have a higher degree of s than their denominators, realize that this shows that the current will go to infinity in that leg as the frequency goes to infinity. Of course, at some frequency and for some current value, the voltage source will no longer be able to supply increased

current and the capacitor will no longer be able to handle such current levels. The equations, therefore, represent an ideal behavior that cannot be physically accurate for all values.

The denomenator of the total impedance, $Z_{thevenin}$ is the denomenator shared by all transfer functions describing the dynamics of this parallel circuit. Matching terms to the general Q representation gives the natural resonant frequency, ω_n and the quality factor, Q to be:

$$\omega_n = \frac{1}{\sqrt{LC}} \tag{2.42}$$

$$\frac{\omega_n}{Q} = \frac{1}{RC} \Rightarrow Q = RC\omega_n \tag{2.43}$$

The natural resonant frequency, ω_n retains the same formulation as seen in the series RLC topology while the quality factor, Q, is now quite different from its previous definition. Because Q is proportional to R, as the power dissipated across the resistor *decreases* as R is increased, the value of Q increases with increasing R. Furthermore, in a parallel topology, the impedance of the capacitor is directly proportional the value of Q instead of the impedance of the inductor.

The design of parallel RLC circuits is identical to that for series RLC circuits. Input source specifications and desired output requirements are matched to an operating frequency (ω_n) and a Q value. However, this analysis assumes that the components follow linear, ideal behavior. When the components represent real parts, this generally holds true. When these lumped parameter components represent parasitic or distributed electromagnetic effects, these models often fail due to nonlinearities in their behavior.

2.5.1 Lumped Parameter Limitations

A parasitic capacitance in the context of a wound inductor implies that current will be travelling up and down the sides of the coil as well as inside the wire itself. If the coil is driven with a greater than DC frequency, there will be a net current through this parasitic capacitance, effectively through the insulation between the adjacent turns and to ground. As the wire and its insulation heats up, failure is more likely to occur. If the coil is driven at too high a frequency, such that the primary method of conduction is through the parasitic capacitance, acting as a short, instead of through the inductor, then the probability of insulation failure is greatly increased. In addition, power is wasted because this capacitance

has the resistance of the insulation in series with it.

In order to build and properly tune a coil, there are two options. One option is to procure an impedance bridge analyzer. This device measures the impedance between two terminals of an RLC network while exciting it at a given frequency. As the impedance of the circuit is found, it is important to not stand too close to it during operation as any proximal objects will affect its resonance by changing its capacitance to ground. Another method is to build a second, smaller inductor with an adjustable magnetic core that can be wired in series with a main, fixed-inductance coil to be tested. The magnitude of the output voltage can be observed for a given input voltage at a fixed, known frequency. As the tunable coil is adjusted, the measured response will peak. The total inductance of the circuit along with the parasitic capacitance has a natural resonant frequency, ω_n that corresponds to the driving frequency, ω_{driven}.

2.6 Summary of Results

In this chapter, two general methods for describing second order resonant systems were described, the damping ratio, ξ, representation and the Q representation. While equivalent, the Q representation will be more applicable to later work. Models for the capacitor and inductor including their parasitics were formulated and their limiting behavior at high and low frequencies was discussed. For the two types of second order topologies, series and parallel, it remains to find the Q and the resonant frequency in order to use the general formulas for frequency and time domain characterization.

The table below shows the formulas specific to the topologies listed above:

Parameter Estimation	$Q =$	$\omega_n =$
Series	$Q = \frac{\omega_n L}{R}$	$\omega_n = \frac{1}{\sqrt{LC}}$
Parallel	$Q = \omega_n RC$	$\omega_n = \frac{1}{\sqrt{LC}}$

Once these values have been decided, the general frequency domain equation is given by equation 2.19, repeated here:

$$\frac{V_{out}(s)}{V_{in}(s)} = \frac{\omega_n^2}{s^2 + \frac{\omega_n}{Q}s + \omega_n^2}$$

The time domain response depends on the nature of the input signal, but knowing Q gives the following information about the frequency and time domain responses:

- The frequency domain voltage gain when the system is driven at ω_{peak}
- The number of cycles in the time domain transient response before the response reaches steady state.
- The amount of time before the system is damped, $t \approx \frac{2\pi N_{cycles}}{\omega_n}$
- $Q = 0.5$ represents a critically damped system, anything less is overdamped, anything above is underdamped.

Understanding Q will greatly aid in understanding results when multiple second order systems are coupled together.

Chapter 3

Coupled Resonate RLC Networks

A Tesla coil system is a coupled resonate RLC network. It acts as a transformer, taking energy input applied to the primary circuit and converting it into an oscillating voltage or current waveform at the output. Regardless of claims in many books about the unlimited deliverable power of a Tesla coil, the energy output of the coil is always less than the energy put into it. The "magic" behind Tesla coil operation is the use of resonant circuits coupled in such a way as to take energy stored in the primary side of the circuit and transfer it onto the secondary coil in a modified state. This chapter explores the underlying theory of Tesla coils and other coupled resonant topologies that exhibit similar behavior.

Any circuit with two or more energy storage devices is called a resonating network. For the second order case examined in the previous chapter, there were only two energy storage devices: a capacitor and an inductor. These two energy storage devices give the circuit, regardless of its topology, a single resonant frequency. Circuits with multiple pairs of energy storage elements have multiple resonant frequencies. These frequencies represent the speed of energy transfer between inductors and capacitors in the circuit. The power behind the lumped parameter model is that it takes a geometrically and spatially dependent system, such as a Tesla coil, containing distributed inductances and capacitances and converts it into an electrical circuit model that can be analyzed with the tools of circuit theory instead of electromagnetic field theory. The price paid for this convenience is a loss of information concerning losses in the system, some higher order parasitic effects, and higher order harmonics of the system. When these effects are significant, modeling these is better handled with a distributed model that better accounts for the underlying electromagnetic theory.

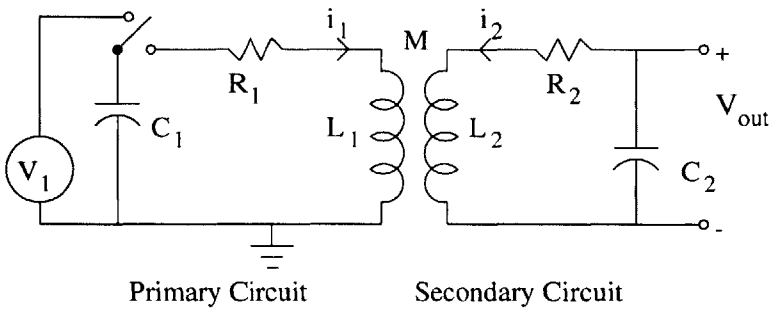

Figure 3-1: Two second order circuits with inductive coupling.

When combining two second order circuits, each with its own resonant frequency and Q factor, the behavior of the total, fourth order system is not simply a sum, difference, or average of the two constituent circuits' parameters. Instead, different parts of the circuit resonate at different frequencies related to the original independent fundamental frequencies. As the system is driven by an external source, the energy it transfers to the circuit is moved between the energy storage elements of the circuit according to each devices' constitutive relations. The result is that the circuits will load one another and affect their natural resonance frequencies and individual Q factors.

A basic fourth order topology is shown in Figure 3-1. All losses in each subcircuit are modelled by a single resistance. The switch in the primary circuit represents the power supply that is driving the circuit. When the switch is open, the voltage source acts to charge the capacitor, C_1, to a voltage V_{source}. When the switch is closed, the capacitor discharges its energy electrically via a direct wired connection to the primary elements. The primary coil, L_1, magnetically coupled to the secondary coil, L_2, induces a voltage that creates current through the secondary coil. Solving for the dynamics of this system requires a through understanding of the both the voltage and current dynamics in both the time and frequency domain. Most critical will be how the waveforms of the primary circuit compare to the waveforms in the secondary.

3.1 Derivation of Dynamics in the Frequency Domain

A set of solutions describing the operation of the coupled resonate system is first presented in the frequency domain. The simplified expressions show optimal relationships between

the primary and secondary network parameters and how frequency affects the nature of the induced waveforms in the secondary.

First, define the series impedances in the primary and secondary as Z_1 and Z_2, respectively:

$$Z_1 = R_1 + j(\omega L_1 - \frac{1}{\omega C_1}) \tag{3.1}$$

$$Z_2 = R_2 + j(\omega L_2 - \frac{1}{\omega C_2}) \tag{3.2}$$

These impedances are defined for the circuit elements in series. To begin each derivation, Kirchhoff's rules are used on the lumped parameter circuit. All assumptions underlying those rules are applicable.

3.1.1 Derivation of the System Transfer Function

For a system driven by an input of the form $V_{in}(s)$, a transfer function $H(s)$ can be derived that relates the input, $V_{in}(s)$ to an output $V_{out}(s)$. In keeping with standard notation, the frequency domain variables are written in upper case letters to distinguish them from their time domain counterparts. To begin, Kirchhoff's voltage equations are written for going around the primary and secondary circuits below:

$$\begin{cases} V_{in} = I_1 Z_1 + j\omega M I_2 \\ -j\omega M I_1 = I_2 Z_2 \end{cases}$$

The second equation utilizes Faraday's and Lenz's laws to find the induced EMF in the circuit in the form of a coupled inductance. Solving the second equation for I_2 and then plugging it in the first equation to solve for I_1 yields:

$$I_1 = \frac{V_{in}}{Z_1 + \frac{(\omega M)^2}{Z_2}} \tag{3.3}$$

$$I_2 = \frac{-j\omega M I_1}{Z_2} = \frac{-j\omega M V_{in}}{Z_1 Z_2 + (\omega M)^2} \tag{3.4}$$

The effect of the secondary coupled to the primary is identical to that of an additional

impedance in the series path. Instead of the current in the primary being a simple voltage divided by its own impedance, there is an additional impedance of $\frac{(\omega M)^2}{Z_2}$. This is due to the back EMF from the coupled secondary, with the sign according to Lenz's law. The secondary coil, having its own voltage produced by the primary, loads the primary in an effort to oppose the creation of flux in its inductor. This effect appears as a drop in the voltage around the primary circuit loop, acting as an additional impedance.

The output voltage on the secondary coil, measured as the voltage across the parasitic capacitance is given as:

$$V_{out} = I_2 \frac{1}{j\omega C_2} = \frac{-MV_{in}}{C_2(Z_1 Z_2 + (\omega M)^2)} \tag{3.5}$$

$$\frac{V_{out}}{V_{in}} = \frac{-M}{C_2[(R_1 + L_1 s + \frac{1}{C_1 s})(R_2 + L_2 s + \frac{1}{C_2 s}) + (sM)^2]} \tag{3.6}$$

This last equation is the transfer function, $H(s)$ of the coupled second order resonant system. The frequency term, ω is replaced with the more general Laplacian frequency operator s.

One practical restriction on the type of inputs, $V_{in}(s)$, deals with the method of driving the system shown in Figure 3-1. The switching time of the leftmost switch must be brief compared to the frequency of the system oscillations. In other words, for a continuous train of pulsed responses, $V_{in}(s) = V \sum \delta(t - t_o)$, the switch on the primary should be able to charge C_1 in a time much less than the decay time of the system. A good analogy is to think of the ringing of a church bell. The bell knocker is pulled upward, giving it a set amount of stored energy (corresponding to the voltage source charing the primary capacitor). The knocker is then quickly released in relation to the duration of the bell's ringing, striking the bell and causing it to oscillate at its resonant frequency. When the bell's ringing dies out, the bell is knocked again. The action of the impact between the knocker and the bell can be approximated as an impulse. If the knocker is slowly released to ring the bell, the behavior of the system will be changed.

By introducing new parameters, it is possible to further manipulate the above equations. First, the output voltage equation 3.6 is expanded and the mutual inductance is expressed as: $M = k\sqrt{L_1 L_2}$.

$$\frac{V_{out}}{V_{in}} = \frac{-k\sqrt{L_1 L_2}}{C_2((R_1 + L_1 s + \frac{1}{C_1 s})(R_2 + L_2 s + \frac{1}{C_2 s}) - s^2 k^2 L_1 L_2)} \tag{3.7}$$

Next, the grouped terms are expanded and ordered by their degree in s:

$$\frac{V_{out}}{V_{in}} = \frac{-k\sqrt{L_1 L_2} C_1 s^2}{\left\{ \begin{array}{l} (1-k^2) C_1 C_2 L_1 L_2 s^4 + (R_1 L_2 C_2 C_1 + R_2 L_1 C_1 C_2) s^3 \\ +(R_1 R_2 C_1 C_2 + L_1 C_1 + L_2 C_2) s^2 + (R_1 C_1 + R_2 C_2) s + 1 \end{array} \right.} \tag{3.8}$$

The following network parameter substitutions are made: $\omega_i = \frac{1}{\sqrt{L_i C_i}}$ and $Q_i = \frac{\omega_i L_i}{R_i}$. The series formula for Q is used as both the primary and secondary circuits are modelled as series circuits. If either circuit is modelled as a parallel circuit, then the value $Q_i = \frac{R_i}{\omega_i C_i}$ must be used. These parameters are introduced by dividing the numerator and denomenator of equation 3.8 by the factor $\frac{1}{L_1 L_2 C_1 C_2}$. These substitutions yield:

$$\frac{V_{out}}{V_{in}} = -\sqrt{\frac{L_2}{L_1}} \frac{s^2 \omega_2^2 k}{\left\{ \begin{array}{l} (1-k^2) s^4 + (\frac{\omega_1}{Q_1} + \frac{\omega_2}{Q_2}) s^3 + (\omega_2^2 + \omega_1^2 + \frac{\omega_1 \omega_2}{Q_1 Q_2}) s^2 \\ +\omega_1 \omega_2 (\frac{\omega_2}{Q_1} + \frac{\omega_1}{Q_2}) s + \omega_1^2 \omega_2^2 \end{array} \right.} \tag{3.9}$$

or, alternately,

$$\frac{V_{out}}{V_{in}} = -\frac{M}{L_1} \frac{s^2 \omega_2^2}{\left\{ \begin{array}{l} (1-k^2) s^4 + (\frac{\omega_1}{Q_1} + \frac{\omega_2}{Q_2}) s^3 + (\omega_2^2 + \omega_1^2 + \frac{\omega_1 \omega_2}{Q_1 Q_2}) s^2 \\ +\omega_1 \omega_2 (\frac{\omega_2}{Q_1} + \frac{\omega_1}{Q_2}) s + \omega_1^2 \omega_2^2 \end{array} \right.} \tag{3.10}$$

The denomenator represents the characteristic polynomial of the system; in terms of s, it gives the frequency domain expression that dictates exactly how the system will respond to inputs for all allowable values of its parameters.

The numerator of these transfer functions warrants explanation. The leading factor from equation 3.9, $-\sqrt{\frac{L_2}{L_1}}$ is expected from the results seen thus far. The negative sign is due to the defined direction of current flow in the secondary. The reason for an $s\omega_2$ term and why it is squared is for two reasons. One is to keep the units consistent with the denomenator i.e. with a net fourth order frequency term on top and bottom. The other, more fundamental reason, requires one factor of $s\omega_2$ to transfer current from the primary to secondary circuit

and another factor to turn this secondary current into a voltage. Mathematically, the factor of $-j\omega$ from the induced secondary current expression $I_2 = -j\omega_2 M I_1/Z_2$ yields one factor of $s\omega$ while the other factor comes from the frequency domain equivalent of converting the current to voltage, $v_{out} = L_2 \frac{d\, i_2}{dt}$. The secondary voltage is actually taken over the capacitor, but it gives the equivalent terms via $\omega = \frac{1}{\sqrt{LC}}$ mathematically. The k in equation 3.9 is more intuitively explained by the form of equation 3.10. The factor of $k\sqrt{\frac{L_2}{L_1}}$ is a different form of $\frac{M}{L_1}$, a ratio of inductances that act as a voltage divider between secondary and primary.

It is important to note that equations 3.9 and 3.10 are equivalent forms of the transfer function, $H(s)$, that completely describe the system dynamics. Any input of the form $V_{in}(s)$ multiplied by the transfer function will give the response in the sinusoidal steady state. While time domain expressions are useful for checking the observed measured waveforms against the theoretical model, deriving new expressions for each method of drive (each equivalent expression for $V_{in}(s)$) is mathematically intensive. Frequency domain techniques offer a convenient system of deriving output expressions for each drive method.

3.1.2 Solution with primary and secondary tuned together

When the natural resonant frequencies of the primary and secondary circuits are tuned together to the same frequency such that $\omega_1 = \omega_2 = \omega_n$, the behavior of the output voltage waveform depends largely on the value of the coupling coefficient, k. Equation 3.9 can be manipulated with the assumptions below to give equation 3.11.[32] This ratio gives a convenient expression for determining the relative steady state output magnitude when the system is driven at a particular frequency, ω not necessarily equal to the self resonant frequency, ω_n.

$$\frac{V_{out}}{V_{in}} = \frac{-1}{\alpha^2}\sqrt{\frac{L_2}{L_1}}\frac{k}{(k^2 + \frac{1}{Q_1 Q_2} - (1 - \frac{1}{\alpha^2})^2 + j(1 - \frac{1}{\alpha^2})(\frac{1}{Q_1} + \frac{1}{Q_2}))} \tag{3.11}$$

For this expression, it is assumed that the self resonant frequencies are equal: $\omega_{1,2} = \omega_n$, the system is constrained to oscillate at a frequency $s = j\omega$, and $\alpha = \frac{\omega}{\omega_n}$ is the ratio of these two frequencies. As the ratio of the inductances is dependent on the value of the quality factors, equation 3.11 must be restated as:

$$\frac{V_{out}}{V_{in}} = \frac{-1}{\alpha^2}\sqrt{\frac{Q_2R_2}{Q_1R_1}}\frac{k}{(k^2 + \frac{1}{Q_1Q_2} - (1-\frac{1}{\alpha^2})^2 + j(1-\frac{1}{\alpha^2})(\frac{1}{Q_1}+\frac{1}{Q_2}))} \tag{3.12}$$

When $\alpha = 1$, corresponding to a system resonating at ω_n, the AC steady state voltage gain of equation 3.11 reduces to:

$$\frac{V_{out}}{V_{in}} = -\sqrt{\frac{L_2}{L_1}}\frac{k}{k^2 + \frac{1}{Q_1Q_2}} = -\sqrt{\frac{Q_2R_2}{Q_1R_1}}\frac{k}{k^2 + \frac{1}{Q_1Q_2}} \tag{3.13}$$

This voltage gain is maximized by taking a derivative with respect to k and taking a second derivative to show negative concavity. The result is a maximizing value of k defined as k_{crit}.

$$k_{crit} = \frac{1}{\sqrt{Q_1Q_2}} \tag{3.14}$$

$$\frac{V_{out}}{V_{in\ crit}} = -\sqrt{\frac{L_1}{L_2}}\frac{\sqrt{Q_1Q_2}}{2} = -\frac{Q_2}{2}\sqrt{\frac{R_2}{R_1}} = -\frac{\omega_n L_2}{\sqrt{R_1R_2}} \tag{3.15}$$

This value of critical coupling corresponds to a mutual inductive impedance of:

$$\omega_n M_{crit} = \sqrt{R_1R_2} \tag{3.16}$$

Using this equation gives another expression for the AC steady state voltage gain at $k = k_{crit}$:

$$\frac{V_{out}}{V_{in}}|_{crit} = -\frac{L_2}{2M_{crit}} \tag{3.17}$$

Figure 3-2 shows how the magnitude of the output voltage gain *at the frequency* ω_n varies with the relative value of the coupling coefficient. For operation at a fixed frequency of ω_n, a coupling coefficient of $k = k_{crit}$ represents an optimum voltage gain.

This point is quite subtle and cannot be overemphasized: If the coupled system is constrained to run at ω_n, the optimum output voltage gain will occur for $k = k_{crit}$. However, if the system is allowed to freely oscillate, the output voltage gain may indeed be greater, depending on the mismatch of the quality factors, as shown below.

Equation 3.11 can also be solved to maximize voltage gain over frequency. Taking its derivatives to find local maxima yields two solutions. These solutions are seen graphically in Figures 3-3 through 3-7 for various k and quality factors, under the constraint $k_{crit} = 0.01$

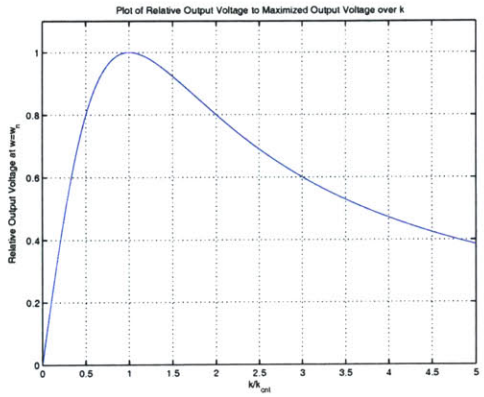

Figure 3-2: A plot of voltage gain at the frequency $\omega = \omega_n$ over a range of $\frac{k}{k_{crit}}$

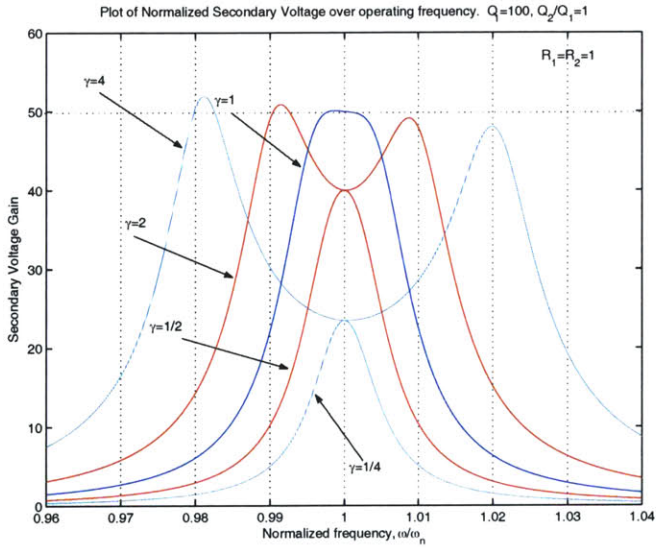

Figure 3-3: Plot of secondary voltage gain over normalized frequency, $Q_1 = Q_2 = 100$, $R_1 = R_2 = 1$. $\gamma = \frac{k}{k_{crit}}$

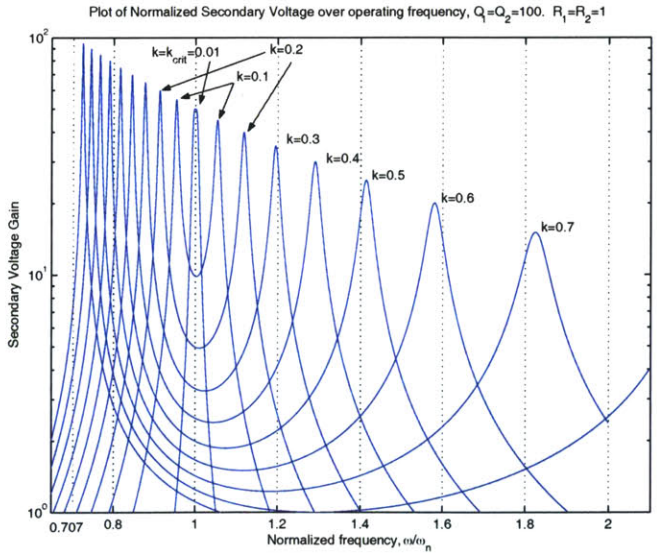

Figure 3-4: Plot of secondary voltage gain for $Q_1 = Q_2 = 100$ and larger k

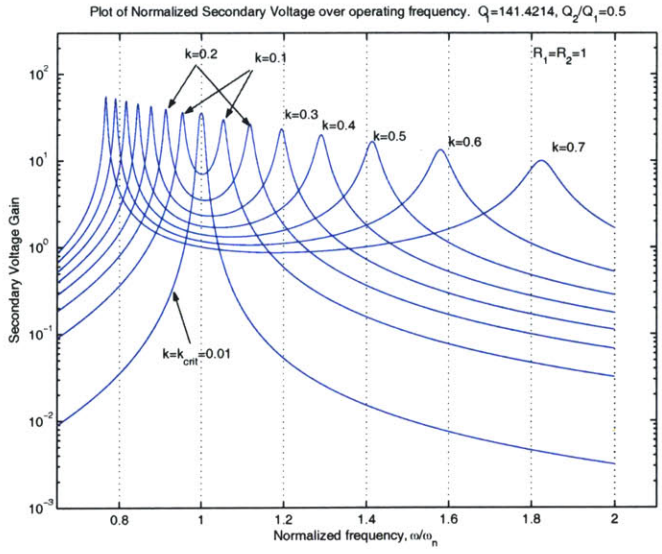

Figure 3-5: Plot of secondary voltage gain for $Q_1 = 141.4$, $\frac{Q_2}{Q_1} = \frac{1}{2}$, and larger k

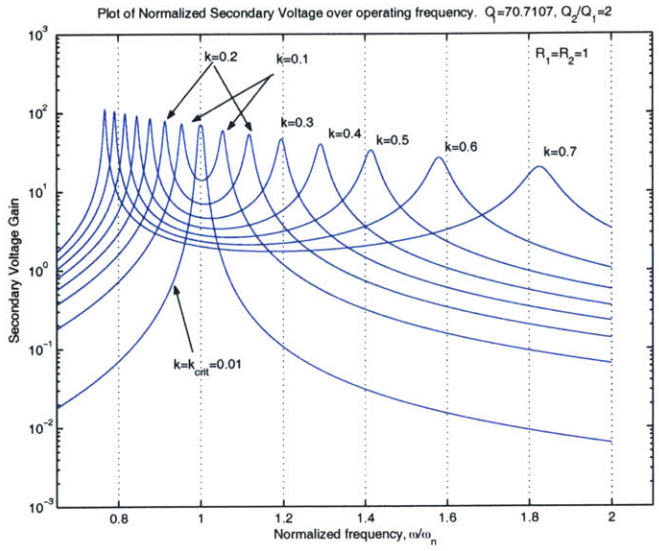

Figure 3-6: Plot of secondary voltage gain for $Q_1 = 70.7$, $\frac{Q_2}{Q_1} = 2$, and larger k

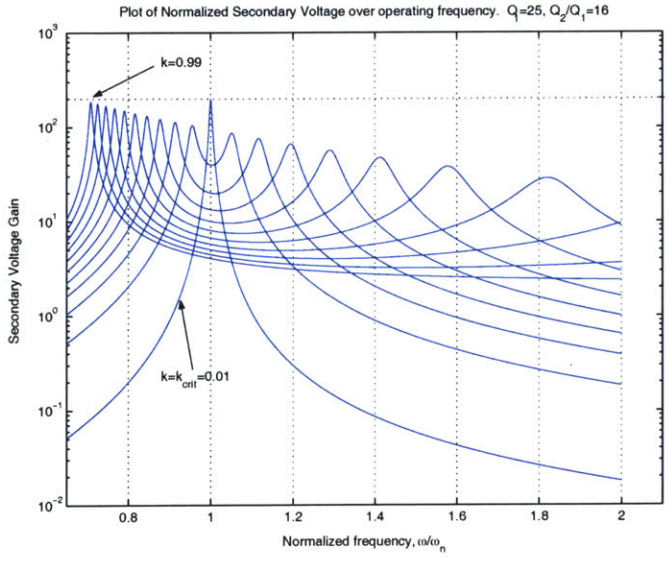

Figure 3-7: Plot of secondary voltage gain for $Q_1 = 25$, $\frac{Q_2}{Q_1} = 16$, and larger k

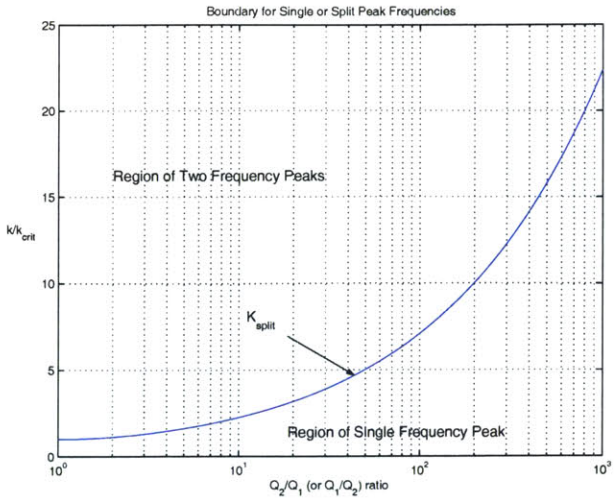

Figure 3-8: Plot of $\frac{Q_2}{Q_1}$ versus $\frac{k}{k_{crit}}$ ratio boundary condition for single or split peak frequency response

in all these plots. Figure 3-3 shows how the voltage gain peak rises at the frequency ω_n only splitting into two peaks above $\frac{k}{k_{crit}} = \gamma = 1$ in this case. However, these peaks do not have equal magnitudes and are not symmetrically split about the self resonant frequency ω_n. Note that when the quality factors are not equal, the voltage gain peak at ω_n does not split at $\gamma = 1$. Instead, it splits under the condition $k \geq k_{split}$ shown in equation 3.18 below.

$$k \geq k_{split} = \frac{1}{\sqrt{2}}\sqrt{\frac{1}{Q_1^2} + \frac{1}{Q_2^2}} \tag{3.18}$$

Figure 3-8 shows the ratio of quality factors and relative k needed for the split in resonant frequency peaks to occur.

As k gets larger the lower peak grows in magnitude and asymptotically approaches the frequency $\frac{\omega_n}{\sqrt{2}}$. The upper peak decreases in magnitude and its frequency asymptotically approaches infinity. When the quality factors are unequal, there is a drop in voltage gain when the peak splits into two. The magnitude of this drop is dependent on the ratio of the quality factors, $\frac{Q_2}{Q_1}$. For $Q_1 Q_2 = 100^2$ ($k_{crit} = 0.01$), then for the condition $\frac{Q_2}{Q_1} > 16$ or $\frac{Q_1}{Q_2} > 16$, the secondary voltage gain at $k = k_{crit}$ is greater than that at $k = 1$. The value of $\frac{Q_2}{Q_1}$ at which the secondary voltage gain is greater at k_{crit} than at unity depends on the product of the quality factors.

Terman[32] gives a derivation to determine these peak frequency magnitudes and gives curves for various conditions showing the relative magnitude of the output voltage for values of $\frac{k}{k_{crit}}$ and $\frac{\omega_{peak}}{\omega_n}$. The derivative of equation 3.11 is taken to find its relative maxima. The frequency locations of these maxima are given in equation 3.19.

$$\omega_{peaks} = \frac{\omega_n}{\sqrt{1 \pm k\sqrt{(1 - \frac{k_{crit}^2}{2k^2}(\frac{Q_1}{Q_2} + \frac{Q_2}{Q_1}))}}} \tag{3.19}$$

This equation assumes that the factor $(1 - \frac{1}{\alpha^2})$ is constant. The two peak resonant frequencies are defined as ω_{upper} and ω_{lower} with $\omega_{upper} \geq \omega_{lower}$. When equation 3.18 is satisfied with $k \geq k_{split}$, these two resonant frequencies give rise to a beat pattern in the time domain waveforms. For the condition $k < k_{split}$, equation 3.19 shows that there is only one frequency peak at ω_n. This implies that there will be one resonant frequency present in the response output.

Pole-Zero plots give a geometric picture of how the system gain and resonant frequencies change as the coupling coefficient changes from zero to unity. The transfer function used is the voltage gain expressed in equation 3.11. The four poles assume the form $s_{upper} = -\zeta_{upper} \pm j\omega_{peaks}$ and $s_{lower} = -\zeta_{lower} \pm j\omega_{peaks}$ where ω_{peaks} represents ω_{upper} and ω_{lower} (for $k \geq k_{split}$) while ζ represents the damping coefficient associated with the upper and lower system resonant frequency. As these poles are in the form of complex conjugates, they represent time domain solutions proportional to a sum of two damped sinusoids. The upper pole always has a greater damping coefficient than the lower pole.

As k approaches unity, the system reduces to a third order polynomial with the two upper poles coalescing into a single pole at negative infinity. The remaining two lower poles exponentially approach the imaginary axis at $\pm\frac{\omega_n}{\sqrt{2}}$. This is consistent with the operational dynamics of an ideal transformer. When an ideal transfer is excited with an impulse, the system resonates sinusoidally and indefinitely at a single resonant frequency.

3.1.3 Physical interpretation of $\omega_1 \neq \omega_2$

When the primary and secondary circuits are not tuned to the same frequency, ω_n, the mathematics describing the situation becomes complicated. To better understand the dynamics, a physical intuition of what happens must be developed.

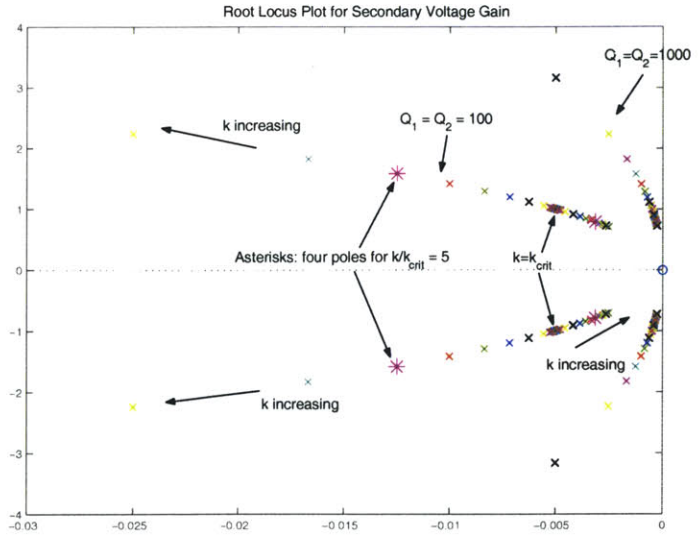

Figure 3-9: A Pole-Zero plot for the Secondary Voltage. Notice how range of Q affects the values of ζ and ω_{peaks}. As k approaches unity, poles go to negative infinity and $j\omega$ axis.

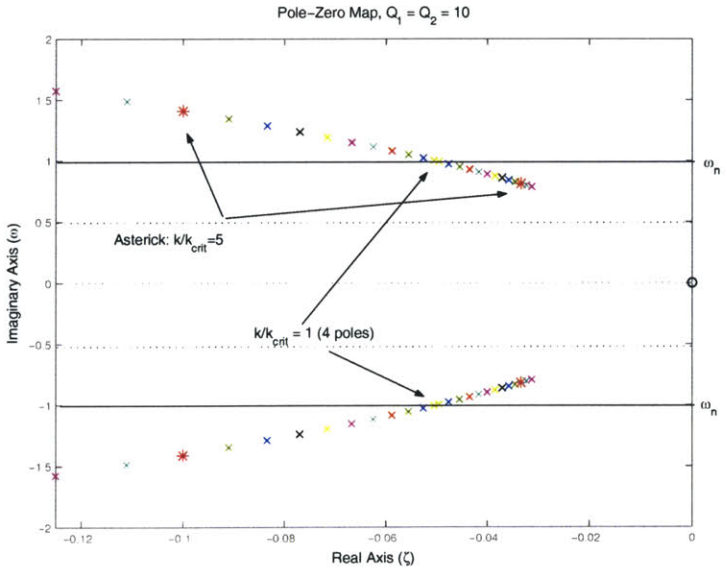

Figure 3-10: $Q_1 = Q_2 = 10$. No pole breaches the $\frac{\omega_n}{\sqrt{2}}$ frequency limit.

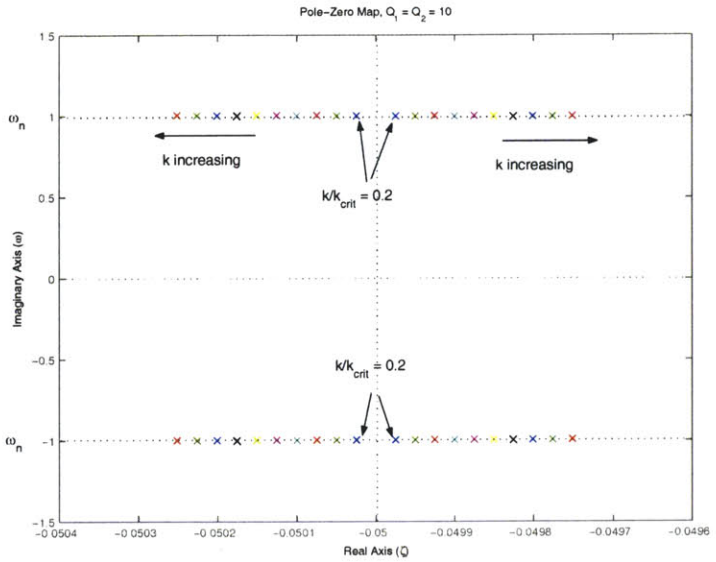

Figure 3-11: A plot for $k < k_{crit}$. $Q_1 = Q_2 = 10$. System oscillates at ω_n.

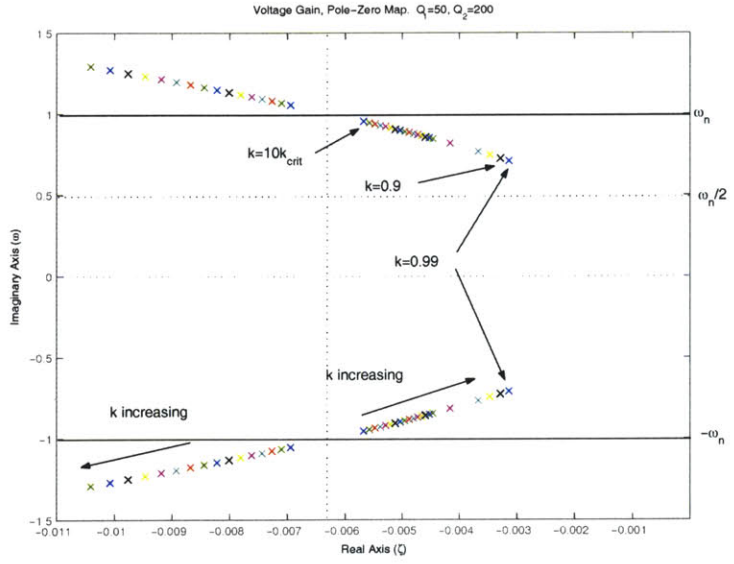

Figure 3-12: Plot for large k. $Q_1 = 50, Q_2 = 200$. Note that for all pole-zero plots, real component, ζ centered about quantity $(\frac{1}{Q_1} + \frac{1}{Q_2})^2$.

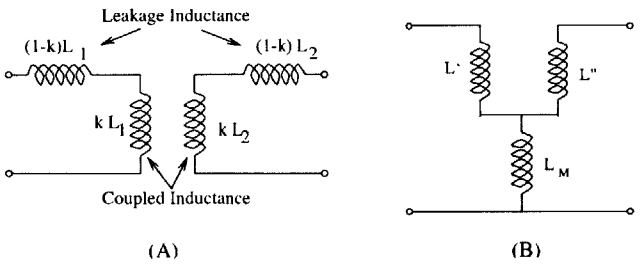

Figure 3-13: A and B are mathematically equivalent circuits describing the magnetic coupling in terms of inductive coupling.

When the two circuits are far enough away, their coupling is effectively zero, $k = 0$. Each circuit has its own damping coefficient and resonant frequency determined by the characteristics of the circuit. As the two circuits are brought closer together, the inductors, producing magnetic flux, begin to couple. The inductor in the secondary circuit converts this coupled or linked flux into a voltage. The primary circuit sees an additional load across its inductor as the flux it produces is being taken by the secondary. Two topologically equivalent circuits that describes this relationship are shown in Figure 3-13. This topology gives a clearer picture of how the coupling between the two physically separate transformers grows as k increases. Figure A shows the physically separate inductors broken up into coupled and leakage inductances even though they are part of the same physical inductor. The coupled inductances grow as k increases. The greater k, the more flux transferred between the two coupled inductors. The leakage inductors do not share or link flux with the other circuit. Instead, they serve as an energy storage element.

Figure B shows an electrically and mathematically equivalent circuit. The equations relating L_1, L_2, and M to the values of L', L'', and L_M are shown below:

$$L_M = -M = -k\sqrt{L_1 L_2} \tag{3.20}$$

$$L' = L_1 + k\sqrt{L_1 L_2} \tag{3.21}$$

$$L'' = L_2 + k\sqrt{L_1 L_2} \tag{3.22}$$

These are easily derived by the definition of $k = \frac{M}{\sqrt{L_1 L_2}}$ and setting $L_1 = L' + L_M$. As k increases to unity, the leakage inductance goes to zero.

The resonant frequency of a system is the rate of energy transfer between energy storage

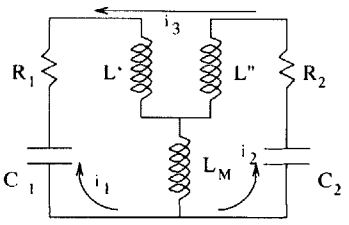

Figure 3-14: A mathematical model of the coupled system. The magnetic coupling is replaced with inductive coupling. Operation is identical.

elements. As the coupling k between the two circuits increases, the four energy storage elements exchange energy amongst themselves, i.e. there are resonant frequencies involving C_1 and L_1, C_1 and L_2 as well as C_2 and L_1 and C_2 and L_2. When the two circuits are tuned to the same frequency, these four resonant frequencies reduce to two.

Figure 3-14 shows, using the B transformation of Figure 3-13, the paths between the four elements. For most practical values of Q and k, the system has at least two resonant frequencies determined by the system moving energy from the primary capacitor to the set of inductors to the secondary capacitance and back again. However, for very small Q and $k < k_{split}$, the system response decays before any oscillations occur.

3.1.4 Equivalent Input/Output Impedances

For design purposes, it is useful to compute an equivalent input and output impedance for the circuit. These equivalent impedances are known as Thevenin equivalent impedances; they are useful quantities if this resonant circuit is to be used in any sort of larger system where it will be coupled to an input or output device. A model showing where these impedances are computed is shown in Figure 3-15.

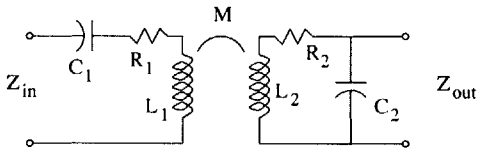

Figure 3-15: A model showing the ports used to compute the Thevenin equivalent input and output impedances

To find these impedances, it is first necessary to recall some previous definitions for the series impedance of the primary and secondary. Equations 3.1 and 3.2, repeated below,

define the series impedance of the primary and secondary circuits when there is no coupling ($k = 0$).

$$Z_1 = R_1 + j(\omega L_1 - \frac{1}{\omega C_1})$$
$$Z_2 = R_2 + j(\omega L_2 - \frac{1}{\omega C_2})$$

The effect of the coupling is to effectively add an impedance in series with these elements. The magnitude of this coupled impedance is $Z_{coupled} = \frac{-(sM)^2}{Z_1}$, as derived in equations 3.3 and 3.4.

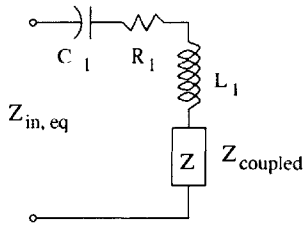

Figure 3-16: Schematic of Equivalent Primary Circuit

An equivalent circuit is shown in Figure 3-16. The initial charge on the capacitor is shown as a voltage source. However, when computing the Thevenin impedance at the terminals shown, this voltage source is shorted. Summing the four impedance elements together gives $Z_{in} = Z_1 + Z_{coupled}$ which is expressible as:

$$Z_{in} = Z_1 s \frac{(sM)^2}{Z_2} = R_1 + L_1 s + \frac{1}{C_1 s} - \frac{(sM)^2}{R_2 + L_2 s + \frac{1}{C_2 s}} \tag{3.23}$$

The output impedance is more complicated to calculate in that the secondary capacitance is in parallel with the output terminals. The voltage induced on the secondary can be modelled as a voltage source supplying current to the secondary. Because of symmetry, the coupled impedance remains $Z_{coupled} = \frac{-(sM)^2}{Z_1}$. The output impedance is computed by finding the voltage across the capacitor in the secondary due to the induced voltage. Using the expression for the secondary current derived in equation 3.4 and an induced voltage magnitude of $V_{induced} = \frac{-sMV_{in}}{Z_1}$ yields:

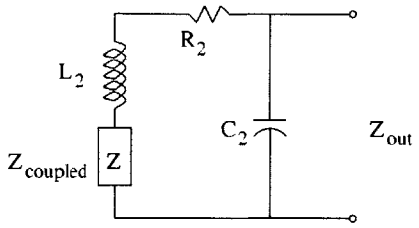

Figure 3-17: Schematic of Equivalent Secondary Circuit Impedance

$$I_2 = \frac{-j\omega M V_{in}}{Z_1 Z_2 + (\omega M)^2}$$
$$Z_{out} = \frac{V_{induced}}{I_2} \tag{3.24}$$

This can be expanded to give:

$$Z_{out} = \frac{\begin{cases} (M^2 - L_1L_2)C_1s^3 - C_1(L_1R_2 + L_2R_1)s^2 \\ -(C_1R_1R_2 + L_2)s - R_2 \end{cases}}{\begin{cases} (M^2 - L_1L_2)C_1C_2s^4 - C_1C_2(L_1R_2 + L_2R_1)s^3 \\ -(C_1(C_2R_1R_2 + L_1) + C_2L_2)s^2 - (C_1R_1 + C_2R_2)s - 1 \end{cases}} \tag{3.25}$$

An equivalent circuit is shown in Figure 3-17. For $k \leq k_{crit}$ or k small ($k < 0.1$), the resonant frequencies of the coupled system ω_{upper} and ω_{lower} are exactly or close to the independent resonant frequency ω_n, the input and output impedances can be expressed as the following.

$$Z_{in}|_{s=\omega_n} = R_1 + \frac{\omega_n^2 k^2 L_1 L_2}{R_2} \tag{3.26}$$
$$Z_{out} = \frac{\omega_n R_1 L_2 - j(R_1R_2 + \omega_n^2 L_1 L_2 k^2)}{\omega_n(R_1R_2C_2 + L_1k^2)} \tag{3.27}$$

Rewriting these Thevenin impedances in terms of the network parameters of the coupled circuits gives:

$$Z_{in}|_{\omega_n} = R_1(1 + kQ_1Q_2) \tag{3.28}$$

$$Z_{out}|_{\omega_n} = \sqrt{\frac{L_2}{C_2}}\frac{(Q_2 - j(1 + k^2 Q_1 Q_2))}{1 + k^2 Q_1 Q_2} \tag{3.29}$$

An interesting feature of the output resistance is that it is proportional to the characteristic impedance of a transmission line. Furthermore, Z_{out} always has a resistive and capacitive component in series. There is no physically consistent mathematical substitution for one of the parameters that will make it appear purely resistive or capacitive. However, for k small ($k \approx k_{crit}$) and $Q_2 \gg 1$, the resistive component will dominate the expression giving:

$$Z_{out} \approx \sqrt{\frac{L_2}{C_2}}\frac{Q_2}{1 + k^2 Q_1 Q_2} \tag{3.30}$$

For $k = k_{crit}$, these Thevenin impedances reduce to:

$$Z_{in}|_{crit} = 2R_1 \tag{3.31}$$

$$Z_{out}|_{crit} = \sqrt{\frac{L_2}{C_2}}\frac{Q_2 - 2j}{2} \approx \sqrt{\frac{L_2}{C_2}}\frac{Q_2}{2} \tag{3.32}$$

The input impedance for $k = k_{crit}$ is determined solely by the resistance of the primary circuit while the output impedance solely by the properties of the secondary coil. The critical coupling value is the point where the coupled impedance seen by each side is determined by the properties of the individual circuit's parameters.

At this point, it is advantageous to derive the time dynamics of the coupled system to observe the effect of the coupling coefficient and damping on the secondary waveforms.

3.2 Derivation of Dynamics in the Time Domain

The most direct and probably the most mathematically intensive approach to solving the dynamics of a couple system in the time domain is to analytically solve the system's characteristic polynomial. The currents $i_1(t)$ and $i_2(t)$ in each loop of the two circuits are found leading to expressions for voltage and energy using the constitutive relations of the circuit elements.

As in the frequency domain, the voltage around the two loops of the circuit in Figure 3-1 are summed, with V_{in} representing the magnitude of the initial charge on the capacitor C_1 before the switch is closed. Using KVL in terms of the system currents to find the sum of the voltages yields:

$$\int \frac{1}{C_1} i_1(t)dt + R_1 i_1(t) + L_1 \frac{di_1(t)}{dt} + M\frac{di_2(t)}{dt} = V_{in} \tag{3.33}$$

$$\int \frac{1}{C_2} i_2(t)dt + R_2 i_2(t) + L_2 \frac{di_2(t)}{dt} + M\frac{di_1(t)}{dt} = 0 \tag{3.34}$$

The voltage in the second loop is set to 0 as there is no external source driving it. The source of $i_2(t)$ is the induced voltage due to the coupling of the inductors, an effect that is taken into account through the mutual inductance, M. By solving equation 3.33 for $\frac{di_2(t)}{dt}$ and taking two time derivatives of equation 3.34, a general fourth order differential equation can be found:

$$\begin{aligned} i_1(t) + (R_1C_1 + R_2C_2)\frac{di_1(t)}{dt} + (L_2C_2 + L_1C_1 + R_1R_2C_1C_2)\frac{d^2i_1(t)}{dt^2} \\ + C_1C_2(L_2R_1 + L_1R_2)\frac{d^3i_1(t)}{dt^3} - (M^2 - L_1L_2)C_1C_2\frac{d^4i_1(t)}{dt^4} = 0 \end{aligned} \tag{3.35}$$

The currents, $i_1(t)$ and $i_2(t)$ are interchangeable in the above equation due to the symmetry of the two coupled differential equations.

To solve for the currents explicitly there must be four constraining equations, as there is a fourth order differential equation. The first two conditions can be stated as $i_1(t=0) = 0$ and $i_2(t=0) = 0$ meaning that the system is at static rest before it is excited. The second two conditions state that the initial charges on the primary and secondary capacitances are $Q_{1,o} = C_1V_{in}$ and $Q_{2,o} = 0$.

The system of second order equations above (3.33 and 3.34) have solutions that are symmetric due to the symmetric nature of the circuit. The general form of the solution is $C_{upper}e^{-\lambda_{upper}t} + C_{lower}e^{-\lambda_{lower}t}$. The characteristic polynomial is found by multiplying the following:

$$\begin{cases} 1 + R_1C_1\lambda_{lower} + L_1C_1\lambda_{lower}^2 = -C_1M\lambda_{upper}^2 \\ 1 + R_2C_2\lambda_{upper} + L_2C_2\lambda_{upper}^2 = -C_2M\lambda_{lower}^2 \end{cases}$$

Separating the λ_{upper} and λ_{lower} terms is called a separation of variables. Cross multiplying and dropping the subscript yields the same result as taking derivatives of the KVL equations and substituting to find a fourth order differential equation in terms of i_1 or i_2

alone. The result of this operation is the characteristic polynomial.

$$1 + (R_1C_1 + R_2C_2)\lambda + (R_1C_1R_2C_2 + L_1C_1 + L_2C_2)\lambda^2 + (L_1C_1R_2C_2 + R_1C_1L_2C_2)\lambda^3 + L_1C_1L_2C_2\lambda^4 = M^2C_1C_2 \quad (3.36)$$

This characteristic polynomial is identical to the denomenator of the input/output voltage ratio seen in the frequency domain relation (equation 3.9). The dynamics of the coupled resonant circuits are completely described by this expression. However, this characteristic polynomial is extremely difficult to solve analytically. Putting this equation into a symbolic solver does not give any insight into designing a better circuit as it is unclear how a given component value affects both the resultant frequencies and damping coefficients. For that reason, the parameters of self resonant frequency, ω_1 and ω_2, and the frequencies of the original uncoupled circuits and quality factor, Q_1 and Q_2, are introduced. With these substitutions: $\omega_i = \frac{1}{\sqrt{L_iC_i}}$, $Q_i = \omega_i\frac{L_i}{R_i}$, and $M = k\sqrt{L_1L_2}$, the characteristic polynomial is restated as it was in the frequency domain equation 3.10. This characteristic polynomial has identical solutions to the general fourth order differential equation derived in equation 3.35.

$$(1-k^2)\lambda^4+(\frac{\omega_1}{Q_1}+\frac{\omega_2}{Q_2})\lambda^3+\omega_1\omega_2(\frac{\omega_1}{\omega_2}+\frac{\omega_2}{\omega_1}+\frac{1}{Q_1Q_2})\lambda^2+\omega_1\omega_2(\frac{\omega_1}{Q_2}+\frac{\omega_2}{Q_1})\lambda+\omega_1^2\omega_2^2 = 0 \quad (3.37)$$

The difference between this formulation and that of the frequency domain is the distinction between the two self resonant frequencies of the individual circuits. In the frequency domain derivation, the case where the two self resonant frequencies, ω_1 and ω_2 are unequal is only briefly discussed due to the greatly simplified nature of the frequency domain solution when they are set equal. The general analysis is carried out using the Laplacian frequency operator, s, where any complex frequency $s = \alpha + j\omega$ can be used to drive the system. In the time domain solution, the case of differing self resonant frequencies is discussed for completeness while the case of a pulsed system operated at a frequency ω of the same order of magnitude as the peak frequencies ω_{upper} or ω_{lower} is not discussed here. In other words, it is assumed that the system is allowed to freely oscillate and damps itself out before the

next impulse is delivered.

3.2.1 Freely Resonating Time Domain Solution for $\omega_1 = \omega_2$

Plugging into the characteristic polynomial $\lambda = \zeta \pm j\omega$ and expanding yields the complete solution. These solutions can be greatly simplified and solved by hand if terms of order $(\frac{\zeta}{\omega})^2$ and higher are assumed to be much less than unity and ignored. This leads directly to the condition that the damping coefficients ζ_{lower} and ζ_{upper} will be much smaller than the resonant frequencies. From this, the characteristic polynomial can be decomposed into real and imaginary parts: [24]

$$\begin{cases} Re: \ (1-k^2)\omega^4 - (\omega_1^2+\omega_2^2)\omega^2 + \omega_1^2\omega_2^2 = 0 \\ Im: \ (2(1-k^2)\omega^2 - (\omega_1^2+\omega_2^2))\zeta - ((\frac{\omega_1}{2Q_1}+\frac{\omega_2}{2Q_2})\omega^2 - \frac{\omega_1\omega_2}{2}(\frac{\omega_2}{Q_1}+\frac{\omega_1}{Q_2})) = 0 \end{cases}$$

Solving yields the required four solutions:

$$Re\{\lambda\} = \zeta_{upper} = \frac{(\omega_1 Q_2 + \omega_2 Q_1)\omega_{upper}^2 - \omega_1\omega_2(\omega_2 Q_2 + \omega_1 Q_1)}{2Q_1Q_2(2(1-k^2)\omega_{upper}^2 - (\omega_1^2+\omega_2^2))} \tag{3.38}$$

$$Re\{\lambda\} = \zeta_{lower} = \frac{(\omega_1 Q_2 + \omega_2 Q_1)\omega_{lower}^2 - \omega_1\omega_2(\omega_2 Q_2 + \omega_1 Q_1)}{2Q_1Q_2(2(1-k^2)\omega_{lower}^2 - (\omega_1^2+\omega_2^2))} \tag{3.39}$$

$$Im\{\lambda\} = \omega_{upper} = \sqrt{\frac{(\omega_1^2+\omega_2^2) + \sqrt{(\omega_1^2+\omega_2^2)^2 - 4(1-k^2)\omega_1^2\omega_2^2}}{2(1-k^2)}} \tag{3.40}$$

$$Im\{\lambda\} = \omega_{lower} = \sqrt{\frac{(\omega_1^2+\omega_2^2) - \sqrt{(\omega_1^2+\omega_2^2)^2 - 4(1-k^2)\omega_1^2\omega_2^2}}{2(1-k^2)}} \tag{3.41}$$

For the case where the self resonant frequencies are equal, $\omega_1 = \omega_2$, these solutions reduce to the following:

$$Re\{\lambda\} = \zeta_{upper} \approx \frac{\omega_n}{4}\frac{1}{1-k}(\frac{1}{Q_1}+\frac{1}{Q_2}) \tag{3.42}$$

$$Re\{\lambda\} = \zeta_{lower} \approx \frac{\omega_n}{4}\frac{1}{1+k}(\frac{1}{Q_1}+\frac{1}{Q_2}) \tag{3.43}$$

$$Im\{\lambda\} = \omega_{upper} \approx \frac{\omega_n}{(1-k)^{1/2}} \tag{3.44}$$

$$Im\{\lambda\} = \omega_{lower} \approx \frac{\omega_n}{(1+k)^{1/2}} \tag{3.45}$$

The solutions presented here imply that there will always be two distinct peak frequen-

cies ω_{upper} and ω_{lower} for all $k > 0$. This is due to the approximations made during the derivation, that the damping ratio is much smaller than the quality factor of either circuit. For $k \leq k_{split}$ and the Q's small, this assumption is not strictly valid. Physically, the primary cannot transfer enough energy to the secondary for their output waveforms to have beats. This is analogous to the second order case of critical damping. For $Q < 0.5$, the energy lost by the circuit is too great for oscillations to appear in the response.

If k is a relatively large number, implying a strong coupling between the two inductors, then the difference in the resonant frequencies becomes quite large. As k approaches 1, then the upper resonant frequency, ω_{upper} and the damping coefficient ζ_{upper} approach infinity. Physically, the beat pattern predicted in the frequency domain derivation will be damped out and will result in a decaying sinusoidal waveform. This is expected as ideal transformers with $k \approx 1$ do not exhibit beat patterns when pulsed. There is no defined cut-off value of the coupling coefficient where this occurs, but instead happens in an exponential fashion as the frequencies become more mismatched.

The expressions for the currents are given by the above parameters and the derived initial conditions in a typical second order differential equation solution form.

$$i_1(t) = -\frac{V_{in}}{2\omega_n^2 L_1}\left[\omega_{lower}e^{-\zeta_{lower}t}\sin(\omega_{lower}t) + \omega_{upper}e^{-\zeta_{upper}t}\sin(\omega_{upper}t)\right] \quad (3.46)$$

$$i_2(t) = \frac{V_{in}}{2\omega_n^2\sqrt{L_1 L_2}}\left[\omega_{upper}e^{-\zeta_{upper}t}\sin(\omega_{upper}t) - \omega_{lower}e^{-\zeta_{lower}t}\sin(\omega_{lower}t)\right] \quad (3.47)$$

Inserting the approximate relations for the resonant peak frequencies ω_{upper} and ω_{lower} yields:

$$i_1(t) \approx -\frac{V_{in}}{2\omega_n L_1}\left[\frac{e^{-\zeta_{lower}t}}{\sqrt{1+k}}\sin(\frac{\omega_n}{\sqrt{1+k}}t) + \frac{e^{-\zeta_{upper}t}}{\sqrt{1-k}}\sin(\frac{\omega_n}{\sqrt{1-k}}t)\right] \quad (3.48)$$

$$i_2(t) \approx \frac{V_{in}}{2\omega_n\sqrt{L_1 L_2}}\left[\frac{e^{-\zeta_{upper}t}}{\sqrt{1-k}}\sin(\frac{\omega_n}{\sqrt{1-k}}t) - \frac{e^{-\zeta_{lower}t}}{\sqrt{1+k}}\sin(\frac{\omega_n}{\sqrt{1+k}}t)\right] \quad (3.49)$$

For validity, the limiting cases for $k = 0$ and $k = 1$ are computed, even though this model is not entirely accurate up to these points. At $k = 0$, there is no coupling and the current $i_2(t)$ should not be influenced by the primary. Conversely, for $k = 1$, the behavior should be that of an ideal transformer. The currents should be identical within a turns ratio defined by the inductances. At $k = 1$, the upper pole is damped out by an infinitely

large exponential.

$k = 1$

$$i_1(t) = -\frac{V_{in}}{2\sqrt{2}\omega_n L_1} e^{-\zeta_{lower} t} \sin(\frac{\omega_n t}{\sqrt{2}}) \tag{3.50}$$

$$i_2(t) = -\frac{V_{in}}{2\omega_n \sqrt{2 L_1 L_2}} e^{-\zeta_{lower} t} \sin(\frac{\omega_n t}{\sqrt{2}}) \tag{3.51}$$

$k = 0$

$$i_1(t) = -\frac{V_{in}}{\omega_n L_1} e^{-\zeta_0 t} \sin(\omega_n t) \tag{3.52}$$

$$i_2(t) = 0 \tag{3.53}$$

These equations yield waveforms that behave as expected in the limiting cases. Remember that the damping coefficients in the first case are dependent on k. In the last case, $\zeta_0 = \frac{\omega_n}{4}(\frac{1}{Q_1} + \frac{1}{Q_2})$.

Time Domain Characteristics for $R_{1,2} = 0$

When the quality factors go to infinity, for $k_{split} < k \ll 1$, the coupled networks exhibit a beat pattern. The purpose of this section is to examine the ideal behavior of the system before the energy is dissipated and the system is dominated by losses.

If loss mechanisms are not present, then the behavior of the system is due solely to the coupling of the two LC networks. This explains the purely sinusoidal behavior. Figure 3-18 illustrates the time domain behavior of the currents for $k = 0.01$ and $k = 0.1$. These current waveforms exhibit a "beat frequency", that is, instead of simple sinusoidal oscillations, these waveforms appear to have an envelope waveform that bound them. The characteristics of this envelope function and its frequency, called the beat frequency are discussed momentarily. Note that the leading coefficients of these currents are set to unity and the time axis is normalized such that $t = \frac{2\pi x}{\omega_n}$ where x is the normalized, unitless time. These modifications have consequences; while the currents appear to have equal magnitude in these plots, the current $i_2(t)$ will be multiplied by a turns ratio that is buried inside the inductance terms, L_1 and L_2. The purpose in neglecting losses and scaling factors is to clarify the relationship between $i_1(t)$ and $i_2(t)$ in terms of the phase angle, oscillation frequency, beat frequency, as well as the influence of the independent frequencies ω_1, ω_2 and the coupling coefficient, k.

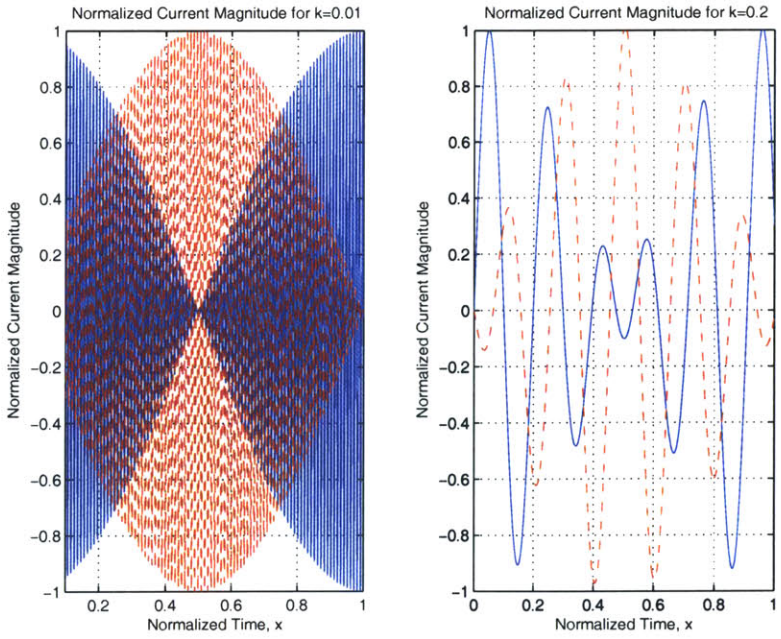

Figure 3-18: A plot comparing the envelope frequencies for $k = 0.01$ (left) and $k = 0.2$ (right). $k \gg k_{crit}$

i. Phase Relations

One interesting aspect of these current waveforms is how "orthogonal" they are to one another for various values of k, i.e. how the phase between their beat pattern changes. The smaller k the smaller the one current waveform is while the other is maximum. As k approaches unity, the two waveforms overlap such that each experiences a relative maximum at the same time. In this sense, k can be thought of as a phase angle between the primary and secondary waveforms. This relative phase relationship holds for both the waveforms themselves as well as the functions that appear to be bounding or constraining the oscillating waveforms, as the value of k goes from unity to zero, the current waveforms go from perfectly in phase to 90^o out of phase.

To understand how the envelope and relative phase of the current waveforms changes with the coupling coefficient, k, it is necessary to go back to the differential equations used to solve for the currents and instead of breaking the solution into real and imaginary parts which leads to the sine terms, keep the solution in the form of $e^{\lambda t}$. The envelope function that follows the current waveforms has the form $C_1 \sin\left(\frac{\omega_{upper}-\omega_{lower}}{2}t + \phi\right)$, where C_1 is a

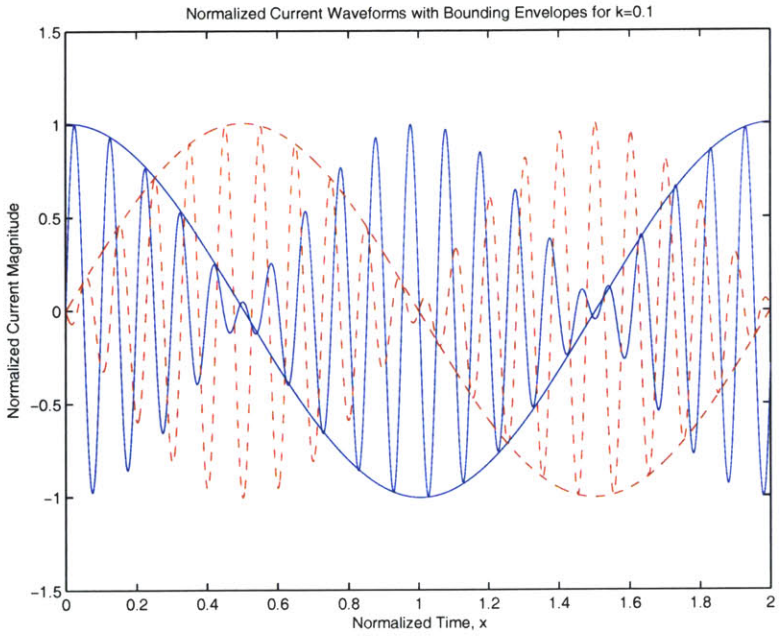

Figure 3-19: Plot of Normalized Current Waveforms with Bounding Envelopes, $k = 0.1$

constant that combines the magnitudes of the individual sine terms in the current equations and ϕ adjusts the phase to properly align the envelope waveform. This expression is most easily found by taking the currents as a complex phaser of the form $\underline{I_1} = I_1 e^{\omega t + \phi}$ and solving for the magnitude and phase. Tailored for the individual currents, the envelope waveforms are given by the following equations.

$$I_{env1}(t) = \pm \frac{1}{\sqrt{1-k^2}} \sin\left(\frac{\omega_{upper} - \omega_{lower}}{2} t + (1-k^2)\frac{\pi}{2}\right) \tag{3.54}$$

$$I_{env2}(t) = \pm \frac{1}{\sqrt{1-k^2}} \sin\left(\frac{\omega_{upper} - \omega_{lower}}{2} t\right) \tag{3.55}$$

Figure 3-19 shows how these envelope waveforms bound the current waveforms. As k increases from 0 to 1, the two envelopes overlap and eventually, at perfect coupling, $k = 1$, become identical. Figure 3-20 shows this tradeoff.

The beat frequency $f_{beat} = \frac{\omega_{upper} - \omega_{lower}}{2\pi}$ is *twice* the frequency of this envelope and dictates the rate at which energy is exchanged between the two sides of the circuit. The individual oscillations of the current waveforms themselves represent the current magnitude

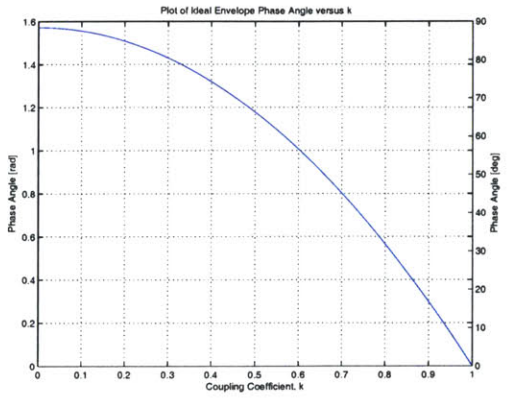

Figure 3-20: Plot of Relative Envelope Phase Angle versus k. System breaks down as k approaches unity and the upper pole becomes infinitely damped.

between the inductor and capacitor on each side of the oscillator as they exchange energy between themselves.

ii. Beats

The beats of the response waveform are defined by the zero crossings of their envelope functions shown in equations 3.54 and 3.55. Each complete half cycle between two zero crossings of the envelope represents one beat. This definition implies that the primary waveform in Figure 3-19 between the origin and the first zero crossing of its bounding envelope is not a beat. However, the secondary response, between the origin and its first envelope zero crossing, shows one beat.

The beats arise mathematically from the coupling of the two second order circuits. Each circuit has its own characteristic solution of the form $i(t) = Ce^{(-\alpha+j\omega)t}$. When these two circuits couple, their oscillating frequencies and damping coefficients shift, as derived in the previous section. However, when their solutions multiply, the resonant frequencies add and subtract to produce harmonics. These harmonics manifest themselves as beats. To illustrate, consider the following trigonometric identity:

$$\cos(\omega_{upper}t) \cdot \cos(\omega_{lower}t) = \frac{1}{2}[\cos((\omega_{upper} + \omega_{lower})t) + \cos((\omega_{upper} - \omega_{lower})t)] \quad (3.56)$$

There are two beat frequencies, the lower of which produces the beat envelope. The higher beat frequency is damped out such that its effects are usually negligible.

ii. Waveform Cycle Count

Another condition is the number of complete waveform cycles that occur during one beat, i.e. the number of complete waveform cycles between zero crossings of the envelope function. As seen in previous plots, the number of waveform cycles appears inversely proportional to the value of k. To determine the relationship exactly, first start with the time it takes the beat waveform to reach its peak:

$$\tilde{T}_{peak} = \frac{0.5}{f_{beat}} = \frac{\pi}{\omega_{upper} - \omega_{lower}} \tag{3.57}$$

$$\tilde{T}_{peak} \approx \frac{\pi(k + \frac{5k^2}{8})}{\omega_n} \approx \frac{\pi k}{\omega_n} \tag{3.58}$$

Equation 3.58 uses a Taylor expansion to reduce the expressions for ω_{upper} and ω_{lower}, neglecting third and higher order terms. The condition $\tilde{T}_{peak} = T_{peak}$ holds if there is no phase shift in the envelope waveform. If there is a phase shift then the two are related by: $T_{peak} = \tilde{T}_{peak} + \frac{\pi k}{\omega_n}$ where the same Taylor expansion is again used. This result is arrived at by setting the *sine* term in equation 3.54 to zero and solving.

Now, the number of cycles in a complete beat time period is $\frac{1}{k}$ to second order. In practice, there may be a slight perturbation on the order of $\frac{1}{k^3}$; these perturbations occur during the zero crossings of the envelope function. Therefore, the number of waveform cycles from a zero of the envelope function to the maximum of the envelope function is approximately:

$$N_{peak} \approx \frac{1}{2k} \tag{3.59}$$

This is found by setting the argument of the *sine* term from the envelope equation to $\pi/2$, solving for the time, normalizing it, and then dividing π by the product of this normalized time to peak and the average of the two resonant frequencies. The following equations illustrate:

$$X_{peak} = \frac{\omega_n}{2\pi} \frac{k\pi}{\omega_n} \tag{3.60}$$

$$\frac{\omega_{upper} + \omega_{lower}}{\omega_n} N_{cycle} X_{peak} = 1 \tag{3.61}$$

The second equation equals one due to its normalization; as X_{peak} is solved for the normalized time to get to a peak instead of an entire period of the envelope, N will solve to the

average number of cycles to get to the envelope peak.

Solving for the output voltage

With the current waveforms and envelope functions understood, it remains to solve for the voltage across the secondary coil. The Tesla secondary coil is modelled by the lumped parameters, L_2, R_2, and C_2. Thus, it is important to take the voltage across the secondary parasitic capacitance instead of across the secondary inductance.

$$v_{out}(t) = \int_0^t \frac{i_2(t)}{C_2}\, dt \tag{3.62}$$

$$v_{out}(t) = \frac{V_{in}}{2}\sqrt{\frac{L_2}{L_1}}\Big[\frac{\omega_{lower}e^{-\zeta_{lower}}(\omega_{lower}\cos(\omega_{lower}t) + \zeta_{lower}\sin(\omega_{lower}t))}{\zeta_{lower}^2 + \omega_{lower}^2} - \frac{\omega_{upper}e^{-\zeta_{upper}}(\omega_{upper}\cos(\omega_{upper}t) + \zeta_{upper}\sin(\omega_{upper}t))}{\zeta_{upper}^2 + \omega_{upper}^2}\Big] \tag{3.63}$$

If the damping ratio ζ squared is considered much less than the resonant frequency squared, then the output voltage can be closely approximated as:

$$v_{out}(t) \approx \frac{V_{in}}{2}\sqrt{\frac{L_2}{L_1}}\Big[e^{-\zeta_{lower}t}\cos(\omega_{lower}t) - e^{-\zeta_{upper}t}\cos(\omega_{upper}t) + \frac{\zeta_{lower}}{\omega_{lower}}e^{-\zeta_{lower}t}\sin(\omega_{lower}t) - \frac{\zeta_{upper}}{\omega_{upper}}e^{-\zeta_{upper}t}\sin(\omega_{upper}t)\Big] \tag{3.64}$$

or, even more simply,

$$v_{out}(t) \approx \frac{V_{in}}{2}\sqrt{\frac{L_2}{L_1}}\Big[e^{-\zeta_{lower}t}\cos(\omega_{lower}t) - e^{-\zeta_{upper}t}\cos(\omega_{upper}t)\Big] \tag{3.65}$$

The voltage across the other components follows similarly when the *sine* terms of order $\frac{\zeta_i}{\omega_i}$ are considered much less than unity.

$$v_{C1}(t) \approx \frac{V_{in}}{2}\Big[e^{-\zeta_{upper}t}\cos(\omega_{upper}t) + e^{-\zeta_{lower}t}\cos(\omega_{lower}t)\Big] \tag{3.66}$$

$$v_{L2}(t) \approx \frac{V_{in}}{2\omega_n^2}\sqrt{\frac{L_2}{L_1}}\Big[\omega_{upper}^2 e^{\zeta_{upper}t}\cos(\omega_{upper}t) - \omega_{lower}^2 e^{\zeta_{lower}t}\cos(\omega_{lower}t)\Big] \tag{3.67}$$

$$v_{L1}(t) \approx -\frac{V_{in}}{2\omega_n^2}\Big[\omega_{lower}^2 e^{\zeta_{lower}t}\cos(\omega_{lower}t) + \omega_{upper}^2 e^{\zeta_{upper}t}\cos(\omega_{upper}t)\Big] \tag{3.68}$$

where, for reference,

$$Re\{\lambda_1\} = \zeta_{lower} \approx \frac{\omega_n}{4}\frac{1}{1+k}(\frac{1}{Q_1}+\frac{1}{Q_2})$$
$$Im\{\lambda_1\} = \omega_{upper} \approx \frac{\omega_n}{(1-k)^{1/2}}$$
$$Re\{\lambda_2\} = \zeta_{upper} \approx \frac{\omega_n}{4}\frac{1}{1-k}(\frac{1}{Q_1}+\frac{1}{Q_2})$$
$$Im\{\lambda_2\} = \omega_{lower} \approx \frac{\omega_n}{(1+k)^{1/2}}$$

When plotting the voltage, as with the currents, the damping coefficients are assumed to be zero for now such that the decaying exponentials reduce to unity. Furthermore, the leading coefficient $\frac{V_{in}}{2}\sqrt{\frac{L_2}{L_1}}$ is normalized to unity. Remember that this is not an accurate physical model since the ratio of the inductors affected the values of the quality factors. However, while examining the relationships between the primary and secondary voltage waveforms, it is convenient to ignore these effects temporarily. Figure 3-21 shows the voltage waveforms across the primary and secondary capacitances. Notice how closely the current and voltage waveform behavior parallel one another. Notice also that the voltage follows a beat pattern and its bounding envelopes can be described by the same equations used for the current envelopes, equations 3.54 and 3.55.

Notice also that the magnitude of k dictates the number of voltage waveform oscillations it takes for the voltage to rise from zero to a maximum, just as with the current waveforms. As the arguments of the sinusoid and cosinusoid terms are identical to those of the current waveform relations, the relationships between T_{peak} and N_{peak} are identical to those of equations 3.58 and 3.59.

3.2.2 Energy and Power

With the voltage and currents known on each side of the coupled oscillator, the power and energy transfer characteristics of the circuit are known as well. Figure 3-22 shows the instantaneous power across the inductors L_1 and L_2. The difference between the two waveforms at an envelope peak is the amount of energy overlap. This is power that is still in the primary when the secondary has reached its peak (or vice versa). From an efficiency standpoint, this is wasted power in that it does not contribute to the energy or voltage available at the output. For this derivation, there is a fixed amount of energy present in

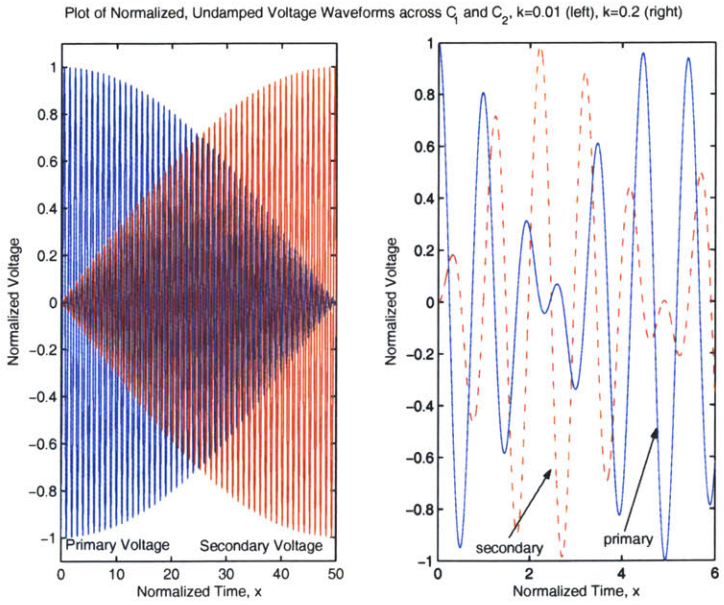

Figure 3-21: Plot of Normalized Voltage Waveforms across the primary and secondary capacitances, k=0.01 (left), 0.2 (right)

this system for all time, neglecting losses, of $E(t) = E_{initial} = \frac{1}{2}C_1V_{in}^2$ due to the initial conditions of C_1 having an initial voltage V_{in}. The energy across the inductor, L_2 is given by $E_{L2} = \frac{1}{2}L_2i_2^2(t)$.

Figure 3-23 is a graph superimposing the secondary coil voltage, $v_{L2}(t)$ with the energy stored in the coil for two values of the coupling coefficient, $k = 0.03$ and $k = 0.2$. To achieve maximum efficiency the coil energy should peak when the voltage across it peaks. This ensures that a maximum amount of energy is available during the output voltage peak. The closer to zero the coupling coefficient, k, is, the more in phase the peak coil voltage will be with the energy peak.

The energy in the secondary is due to the flux produced by the primary inductor coupling to the secondary, as described in the frequency domain derivation (see Figure 3-14). As previously stated, the beats of the system for the range of k: $k_{crit} \leq k \ll 1$ represent energy moving between the primary and secondary circuits. Figure 3-24 shows the total normalized energy of the primary and secondary over normalized time when damping is negligible. Under this condition, the quality factors tend towards infinity, and the system dynamics are dominated by the coupled LC network parameters. Thus, beats are present.

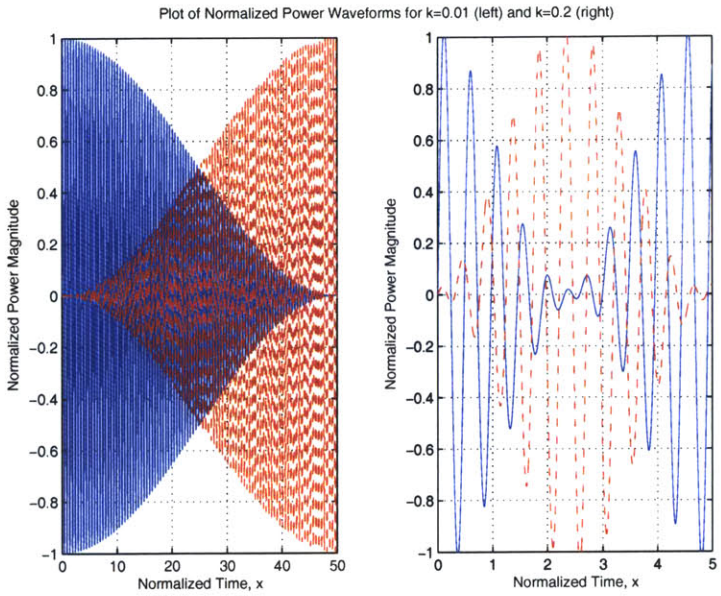

Figure 3-22: Plot of Instantaneous Power $L_2 i_2 \frac{d\, i_2}{dt}$ on Each Side, k=0.01 (left), k=0.2 (right)

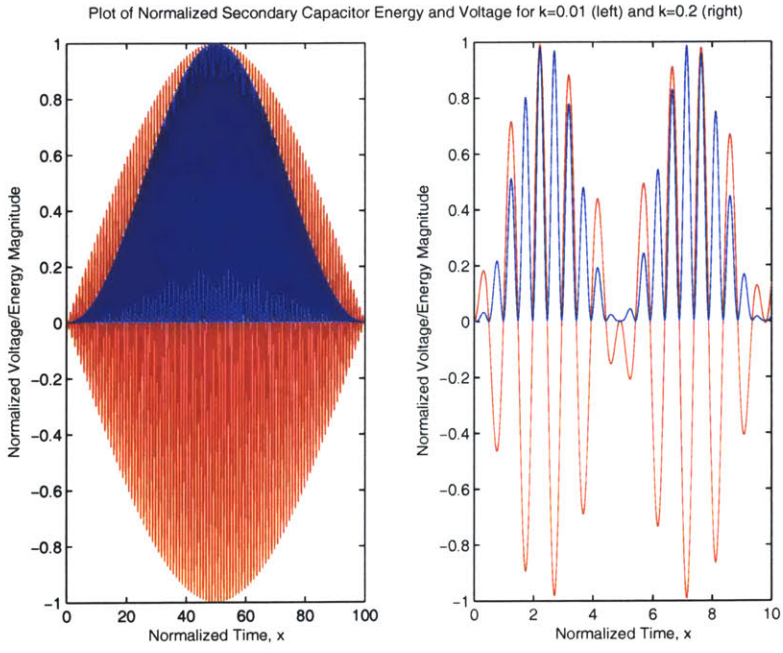

Figure 3-23: Plot Superimposing Voltage and Energy across the Secondary Coil, $k = 0.01$ (left), $k = 0.2$ (right)

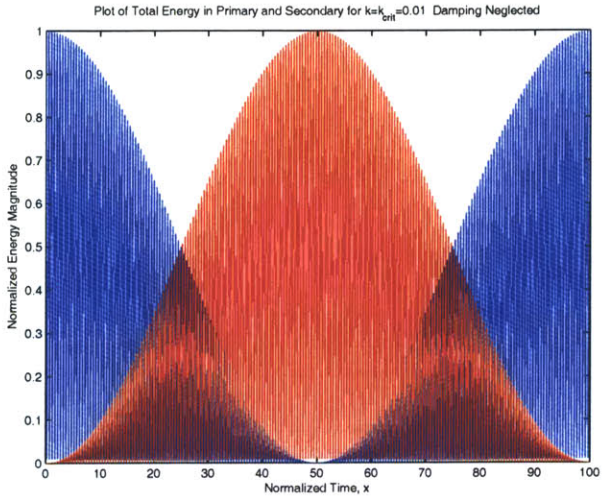

Figure 3-24: Plot of Total Normalized Energy in Primary and Secondary when damping is negligible. $k = 0.01$

The total energy expressions are given by the following:

$$E_{primary} = \frac{1}{2}C_1 v_1(t)^2 + \frac{1}{2}L_1 i_1(t)^2 \tag{3.69}$$

$$E_{secondary} = \frac{1}{2}C_2 v_{out}(t)^2 + \frac{1}{2}L_2 i_2(t)^2 \tag{3.70}$$

3.2.3 Time Domain Solution for $\omega_1 \neq \omega_2$

The general solution to the characteristic polynomial presented in equations 3.40 through 3.41 is restated below:

$$Re\{\lambda\} = \zeta_{lower} = \frac{(\omega_1 Q_2 + \omega_2 Q_1)\omega_{lower}^2 - \omega_1\omega_2(\omega_2 Q_2 + \omega_1 Q_1)}{2Q_1Q_2(2(1-k^2)\omega_{lower}^2 - (\omega_1^2 + \omega_2^2))}$$

$$Re\{\lambda\} = \zeta_{upper} = \frac{(\omega_1 Q_2 + \omega_2 Q_1)\omega_{upper}^2 - \omega_1\omega_2(\omega_2 Q_2 + \omega_1 Q_1)}{2Q_1Q_2(2(1-k^2)\omega_{upper}^2 - (\omega_1^2 + \omega_2^2))}$$

$$Im\{\lambda\} = \omega_{upper} = \sqrt{\frac{(\omega_1^2 + \omega_2^2) + \sqrt{(\omega_1^2 + \omega_2^2)^2 - 4(1-k^2)\omega_1^2\omega_2^2}}{2(1-k^2)}}$$

$$Im\{\lambda\} = \omega_{lower} = \sqrt{\frac{(\omega_1^2 + \omega_2^2) - \sqrt{(\omega_1^2 + \omega_2^2)^2 - 4(1-k^2)\omega_1^2\omega_2^2}}{2(1-k^2)}}$$

Again, it is assumed that $0 < k \ll 1$.

The difference between the two system resonant frequencies is a useful quantity to

calculate. This difference is called the bandwidth of the system. It is given by the difference between ω_{upper} and ω_{lower}, not ω_1 and ω_2. While for the general case, this quantity is not easily expressed in a simplified form, when $\omega_1 = \omega_2$, there is a useful expression for the bandwidth. Equation 3.72 illustrates.

$$\omega_{BW} = \omega_{upper} - \omega_{lower} = \omega_n(\frac{1}{\sqrt{1-k}} - \frac{1}{\sqrt{1+k}}) \tag{3.71}$$

$$\omega_{BW} \approx \omega_n(k + \frac{5k^3}{8}) \tag{3.72}$$

For k small, the bandwidth equation can be estimated as $\omega_{BW} \approx \omega_n k$. The time period of the envelope function can then be expressed as $T_{env} \approx \frac{4\pi}{\omega_n k}$. Using this result, it can be shown that, for $k^2 \ll 1$, the value of the coupling coefficient is $k = \frac{\omega_{beat}}{\omega_{avg}}$, where ω_{beat} is the beat frequency, $\frac{\omega_{upper}-\omega_{lower}}{2}$ and ω_{avg} is the mean (average) oscillation frequency (frequency of the waveform zero crossings) of the current or voltage waveform.[24]

When the currents are expressed in their more general form in terms of their original, assumed distinct, self resonant frequency and upper and lower quantities, they are:

$$i_1(t) = -\frac{V_{in}}{2\omega_1^2 L_1}\left[\omega_{lower}e^{-\zeta_{lower}t}\sin(\omega_{lower}t) + \omega_{upper}e^{-\zeta_{upper}t}\sin(\omega_{upper}t)\right]$$

$$i_2(t) = \frac{V_{in}}{2\omega_2^2(L_1L_2)^{1/2}}\left[\omega_{upper}e^{-\zeta_{upper}t}\sin(\omega_{uppper}t) - \omega_{lower}e^{-\zeta_{lower}t}\sin(\omega_{lower}t)\right]$$

The voltages across the inductors and capacitors have forms similar to those presented in the previous section. Illustrating how these two currents relate to one another, they are plotted. Again ignoring the leading coefficients and allowing the damping coefficients, ζ_{lower} and ζ_{upper} to go to zero, the plots are seen in Figures 3-25 and 3-26. Note that the frequency dependency in the leading coefficients is not included in the graphs, but, as the basis for a normalized, unitless time factor 'x', where $x = \omega t/(2\pi)$ is different for each current waveform, it is not used.

Figure 3-26 shows the primary and secondary current waveforms when the base frequencies are grossly mismatched. The system frequencies ω_{upper} and ω_{lower} create a beat frequency that strongly dominates the shape of the output.

Figure 3-27 shows a plot of secondary coil voltage and energy (the waveform that is

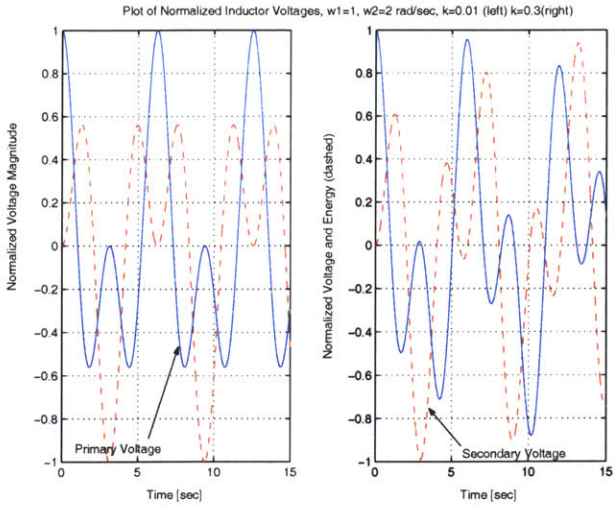

Figure 3-25: Plot of Normalized Inductor Waveforms for $\omega_1 = 1, \omega_2 = 2, k = 0.01$ (left), $k = 0.3$ (right)

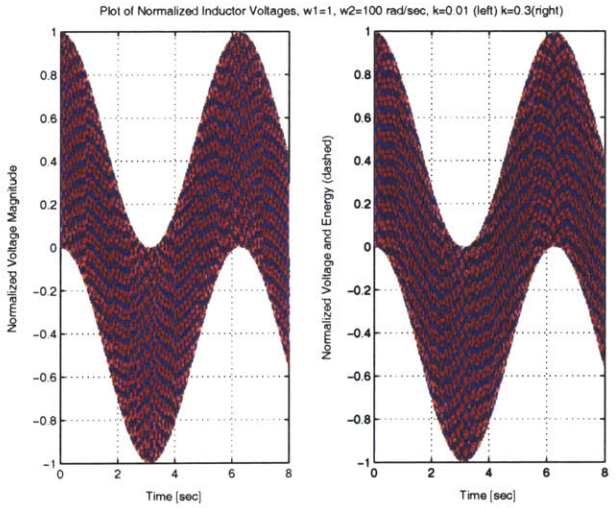

Figure 3-26: Plot of Normalized Voltage Waveforms for $\omega_1 = 1, \omega_2 = 100, k = 0.01$ (left), $k = 0.2$ (right)

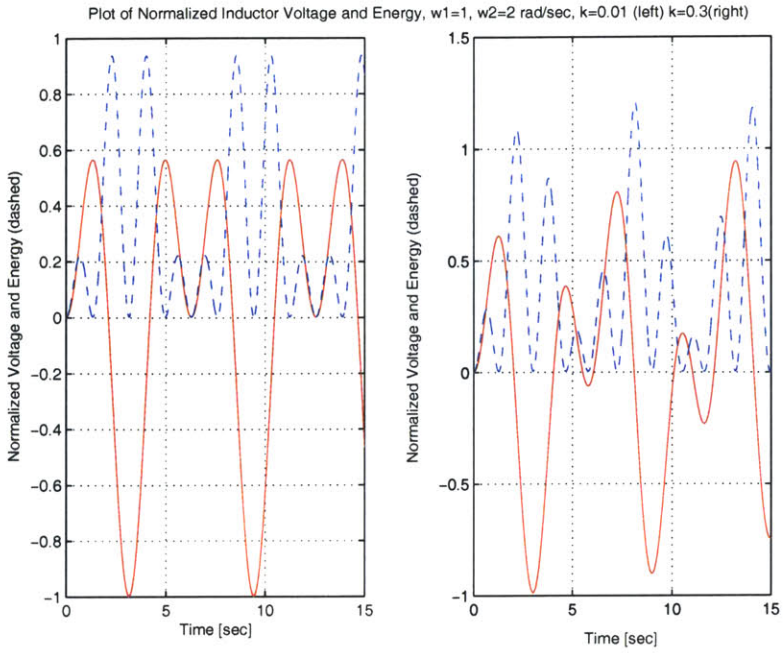

Figure 3-27: Plot of Normalized Secondary Coil Voltage and Energy, $\omega_1 = 1, \omega_2 = 2, k = 0.01$ (left), $k = 0.3$ (right)

always positive represents the inductor energy). The peaking of secondary coil voltage and energy is shifted when the self resonant frequencies are offset by a factor. Notice that the peak magnitudes of the waveforms have not changed, only the relative phase angle of the waveforms.

3.2.4 Perturbation Analysis

While the mathematical convenience, design simplification, and operational efficiency of having the two independent resonant frequencies, ω_1 and ω_2, equal has been made, it will be near impossible to do so in the laboratory. To analyze the effects of having a slight mismatch will have on the behavior of the system, a condition on the self resonant frequencies is imposed.

$$\omega_2 = \omega_1 + \delta \tag{3.73}$$

where δ represents some frequency perturbation. The system resonant frequencies from equations 3.41 and 3.41 are computed with $\omega_1 + \delta$ substituted for ω_2.

Working with the solutions presented in the $\omega_1 \neg \omega_2$ section, equations 3.41 and 3.41, the perturbation yields:

$$\omega_{upper} = \frac{\omega_n}{\sqrt{1-k}}\sqrt{1+\frac{\delta}{\omega_n}} \tag{3.74}$$

$$\omega_{lower} = \frac{\omega_n}{\sqrt{1+k}}\sqrt{1+\frac{\delta}{\omega_n}} \tag{3.75}$$

Next, using the voltage equations, the effect of the perturbation can be seen in Figure 3-28. There is little effect on the voltage waveform. The effect of having a 10% frequency drift does not significantly change the number of cycles in a beat period nor the time to peak. Note that while the magnitude does not appear to be affected, a frequency perturbation will affect the damping coefficients, ζ_{lower} and ζ_{upper}, and they will be larger for a larger perturbation. A more complete solution, showing where higher order terms are dropped and Taylor substitutions made is shown in appendix A.

While the perturbation does not fundamentally affect the relationship between k and the number of cycles to peak, it does affect the apparent normalized time it takes to reach that peak. As expected, the perturbation gives the appearance of a shifted natural resonant frequency, ω_n. Using the relations derived in equations 3.75 and 3.75, the offset between the two normalized times to peak, X_{peak} and X'_{peak}, for a given resonant frequency perturbation of $\frac{\delta}{\omega_n}$ percent can be expressed as a percentage of .

$$\frac{X'_{peak}}{X_{peak}} = \frac{\frac{2\pi T_{peak}}{\omega_n}}{\frac{2\pi T_{peak}}{\omega_n\sqrt{1+\frac{\delta}{\omega_n}}}} \approx 1 - \frac{\delta}{2\omega_n} \tag{3.76}$$

In Figure 3-28, notice that the 10% shifted plot is approximately 1/4 of a cycle ahead of the nominal secondary voltage plot. This result is accurately predicted from the above equation. Note that this result is essentially a scaling of the axes. This scale factor, multiplied by the original X_{peak}, gives the normalized time to the new peak. The relationship between k_{eff} and k, where k_{eff} is the apparent 'k' needed to get the peak value in the scaled X' system is given by the following relationship.

$$k_{eff} = k\sqrt{1+\frac{\delta}{\omega_n}} \tag{3.77}$$

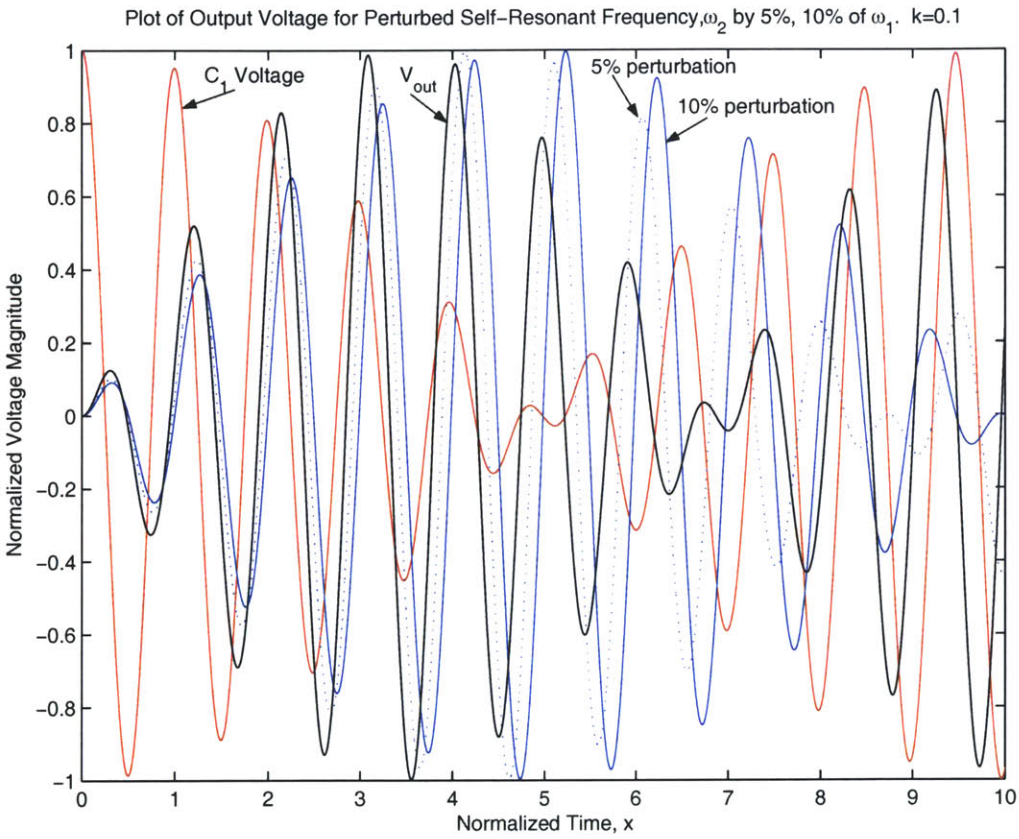

Figure 3-28: Plot of Frequency Perturbations in Voltage Waveform. $\delta/\omega = [0, 5\%, 10\%]$, $k = 0.1$

Note that while operating a Tesla coil, it would be extremely difficult to determine whether the primary and secondary are tuned to the exact same individual resonant frequency, ω_n. Consequently, it would be unwise to use k_{eff} and X'_{peak} parameters in the design procedure until fine tuning the coil.

3.3 Shaping the Damped Output Voltage Waveform

The value of k and the quality factors determine the behavior of the time domain waveforms. The time domain derivation considers the case of large and approximately equal Q's and a coupling coefficient constrained by: $0 < k \ll 1$. There are three regimes of waveforms determined by the relative value of the coupling coefficient. They are: (1) $0 < k < k_{crit}$, (2) $k = k_{crit}$, (3) $k_{crit} < k \ll 1$, and (4) $k_{crit} \ll k < 1$. These four regimes correspond almost exactly to those of the second order system: overdamped, critically damped, and underdamped, respectively. The characteristics and behavior of the system waveforms are explained in each of the following sections.

3.3.1 Case: $0 < k \leq k_{crit}$

When k falls between these two values, the waveforms of the output oscillate at a the self-resonant frequency, ω_n. Thus, there are *no* beats in the output waveform. Figure 3-29 illustrates this condition. While the initial magnitude of the output voltage appears to go as the inverse square root of the product of the quality factors, i.e. $V_{out} \sim \frac{1}{\sqrt{Q_1 Q_2}}$, this is only because the value of k in this example is constrained to be less than k_{crit}. Holding other network parameters constant, if the quality factors are increased, the initial peak output voltage will increase.

The envelope function that bounds these output voltage waveforms is given by the equation 3.78.

$$v_{env}(t) = V_{in}\sqrt{\frac{L_2}{L_1}}e^{-\frac{1}{4}\omega_n t\frac{Q_1+Q_2}{Q_1 Q_2}}\sin\left(\frac{\omega_{upper}-\omega_{lower}}{2}t\right) \tag{3.78}$$

From this envelope equation discussed in greater detail below, it is possible to tailor the output voltage to meet many design specifications. Notice that for $k = k_{crit}$ the envelope waveform goes slightly negative at the rail. This is the smallest value of k for which this occurs. This marks the transition from an undercoupled system to a critically coupled system. In terms of second order equations, this value of k marks the difference between an

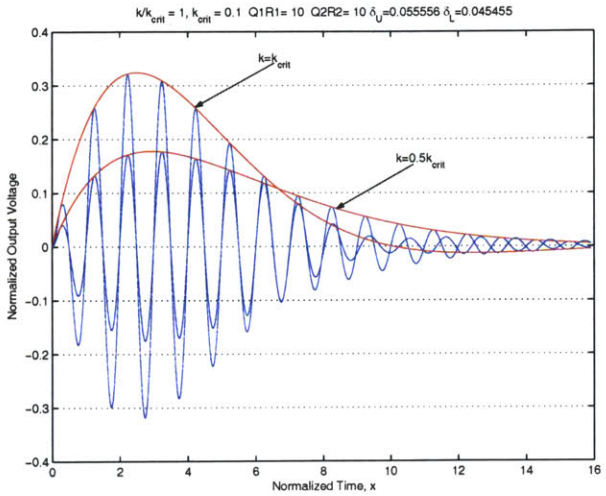

Figure 3-29: Plot for subcritical $k = \frac{1}{2}k_{crit}$ and $k = k_{crit}$. $Q_1 = Q_2 = 10$. Note the envelope functions.

overdamped system to a critically damped system. For larger k and equal Q's, the output response shows beats.

The limitations of this bounding envelope become apparent when the quality factors are mismatched and the coupling is below k_{crit}. Figure 3-30 illustrates this deficiency. This is a direct result of the neglected second and higher order terms in the formulation of the time domain. A more more exact bounding envelope equation would contain more terms to account for these dynamics.

When $k = k_{crit}$

When $k = k_{crit}$, the frequency domain derivation gives a maximum steady state output voltage gain. However, this does not correspond to a maximum output voltage peak for a pulse drive in the time domain. It means that, when the quality factors are roughly equal, this is the coupling that yields a maximum gain when the system is driven at the frequency ω_n. Also, it is important to remember that the output voltage does not reach a maximum until the system has already lost some of its initial energy through dissipation in R_1 and R_2.

Instead, $k = k_{crit}$ signifies the point where the two circuits are impedance matched to one another as shown in equation 3.16 during the derivation of the Thevenin equivalent

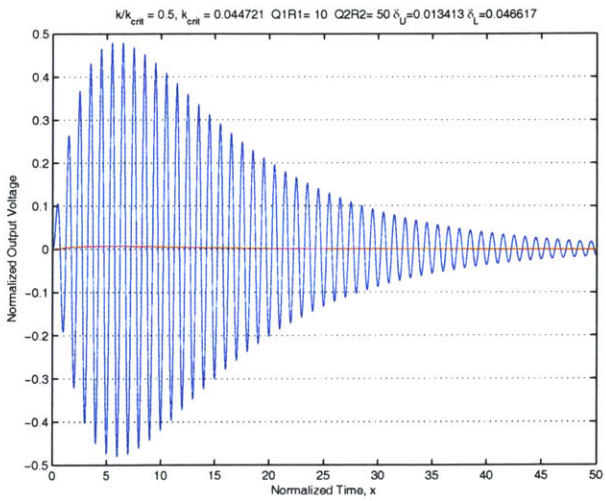

Figure 3-30: Output voltage for $k = \frac{1}{2}k_{crit}$ with quality factors mismatched by factor of 5. The approximate bounding envelope equation fails.

impedances. This is analogous to the case of power dissipation between two resistors in series across a voltage source; they dissipate a maximum of energy when their values are equal. If the impedance of the source used to energize the primary capacitor is equal to the Thevenin input impedance of the primary and a load resistor matched to the Thevenin equivalent output impedance is placed across the output of the secondary, a maximum amount of power can be transferred from source to load. If the situation is compared to a standard transmission line, then the energy of the primary is entirely transferred to the secondary with a minimum of loss in only one beat (corresponding to one zero crossing of the bounding envelope for the primary.

3.3.2 Case: $k_{crit} < k \ll 1$

This is the regime of solutions that was shown in the idealized time domain plots above in Figures 3-18 through 3-21. When quality factors are equal and the coupling coefficient falls within this range, the system waveforms exhibits a beat pattern that represents energy being transferred back and forth between the primary and secondary circuits. When the quality factors are mismatched, beats occur for $k = k_{split}$, as shown in equation 3.18 and Figure 3-8. In this section, it is assumed that the beats emerge for $k > k_{crit}$. The emergence of beats is a consequence of the relation between the two peak resonant frequencies of the

system. When $k > k_{crit}$, the system poles begin to move more quickly, causing the system resonant frequencies to change and the damping coefficients to change even faster.

The values for the peak frequencies and damping coefficients as given during the time domain derivation in the previous section are:

$$\omega_{peaks} = \frac{\omega_n}{\sqrt{1 \pm k}}$$
$$\zeta = \frac{\omega_n(\frac{1}{Q_1} + \frac{1}{Q_2})(\omega_{peaks}^2 - \omega_n^2)}{(1-k^2)\omega_{peaks}^2 - \omega_n^2}$$

where when the peak values are separated and defined as "upper" and "lower" yield:

$$\zeta_{upper} = \frac{\omega_n}{4}(\frac{1}{Q_1} + \frac{1}{Q_2})\frac{\omega_{upper}^2 - \omega_n^2}{(1-k^2)\omega_{upper}^2 - \omega_n^2} \tag{3.79}$$

$$\zeta_{lower} = \frac{\omega_n}{4}(\frac{1}{Q_1} + \frac{1}{Q_2})\frac{\omega_{lower}^2 - \omega_n^2}{(1-k^2)\omega_{lower}^2 - \omega_n^2} \tag{3.80}$$

These damping coefficients are real with the following constraint which is identical to equation 3.18. When k is less than or equal to this quantity, then the system waveforms are identical to the case for $0 < k < k_{crit}$.

$$k > \frac{k_{crit}}{\sqrt{2}}\sqrt{\frac{Q_1}{Q_2} + \frac{Q_2}{Q_1}} \tag{3.81}$$

In this regime of k, there are four properties of the characteristic system waveform that can be described.

- Peak Magnitude of the Secondary
- The Decay Rate of the Waveform
- Number of Beats
- Number of Cycles Inside each Beat

The following analysis assumes that the quality factors, Q_i are "large enough" to not damp out the waveform before a the desired dynamics have occurred.

Furthermore, the difference of the peak frequencies, $\omega_{upper} - \omega_{lower}$ requires a Taylor

expansion to allow for simplifications in the following equation. The expansion is:

$$\omega_{upper} - \omega_{lower} = \omega_n(\frac{1}{\sqrt{1-k}} - \frac{1}{\sqrt{1+k}}) \approx \omega_n(k + \frac{5k^3}{8}) \tag{3.82}$$

The third order term is negligible for $k \ll 1$.

Peak Magnitude of the Secondary

The peak magnitude of the secondary output voltage waveform is easily computed once the envelope function of these damped waveforms is found. This envelope function is similar in form to those derived for the undamped case. The damped exponential term is simply the first order Taylor expansion of the average of the two damping coefficients. For this regime of k, the envelope function is expressible as:

$$V_{env}(t) = V_{in}\sqrt{\frac{L_2}{L_1}}e^{-\frac{1}{4}\omega_n t\frac{Q_1+Q_2}{Q_1Q_2}}\sin(\frac{\omega_{upper} - \omega_{lower}}{2}t) \tag{3.83}$$

The time constant of the exponential is an important quantity in the following analysis. It is defined as:

$$e^{-t/\tau_{eff}} \Rightarrow \tau_{eff} \equiv \frac{4Q_1Q_2}{\omega_n(Q_1+Q_2)} \tag{3.84}$$

The initial part of equation 3.83, $V_{in}\sqrt{\frac{L_2}{L_1}}$ is directly proportional the initial peak magnitude of the output voltage. The actual magnitude of the initial peak is found by finding the maximum of the envelope waveform. Taking a derivative in time and setting it to zero solves to:

$$t_{peak} = \frac{2}{\omega_{upper} - \omega_{lower}}\arctan(\frac{2(\omega_{upper} - \omega_{lower})}{\omega_n}\frac{Q_1Q_2}{Q_1+Q_2}) \tag{3.85}$$

If a Taylor series is used to reduce the tangent expression, it will give a result greater than the true result. Because of the sensitivity of k in this equation, the expansion should include at least third order terms.

Inserting the expression for t_{peak} into the voltage envelope equation 3.83 yields an expression that does not lend itself to easy manipulation. Figure 3-31 plots the maximum peak voltage versus Q (Q_1 is set equal to Q_2) with k as a parameter. The results have been normalized by the input voltage and transformer gain ratio, $V_{in}\sqrt{\frac{L_2}{L_1}}$ to show the maximum peak of the exponential and *sine* term. Notice that the peak magnitude is approximately 48% of the input voltage, regardless of the Q chosen. One assumption, however, is that

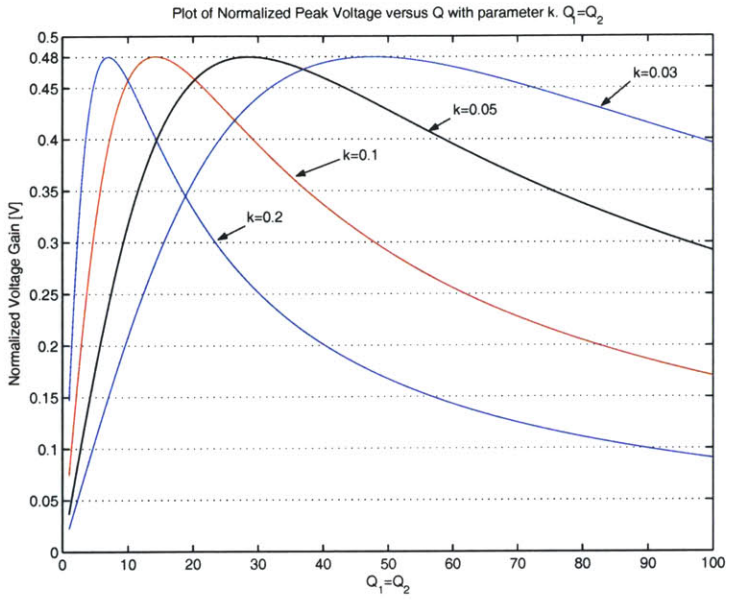

Figure 3-31: Plot of the normalized peak voltage versus Q with parameter k. Note that $\omega_n = 1$, $Q_1 = Q_2$, and $R_1 = R_2 = 1$.

$k \ll 1$. The parameters Q and k dictate the shape of the peak response voltage.

Taking the ratio of $\frac{k}{k_{crit}}$ at the Q for which the maximum peak voltage occurs gives a ratio between 1.2 and 1.55 over the range of k, as observed numerically. The maximum peak output voltage will occur when the system has between one and two beats.

Decay Rate of the Waveform

The decay rate of the voltage waveform is given by the effective time constant of the exponential term in equation, τ_{eff}. This term depends only on the quality factors of the primary and secondary circuits. The greater those quantities, the slower the decay rate, the less energy is lost as it moves from primary to secondary and back.

$$\tau_{eff} = \frac{4Q_1Q_2}{\omega_n(Q_1 + Q_2)}$$

It is this decay rate that detracts from the maximum realizable voltage gain of the system. This is a direct result of the energy losses of the system and the time it takes for the output to reach a peak voltage.

Number of Beats

The approximate number of beats in the waveform is given by the expression:

$$\gamma = \frac{k}{k_{crit}} \approx N_{beats} \tag{3.86}$$

This ratio equates directly with the quality factor of a second order system in determining the approximate number of cycles until damped out. With this analogy, γ above counts the number of beats until time $3\tau_{eff}$. After three time constants, the magnitude of the signal is at most 5% of the initial peak magnitude.

First, the time period of the beat frequency is half of the frequency inside the sinusoid term of equation 3.83 as there are two beats for each full cycle. The time period of each beat is:

$$T_{beat} = \frac{1}{2}(2\pi)\frac{2}{\omega_{upper} - \omega_{lower}} \tag{3.87}$$

Next, the exponential in equation 3.83 only affords an amount of time, $3\tau_{eff}$ before the bounding envelope is effectively zero. This means that there is only enough time for approximately $N_{beats} = \frac{3\tau_{eff}}{T_{beat}}$ beats. This expression works out to:

$$N_{beats} \approx \frac{6\sqrt{Q_1 Q_2}}{\pi(Q_1 + Q_2)}\frac{k}{k_{crit}} \tag{3.88}$$

where again the Taylor series in equation 3.82 is used to simplify the square roots from the peak frequencies, $\omega_{upper}, \omega_{lower}$. For $k < 5k_{crit}$, the quality factors can differ by a factor of 5 and still have γ give an accurate count. Note that γ is a conservative bound. For large, equal quality factors and a relatively large value of $\frac{k}{k_{crit}}$, γ will underestimate the number of beats by one.

Number of Cycles Inside each Beat

The number of oscillations inside each beat is given by:

$$N_{cycles} \approx \frac{1}{k} \tag{3.89}$$

This formulation is a result of the Taylor series in equation 3.82 and equation 3.59 derived in a previous section. This formula assumes that k^2 is negligible compared to unity. This

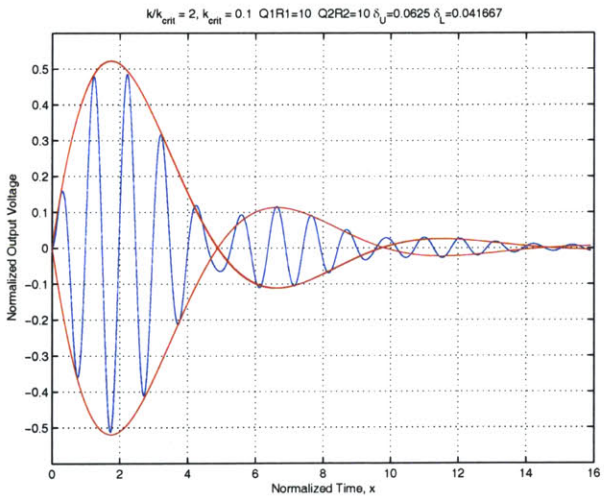

Figure 3-32: Normalized Plot of $\frac{k}{k_{crit}} = 2, Q_1 = Q_2 = 100$. Notice two large beats. Third is less than 5% of the initial peak magnitude. For relatively small values of Q, the envelope is still accurate.

result is seen graphically if the time axis is normalized to

$$t = \frac{2\pi x}{\omega_n} \tag{3.90}$$

This normalization leads to each cycle of the waveform corresponding to one unit of "unitless" or normalized time, x. A more exact formulation is found if the internal frequency is realized to be $\frac{\omega_{upper}+\omega_{lower}}{2}$. A Taylor expansion gives $\omega_n(1 + \frac{3k^2}{8})$. If this is substituted into the above equation, a more exact counting of beats is possible. If instead, it is more convenient to normalize the time axis to the number of beats, then the beat frequency $\frac{\omega_{upper}-\omega_{lower}}{2}$ can be used instead of ω_n in the above equation. This yields:

$$t = \frac{4\pi}{\omega_n k} x' \tag{3.91}$$

where x' is the new normalized scale for counting beats instead of waveform oscillations. This formula, as the approximation in equation 3.82, is valid for $k \ll 1$.

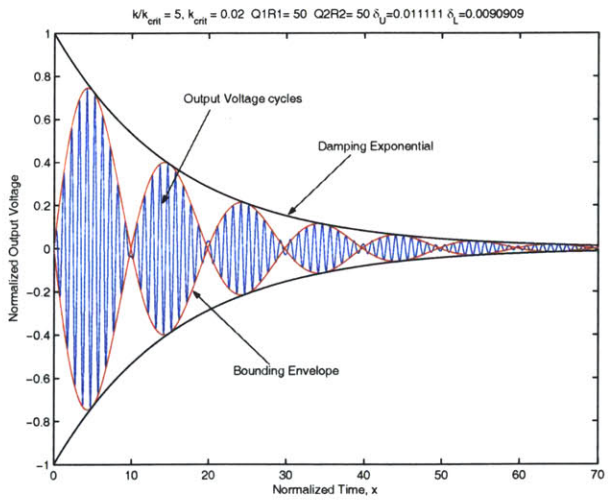

Figure 3-33: Normalized Plot of $\frac{k}{k_{crit}} = 5, Q_1 = Q_2 = 50$. Count five beats. Notice number of internal cycles has increased to $N_{cycles} = \frac{1}{k}$

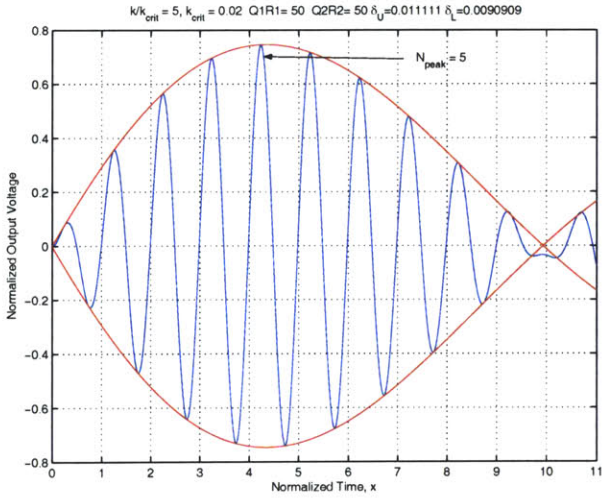

Figure 3-34: Normalized Plot of $\frac{k}{k_{crit}} = 5, Q_1 = Q_2 = 50$. Count $N_{peak} = \frac{1}{2k} = 5$

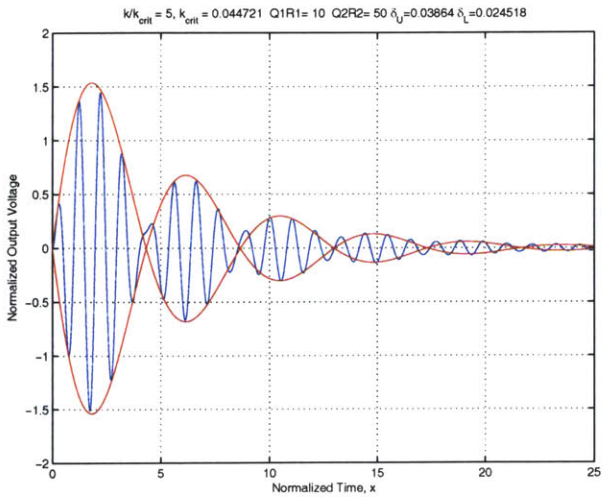

Figure 3-35: Normalized Plot of $\frac{k}{k_{crit}} = 5$. $Q_1R_1 = 10$, $Q_2R_2 = 50$. Unequal Q in this regime of k does not invalidate the envelope function.

3.3.3 Case: $k_{crit} \ll k < 1$

As the coupling coefficient k approaches unity and $k^3 > 10\%k$, the behavior of the system begins to approach that of an ideal transformer. Three quantities regulate how the beats of the previous regime transform into the response seen by typical tightly coupled transformers. The first is the damping coefficient, ζ_{upper}. As k approaches unity, this damping coefficient approaches infinity. Thus, in the output voltage waveform equation, the terms corresponding to the upper pole goes to zero due to an infinitely large damping coefficient and an infinitely large denomenator, $1 - k$.

The system takes on the dominant form as $k \to 1$:

$$v_{out}(t) \approx \frac{V_{in}}{2}\sqrt{\frac{L_2}{L_1}}e^{-\zeta_{lower}t}\cos(\omega_{lower}t) \tag{3.92}$$

The lower pole, $\lambda_{lower} = -\zeta_{lower} \pm j\omega_{lower}$ approaches the resonant frequency $\frac{\omega_n}{\sqrt{2}}$. The damping coefficient ζ_{lower} has a corresponding limiting value of $\zeta_{limit} = \frac{\omega_n}{8}(\frac{1}{Q_1} + \frac{1}{Q_2})$. The output voltage no longer has beats but instead has a primary oscillating frequency of ω_{lower} and a much greater frequency of ω_{upper} that adds or superimposes on the dominant lower waveform in a fashion similar to that of a fourier composition.

Figures 3-36 and 3-37 show the effect of this for identical Q_i. The decay is symmetric

if unequal. When $Q_1 \neq Q_2$, the decay rates are not symmetric and give rise to oscillations that are the remnants of the beats in the previous regime.

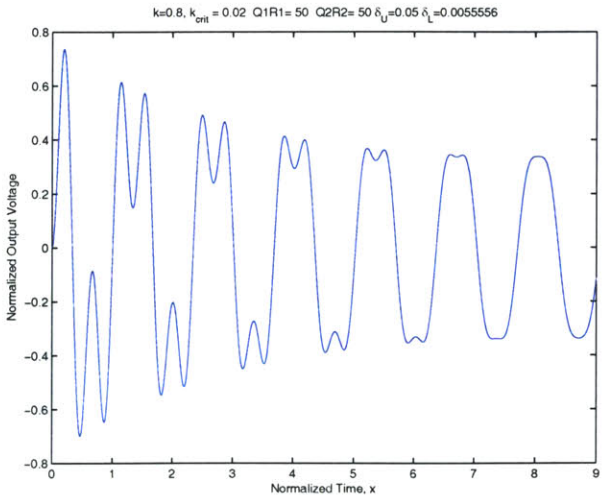

Figure 3-36: Plot for $k = 0.8, k_{crit} = 0.02$. Upper frequency waveform superimposes on lower frequency waveform; they adds similarly to a Fourier composition.

3.3.4 Shaping the System Energy

When damping is present, the system dynamics change considerably as damping strongly influences how much energy is transferred from primary to secondary. For the range $k_{crit} < k \ll 1$, beats are expected and as previously stated, the beats represent energy transfer from primary to secondary and back. Figure 3-39 illustrates; there are two surges in total secondary energy, $E_{secondary}$ corresponding to the peaks in the output voltage. To keep symmetry, there are also two peaks in the total primary energy, $E_{primary}$ corresponding to when the secondary transfers energy back. The damping ratio, even for quite large quality factors $Q_1 = Q_2 = 100$ in these plots, dominate the system dynamics.

When the system is critically coupled, $k = k_{crit}$, there is only one beat. The primary has transferred the maximum amount of energy possible for the values of ω_n, Q_i, and k to the secondary during the first (and only) beat. Any energy sent from the secondary back to the primary is dissipated, as evident from the monotonically decreasing envelope of the total primary energy. The important point here is that **for this value of critical coupling, $k = k_{crit}$, the maximum possible amount of energy capable of being transferred**

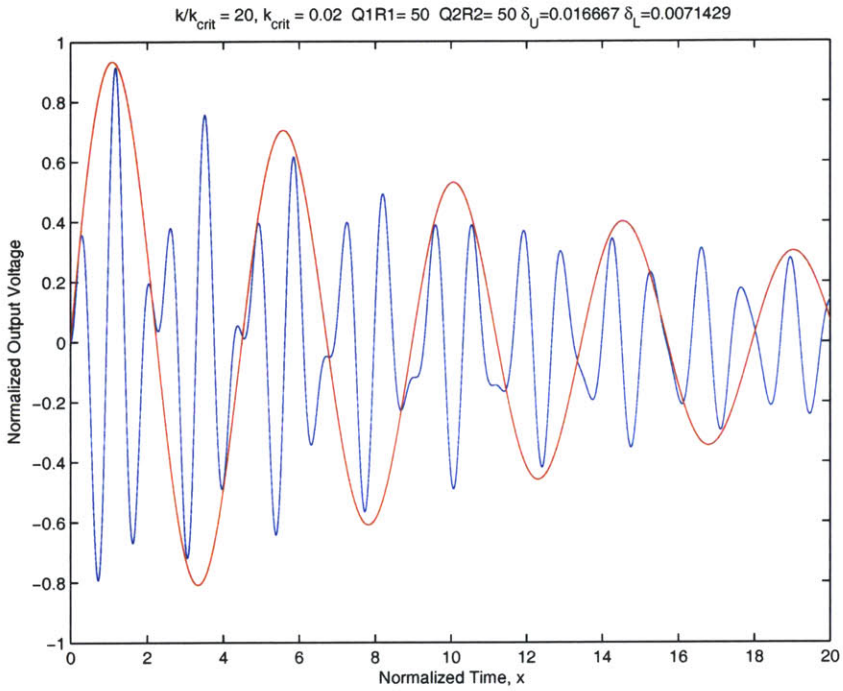

Figure 3-37: Plot for $k = 0.4, k_{crit} = 0.02$. Output beats are gone; envelope breaks down.

was transferred to the secondary.

When the system is coupled below critical coupling, the primary cannot link enough flux to the secondary to transfer enough energy quickly enough before it is dissipated by losses in the secondary. There is only one "sub-beat" representing the total amount of energy gathered by the secondary before it is dissipated. As the coupling approaches k_{crit}, there is enough flux linked to transfer enough energy to the secondary before it is damped out. The output voltage peak does not correspond to the energy peak as it is constrained by the damping exponentials.

The energy for these three regimes of k is analogous to a general second order system with its regimes of overdamped, critically damped, and underdamped. The subcritical coupling case corresponds to the overdamped case, the critical coupling case corresponds to the critically damped case, and the regime for beats is aptly fit for the underdamped case.

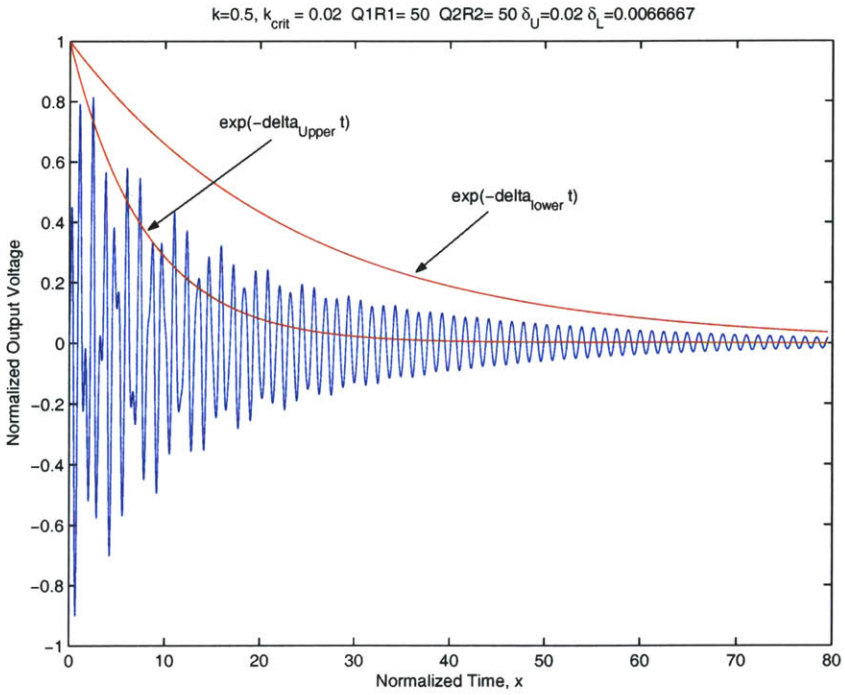

Figure 3-38: Plot for $k = 0.5, Q_1 = 50, Q_2 = 50$. Note how much faster upper frequency waveform decays relative to lower.

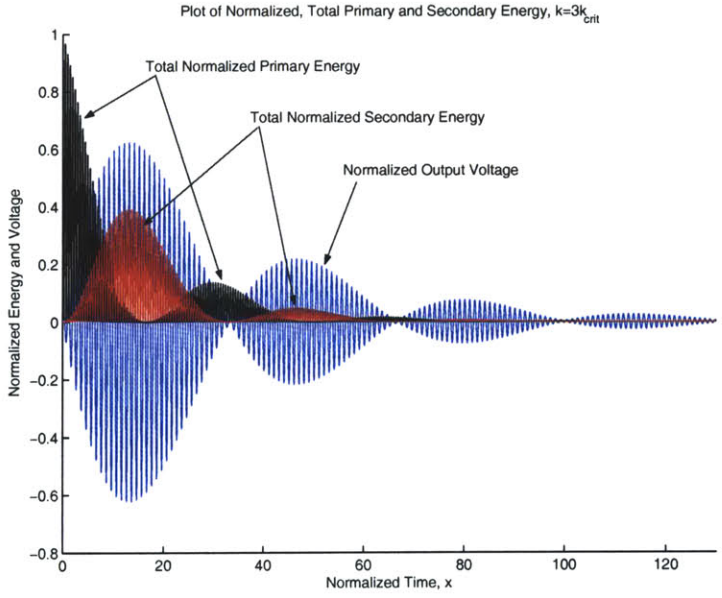

Figure 3-39: Plot of Total Normalized Primary and Secondary Energy. $k = 0.03$, $Q_1 = Q_2 = 100$

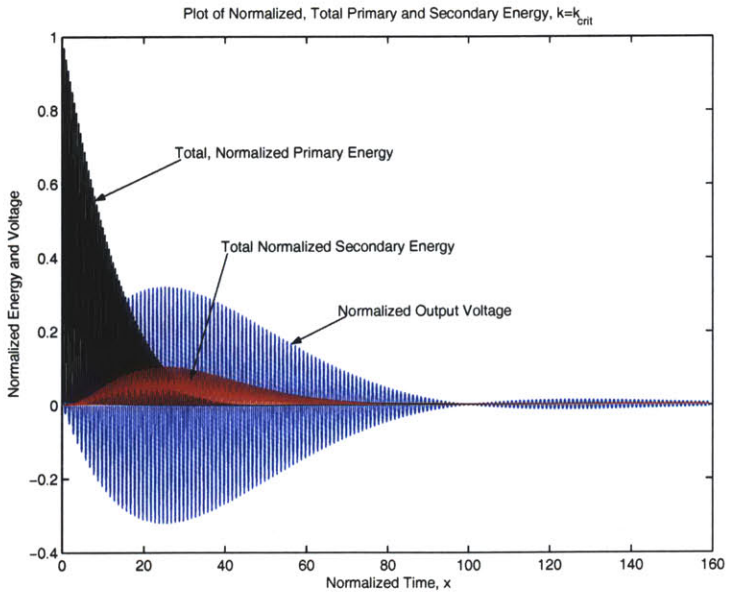

Figure 3-40: Plot of Total Normalized Primary and Secondary Energy for critical coupling. $Q_1 = Q_2 = 100$

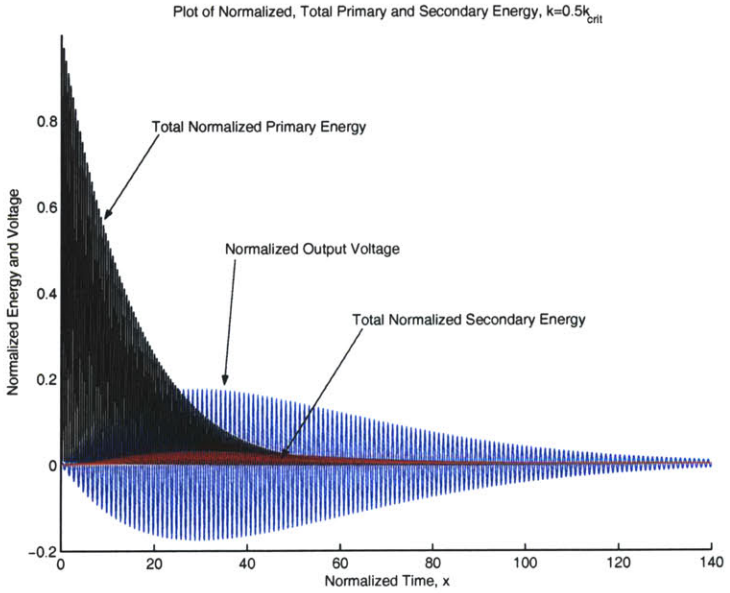

Figure 3-41: Plot of Total Normalized Primary and Secondary Energy for $k = \frac{1}{2}k_{crit}$. $Q_1 = Q_2 = 100$

3.4 Important results from the 4^{th} order system

To reiterate important points in the chapter:

1) The coupling coefficient, k, is the single most important factor in determining the operation of the Tesla coil.

The regime of the coupling coefficient is the reason for its energy transfer characteristics. For $k < k_{crit}$, the output voltage oscillates and rises to a peak value and then decays towards zero. There are no beats in the envelope of the output waveform as there it does not complete two zero crossings. For $k = k_{crit}$, the primary and secondary see matched load impedances. There is only one beat on the secondary response. For $k_{crit} < k \ll 1$, the system has beats and there are two clearly distinct system resonant frequencies, ω_{upper} and ω_{lower} that correspond to resonant frequencies of maximum output in the frequency domain. As k approaches unity, the system becomes a third order polynomial with two "upper" poles coalescing into a single pole at negative infinity. The remaining two poles exponentially approach the imaginary axis. This is consistent with the operational dynamics of an ideal transformer and shown in Figures 3-9 through 3-12.

2) The coupling coefficient can be thought of as a phase angle controller as it controls both the phase angle between the primary and secondary current and voltage waveforms and their respective envelope patterns.

By extension, k also determines the relative phase of the energy between each side of the coupled oscillator. Figure 3-42 illustrates this point. As k approaches unity, the two energy waveforms coalesce such that the energy stored in the primary is identical to the energy stored in the secondary, following the behavior of an ideal transformer. Note that there is no violation of the law of conservation of energy with this phase shifting. Instead, the phase of the energy waveform is only shifted by 90^o.

3) Setting the two self resonant frequencies, ω_1, ω_2 equal leads to both mathematically simpler expressions and fewer parameters that alter the shape of the waveforms.

Calibrating the coupled resonant system to have equal self resonant frequencies allows for mathematically simpler expressions to control and estimate the value of k and other internal parameters such as the damping coefficients ζ_{upper} and ζ_{lower}.

4) The energy transfer characteristics of the coupled system are related to the regime of k.

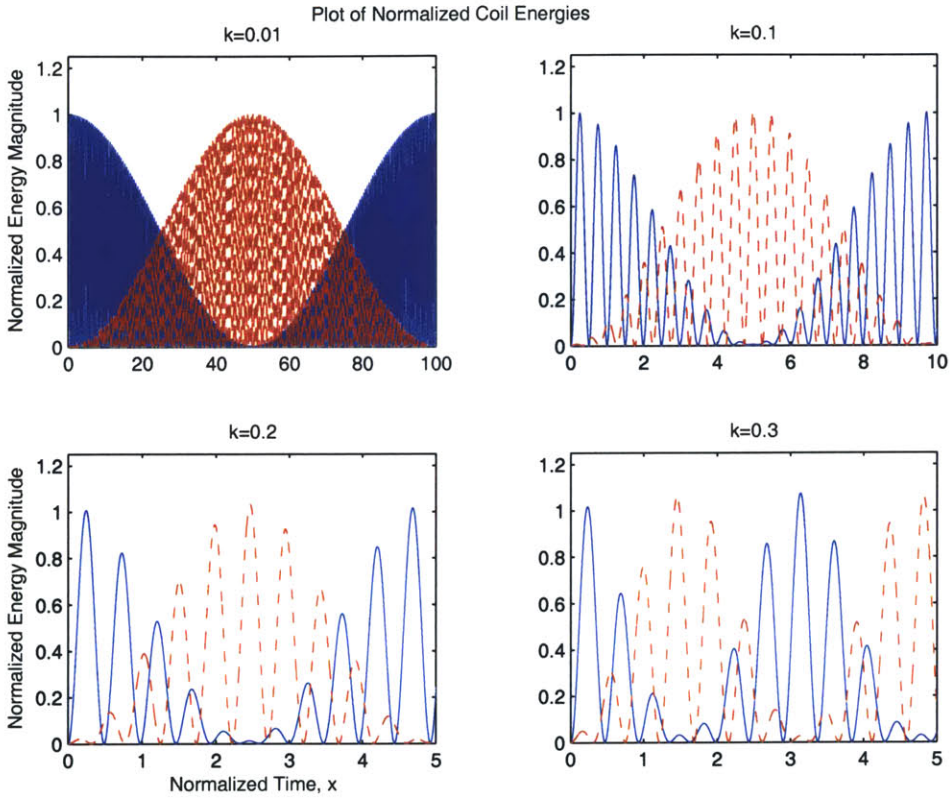

Figure 3-42: Plot of Normalized Energy in Primary and Secondary Coil for $\omega_1 = \omega_2 = 1, k = 0.01, 0.1, 0.3, 0.2$ (clockwise fashion)

For a predetermined amount of energy in the system, all starting out in the primary circuit, the regime of k tells how the secondary and primary transfer energy. For $k_{crit} < k \ll 1$, the secondary and primary exchange energy at the beat frequency. For $k = k_{crit}$, the secondary gives back energy to the primary as fast as it is dissipated from the system. Thus, there is only one beat corresponding to the complete transfer of energy from the primary to secondary. For subcritical k, the energy transferred to the secondary is dissipated faster than it can be transferred. There are no beats in the system.

3.5 Extensions beyond the 4^{th} order resonant system

One serious limitation with the previous derivation is that with all of the previous analysis done on the topology of Figure 3-1, it would seem mathematically impractical to suggest that other, higher order topologies may be better suited to energy transference between two sides of a fourth order circuit. A sixth or eighth order system of unknown topology may yield higher output voltages or more efficient energy transfer. Given the complexity of studying a single fourth order topology in the time and frequency domain, it is necessary to find an alternate method of design. Fortunately, there is a large body of work on analog filter design that allows designers to match impedance specifications, relative component sizes, and input/output voltage ratios to a multiple ordered LC network topology. This requires extensive use of the Laplace frequency domain. The simplicity of using this system is that it allows the designer to set the topology of the system to match desired input/output impedance and voltage ratio specifications.

In the time domain solution, manipulating the characteristic polynomial to achieve certain design specifications is difficult at best. In the frequency domain, there is a procedure for specifying operating frequencies and solving constitutive relations to determine the operating dynamics. The procedure for synthesizing an n^{th} order resonant circuit is beyond the immediate scope of this thesis. For more information on this topic, consult a text on filter design. [36]

Chapter 4

Operating Efficiency

The efficiency of the coupled system depends on how much energy is transferred from the primary to the secondary circuit. For this chapter it is assumed that the system is only excited with a voltage pulse from the charged primary capacitor and left to freely resonate. All derived results are normalized on a per pulse basis. The derived power and energy transfer efficiencies are calculated from the following quantities:

- Energy transferred to the unloaded secondary from the primary
- Power dissipated by the unloaded circuit
- Power transferred to a loaded secondary from the primary
- Energy transferred to a loaded secondary from the primary

Figure 4-1 shows the equivalent lumped parameter circuit with an output load impedance. The output load impedance, R_{load} represents a purely resistive load and could be a matched

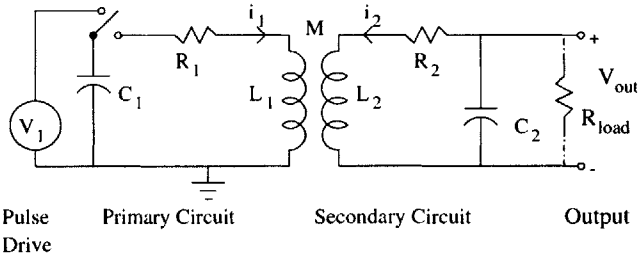

Figure 4-1: Lumped Parameter Model of Tesla Coil with Output Load Resistance

antennae, another circuit, or possibly the surrounding atmosphere itself. This load is assumed, for the purposes of calculation to be real and hence purely dissipative.

4.1 Unloaded Transfer Efficiency

This section concerns the energy transfer and power dissipation characteristics of the unloaded coupled circuits driven by a pulse drive. Using a pulse drive, the energy supplied to the primary circuit is delivered by the voltage source, V_1, to the primary capacitor before the system dynamics are considered. The system is pulsed and left to freely oscillate; there is no further addition of energy to either circuit for the duration of the output response. This implies that the only source of energy for the coupled system is the precharged capacitor, C_1.

4.1.1 Energy Transfer Efficiency of Coupled Circuits

The energy transfer efficiency of the coupled circuits is defined as:

$$\eta_{energy} = \frac{E_{secondary,max}}{E_{primary,max}} \tag{4.1}$$

The maximum energy found on the primary, $E_{primary,max}$, is the amount of energy initially put on the input capacitor C_1 by the voltage source V_1 as there is no other source of energy for the system. This initial energy is given by:

$$E_{primary,max} \equiv E_{init} = \frac{1}{2}C_1V_{in}^2 \tag{4.2}$$

where V_{in} is the voltage on C_1 at time $t = 0$ when the switch disconnects the voltage source from the capacitor and completes a series loop with the primary circuit elements, R_1, L_1, and C_1.

The maximum energy transferred to the secondary is only a fraction of the input energy. The energy found in the secondary circuit is always given by:

$$E_{secondary} = \frac{1}{2}L_2I_{secondary}^2 + \frac{1}{2}C_2V_{C2}^2 \tag{4.3}$$

The voltage across the secondary capacitor is defined to be the output voltage v_{out} of the

coupled system, as shown in Figure 4-1. When this output voltage v_{out} is a maximum, the energy in the capacitor is at a maximum. For the purposes of this discussion, when the energy stored in this capacitor is at a maximum, the energy in the secondary circuit is taken to be a maximum.

When the output voltage v_{out} is a maximum, its time derivative is zero. By the constitutive capacitor relation, $I_{secondary} = C\frac{dv_{out}}{dt} = 0$, the current in the secondary circuit is zero. When the current is zero, the energy stored in the secondary inductor L_2 is zero. Thus, the maximized secondary energy is:

$$E_{secondary,max} = \frac{1}{2}C_2V_{out,max}^2 \tag{4.4}$$

To explicitly determine this maximum secondary energy, it is necessary to first determine the output voltage and its maximum value. The expressions derived in Chapter 3, section 3 detail the dynamics governing the secondary capacitor voltage waveform. The values for the maximum voltage (equations 3.83 and 3.85) and the time, $t = t_{peak}$ at which it peaks are:

$$V_{out,max} = V_{in}\sqrt{\frac{L_2}{L_1}}e^{-\frac{\omega_n(Q_1+Q_2)}{4Q_1Q_2}t_{peak}}\sin(\frac{\omega_{upper}-\omega_{lower}}{2}t_{peak}) \tag{4.5}$$

$$t_{peak} = \frac{2}{\omega_{upper}-\omega_{lower}}\tan^{-1}(\frac{2Q_1Q_2(\omega_{upper}-\omega_{lower})}{\omega_n(Q_1+Q_2)}) \tag{4.6}$$

This yields a maximum secondary energy of:

$$E_{secondary,max} = \frac{1}{2}C_2V_{in}^2\frac{L_2}{L_1}e^{-2(\frac{\omega_n}{4}(\frac{1}{Q_1}+\frac{1}{Q_2})t_{peak})}\sin^2(\frac{\omega_{upper}-\omega_{lower}}{2}t_{peak}) \tag{4.7}$$

Attempts to reduce the above expression through a first or third order Taylor expansion are generally inaccurate because the small argument approximation for the arctangent function is not valid for most values of k used. Furthermore, centering the approximation about k_{crit} does not lead to an algebraically simplified result. It is advisable to use the plot in Figure 3-31 to find the maximum peak voltage. However, this figure does not consider the case of mismatched Q's or large k. While the results of that plot show a 48% maximum peak gain, ideally, as k approaches unity, the system approaches that of an ideal transformer with complete energy transfer.

The peak energy transfer efficiency is obtained as the ratio of equations 4.7 to 4.2,

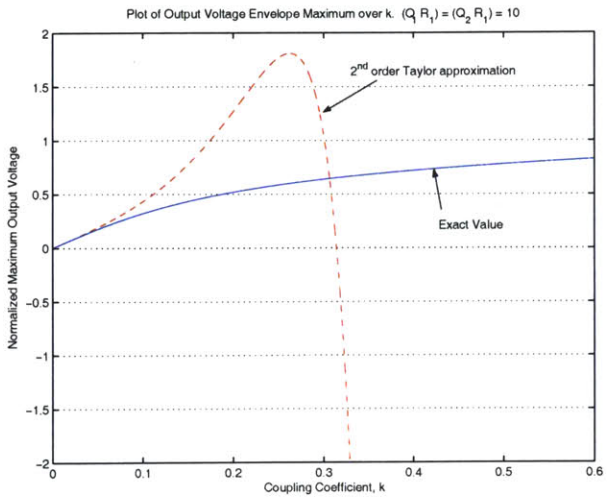

Figure 4-2: Plot of error in the peak output voltage envelope when a 3^{rd} order Taylor expansion centered about zero is used. $k_{crit} = 0.1$.

respectively.

$$\eta_{transfer} = \frac{\frac{1}{2}C_2V_{in}^2\frac{L_2}{L_1}e^{-2(\frac{\omega_n}{4}(\frac{1}{Q_1}+\frac{1}{Q_2})t_{peak})}\sin^2(\frac{\omega_{upper}-\omega_{lower}}{2}t_{peak})}{\frac{1}{2}C_1V_{in}^2} \tag{4.8}$$

The equation below shows an equivalent algebraic expression for the $\sin^2(\cdot)$ term. This expression is found by substituting t_{peak}, in equation 4.6, with its inverse tangent relation $\tan^{-1}(\cdot)$, and solving the triangle.

$$\sin^2(\frac{\omega_{upper}-\omega_{lower}}{2}t_{peak}) = \frac{(2Q_1Q_2(\omega_{upper}-\omega_{lower}))^2}{(\omega_n(Q_1+Q_2))^2+(2Q_1Q_2(\omega_{upper}-\omega_{lower}))^2} \tag{4.9}$$

Reducing this equation under the condition that $Q_1 = Q_2$ and expanding the expressions for the upper and lower frequencies yields:

$$\sin^2(\frac{\omega_{upper}-\omega_{lower}}{2}t_{peak}) = \frac{2kQ^2}{2kQ^2+1-k^2} \tag{4.10}$$

Substituting equation 4.9 into equation 4.8 gives the following:

$$\eta_{transfer} = \frac{4(Q_1Q_2(\omega_{upper}-\omega_{lower}))^2e^{-\frac{\omega_n}{2}\frac{Q_1+Q_2}{Q_1Q_2}t_{peak}}}{(\omega_n(Q_1+Q_2))^2+4(Q_1Q_2(\omega_{upper}-\omega_{lower}))^2} \tag{4.11}$$

where, for the self-resonant frequencies of each side set equal ($L_1C_1 = L_2C_2$), the leading

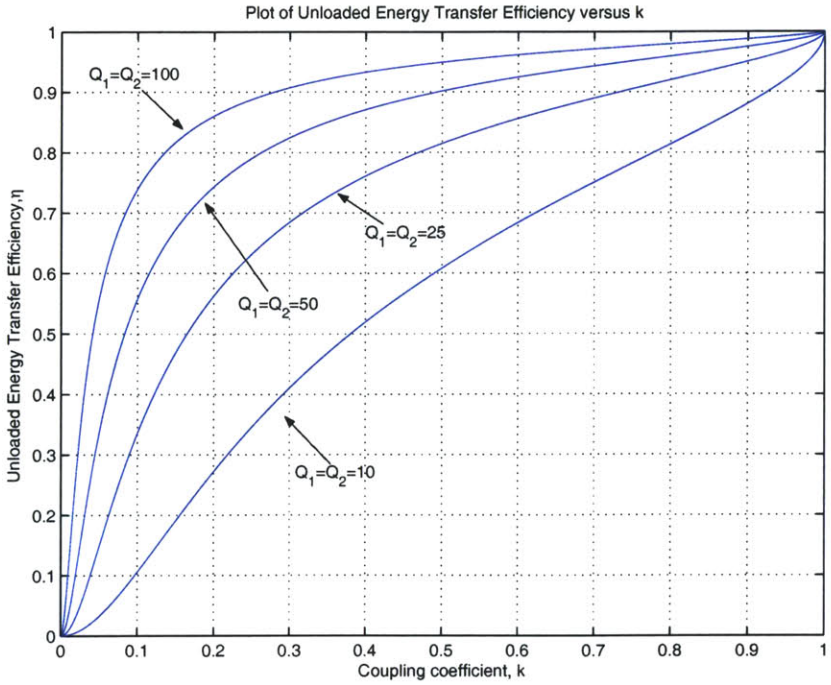

Figure 4-3: Plot showing the tradeoff between coupling coefficient, k and the transfer efficiency η with Q as a parameter.

coefficients of equation 4.8 cancel to unity leaving equation 4.11 that depends only on the network parameters of the system: the quality factors Q_1 and Q_2, the self resonant frequency ω_n, and the coupling coefficient, k.

The maximum efficiency of the system is set primarily by the damped exponential term as the sin^2 term goes from zero to unity over the efficiency curve. Figure 4-3 shows the tradeoff in transfer efficiency versus coupling coefficient, k, with the quality factors as a parameter. The efficiency increases as k approaches unity, but not in a uniform fashion. Taking a derivative of the efficiency expression in equation 4.11 to find a maximum gain (slope) in efficiency versus k will give a result that is close to k_{crit}, but will give a very low efficiency ($k = k_{crit} = 0.1$ for $Q_{1,2} = 10$ yields a 10% efficiency). It can be shown that the maximum $\frac{d\eta}{dQ}$ occurs when the quality factors are equal by solving the derivative of equation 4.8 set equal to zero.

There is no fundamental limit to the unloaded energy transfer efficiency save for constraints on the quality factors and the coupling coefficient. Realistically, switching losses and

parasitic losses will serve to practically constrain the overall Q of the system. Furthermore, increasing k drastically changes the output response waveform. Tradeoffs must be made when designing the coupled system if the shape of the response waveform is important.

4.1.2 Total Energy Dissipated across R_1 and R_2

When the circuit is unloaded and allowed to freely resonate, the resistances R_1 and R_2 are the only source of damping. Thus, all of the energy initially stored in the primary capacitor, $E_{pri} = \frac{1}{2}C_1V_{in}^2$ should be dissipated across these two resistors. The power they dissipate at any given instant is given by $P_{diss} = i^2(t)R$. The equations for the currents, $i_1(t)$ and $i_2(t)$, are taken from the previous chapter.

$$P_{diss,1} \approx \frac{V_{in}^2}{4R_1Q_1^2\omega_n^2}\left(\omega_{lower}e^{\zeta_{lower}t}\sin(\omega_{lower}t) + \omega_{upper}e^{\zeta_{upper}t}\sin(\omega_{upper}t)\right)^2 \quad (4.12)$$

$$P_{diss,2} \approx \frac{V_{in}^2}{4R_1Q_1Q_2\omega_n^2}\left(\omega_{lower}e^{\zeta_{lower}t}\sin(\omega_{lower}t) - \omega_{upper}e^{\zeta_{upper}t}\cos(\omega_{upper}t)\right)^2 \quad (4.13)$$

The approximations made for $i_1(t)$ and $i_2(t)$ in the previous chapter hold, namely that $\frac{\zeta}{\omega} \ll 1$. When the quality factors are substituted for the inductances found in the current equations, the dependence on R_2 seems to be eliminated while both power dissipations appear to depend on the primary resistance, R_1. Actually, the loss terms are buried inside the quality factors; changing their values changes the values of the Q's. Figure 4-4 shows an example of how the dissipated power follows the general behavior expected of this coupled system.

The total energy dissipated by the two resistors is given by the sum of the integrals of equations 4.12 and 4.13. Figure 4-5 shows a running integration of the above dissipated power losses. Integrating the power dissipation over infinite time gives:

$$E_{Diss} = \int_0^\infty P_{Diss,1} + P_{Diss,2}\, dt \quad (4.14)$$

$$E_{Diss} \approx \frac{V_{in}^2Q_2\left[2Q_1(1-\sqrt{1-k^2}) + Q_2 + 3Q_2\sqrt{1-k^2} + 8k^2Q_1^2Q_2\right]}{\omega_nQ_1Q_2R_1(1-k^2)(\sqrt{1+k}+\sqrt{1-k})^2\left[2Q_1 + Q_2 + Q_1^2Q_2(1+8(1-\sqrt{1-k^2}))\right]} \quad (4.15)$$

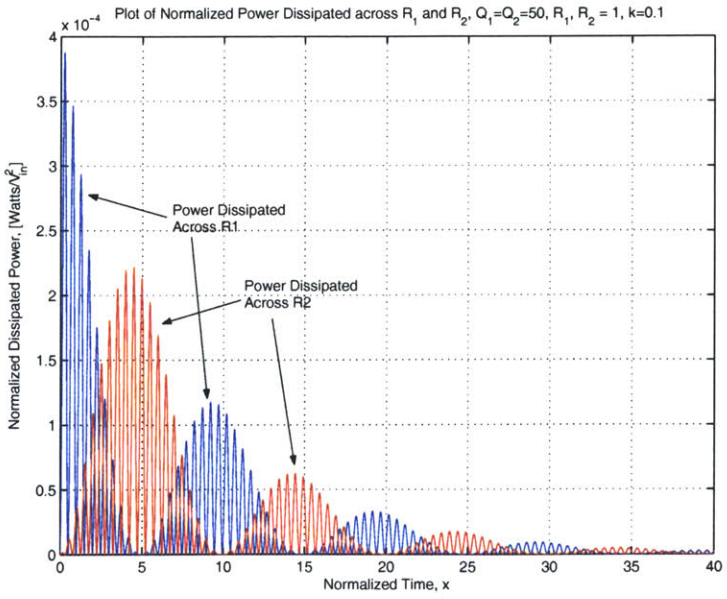

Figure 4-4: Plot of Power Dissipation, normalized by V_{in}^2, through R_1 and R_2. $k = 0.1$, $Q_1 = Q_2 = 50$, $R_1 = R_2 = 1\Omega$.

This result is approximately 1% less than the initial input energy, $E_{in} = \frac{1}{2}C_1V_{in}^2$. This is due to the neglected terms of order $\frac{\zeta}{\omega}$ and higher. Figure 4-5 shows a plot of the total energy dissipated (normalized by V_{in}^2) across each resistor versus normalized time. Notice how the rate of energy dissipation slows when the voltage waveform has nulls between the beats. The upper plot shows the sum of both energy dissipations; it is a monotonically increasing function. For these calculations, the input energy, normally expressed as $E_{in} = \frac{1}{2}C_1V_{in}^2$ is calculated as $E_{in} = \frac{V_{in}^2}{2\omega_n Q_1 R_1}$ through the substitution $C_1 = \frac{1}{\omega_n Q_1 R_1}$. Changes to Q and k change the locations of the flat regions in the plot by changing the location and amount of nulls in the output response waveform, but the general form of this plot remains unchanged.

In conclusion, this energy dissipation calculation shows that the primary and secondary losses, when equal, dissipate approximately equal amounts of energy although the losses in the primary slightly dominate those in the secondary. Furthermore, these results serve as a check to the self consistency of the response waveforms as the total energy losses in the isolated circuit sums to unity, as expected.

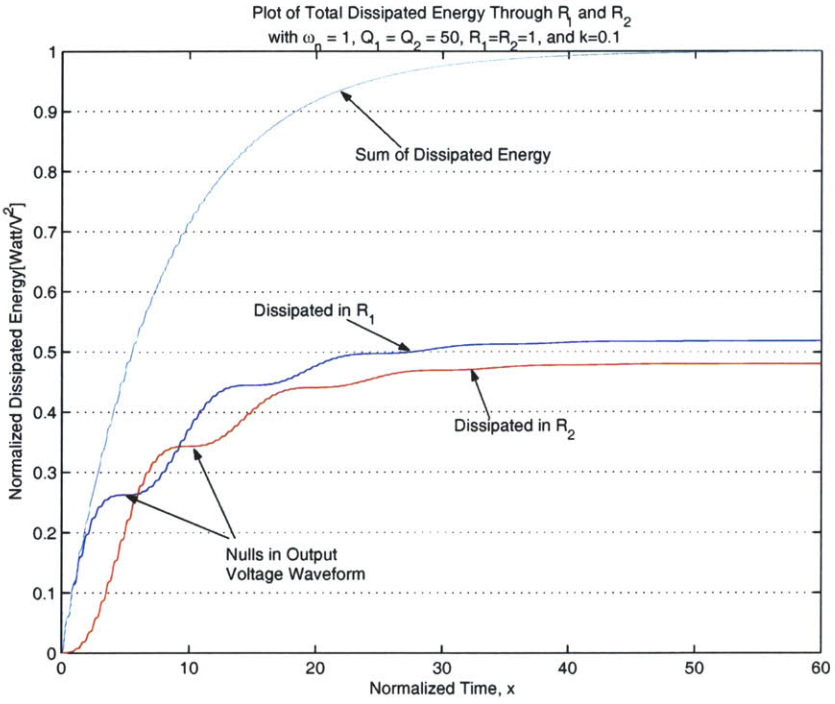

Figure 4-5: Plot of normalized total energy dissipated across each resistor over normalized time. Top plot shows sum of both energy losses. $Q_1 = Q_2 = 50$, $R_1 = R_2 = 1$, $\omega_n = 1$, $k = 0.1$

4.2 Loaded Transfer Efficiency

Consider the efficiency of transferring energy into a resistive load, R_{load}, as shown in Figure 4-1. This load is connected across the secondary capacitance. The energy input to the system remains unchanged, given by equation 4.2: $E_{in} = \frac{1}{2}C_1V_{in}^2$. As before, this energy is both the input energy and the maximum energy found on the primary side.

On the secondary side, the total output energy is defined to be the power dissipated by the load integrated over the lifetime of the output waveform. The output voltage across the load resistor is found by using the equivalent output impedance Z_{out} in a Thevenin or Norton equivalent circuit. As derived in the previous chapter in equation 3.30, this Thevenin impedance is:

$$Z_{out} \approx \sqrt{\frac{L_2}{C_2}}\frac{Q_2}{1+k^2Q_1Q_2} \tag{4.16}$$

$$v_{out}(t) \approx \frac{V_{in}}{2}\sqrt{\frac{L_2}{L_1}}\left[e^{-\zeta_{lower}t}\cos(\omega_{lower}t) - e^{-\zeta_{upper}t}\cos(\omega_{upper}t)\right] \tag{4.17}$$

The output impedance equation assumes that $Q_2 \gg 1+k^2Q_1Q_2$ while the output voltage equation, listed above, assumes that $\frac{\zeta}{\omega_n} \ll 1$. This output voltage changes with the addition of a resistive load. Its new value is found by taking a voltage ratio between Z_{out} and R_{load}. This yields:

$$v_{load}(t) = v_{out}(t)\Big(\frac{R_{load}}{R_{load}+Z_{out}}\Big) \tag{4.18}$$

4.2.1 Loaded Power Transfer

To compute the energy delivered to the load, it is convenient to find the power delivered to the load, R_{load}. This power is computed as $P_{load} = \frac{v_{out}^2}{R_{load}}$. This can be expressed as:

$$P_{load} = (\frac{v_{out}}{R_{load}+Z_{out}})^2 R_{load} = \frac{V_{out}^2}{R_{load}}(\frac{\alpha}{1+\alpha})^2 \tag{4.19}$$

where $\alpha \equiv \frac{R_{load}}{Z_{out}}$ is the ratio of the load resistance to the Thevenin equivalent output impedance.

The power delivered to the load is maximized when the impedances are matched, i.e. $R_{load} = Z_{out}$. Substituting equation 4.16 for R_{load} and equation 4.5 for v_{load} in equation 4.19 yields:

$$P_{load} = \frac{V_{in}^2}{16}\frac{(1+k^2Q_1Q_2)}{R_1Q_1Q_2}\Big[e^{-\delta_{lower}t}\cos(\omega_{lower}t) - e^{-\delta_{upper}t}\cos(\omega_{upper}t)\Big]^2 \tag{4.20}$$

Figure 4-6 shows this power dissipated across a matched load resistor for two values of the quality factors (set equal).

4.2.2 Loaded Energy Transfer Efficiency

With the expression for the total power dissipated in R_{load} as a function of time, the total energy dissipated by the load is found by integrating equation 4.19.

$$E_{out} = \int_0^\infty P_{load}\, dt = \int_0^\infty \frac{(v_{out}(t))^2}{R_{load}}\, dt \tag{4.21}$$

Inserting equations 4.16 through 4.18 into equation 4.21 yields:

$$E_{out} = \int_0^\infty (v_{out}^2(\frac{R_{load}}{R_{load}+Z_{out}})^2\frac{1}{R_{load}})\, dt \tag{4.22}$$

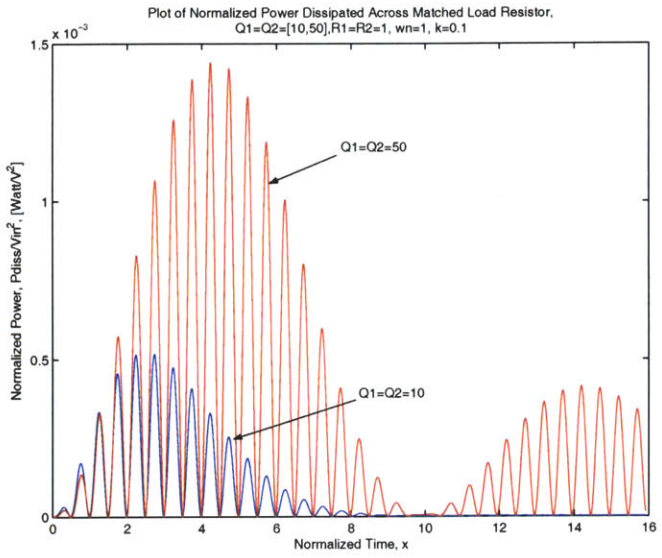

Figure 4-6: Plot of normalized power dissipated across a matched load resistor. $Q_1 = Q_2 =$ 10 and 50, $\omega_n = 1$, $k = 0.1$

To find the loaded energy transfer efficiency, equation 4.22 is integrated, divided (normalized) by the maximum input energy $E_{in} = \frac{1}{2}C_1V_{in}^2$, and finally reduced to:

$$\eta_{load} \approx \frac{1}{8}(\frac{\alpha}{1+\alpha})^2 \frac{1}{C_2 R_{load}} \Big[\frac{1}{\zeta_{upper}} + \frac{1}{\zeta_{lower}} - \frac{4(\zeta_{upper}+\zeta_{lower})}{(\zeta_{upper}+\zeta_{lower})^2 + (\omega_{upper}-\omega_{lower})^2}\Big] \quad (4.23)$$

where $\alpha \equiv \frac{R_{load}}{Z_{out}}$ is again the ratio of output load resistance to the coil's Thevenin equivalent output impedance. Terms of order $\frac{\zeta}{\omega}$ are neglected when computing the integral of equation 4.22 as it greatly simplifies in the integration of the above expression. This integration is performed with more detail in appendix A.

To get as large of a power transfer as possible, the load resistance, R_{load} should be set equal to Z_{out} by the maximum power transfer theorem. The theorem states that the maximum power across a load will occur when its impedance equals the complex conjugate of the Thevenin equivalent impedance of the source. As Z_{out} is taken to be purely resistive, $\alpha = 1$, $R_{load} = Z_{out}$, and the efficiency becomes:

$$\eta_{matched} \approx \frac{\omega_n}{32Q_2}(1+(\frac{k}{k_{crit}})^2)\Big[\frac{1}{\zeta_{upper}} + \frac{1}{\zeta_{lower}} - \frac{4(\zeta_{upper}+\zeta_{lower})}{(\zeta_{upper}+\zeta_{lower})^2 + (\omega_{upper}-\omega_{lower})^2}\Big] \quad (4.24)$$

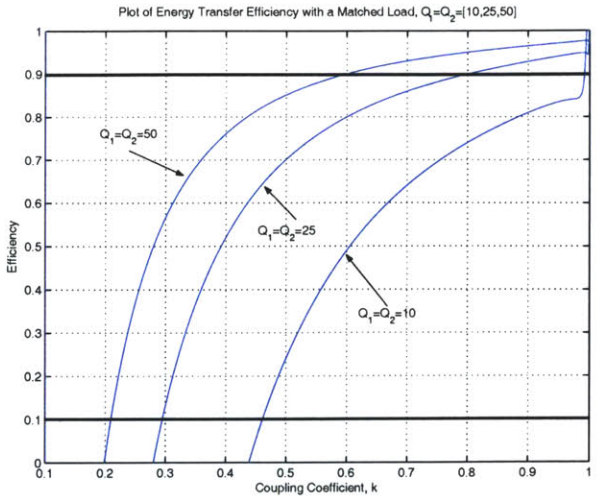

Figure 4-7: Plot of Loaded Energy Efficiency (equation 4.23) versus coupling coefficient with matched load resistance. These plots are *not* accurate above the 90% or below the 10% efficiency marks due to approximations made during the integration of equation 4.22.

Figure 4-7 shows a plot of the loaded energy transfer efficiency versus the coupling coefficient, k. Again, the sensitivity of the transfer efficiency versus k is apparent as the efficiency rises greatly for a relatively small change in coupling and then flattens out as the coupling approaches unity. This plot is formulated from equation 4.23 and as such, the approximations made limit the accuracy of this plot. For efficiencies above 90% or below 10%, consult the full solution to the integral shown in appendix A. One important item is that for $k \approx k_{crit}$, the loaded transfer efficiency is well below 10%. The *energy* transfer efficiency when operating with a matched load is quite poor.

In conclusion, the coupled resonant system is not efficient when operating with a small coupling coefficient in the range $0 \leq k \ll 1$. This is expected as standard transformers strive to keep k as close to unity as possible to avoid efficiency losses. While many antennae systems are impedance matched to their sources to maximize the amount of radiated power, the efficiency of the loaded coupled resonant system is low. However, if the secondary circuit is used for another purpose, increasing the load impedance would increase the overall energy transfer efficiency in the limit to that shown in the unloaded energy transfer section.

Chapter 5

Tesla Coil Design Constraints and Tradeoffs

Using the results of the previous chapters, it is now possible to design a coupled resonant system tailored to a specific use by setting certain parameters and system specifications. This chapter outlines methods of design that do not depend solely on component values or difficult to measure internal parameters. Instead, the approach is to determine component values to match the intended operational specifications of the resonant system.

5.1 Explanation of Variables, Parameters, and Assumptions

There are seven unknowns that define the resonant system described thus far:

The primary inductor value:	L_1
The primary circuit capacitance:	C_1
The primary circuit parasitic resistance:	R_1
The secondary coil inductance:	L_2
The secondary coil parasitic capacitance:	C_2
The secondary coil parasitic resistance:	R_2
The coupling coefficient:	k

The schematic of the system is shown again in Figure 5-1. To attain desired operation, certain response quantities and their constraining equations are used. The equations listed here are taken directly from the previous chapters. For convenience, they are presented in

terms of both circuit elements and their corresponding network parameters.

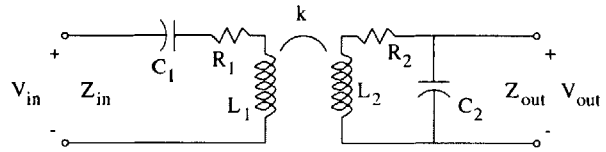

Figure 5-1: Schematic showing the coupled resonant circuits as well as their input and output ports.

The impedance equations, 5.10 and 5.12, are computed at the terminals shown in Figure 5-1. Equations 5.8 and 5.9 (the steady state voltage gain), 5.15 and 5.16 (the pulse driven peak voltage gain), as well as 5.10, 5.11, 5.12, and 5.13 (the input and output AC steady state impedance) all require that the primary and secondary circuits resonate at identical frequencies, $\omega_1 = \omega_2$ denoted ω_n. Furthermore, equations 5.10, 5.11, 5.12, 5.13, and 5.14 also require a small k, approximately $k < 0.1$.

Response Quantities:

Coupling Coefficient

$$k \equiv \frac{M}{\sqrt{L_1 L_2}} \tag{5.1}$$

Natural resonant frequency of the primary circuit

$$\omega_1 = \frac{1}{\sqrt{L_1 C_1}} \tag{5.2}$$

Natural resonant frequency of the secondary circuit

$$\omega_2 = \frac{1}{\sqrt{L_2 C_2}} \tag{5.3}$$

Quality factor of the primary circuit

$$Q_1 = \frac{1}{R_1}\sqrt{\frac{L_1}{C_1}} \tag{5.4}$$

$$Q_1 = \frac{\omega_1 L_1}{R_1} \tag{5.5}$$

Quality factor of the secondary circuit

$$Q_2 = \frac{1}{R_2}\sqrt{\frac{L_2}{C_2}} \tag{5.6}$$

$$Q_2 = \frac{\omega_2 L_2}{R_2} \tag{5.7}$$

AC steady state voltage gain

$$\frac{V_{out}}{V_{in}} = \frac{-kL_2}{k^2\sqrt{L_1L_2} + R_1R_2\sqrt{C_1C_2}} \tag{5.8}$$

$$\frac{V_{out}}{V_{in}} = -\sqrt{\frac{Q_2R_2}{Q_1R_1}}\left(\frac{k}{k^2 + \frac{1}{Q_1Q_2}}\right) \tag{5.9}$$

AC steady state input impedance of the coupled circuits

$$Z_{in}|_{s=\omega_n} = R_1 + \frac{k^2L_1}{R_2C_2} \tag{5.10}$$

$$Z_{in} = R_1(1 + k^2Q_1Q_2) \tag{5.11}$$

AC steady state output impedance of the coupled circuits

$$Z_{out} = \frac{R_1L_2 - j\sqrt{L_2C_2}(R_1R_2 + k^2\frac{L_1}{L_2})}{R_1R_2C_2 + k^2L_1} \tag{5.12}$$

$$Z_{out} = \sqrt{\frac{L_2}{C_2}}\left(\frac{Q_2 - j(1 + k^2Q_1Q_2)}{1 + k^2Q_1Q_2}\right) \tag{5.13}$$

Number of waveform cycles to peak secondary output voltage

$$N_{peak} = \frac{1}{2k} \tag{5.14}$$

Maximum pulse driven secondary voltage peak

$$V_{out,max} = V_{in}\sqrt{\frac{L_2}{L_1}}e^{-\frac{\omega_n(Q_1+Q_2)}{4Q_1Q_2}t_{peak}}\sin\left(\frac{\omega_{upper} - \omega_{lower}}{2}t_{peak}\right) \tag{5.15}$$

$$t_{peak} = \frac{2}{\omega_{upper} - \omega_{lower}}\tan^{-1}\left(\frac{2Q_1Q_2(\omega_{upper} - \omega_{lower})}{\omega_n(Q_1 + Q_2)}\right) \tag{5.16}$$

Peak energy transfer efficiency

$$\eta = \frac{E_{peak,C_2}}{E_{peak,C_1}} = \frac{\frac{1}{2}C_2V_{in}^2\frac{L_2}{L_1}e^{-2(\frac{\omega_n}{4}(\frac{1}{Q_1}+\frac{1}{Q_2})t_{peak})}\sin^2(\frac{\omega_{upper}-\omega_{lower}}{2}t_{peak})}{\frac{1}{2}C_1V_{in}^2} \tag{5.17}$$

5.2 Component Estimation and Physical Constraints

Before the design tradeoffs are discussed, it is necessary to outline how the geometry and operation of the Tesla coil affects the seven lumped parameter component values. The issues discussed are: formulas relating inductance and capacitance to geometry, parasitic resistances found in the primary and secondary, and the self-resonant frequency of a given coil geometry.

5.2.1 Estimating Inductance

Simple models for computing the inductance of a structure relate it to an idealized solenoid. More accurate numeric models exist and are explained below. A range of formulas is given as there are a variety of inductor geometries besides solenoids used in Tesla coil construction. Note that these formulas shown do *not* account for a ground plane. The presence of a ground plane will serve to increase the measured inductance.

Long solenoid model

This model follows directly from Ampere's law. It assumes that the magnetic field inside the coil is constant. This assumption is reasonably true for the height of the solenoid approximately eight times greater than the radius, $b > 8a$ where a, b are the average radius and height, respectively. They are defined in Figure 5-2. A derivation is shown in appendix B. The inductance relation is:

$$L_{solenoid} = \frac{\mu_0 N^2 \pi a^2}{b}\ [Henry] \tag{5.18}$$

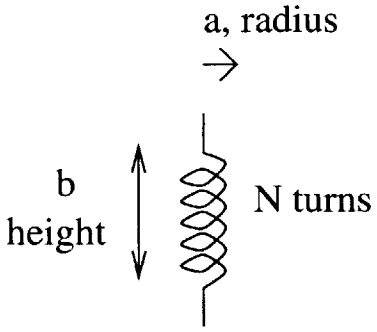

Figure 5-2: Cartoon of a Solenoid Inductor with Marked Dimensions

where μ_0 is the permeability of free space equal to $4\pi \cdot 10^{-6}$ $[Henry/meter]$ and a, b are expressed in meters.

Wheeler's Formula

A common practical method of calculating the inductance of a uniform cylindrical solenoid is Wheeler's formula.[33] [38] It is an empirical formula used primarily in designing RF, air core coils. It is useful in calculating inductances for short coils. It is given by equation 5.19.

$$L_{solenoid} = \frac{a^2 N^2}{9a + 10b} \ [\mu H] \tag{5.19}$$

Note that a and b are expressed in inches. This formula holds for single layer wound solenoids (no wire wrapped on top of another) and holds to within 5% of the measured value for $b > 0.8a$.

Lundin's Formula

For comparison, there is a more accurate formula to compute the inductance of a solenoid known as Lundin's formula. It is derived from first principles and is quite accurate.[20]

$$L = \frac{\mu_0 N^2 \pi a^2}{b}[f(\frac{4a^2}{b^2}) - \frac{4}{3\pi}\frac{2a}{b}] \ [H] \tag{5.20}$$

$$f(x) = \frac{1 + 0.383901x + 0.017108x^2}{1 + 0.258952x}, \ 0 \leq x \leq 1 \tag{5.21}$$

While this formula is accurate up to three parts per million Henries, it is both a nonlinear

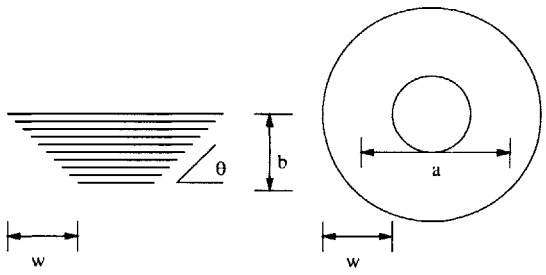

Figure 5-3: Diagram of a tapered coil inductor. Side (left) and top (right) views are shown.

function of the coil's size and difficult to work with in equations when substituting an expression for inductance. However, if a coil is already built, this formula usually gives a much better prediction of inductance than Wheeler's formula.

Tapered Inductor

Another common coil geometry is the tapered coil. An illustration of its shape is shown in Figure 5-3. The formula used to compute its inductance is based on Wheeler's work.[38]

$$L_x = \frac{(Na)^2}{9a + 10b} \tag{5.22}$$

$$L_y = \frac{(Na)^2}{8a + 11w} \tag{5.23}$$

$$L = \sqrt{(L_x \sin(\theta))^2 + (L_y \cos(\theta))^2}\ [\mu H] \tag{5.24}$$

The computed inductance, L has units of μH, a is the average radius of the tapered coil in inches, b is the height of the coil in inches, N is the number of turns, w is the amount of taper in inches, and θ is the angle of the taper in degrees.

Spiral Pancake Inductor

The spiral shaped inductor is sometimes seen as the primary on a Tesla coil system. The height (thickness) of the inductor is the diameter of the wire used in its construction. Figure 5-4 illustrates its geometry. The inductance is given by:

$$L = \frac{(Na)^2}{8a + 11w}\ [\mu H] \tag{5.25}$$

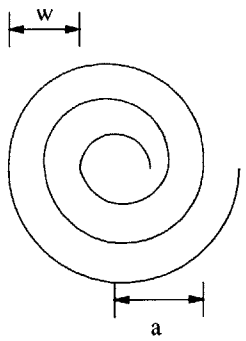

Figure 5-4: Diagram of a spiral pancake inductor. Top view is given with defining parameters.

where the computed inductance, L has units of μH, a is the average radius of the pancake in inches, w is the width of the coil in inches, and N is the number of complete turns.

Inductance of Straight Wire

For estimating the parasitic inductance of the wires used to connect components, it is necessary to compute the inductance of a wire above a ground plane.

$$L_{wire} = 0.2l(ln(4\frac{l}{d}) - 0.75)\ nH \tag{5.26}$$

where l is the length in millimeters and d is the wire diameter in millimeters. Figure 5-5 gives an illustration of such a lead inductance component.

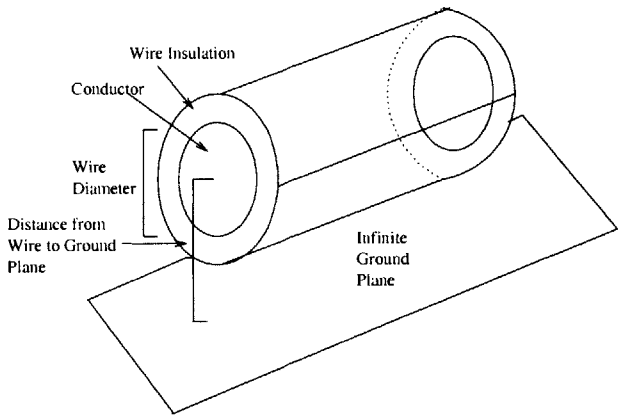

Figure 5-5: Diagram of a wire over an infinite ground plane used to compute inductance.

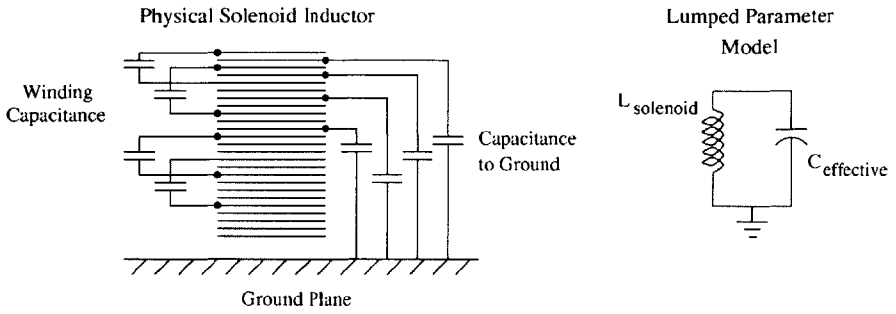

Figure 5-6: Diagram showing physical solenoidal inductor (left) with associated capacitances and idealized lumped parameter model (right)

5.2.2 Estimating Capacitance

The inductors presented in the previous section are shown in previous chapters as requiring a capacitor in order to resonate. Practically, the parasitic and distributed capacitances found in the physical inductor structure are often used to produce a resonant system. Figure 5-6 shows a typical orientation for an inductor.

Calculating these distributed capacitances between the coil's windings and between the coil and ground requires tedious calculations using electromagnetic field equations. Fortunately, the effective capacitance for a single layer solenoidal inductor has already been experimentally measured.

Medhurst Capacitance

Medhurst [21] gives a table for estimating the effective capacitance, C_o, of a single layer solenoidal coil with mean radius a and length b oriented as shown in Figure 5-6. The capacitance is measured between the top winding of the coil and the grounded bottom winding. Thus, this capacitance takes into account the capacitance between the coil windings and between the coil and the earth ground plane. Medhurst's formula is:

$$C_0 \approx 2Ha \ [pF] \tag{5.27}$$

where a is the radius of the solenoid in centimeters and H is a factor based on the table (Table V in Medhurst's publication):

$\frac{b}{2a}$	H	$\frac{b}{2a}$	H	$\frac{b}{2a}$	H
50	5.8	5.0	0.81	0.70	0.47
40	4.6	4.5	0.77	0.60	0.48
30	3.4	4.0	0.72	0.50	0.50
25	2.9	3.5	0.67	0.45	0.52
20	2.36	3.0	0.61	0.40	0.54
15	1.86	2.5	0.56	0.35	0.57
10	1.32	2.0	0.50	0.30	0.60
9.0	1.22	1.5	0.47	0.25	0.64
8.0	1.12	1.0	046	0.20	0.70
7.0	1.01	0.90	0.46	0.15	0.79
6.0	0.92	0.80	0.46	0.10	0.96

Medhurst, through experimental verification, quotes these numbers as being accurate to within 5.0%.

Capacitance of a Wire

The capacitance of a wire oriented parallel to a ground plane, the same geometry as Figure 5-5, is given by the formula:

$$C_{leads} = \frac{0.55\epsilon_{eff}}{\ln(\frac{2height}{radius})}\ pF/cm \tag{5.28}$$

The relative permittivity, ϵ_{eff}, is usually 1 in air. The radius is the radius of the wire used, the height is the distance between the wire and the groundplane. Note that the above formula gives the capacitance between a wire to a groundplane per centimeter of wire.[37]

5.2.3 Estimating the resistance

The resistances found in the Tesla coil are typically parasitic. The goal here is to provide a bounding value for estimation purposes. In this analysis the parasitic resistances due to eddy currents and dielectrics are neglected. The resistance found for a wire element in a Tesla coil can be separated into two components. The first term is a bulk resistance while

the second term accounts for the power loss by radiation.

$$R_{total} = \Phi_M \Phi_{AC} R_{DC} + R_{radiation} \tag{5.29}$$

DC resistance

The DC resistance of a length of wire is a due to the bulk resistivity of the material used and its conducting geometry. A straightforward formula is given by 5.30.

$$R_{dc} = \rho_{wire} \frac{length}{Area_{wire}} = \rho_{wire} \frac{length}{\pi \cdot radius^2} \ [\Omega] \tag{5.30}$$

For multiply stranded wiring, the per strand resistance is divided by the number of individual strands in the stranded bundle.

The bulk resistivity for copper is $\rho_{copper} = 1.68 \cdot 10^{-8} \Omega m$. A common wire size to use is 24 gauge wire. It has a conductive diameter of 0.51mm so this gauge wire has a bulk resistance of 0.0825 ohms per meter at $20^o C$.

The temperature of the wire itself has a scaling effect on the DC resistance, altering its value through the relation:

$$R_{T2} = R_{T1}(1 + \alpha \Delta T) \tag{5.31}$$

where the temperature coefficient $\alpha_{copper} = 3.9 \cdot 10^{-3} \ [K^{-1}]$. Measuring the resistance of the secondary coil windings before and after operation can give an indication of how hot the wiring gets.

AC resistance

The AC resistance of a wound coil represents a significant portion of the resistance of the wire used in the system. At DC conditions, current is uniformly distributed through a cross-section of wire. Under AC conditions, the current tends to remain near the outer surface of the conductor. The effective depth of penetration of the current is called the skin depth, δ. The current travelling through a smaller cross sectional area of wire equates to a higher resistance.

The skin depth varies inversely with frequency according to the equation:[31]

$$\delta = \frac{1}{\sqrt{\pi f \mu \sigma}} \ [m] \tag{5.32}$$

The constant μ is the permeability of the the wire (for copper, $\mu = \mu_0$), σ is the conductivity of the wire and f is the operating frequency in Hertz. For standard copper wire, this skin depth coefficient reduces to the following:

$$\delta = \frac{0.066}{\sqrt{f}} \; [meters] \tag{5.33}$$

Depending on the ratio of this skin depth coefficient to the radius of the wire, there are tables that give a multiplier to convert the DC resistance to an equivalent AC resistance. [17, ch.6, page 7]. The cited reference gives a detailed analysis of this situation as well as a proof for the presented formula and tables.

$\frac{a}{\delta}$	$\Phi_{AC} = \frac{R_{AC}}{R_{DC}}$
1	1.020
2	1.263
3	1.763
4	2.261
5	2.743
6	3.221
7	3.693
8	4.154

The multiplying factor, Φ_{AC} is defined as the ratio of AC to DC resistance. Hence, at a given frequency, f.

$$R_{AC} = \Phi_{AC} \cdot R_{DC} \tag{5.34}$$

Some texts on electromagnetism cite the formula: $R_{AC} = R_{DC}(\frac{a}{2\delta})$, but this is only valid for $\delta \ll a$, which does not hold for smaller gauge wiring found on most coils.

Proximity effect

The proximity effect stems from the adjacent turns of a long solenoid being wound close together. The electrons comprising the current are confined to the outside of the wire due to the same electrodynamics that cause the skin effect in a single wire. The adjacent conducting turns of a tightly wound solenoid coil act to cause the currents to stay nearer the outer radius of the wound coil. This acts as an added resistance. Medhurst [21] gives

the following formula for converting the AC resistance into the proximity resistance.

$$R_{proximity} = \Phi_M R_{AC} \tag{5.35}$$

Φ_M is a number based on two quantities: the ratio of the total length of wire in the coil, T to the coil's radius, a and the ratio of the diameter of the wire itself, d and the distance between the wires' centers of two adjacent turns, z.

T/a

$\frac{d}{z}$	2	4	8	12	16	20	∞
1	5.55	4.10	3.54	3.31	3.20	3.23	3.41
0.9	4.10	3.36	3.05	2.92	2.90	2.93	3.11
0.8	3.17	2.74	2.60	2.60	2.62	2.65	2.81
0.7	2.47	2.32	2.27	2.29	2.34	2.37	2.51
0.6	1.94	1.98	2.01	2.03	2.08	2.10	2.22
0.5	1.67	1.74	1.78	1.80	1.81	1.83	1.93
0.4	1.45	1.50	1.54	1.56	1.57	1.58	1.65
0.3	1.24	1.28	1.32	1.34	1.34	1.35	1.40

Medhurst's analysis assumes that the operating frequency is large, as his tables and data were gathered at 1 MHz. For much lower frequencies, the proximity effect is negligible, $\Phi_M = 1$.

The total resistance of the coil thus far can be approximated as:

$$R_{coil,bulk} = \Phi_M \Phi_{AC} R_{DC} \tag{5.36}$$

Radiation resistance

The radiation resistance arises when the coil structure radiates electromagnetic energy like an antenna. The radiation resistance is not strictly a measure of loss in the antennae but is analogous to the characteristic impedance, Z_o of a transmission line. The formula for

computing the effective resistance of an ideal Hertzian dipole is:[31, chatper 9]

$$R_{rad} = \frac{2P_{rad}}{|I|^2}\frac{\eta_0}{6\pi}(kd)^2 \approx 20(kd)^2 \ [\Omega] \tag{5.37}$$

where $\eta_0 \approx 377\Omega$ is the characteristic impedance of space, k is the wave number in radians per meter ($\frac{\omega}{c}$), and d is the dipole length in meters. Specific formulas for various inductor geometries can be derived from equations found in the references.

The value of the resistance varies depending on the coil structure and the frequency of the system, ω_{upper} in this case. If the wavelength of these frequencies ($\lambda = \frac{2\pi c}{\omega_{upper}}$ where c is the speed of light) is much greater than the length of the secondary coil, then the radiation resistance can be neglected when modelling the resistance of the system. For the primary circuit, if the lengths of all connecting wires are kept short, the effect of radiation resistance can be ignored when compared to other parasitic resistances.[17, chapter 6] For illustration, if the secondary coil is a solenoid of length 10cm and is resonating with frequency of $f_n = 100$kHz, then its radiation resistance is (approximating it as an ideal Hertzian dipole) approximately 0.87Ω. This resistance is proportional to the peak power radiated by the coil.

To conclude, the total parasitic resistance of a coil found thus far can be approximated as:

$$R_{coil} = R_{rad} + \Phi_M \Phi_{AC} R_{DC} \tag{5.38}$$

5.2.4 Determining a Self-Resonant Frequency of the Secondary Coil

If the system operating frequencies are of importance in designing the system, then it is necessary to ensure the secondary coil resonates at this frequency in order to extract optimal performance. An empirical formula for the self-resonant frequency of a solenoidal coil is given in equation 5.39.[1, chapter 23] It is found by correlating Wheeler's data for computing coil inductances with Ampere's Law to find the natural resonant frequency of the solenoid coil structure.

$$\omega_{n,self} = \frac{8.16 \cdot 10^7 (b_2/a_2)^{1/5}}{N_2 a_2} \ [rad/sec] \tag{5.39}$$

As before, a_2 is the coil radius and b_2 is the coil height, in meters. The length of coil, b_2 is of little consequence in determining the self-resonant frequency. This formula holds only for air core solenoidal coils and requires that $\frac{b_2}{a_2} \geq 2$. If the fifth root of this ratio is not

much more than unity, it can be neglected.

The coil designer is free to constrain the secondary coil geometry as approximately:

$$N_2 a_2 \approx \frac{8.16 \cdot 10^7}{\omega_{n,self}} \tag{5.40}$$

and choose the desired values of N_2 and a_2 separately. In most cases, $\omega_{n,self}$ is chosen to be ω_n.

5.3 Design Tradeoffs

Most resonant system designs aim to optimize only one or two parameters and allow the others to be set by engineering tradeoffs. The follows sections outline how to theoretically achieve such optimizations.

5.3.1 Design Tradeoffs for Maximizing AC Steady State Voltage Gain

One commonly maximized parameter is the AC steady state voltage gain. Steady state voltage gain is different from the peak secondary voltage in that these two parameters arise from two different methods of driving the coupled system. The steady state voltage gain is determined from the value of the frequency domain transfer function, repeated below, evaluated at the frequency of interest.

$$\frac{V_{out}}{V_{in}} = -\sqrt{\frac{L_2}{L_1}} \frac{s^2 \omega_2^2 k}{\begin{cases} (1-k^2)s^4 + (\frac{\omega_1}{Q_1} + \frac{\omega_2}{Q_2})s^3 + (\omega_2^2 + \omega_1^2 + \frac{\omega_1 \omega_2}{Q_1 Q_2})s^2 \\ +\omega_1 \omega_2 (\frac{\omega_2}{Q_1} + \frac{\omega_1}{Q_2})s + \omega_1^2 \omega_2^2 \end{cases}}$$

When the resonant frequencies of the primary and secondary are tuned together and the system is operated at ω_n, the voltage gain equations are those given at the beginning of the chapter, equations 5.8 and 5.9. As previously shown, maximizing these gains occurs when the coupling coefficient is equated to $k = k_{crit} = \frac{1}{\sqrt{Q_1 Q_2}}$. This gives a steady state voltage gain equal to:

$$V_{gain} = \frac{V_{out}}{V_{in}} = -\frac{1}{2} \frac{\omega_n L_2}{\sqrt{R_1 R_2}} \tag{5.41}$$

Practically, the designer is limited in voltage gain by the self-resonant frequency of the secondary coil which, for solenoids whose height is greater than its diameter, goes as

equation 5.39: $\omega_{n,self} = \frac{8.16 \cdot 10^7 (b_2/a_2)^{1/5}}{N_2 a_2}$ [rad/sec]. Substituting this into equation 5.41 above and expressing the inductance in terms of its geometry via Wheeler's formula (equation 5.19) yields:

$$V_{gain,SSS} \approx -40.8 \frac{b_2^{1/5} a_2^{4/5} N_2}{(9a_2 + 10b_2)\sqrt{R_1 R_2}} \tag{5.42}$$

Note that this gain is only valid when the system is operating in the sinusoidal steady state.

The most direct way to build voltage gain is to use more turns on the secondary coil. However, adding turns does increase the length of the solenoid and detracts from its inductance. When modelling the performance of the system, remember that the coil inductance formulas often stipulate that the height of the solenoid must be greater than the radius by some amount for the approximation to hold. As the loss terms in the denomenator are rooted, increasing the turns on the inductor, N_2, should still increase the voltage gain as the resistive losses are low for low frequencies. At higher frequencies, however, expressions for the loss terms are multiplied by the skin depth multiplier Φ_{AC} and the proximity multiplier, Φ_M such that the adding more turns may not yield increased voltage gain.

5.3.2 Design Tradeoffs for a Set Frequency and Input Impedance

If the Tesla coil is part of a larger system, it is important to match the operating characteristics of the preceding and following system to those of the Tesla coil for efficient operation. The operating frequency of the Tesla coil should be set equal to that of the other system and the coil's input impedance should either match that of the preceding system for impedance matching or be much greater to minimize loading. If the input and output impedances wish to be tailored using these Thevenin equivalent impedance formulas, the system *must* be operated in the sinusoidal steady state.

Using the input impedance formula in equation 5.11 and expressing the quality factors in terms of their constitutive elements yields:

$$Z_{in} = R_1 (1 + k^2 \frac{\omega_n^2 L_1 L_2}{R_1 R_2}) \tag{5.43}$$

This expression can be expanded as:

$$Z_{in} = R_1 + k^2 \frac{\omega_n^2 L_1 L_2}{R_2} \tag{5.44}$$

If the input resistance must be as small as possible, there are several options to achieve this. If it is feasible to have a very large secondary coil resistance, then the value of R_2 can be made as large as desired, yielding $Z_{in} \approx R_1$. This is at the expense of a large Q_2. Increasing R_2 will degrade coil performance, introduce large damping, and limit voltage gain. Otherwise, the coupling coefficient, k, can be made very small (less than 0.01), although this will require some amount of physical spacing to achieve this little coupling. Orienting the coils such that the flux from each coil is propagating orthogonally to one another may allow the coils to be brought closer together while achieving the same low coupling.

If the input resistance needs to be reasonably insensitive to the secondary parameters, it is necessary to constrain the coupling coefficient. Substituting $k_{crit} = \frac{1}{Q_1 Q_2}$ for k in the input impedance equation 5.43 gives:

$$Z_{in} = R_1 + R_1 = 2R_1 \tag{5.45}$$

With the constraint $k = k_{crit}$, the input impedance appears to only be sensitive to the resistance of the primary circuit. The price for this is keeping k matched to k_{crit}. This is difficult to do in practice unless the primary voltage waveform is monitored for a single zero crossing of its envelope function. This signifies that $k \approx k_{crit}$ as long as the quality factors are approximately equal, the two circuits are tuned to ω_n, and the system is operating in the sinusoidal steady state.

If a specific input impedance, Z_{in} is desired, it is necessary to tailor the inductances of the primary and secondary coils to match this. Rearranging the input impedance equation gives:

$$(Z_{in} - R_1)R_2 = k^2 \omega_n^2 L_1 L_2 \tag{5.46}$$

This equation shows a marked asymmetry between the effects of the primary and secondary resistors. If the secondary coil has a self resonant frequency, ω_n expressible as equation 5.39, then geometric parameters can be used to express ω_n, L_2, and give an approximation to R_2. This leaves L_1, R_1, and k as free parameters.

5.3.3 Design Tradeoffs for Time Domain Output Waveforms

As seen in a previous chapter, the voltage across the secondary coil, $v_{out}(t)$, can be controlled by the selection of certain circuit constraints. One way to tailor an output waveform is to follow a sequence of selection steps. The steps presented here are applicable only if the system is driven with a pulse, not if it is driven in the sinusoidal steady state.

1. Number of beats
2. Number of waveform cycles inside each beat
3. Time to secondary voltage peak
4. Magnitude of secondary output voltage peak

To restate previous definitions, the ratio $\gamma = \frac{k}{k_{crit}}$ approximates the number of beats that occur before the system decays to less than 5% of its peak output voltage through the following equation:

$$N_{beats} = \frac{6}{\pi}\frac{\sqrt{Q_1 Q_2}}{Q_1 + Q_2}\gamma \tag{5.47}$$

For $Q_1 = Q_2$, this equation reduces to the familiar $N_{beats} = \frac{3}{\pi}\gamma \approx \gamma$. A beat, as previously defined, is the result of the bounding envelope that governs the shape of the time domain response. The response waveform between two zero crossings (one half of a complete envelope cycle) is termed one beat.

Determining the number of waveform cycles that occur within each beat gives k according to the relation: $N_{cycles} \approx \frac{1}{k}$. The product of the number of beats and cycles yields:

$$N_{beats} N_{cycles} = \frac{6}{\pi}\frac{Q_1 Q_2}{(Q_1 + Q_2)} \tag{5.48}$$

which for $Q_1 = Q_2$ approximates to $N_{beats} N_{cycles} \approx Q$. These results are further explained in Chapter 3, section 3.

Determining the time to the output voltage peak of the secondary response requires taking a derivative of the bounding envelope function that describes the secondary response. Solving this derivative equal to zero gives t_{peak}, the time when the secondary achieves a maximum voltage, as shown in equation 5.16.

$$t_{peak} = \frac{2}{\omega_{upper} - \omega_{lower}} \tan^{-1}\left(\frac{2Q_1 Q_2(\omega_{upper} - \omega_{lower})}{\omega_n(Q_1 + Q_2)}\right) \tag{5.49}$$

With the substitution of equation 5.48, this can be expressed as:

$$t_{peak} \approx \frac{2}{\omega_{upper} - \omega_{lower}} \tan^{-1}\left(\frac{(\omega_{upper} - \omega_{lower})N_{beats}N_{cycles}}{\omega_n}\right) \tag{5.50}$$

Practically, as the time to peak goes inversely as the self-resonant frequency, ω_n, this time can be scaled arbitrarily by setting ω_n. If the Tesla coil is set to discharge at this output voltage peak, then this t_{peak} is best thought of as a time delay between input pulse and output voltage peak.

The value of the secondary output voltage peak magnitude at time $t = t_{peak}$ is given by the following equation, repeated from equation 5.15:

$$V_{out,max} = V_{in}\sqrt{\frac{L_2}{L_1}}e^{-\frac{\omega_n(Q_1+Q_2)}{4Q_1Q_2}t_{peak}} \sin\left(\frac{\omega_{upper} - \omega_{lower}}{2}t_{peak}\right) \tag{5.51}$$

Substituting in equation 5.48 in the exponential yields:

$$V_{out,max} = V_{in}\sqrt{\frac{L_2}{L_1}}e^{-\frac{3\omega_n}{2\pi N_{beats}N_{cycles}}t_{peak}} \sin\left(\frac{\omega_{upper} - \omega_{lower}}{2}t_{peak}\right) \tag{5.52}$$

The exponential in this expression is sensitive to approximations; using a Taylor series to of less than 5^{th} order to express t_{peak} will result in significant errors.

5.4 Adjusting for frequency mismatch

Meeting the condition that the self resonant frequencies match, $\omega_1 = \omega_2$, is extremely difficult to achieve in practice. Variations in the atmospheric humidity or temperature effects can change the values of the parasitic resistances, the capacitances of the components, and even the coupling between the inductors. Thus, it is important to find methods to determine when the two frequencies are "close enough". One method is to manually tune the coils using a variable capacitor, another is to use an electrical feedback loop, such as a phase locked loop, to control the resonant frequencies.

While it is possible to also change the primary or secondary inductance by adding a permeable material inside of its coil form, this will also affect the secondary coil's effective inductance as well as its own self-resonant frequency. Altering the resonant frequency should not include altering the coupling coefficient, k or the critical value, k_{crit}. This implies that

the capacitance is probably the best component to vary to achieve matched resonance.

5.4.1 Constructing a coil with a specific k

The goal of this section is give procedures for getting k close to a desired value, specifically k_{crit}. While $k_{crit} \equiv \frac{1}{Q_1 Q_2}$, this is only a number, not a method to find k or adjust it to equal k_{crit}. The parameter k falls from the definition of the mutual inductance between the primary and secondary coil, $M = k\sqrt{L_1 L_2}$. It is a measure of the amount of flux linking the coils to one another.

One easy method to find k_{crit} experimentally is to count the number of beats in the output time domain response, assuming the Q's are relatively equal. Remember that the number of beats seen before decay goes as: $N_{beats} = \frac{6\sqrt{Q_1 Q_2}}{\pi(Q_1+Q_2)} \frac{k}{k_{crit}}$, which approximates to $N_{beats} \approx \frac{k}{k_{crit}}$ for Q's of the same order of magnitude. This method only works for a pulse driven system.

If the system is operating in the sinusoidal steady state, then the easiest way to find k_{crit} is to observe the secondary voltage waveform. It reaches a maximum for $k \approx k_{crit}$, although the change in voltage gain around $k \simeq k_{crit}$ is minimal.

These procedures do not work if the primary and secondary are not tuned within a few percent to the same resonant frequency. If the coils are mistuned, there is no simple procedure for determining k or when $k = k_{crit}$ save through measuring flux and watching for peaks in the output voltage waveform, although they may be misshaped beats.

5.5 Design Example

This design example illustrates the process presented in the above sections. The specification for this design is:

- $10kV$ secondary voltage output
- Output frequency of 1MHz
- 10 waveform cycles per beat on the secondary output
- 2 beats on the secondary output

First, it is assumed that the system has no external loading. Furthermore, by specifying a specific time domain output response, a pulse driven system is implied. Because the output

waveform must resonate at 1MHz, the secondary coil must be constrained to resonate at $\omega_n = 2\pi \cdot 1\text{MHz}$. Since this system is being driven with a pulse, it is impossible to have the secondary response ring at any frequency other than ω_n. Using the empirical relation in equation 5.39 gives:

$$N_2 a_2 \approx \frac{8.16 \cdot 10^7}{\omega_{n,self}} = 13.0 \tag{5.53}$$

Assuming a size constraint on the secondary coil radius, a_2 of 5cm. This gives $N_2 = 260$ turns. There is no constraint on the length of the coil as there may need to be spacing between successive turns. If no spacing is allowed, then the length of the coil is the product of the total insulated wire diameter and the number of turns, N_2. An 18 gauge wire, a common magnet wire used in transformers but small for Tesla coil use, has a diameter of 0.001m and has a typical insulation thickness of 5mils, for a total wire diameter of 0.00125m. The coil length is $b_2 = 260 \cdot 0.00125\ m = 0.325$ meters. The voltage per turn that the insulation must withstand is now: $\frac{10kV}{260} = 39\text{V}$ which is completely reasonable for 10mils of insulation between conductors. Using Wheeler's formula (equation 5.19) gives $L_2 = 1.8\text{mH}$ and using the constitutive relation for resonant frequency ($\omega_n = \frac{1}{\sqrt{LC}}$) gives $C_2 = 14.1\text{pF}$.

Next, there should be 2 beats each with 10 waveform cycles apiece. It is thus desired to have 5 cycles before the secondary voltage peaks. This constrains k via $N_{cycles} = \frac{1}{k}$ yielding $k = 0.1$. Assume that $Q_1 \approx Q_2$ such that $N_{beats} = \gamma = \frac{k}{k_{crit}}$ fixing $k_{crit} = 0.05$.

The output voltage of 10kV peak specified is not a gain, hence there is some flexibility in the size of the input voltage source. It is desired to keep this input voltage source as small as possible over the parameters determined thus far. The maximum voltage possible is:

$$V_{out,max} = V_{in}\sqrt{\frac{L_2}{L_1}}e^{-\frac{3\omega_n}{2\pi N_{beats} N_{cycles}}t_{peak}} \sin(\frac{\omega_{upper} - \omega_{lower}}{2}t_{peak}) \tag{5.54}$$

where t_{peak} is found by noting that if it takes 5 waveform cycles of the secondary output to reach a maximum and each cycle takes 2π radians to complete, then it will take approximately $t_{peak} \approx \frac{10\pi}{2\pi \cdot 1MHz}$ or 5μseconds for the secondary output waveform to reach its peak. This value of t_{peak} gives a numeric value:

$$V_{out,max} \approx V_{in}\sqrt{\frac{L_2}{L_1}} \cdot 0.472 \tag{5.55}$$

For an input magnitude of $V_{in} = 10V$, the ratio of inductors is constrained to: $L_2 = 2.18 \cdot 10^6 L_1$. As $L_2 = 1.8\text{mH}$, then $L_1 = 0.83\text{nH}$. Knowing the primary inductance and assuming no stray capacitance in the wiring of the primary, the maximum value of the primary capacitor is $C_1 = 30.7\ \mu\text{F}$.

The individual values of the quality factors are unimportant here so long as their product is constrained to $Q_1 Q_2 = \frac{1}{k_{crit}^2} = 400$ and they are within the same order of magnitude. This is reasonable considering the large resistance of the secondary coil due to the high frequency of operation. The resistance for the 18 gauge wire selected for the secondary is: $R_{DC} = 1.75 \cdot 10^{-4}\ \Omega$ while $\Phi_{AC} = 379$ and $\Phi_M = 1.93$ giving a net secondary coil effective resistance at 1MHz of $R_2 \approx 0.13\ \Omega$. This yields $Q_2 \approx 87$. This is most likely an upper bound to the secondary coil performance.

The use of smaller gauge wire (larger diameter), such as 10 or 12 gauge, would allow for higher quality factors at 1MHz or higher resonant frequencies. However, coils using such large wire are typically large themselves, usually much longer than the secondary coil length $b_2 = 0.325$ meters seen in this example.

Chapter 6

Switching Needs for Frequency and Phase Control of Coupled Resonant Systems

With the behavior of the coupled resonant system described, it remains to drive and control the system such that it produces the desired behavior. While there exist a variety of methods to drive the system, the two methods discussed here are the pulsed and sinusoidal steady state input. Briefly, the pulsed input "kicks" the system such that it self resonates and decays. In the sinusoidal steady state, discussed by Terman [1] [32] [33], the system may be used as a radio frequency amplifier for continuous communications signals.

Another use of the coupled resonant circuit is to coordinate the operation of multiple sets of coupled resonant systems to produce a phased antennae array. By controlling the relative phase of each antennae's output, the net output of electromagnetic energy can be directed to a specified location. For example, many commercial radio stations use multiple phased antennaes to direct the broadcast signal to their coverage regions.

This chapter first explores the methods of driving an individual resonant system. This is followed by methods of frequency and phase control that allow for multiple coils to be linked in parallel to create a phased array.

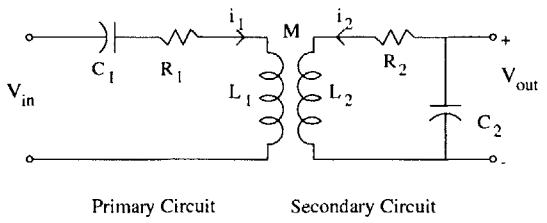

Figure 6-1: Schematic of coupled system configured for driven oscillations at ω_n

6.1 Method of Driving System with Forced Oscillations

Driving the system under the constraint of a forced oscillation requires the primary and secondary circuit to be tuned to the same self resonant frequency as the driving sinusoid frequency. This method of driving the system is precisely how high power radio frequency amplifier transformers operate. In this case, the circuit topology is shown in Figure 6-1. With this method of drive, there is no need for switches in the coupled circuit.

To minimize losses, it is prudent to select a coupling coefficient $k < k_{split}$ so that the two resonant frequencies, ω_{upper} and ω_{lower} converge on ω_n. When the quality factors are approximately equal, the voltage gain of the system is maximized when this driving frequency is equal to the self resonant frequency, ω_n. The details for this reasoning are explained in the resonance chapter in the frequency domain derivation.

6.2 Method of Driving System with Pulse Drive

In order to drive the system with a pulse input, it is necessary to have a circuit topology similar to that shown in Figure 6-2.

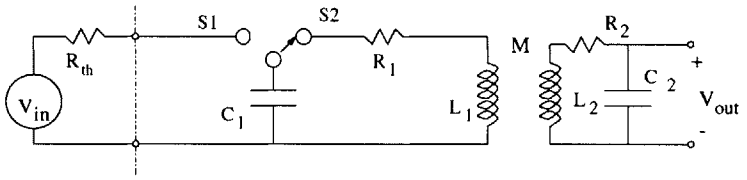

Figure 6-2: Idealized Switched Circuit for producing impulses

The single switch is required to excite the system with a step drive. The switch is located on the primary and first connects an external voltage source to charge the primary capacitor,

C_1. As all voltage sources can be modelled as a Thevenin equivalent source with a source impedance, the primary capacitor will take some time to fully charge, $t_{charge} \approx 5R_{th}C_1$. Charging for five time constants gives a voltage across the capacitor that is approximately 99% of the voltage source terminal voltage. It is important that the primary capacitor have as large a quality factor as possible. If the dielectric has an equivalent leakage resistance of $100M\Omega$, the leakage current when the capacitor is charged to $100V$ is 1μA.

After the primary capacitor is charged, it is switched to the primary coil. This allows the capacitor to discharge through the primary inductor and is the equivalent of a series step drive.

6.2.1 Selection of Switch Topology

There are different types of switches; some manually activated, some electromechanically activated. Examples of a manual switches include push-button switches, mechanical sliders, and contact switches and relays that are energized by the user. One advantage in using these types of switches is the comparatively large current and power ratings they have for a given size. Some disadvantages are switch bouncing, slow activating times, and corrosion on the switch contact surfaces. Switch bouncing describes the action that occurs when the user actuates the switch, the switch moves to make contact with the plate, but during the process, several small, high frequency intermittent contacts occur. This could be due to corrosion on certain parts of the electrode surface interfering with the connection, physical deformations of the switch surface, or mechanical vibration or wiggle of the contacts before solid electrical contact could be made. Corrosion of the switch electrode surfaces is due to environmental conditions if the switch internals are not hermetically sealed as well as chemical effects due to the metallurgy of the electrodes themselves. When the two electrodes approach one another, an electrical arc is created that electrically connects the two electrodes. The electrodes are heated due to this arcing and metal and contaminant ions move between them. Essentially, one electrode electroplates the other resulting in electrode surfaces that are irregular and of varying resistance.

One way to minimize these effects is to use wetted relays. Relays function conceptually in a similar manner to solenoids. When the relay coil is energized, an electrode inside the coil is magnetically moved to physically connect with the opposite electrode. Relays suffer from the same bounce and corrosion problem as mechanically actuated switches, but a type

of relay called a wetted relay uses fluid motion to create contacts between two electrodes. Fluids do not suffer from bouncing problems and greatly mitigate problems due to corrosion and contamination. Mercury wetted relays use mercury in a glass tube to enhance the electrical contact between two electrodes when activated by the relay coil. Mercury switches are useful in that they can handle comparatively large current densities and have a very low on-state resistance, usually less than a tenth of an ohm. However, mercury is toxic to people, harmful to the environment and the relays themselves are expensive and must usually be oriented in a certain fashion to work properly. Furthermore, even though relays are electrically controlled via the energizing coil, these relays cannot be operated above about $50 - 100$Hz. They are acceptable for manually actuated inputs.

Electrically actuated switches include most solid state devices as well as solid state relays that can be driven at above 100Hz. Examples of solid state switch components are BJT's, MOSFET's, IGBT's, SCR's, diodes, and a host of emerging p-n junction semiconductor devices. These devices can be used individually or in combination to create switches that meet certain criteria. The choice of which devices to use to construct a switch depends on the direction and magnitude of the voltages and currents involved and the desired switching speed.

Figure 6-3 shows the requirements of the two switches required for pulsed, self resonating operation. The graphs represent the ideal electrical behavior of the switch when in the state indicated.

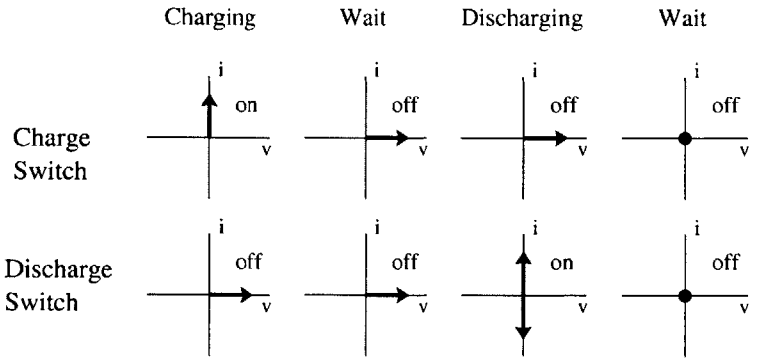

Figure 6-3: Diagram showing voltage and current direction requirements for switch implementation.

The charging switch, the switch located between the voltage source and the primary

capacitor, is responsible for charging the capacitor up to rail voltage. When in the charging state, only this switch is on, allowing charge to flow only onto the capacitor through whatever Thevenin equivalent resistance is inherent to the voltage source and the on-resistance of the switch. Thus, for the capacitor to charge to 99% of the voltage source, the switch must stay on for at least five time constants or $t_{charge} = 5C_1(R_{on} + R_{thevenin})$. This assumes that the equivalent series resistance (ESR) of the capacitor does not have an appreciable effect on the capacitor. If the capacitor is lossy, i.e. has a large ESR, the voltage across the capacitor will be dissipated through this parasitic resistance, generating heat. Thus, it is important to use a high-Q capacitor with ceramic, mica, or polypropylene as a dielectric.

The vertical arrow on the top leftmost plot signifies that when the charging switch is in this state, it is ON, there is ideally no voltage drop across it, and it only conducts current in the forward direction, defined to be from the voltage source to the capacitor. The discharge switch shows a positive voltage, implying that it conducts zero current but must withstand a positive voltage while in the OFF state. Realistically, there will be some voltage drop across the charging switch and some leakage current through the discharge switch. The first wait state is solely to allow the charging switch to turn off before the discharge switch turns on. Both switches *cannot* be on at the same time.

If the switches are electromechanical relays, this first wait state may take on the order of milliseconds or even seconds. If the switches are solid-state devices, this transition can take tens of nanoseconds or microseconds for FET or BJT devices, respectively. The transition time is also influenced by the voltage and current conditions the switches are expected to carry. The specification sheet for the device used will plot the turn on and turn off times under specified conditions.

While it is important to wait for the charging switch to fully turn off before activating the discharge switch, the longer the capacitor is allowed to wait before discharge, the more voltage will be dissipated due to discharge through the parasitic leakages. Once the discharge switch is turned on, the positive voltage arrow on the charge switch shows that it must not conduct current and must block a positive voltage between the voltage source and the RLC network. The positive and negative going current arrows on the discharge plot for the discharge switch imply that there should be no voltage drop across the switch and the current must be able to conduct in either direction.

The final wait stage occurs only after the system is done discharging, usually after a

time $t_{discharge} = 5\tau_{eff}$ discussed in previous chapters. The discharge switch can be opened before this time, but after five time constants, the system has no energy left to radiate or dissipate. This wait state allows the discharge switch to open before the charging switch closes to charge the primary capacitor again. The unacceptable case of having both switches closed simultaneously has already been discussed.

These plots showing the requirements for the two switches are derived from the requirements and behaviors of the system. Realizations for these sets of requirements are shown in Figure 6-4. The devices used in these switch implementations are suggestions, not requirements. [8, chapter 4] These are the more commonly used switches in switched mode power supplies. There are a number of combinations of available semiconductor devices that could duplicate these functions.

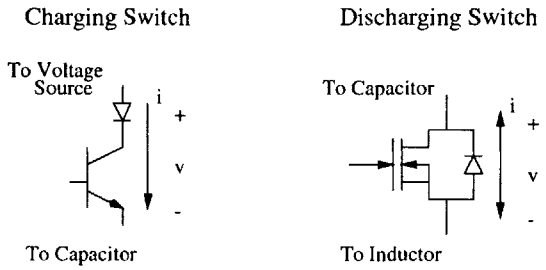

Figure 6-4: Schematic showing possible solid state switch solutions.

6.2.2 Controlling the Switches

For a given set of switches, it remains to find a method to control them. Unless the switches are intended to be switched manually, either by push-button or a throw lever, the switches will need some automated means of operation and a clock to control the timing of their opening and closing. This thesis will only explore electrical control.

Figure 6-5 shows the timing pulses that are used to drive the gates of the transistors used in the switches. This timing scheme could be synthesized by a digital control system such as a pulse-width modulation clock.

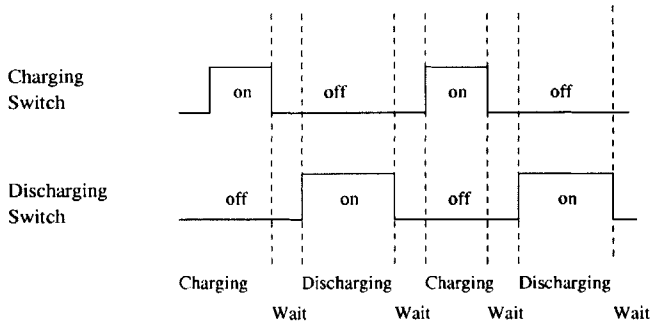

Figure 6-5: Diagram of pulses used to control the switches.

6.3 Controlling the Phased Array

With the primary switching drive and control electronics established for one coupled resonant system, it is possible to build a phased dipole array whereby the primary and secondary circuits of each coupled system oscillating at the same frequency, ω_n. The output radiation pattern from the secondary coils superimposes to create an effective antennae gain pattern that is controlled via the relative phase of the output (secondary) coils to each other. This phenomenon is precisely how radar transmitters and radio broadcasts operate. [31]

Theory of Dipole Arrays

Dipole arrays are used to focus the transmission region of straight wire antennaes. With a single standard antennae, the electromagnetic radiation pattern is produces is uniform in the theta direction around the antennae. This is called omnidirectional transmission. By arranging several straight wire antennaes in a geometric arrangement, usually a line, the net electromagnetic radiation pattern seen by a receiver changes. This radiation pattern is heavily dependent on the distance between the transmitting antennaes and their signals phase relative to each other. These signals add linearly when they intersect. If one signal is 180^o out of phase with the other at a point, they effectively cancel. Any receiver positioned at this cancellation point sees no energy and hence no net signal from the two transmitters.[31, page 438] Of course, the antennaes do not need to be straight; helical antennaes can be made to work in a similar fashion.[31, page 420]

Equation 6.1 describes the gain pattern associated with lossless dipole arrays.

$$Gain(\theta, \phi = 0) \sim \sin^2(\theta) \frac{\sin^2(\frac{N}{2}(\Phi + ka\sin(\theta)))}{\sin^2(\frac{1}{2}(\Phi + ka\sin(\theta)))} \tag{6.1}$$

where N is the number of dipole antennaes present in the array, a is the distance between the antennaes in meters, Φ is the relative phase shift between two adjacent output waveforms of the antennaes, and k is the wave number given by $k = \frac{\omega_n}{c}$. The location of the gain peaks is given by solving for a maximum theta such that $\theta_{max} = -sin^{-1}(\frac{\Phi}{ka})$. If the phase Φ is not constant during output, the peak locations of θ_{max} will change over time.

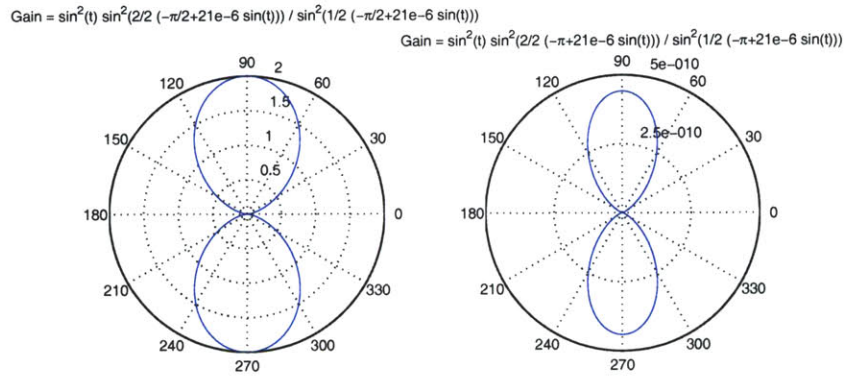

Figure 6-6: Plot of the radiation pattern of two ideal dipole antennaes. The difference between the left and right plots is the relative phase difference of the two outputs. Parameters: $N = 2$, $ka = 21E - 6$, and $\Phi = 90^o$(left) or 180^o (right).

Figure 6-6 shows the far-field gain pattern for two antennaes arranged in a dipole array. The leftmost plot shows the gain pattern for a relative phase shift of 90^0 while the rightmost plots gives the gain pattern for a phase shift of 180^o. Notice the dramatic drop in the gain of the rightmost plot due to this phase shift. The parameters describing these gains are $N = 2$, $\Phi = \frac{-\pi}{2}$ [rad], $k = 2.1$ [meters/rad] (such that $\omega = 2\pi \cdot 10^5$[rad/sec], and $a = 0.5$ [meter]. Note that the two dipoles are arranged on the 0^o to 180^o line on either side of the origin. While the gain pattern is plotted on a 2-D surface, the gain pattern of the dipole array is actually shaped similar to a toroid extending out of the page.

6.3.1 Frequency and Phase Control Using Feedback

While matched inductors and capacitors are easy to propose in theory, they are virtually impossible to build in practice. There will be some degree of frequency mismatch between the primary and secondary coil and between the coils of other systems in the phased array. To correct for these differences, some form of feedback must be used. The feedback could take the form of a variable capacitor attached in parallel to the existing capacitor or simply as a ground plane that can be moved relative to a secondary coil (useful in high voltage settings). The only caveat with using feedback is that some reference must be used. The reference could be a desired frequency that all primary and secondary circuits are tuned to. It could also take the form of a designated "master" coil to which all other resonant circuits are matched.

Once the frequencies of the coils match, in order to set the relative phase of their outputs to construct a phase array, it is necessary to control the relative timing of the activation of the switches in the master and slave circuits. At a set frequency, suppose 100kHz, a time delay of $0.833\mu s$ between the switch activation pulses of the master and slave resonant systems corresponds to a phase delay of 30^o ($\frac{\pi}{6}$ radians) between the output waveforms of the master and slave secondary coils. This relationship is more generally expressed in equation 6.2. The units of time delay are seconds; the units of phase delay are radians.

$$Time\ Delay = \frac{Phase\ Delay}{\omega} = \frac{Phase\ Delay}{2\pi f} \tag{6.2}$$

Thus, a scheme of controlling the relative phases of the secondary waveforms can be realized by implementing a time delay between switching pulses between the two primary circuits. Figure 6-7 shows a diagram of how a phased array system with two coupled systems is made to work. Effectively, the relative phases of the outputs is assumed to be equal to the relative phases of the timing signals. This requires that there be minimal fluctuations in the steady-state turn-on and turn-off times of the switches and that the timing pulses, once set to a delay, do not drift. These assumptions can be removed or greatly reduced by implementing more electronic control over the system.

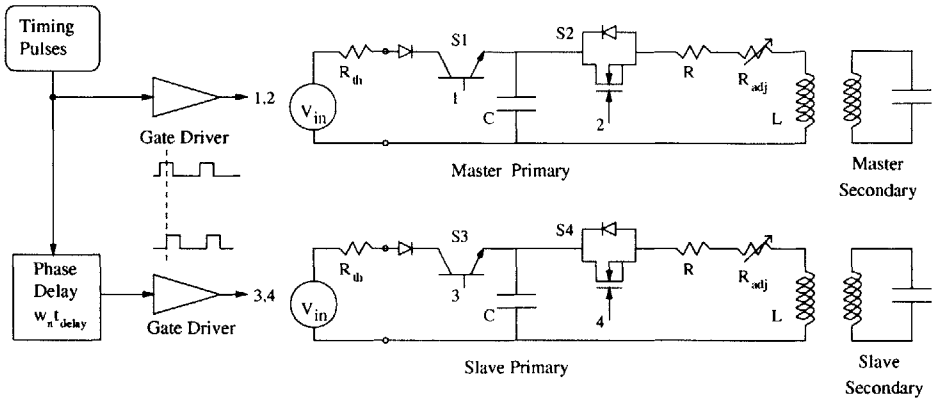

Figure 6-7: Diagram of phased array control scheme. Only one pulse train is shown for simplicity; matching timing pulses are delayed by an amount $\omega_n t_{delay}$

6.3.2 Frequency Control and Matching

Controlling the relative phase delays of the system assumes that the output frequencies are equal. However, each of the four second order systems in Figure 6-7 will ring at a slightly different frequency. One solution to this is to manually tune all other coils after measuring the response of the master secondary coil. However, if the ambient environmental conditions, such as temperature or humidity change or the electromagnetic fields in the room alter due to nearby interference, the coils will change their natural resonant frequency, ω_n. The solution to this is to introduce a feedback circuit that compares the frequency of the master secondary coil to the frequency of another secondary coil, altering its resonant frequency until the two coils match. While there are a handful of ways to accomplish this, one method is to use a phase locked loop.

A phase locked loop, PLL, is a feedback circuit that adjusts its output to a controllable oscillator such that the its frequency exactly matches the frequency of the external input source. The adjustment is made by matching the two oscillations so they remain in phase. Digital and some analog FM radio tuners often use a phase locked loop for improved sound quality.[5]

There are three main components of a phase locked loop system, illustrated in Figure 6-8. The first component is the phase/frequency detector or discriminator (PFD), which is responsible for comparing the two input frequencies and their respective phases. This block outputs a voltage that is proportional to the difference in frequencies or phases, depending

on the specific device used. The second block is a filter, usually a low pass filter that is responsible for correcting for gradual frequency and phase distortions in the received carrier signal. The output is again a voltage that feeds into a voltage controlled oscillator, commonly called a VCO. The VCO is a device that outputs a signal whose frequency is proportional the input voltage. This frequency is feed back into the frequency discriminator. The loop drives itself such that the VCO output frequency is matched to the input reference frequency.[9]

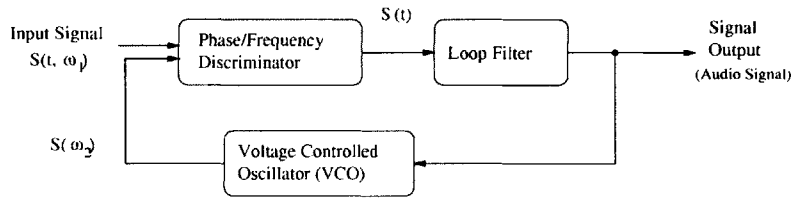

Figure 6-8: Diagram of a generalized PLL loop used in RF applications.

While the topic of phase locked loops spans a breadth of knowledge and applications, it is sufficient to mention here that it is possible to adapt these components into the existing resonant system design. While most PLL integrated circuits incorporate frequency scaling and channel allocations useful in telecommunications and RF applications, these features are useless in this setting. With an appropriate phase/frequency discriminator that contains a four-quadrant multiplier (see the AD9901 specification sheet [3]) and a passive low pass filter to remove the frequency content at approximately ω_n and $2\omega_n$, the frequency feedback system can be implemented. The voltage controlled oscillator (VCO) for our case of a second set of coupled resonant circuits, is the slave resonant coil. To control an LC oscillator via an applied voltage requires the use of a controllable capacitor such as a varactor diode. Alternatively, there are digital components that switch in a capacitance for a given applied bias voltage (see the Xicor X90100 specification sheet [40]). The varactor diode is a diode whose junction capacitance is well characterized over a range of applied reverse bias voltages. If the applied bias voltage goes positive, the diode conducts similarly to a normal diode. Figure 6-9 shows how the slave coils are represented in a lumped parameter model. The leftmost inductor and capacitor are the secondary components of a normal coupled resonant circuit. The tuning capacitor is used for manually tuning the coil before operation to achieve near ω_n operation. The varactor is the diode with the capacitor on its tip and is

electronically adjusted in capacitance value by V_{bias}. The blocking capacitor keeps the DC bias out of the inductor as the secondary coils should have no DC value. If the secondary does have a DC value, it will induce voltages in the primary coils that will interfere with the operation of the switches.

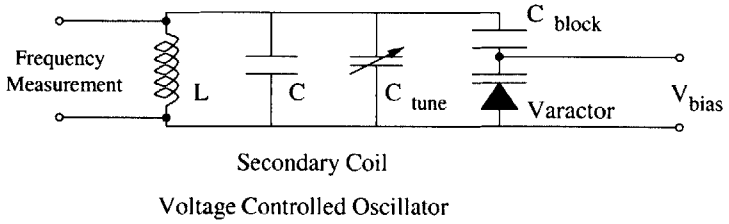

Figure 6-9: Schematic of a secondary coil with a varactor, a voltage controlled capacitor. This circuit is now a voltage controlled oscillator (VCO).

Figure 6-10 shows a diagram of how the frequency matching feedback network works. Even though only the secondary coils are shown, note that all the coils, primary and secondary, could have a feedback network attached to them to keep them locked to approximately the same frequency as the secondary master coil. It is important to keep from loading the coil, however; a high input impedance buffer should be used to avoid distorting the output waveform. A detailed description of how this circuit works will be presented in the following section. For now, the voltage level shifter is used to convert the voltage range from the low pass filter into a corresponding voltage that makes use of the dynamic range of the varactor.

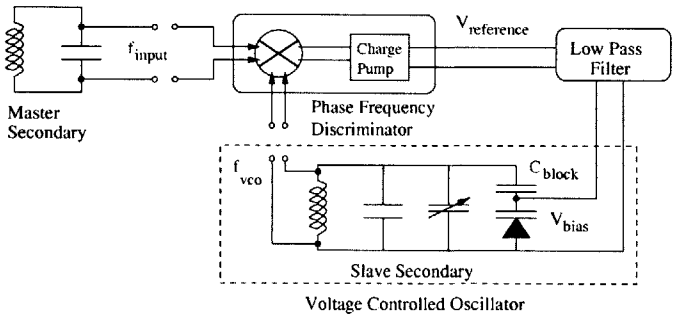

Figure 6-10: Diagram of frequency matching circuit to ensure resonance. Circuit closely follows generalized PLL topology.

Examples of Frequency Matching

The question, for this pulsed system, is how accurate does the phase locked loop need to be? Do the coils need to be matched to within ±1Hz or can they be within 100Hz of one another? The question is a matter of waveform decay time and engineering tradeoffs.

The duration of the output voltage waveform for each input pulse is directly proportional to the quality factor, Q of the system and inversely proportional to the resonant frequency, ω_n. Remembering from the second order systems section that the number of cycles before decay of the output is approximately equal to Q, then the time duration of the output is $t_{output} = 5\tau_{eff} \approx \frac{2\pi}{\omega_n}Q$. Now, if the frequency of another coil deviates from ω_n, by an amount $\Delta\omega$, then the two waveforms are mismatched. While a waveform with a greater frequency will decay faster, assume that the two decay at the same rate (thus, $\Delta\omega \ll \omega_n$). The slave output waveform will get to be 360^o out of phase with the master if:

$$Q\frac{2\pi}{\omega_n} = (Q+1)\frac{2\pi}{\omega_n + \Delta\omega} \tag{6.3}$$

The 360^o phase difference is reflected in the extra cycle (Q+1). Also, the quality factors of both sides are assumed equal. This sets a bound on the frequency deviation:

$$\Delta\omega < \frac{\omega_n}{Q} \tag{6.4}$$

For example, if the master secondary has a $Q = 50$ at $\omega_n = 2\pi \cdot 100\text{kHz/sec}$, then a difference in frequency of 4 kHz yields a 360^o phase difference when the two outputs terminate after 50 cycles. Likewise, a frequency variation of 1kHz yields a 90^o phase difference between the two waveforms after 50 cycles. A generalized formula for the minimum allowable frequency error for a given phase degree error after Q cycles of the secondary master is given by equation 6.5.

$$\Delta\omega \leq \frac{\Phi_{error}}{360^o}\frac{\omega_n}{Q} \tag{6.5}$$

For a resonant frequency of $f_n = 100\text{kHz}$, $Q_{1,2} = 10$, and a desired maximum phase error of $\Phi_{error} = 10$ degrees, the resultant frequency accuracy Δf between the master and slave required is:

$$\Delta f = \frac{10^o}{360^o}\frac{10^5}{10} = 278Hz \tag{6.6}$$

Chapter 7

Building the Coupled Resonators and Control Circuitry

This chapter describes the circuitry used to build a working prototype of the phased array, pulsed resonant system. There were three variants of the system built, one using mechanical, hand-actuated switches to control the charge and discharge cycles. The second used mechanical relays controlled by the timing circuitry. The third variant used timing circuitry and a completely electronic drive method to control the coupled system.

The results of all three variants are recorded in the following sections. The recorded oscilloscope waveforms and data from the mechanically actuated and relay driven system are included with the section describing the properties of the resonant coil and capacitor.

This chapter is divided into five main sections as they pertain to the system construction. The data from the relay and mechanically driven system are incorporated into the fourth section.

- Pulse Timing Circuitry
- Controllable Timing Delay Circuitry
- Switching Devices and Drivers
- Single and Coupled Resonant System Construction
- Tuning and Frequency Feedback Control Circuitry

The circuits and methods used in this chapter are characteristically analog. Much of the control circuitry could be implemented with digital circuitry. Also, the circuit was built on a breadboard, except where indicated, for ease of construction and experimentation. This warranted the use of DIP packaged integrated circuit (IC) chips. Increased operating speed and performance could be attained with the use of surface mount IC's, proper layout on a PC board for decreased parasitic capacitances between traces, and improved isolation between signal and power stages.

7.1 Pulse Timing Circuitry

7.1.1 The LM556 Timer

The timing pulses that control the charge and discharge cycles are generated with an LM556 timer circuit. The LM556 is a dual LM555 packaged in a single IC. It is commonly known as a dual multivibrator in that it uses input pulses to set the delay between output pulses. The frequency and duty ratio of these output pulses are controllable. The details of this output are found in the wiring configuration of the chip, shown in Figure 7-1. This type of application is known as pulse width modulation. This circuit was originally used to control the speed of a fan motor.[22].

For this application, a pulse width modulated clock signal generator found in many switch mode power supplies could be substituted in place of the LM556, but there are two timing pulses needed. In order to keep the two pulses fully controllable in frequency and duty cycle yet locked in relative phase, some manner of feedback, such as a phase locked loop, would be necessary. The method used here to generate the second clock signals uses a more straightforward approach to maintain relative phase control while still allowing user control over the pulse frequency and duty cycle for each pulse.

That there are no leads designated "input" mean that the circuit, when powered on, starts up automatically and generates output pulses. This is accomplished through a technique called bootstrapping, whereby the output is connected back to the input to generate a condition that allows the IC to start correctly – in this case, the output starts out high which charges capacitor C_1 until a large enough voltage is seen by pin 6 (Trigger) to allow the first "input" pulse to be sent to the output. At this point, the circuit operates normally. If the capacitor were charged by the supply voltage rail instead of the output pin of the 555,

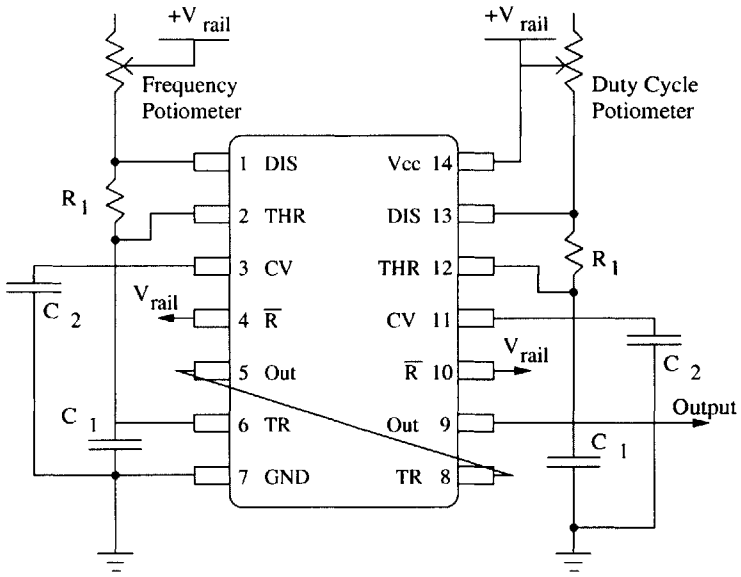

Figure 7-1: Schematic of a 556 dual timer circuit for generating adjustable frequency and duty cycle pulse train

when pin 6 triggered and switched, there would be a current surge through pin 6 to ground while the output was low, possibly destroying the delicate internals of the chip. This surge current is limited to a transient because the output goes low within a few microseconds, depending mostly on the amount of charge in the capacitor. Bootstrapping is not feedback, however, because it is useful only to ensure the circuit starts correctly; traditional feedback uses the output signal to continually change the nature of the input during steady state operation to ensure continued steady state operation.

A discussion is warranted on the pins and their functions on the LM556. Notice also that each side of the LM556 is a complete LM555. Table 7.1.1 outlines the pin functions. For a more complete discussion, see the LM556 specification sheet.[15]

Pin	Function
1	Discharge - Sinks and sources current during pulses
2	Threshold - When voltage reaches a certain level, output pulses
3	Control Voltage - Functions similarly to threshold, used for other applications.
4	Reset - Resets (turns off) the IC when voltage at pin is zero.
5	Output - the output pulses
6	Trigger - Waits for a specific voltage to trigger an output pulse.
7	Ground
8	Trigger
9	Output
10	Reset
11	Control Voltage
12	Threshold
13	Discharge
14	Vcc: +5V supply

The 556 in this application works as follows: it uses the leftmost side of the 556555 to control the frequency of the pulse train while the rightmost 555 controls the duty cycle percentage of the pulses. The duty cycle of the output pulses can span from *almost* zero to *almost* full on. The frequency range is set by the RC network on the leftmost side. The upper frequency limit is due to the slew rates and propagation delays inside the 555 itself. For this particular IC with the components used, the output pulses start becoming slewed when operating above 4MHz.

Consider the left half side of the circuit first. When the circuit is first turned on, the voltage at the threshold (pin 2) is zero because the IC starts out with it internally connected to ground. However, as the trigger (pin 6) is set to respond to voltages less than 1.67V (as per the spec sheet, +5V supply divided by 3) and as it is directly connected to threshold, it immediately disconnects the threshold from ground. Also, when the trigger is less than 1.67V, the output (pin 5) goes high (+5V). The capacitor, $C_1 = 0.1\mu F$, is now charged through the potentiometer (100KΩ max) and $R_1 = 1K\Omega$, for an effective charge time constant of $\tau_{charge} = C_1(R_1 + R_{pot})$. When the capacitor voltage goes high, above 3.3V, the trigger turns off and also turns off the output. The discharge (pin 1) is

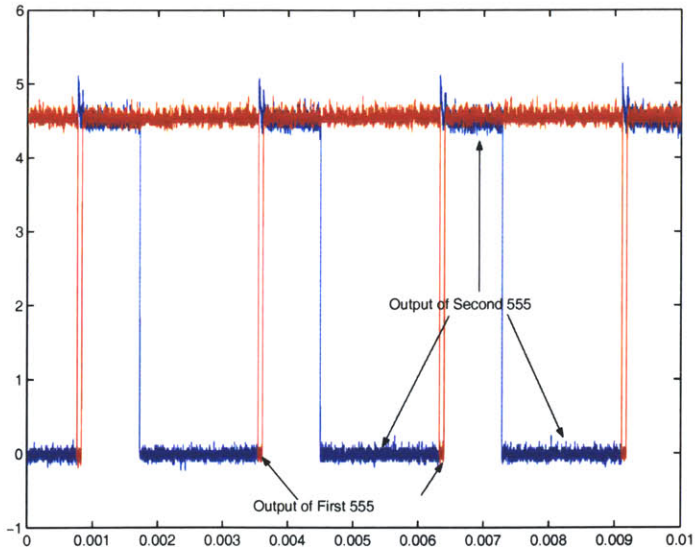

Figure 7-2: Oscilloscope output of the two 555 outputs. The first 555 output controls frequency while the second output controls the duty ratio.

now connected to ground and the charge is removed from the capacitor at a time constant of $\tau_{discharge} = C_1 R_1 = 100\mu s$. Now, the cycle begins; the capacitor discharges to 1.67V, the trigger responds by turning on the output and disconnecting the discharge pin from ground. The capacitor charges up to 3.3V. The trigger pin then sees a high voltage. It responds by turning off the output, connecting the Discharge pin to ground. The capacitor voltage drops back to 1.67V. The cycle repeats indefinitely. By varying the value of the potentiometer, the frequency of charging an discharging and hence the frequency of the output pulses can be regulated. With the frequency of the output pulses determined, it remains to control the duty cycle. With a 56% duty ratio for timing pulse #1 (charging), the repetition charge/discharge frequency is limited to 1.58kHz before the second timing pulse generated by the comparators overlaps the first. Normally, this circuit is run with an $820\mu s$ charge pulse (26% duty ratio), a $780\mu s$ discharge pulse (25% duty ratio) with a period of 3.18ms (314Hz) for each.

The rightmost half of the 556 controls the duty cycle of the output pulses. The circuit here is a mirror image of the left hand side and its operational details are almost identical. However, instead of having the trigger wired to the threshold pin, it is wired to the output of the other 555. The charging and discharging time constants are still set by the equations

before:

$$\tau_{charge} = C_1(R_1 + R_{pot}) \tag{7.1}$$

$$\tau_{dischrage} = C_1 R_1 \tag{7.2}$$

However, the length of the charge cycle determines how long the output pulse stays on before the next pulse comes along, as determined by the frequency of pulses flowing into the trigger (pin 8). If the capacitor charges quickly, i.e. a small value of τ_{charge} and R_{pot}, then the capacitor voltage will quickly reach 3.33V and the output will turn off. If the capacitor charges slowly, i.e. a large value of R_{pot}, then it will take longer for the capacitor to reach 3.33V and the duty cycle will be higher. Note that the duty cycle cannot go above 100%; when the pulse into the trigger goes high as determined by the previous 555, the output of this 555 goes low.

The reset pins, used to turn off the device and reset the system, are tied to the power rail as there is no need to turn the 556 off. Also, the control voltage pin is tied via a 0.01μF capacitor to ground; it is not needed in this application.

Figure 7-3 is a picture of the actual circuit built. Notice the two potentiometers above the LM556 used to control the frequency and duty cycle.

Thus, by using two 555 timers in series, which are conveniently packaged in a single IC, a pulse train with independently determinable frequency and duty cycle can be created. This concludes the generation of one of the two control signals needed to drive the switches. The second control signal could be generated with another 556 IC wired in an identical fashion. However, the relative phase of the two signals could not be easily determined as they would reach trigger and discharge voltages at slightly different times. They would be subject to the internal tolerances of the individual chips and components; there would be no easy way to ensure that the two pulse trains did not have overlapping ON's such that both switches would be on at the same time. The dangers of having both switches on simultaneously are discussed in the previous chapter.

7.1.2 The LM311 Comparator

The solution to this problem could take the form of a phase locked loop or digital logic, but instead a decidedly analog approach was taken. Using the charging waveforms at the

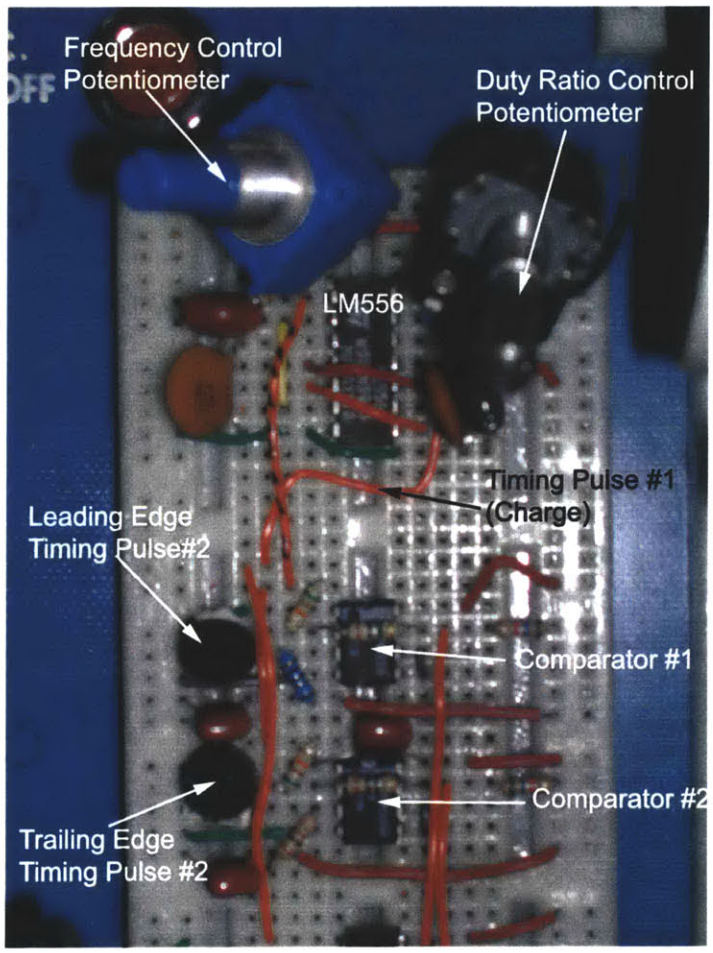

Figure 7-3: A picture of the LM556 and the two LM311 comparators used to generate the timing pulses. The potentiometers on the top left and right control pulse frequency and duty ratio, respectively. The two potentiometers on the left side control the relative spacing between the two pulses.

discharge pins as a reference, a circuit was built that constructed another pulse from the internal 556 waveforms based on different "threshold" values instead of 1.62V and 3.33V used by the internal 556 logic. The discharge pin appeared to be more tolerant to a load than the threshold pin which is why it was chosen.

To construct different threshold points at which to generate a pulse, two LM311 comparators were used. Figure 7-4 shows how they were connected. The input to both comparators is connected directly to the discharge pin (#1) of the LM556. The only difference between the two comparators is the reference voltage applied to the negative input terminal from the resistive voltage divider. This provides the comparator with a voltage at which, when the positive input voltage becomes greater than this reference voltage, the output swings to the supply rail, +5V. The waveforms captured by an oscilloscope in Figure 7-5 illustrates this operation.

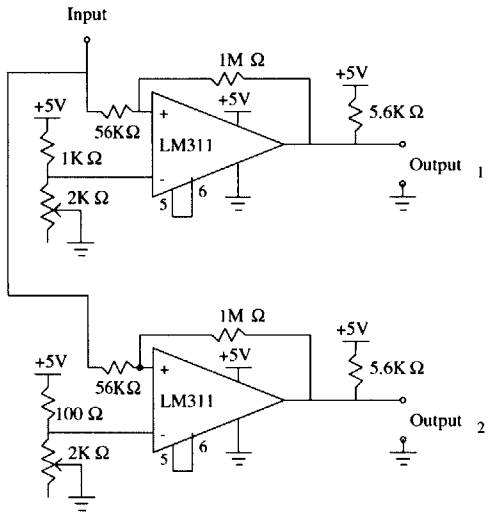

Figure 7-4: Schematic of LM311s used. Note trim and strobe pins 5 and 6 tied together and left floating. Pins 1 and 4 tied to ground.

Essentially, when the input voltage reaches the value defined by the topmost LM311 resistive divider network, the output goes high to +5V. When the input voltage drops below this value, the output goes back to ground. As the reference voltage for each 311 is different, depending on the value of the potentiometer, the output of each 311 will go high at a different point along the charging curve of the input. Thus, there will be some range of voltages for which the top 311 has a high output while the bottom 311 has a low output.

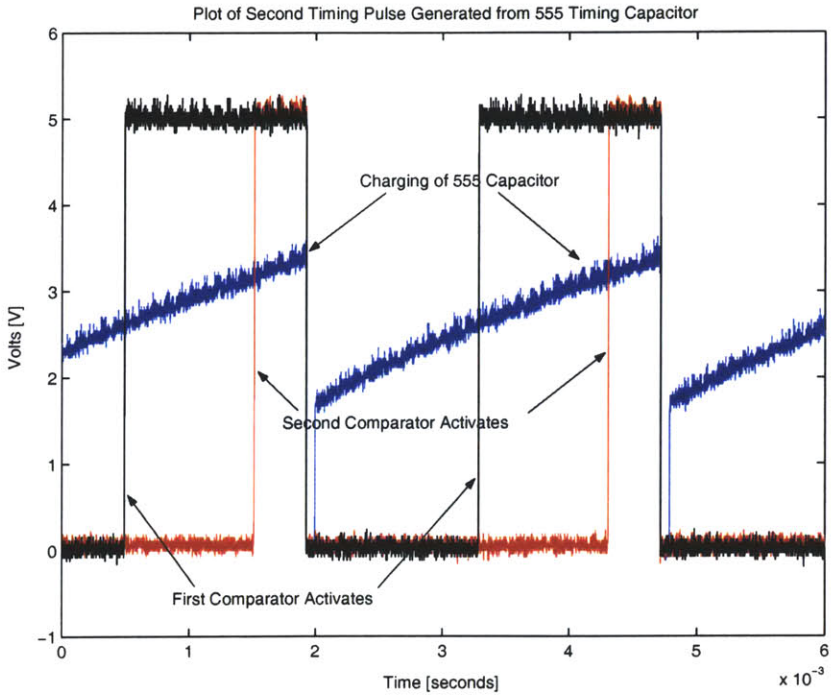

Figure 7-5: Scope waveforms showing the 556 charging waveforms and how they generate they generate the second timing pulse

By using some logic, a timing pulse can be generated by these two waveforms.

A discussion of the operation of the LM311 is warranted. First, a high input impedance relative to the 556 circuit, 51KΩ for this circuit, is necessary so as not to excessively load the input voltage source. If the input is loaded, the frequency of the output pulses of the LM556 timer will fall or become erratic as the discharge pin, when grounded, will try to pull current out of the 311 input. Comparing the input waveform while disconnected and connected to the 311 inputs will immediately show the effects of the 311 input load.

The 1MΩ positive feedback resistor is used for hysteresis. The point of hysteresis is to keep the comparator from acting like a traditional operational amplifier (op-amp). While most linear op-amps use negative feedback to keep their amplifiers working in a linear regime, comparators make use of positive feedback to make its linear regime as small a range as possible. Saturating the output such that it is either at ground or supply voltage is the basis of the comparator's operation. While there is always a very small window of voltages at which the comparator acts like a regular linear amplifier, hysteresis acts to keep

this window as small as possible. For more information regarding the selection of hysteresis resistors and the tradeoffs associated with them, refer to the LM311 specification sheet by National Semiconductor. [14].

Another important and often overlooked point is the output pull up or pull down resistor. For this circuit, a 5.6KΩ pull up resistor is used. Because the LM311 has an open collector output, it cannot pull its output high to the top rail without an external circuit. The benefit of this feature is seen in the application section of the LM311 specification sheet.

7.1.3 The 74HCT86 Quad XOR

The two outputs from the 311 comparators need to be converted into a single timing pulse that does not overlap the timing pulse coming out of the 556 output. The job of keeping the two pulses separate is left to the two potentiometers on the 311 circuits, but the job of converting the two 311 outputs into one timing pulse is left to the quad XOR logic gate, the 74HCT86. The wiring diagram of this IC is shown in Figure 7-6.

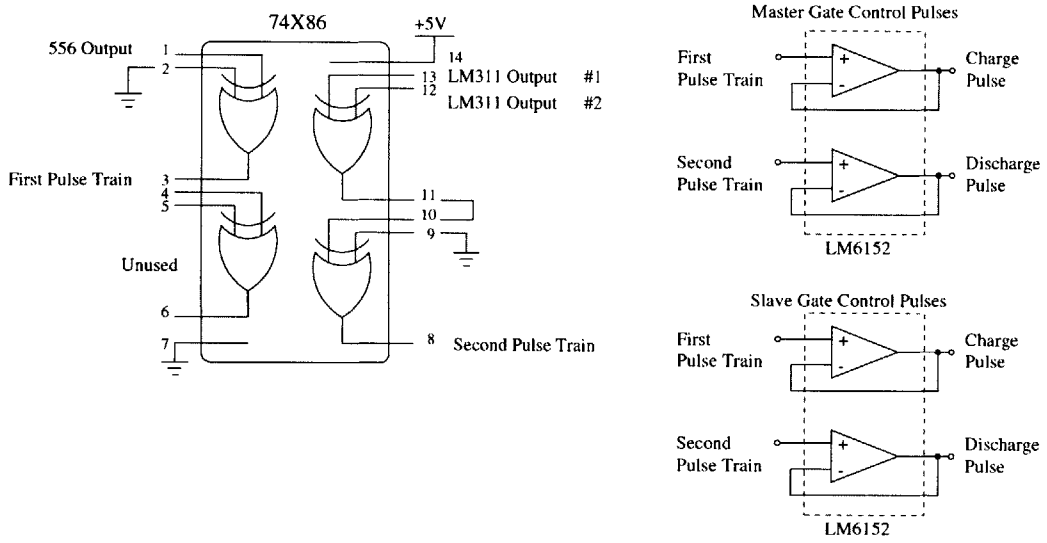

Figure 7-6: Schematic of 74HCT86 quad XOR gate and the buffers it feeds. The buffers carry the signal to the Master and Slave systems. Only three of the four XOR gates are used.

This choice is IC's follows the logic requirements for matching the inputs to the desired outputs, shown in Table 7.1.3. Figure 7-7 gives a pictorial version of this table while Figure 7-8 shows the oscilloscope waveform.

LM311 #1 Input	LM311 #2 Input	Desired Output
HIGH (+5V)	HIGH (+5V)	Low (Ground)
HIGH (+5V)	Low (Ground)	HIGH (+5V)
Low (Ground)	HIGH (+5V)	Don't Care
Low (Ground)	Low (Ground)	Low (Ground)

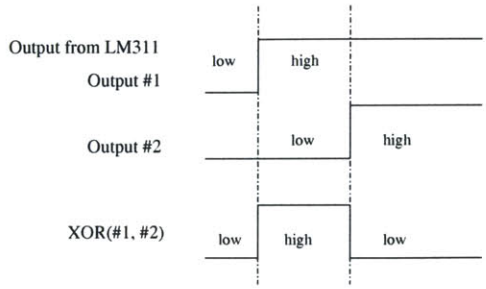

Figure 7-7: Graphical diagram of how the comparator outputs are converted into a timing pulse using the XOR function.

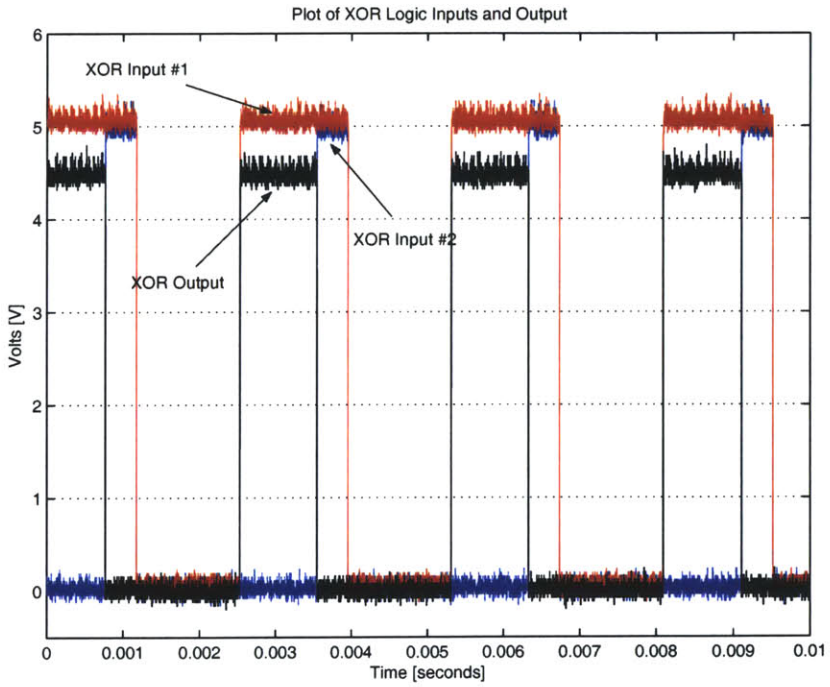

Figure 7-8: Scope waveform showing XOR operation.

The reason both the 556 and the XOR'ed outputs are again XOR'ed is to keep their

output voltages equal. There are many different styles of digital logic; TTL being one type that utilizes a single positive supply of either +3V or +5V. Digital IC's often never give a true +5V output, instead they may output anywhere between 4.25V and 4.85V as seen in the scope waveform. The 74LS logic series of IC's draw relatively large amounts of power and have little tolerance for capacitative loads. The 74HCT logic series has an output stage that can drive a much larger capacitative load.

The two timing signals, after each going through a final XOR are at the same output voltage levels. Figure 7-9 shows the final timing pulses that are sent to the unity gain buffers that feed the delay lines and transistors.

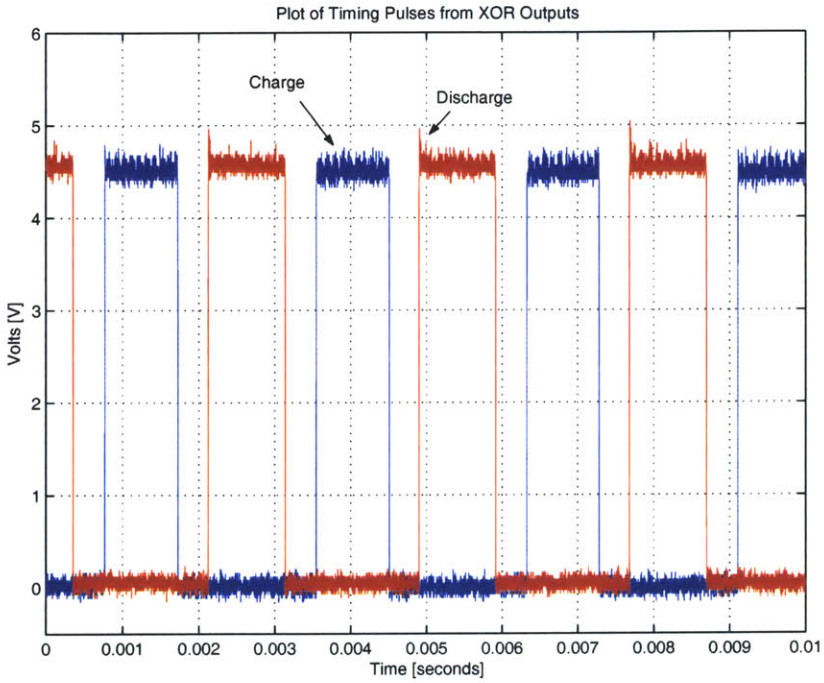

Figure 7-9: Oscilloscope waveforms showing the two timing signals sent to the input buffers of the Master and Slave systems.

7.2 Controllable Time Delay Circuitry

There are three possibilities for purely analog delay lines; one is the bucket brigade series (BBD) of integrated chips, the second is a series of digital delay lines, the third is a capacitor ladder network similar to the BBD but realized in discrete parts or packaged in a delay relay.

This project utilizes the former, the bucket brigade IC, to create a tunable delay lines.[25] The advantage of an analog delay line is that it has an adjustable delay limited mostly by clock skew and the parasitics of the capacitors used to store the signal during the delay. One drawback is the sensitivity of the IC's; they are very sensitive to inter-rail capacitances and parasitics. The digital delay lines, such as the Dallas Semiconductor DS1100 series, come with set delay taps, usually in the nanosecond range which is ideal for high frequency operation. However, adjustable delay tuning is not possible. If slower frequency operation (in the kHz to MHz regime) is required, then analog delay lines are required.

Unfortunately, the original BBD series of chips by Panasonic used for audio signal processing was discontinued when they were bought by another semiconductor manufacturer. Fortunately, another source of BBD chips is available from Visual Sound, Inc., located at www.visualsound.com. They sell the MN3207 analog delay IC and the MN3102 timing IC. No other source for new BBD IC's is available.

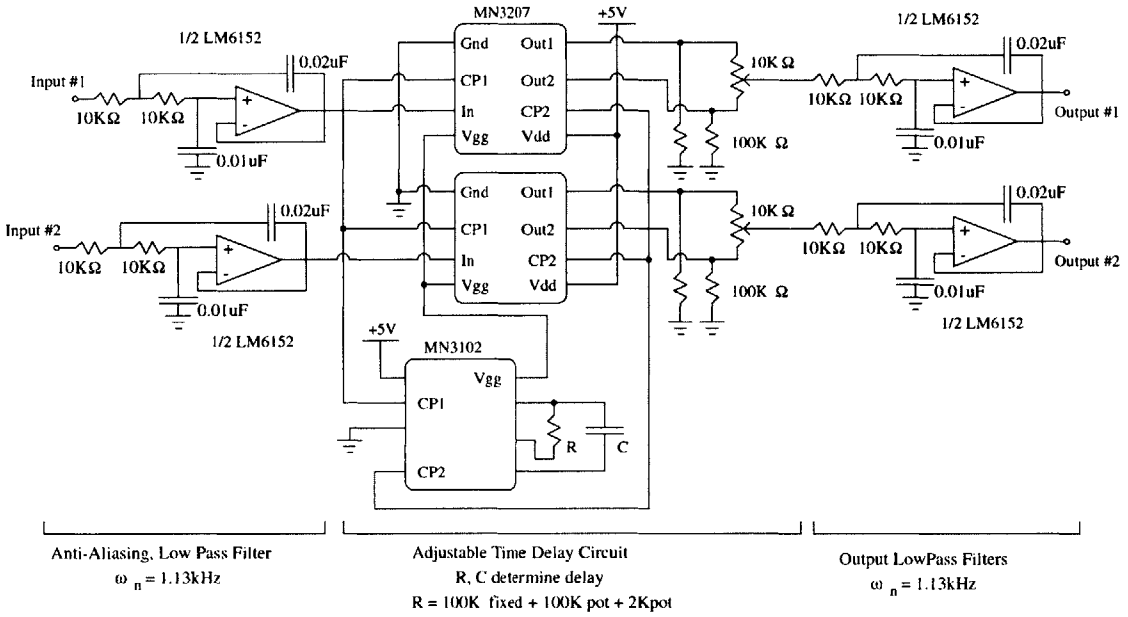

Figure 7-10: Schematic of timing delay circuit used for phase control. Note the need for low pass filters (LPF) at both the output and input to the time delay chips.

Figure 7-10 shows the schematic of the delay line circuitry while Figure 7-11 is a picture of its construction. The time delay is comprised of a delay chip (MN3207) for each of the timing signals plus a clock chip (MN3101) that governs the amount of time delay. The clock

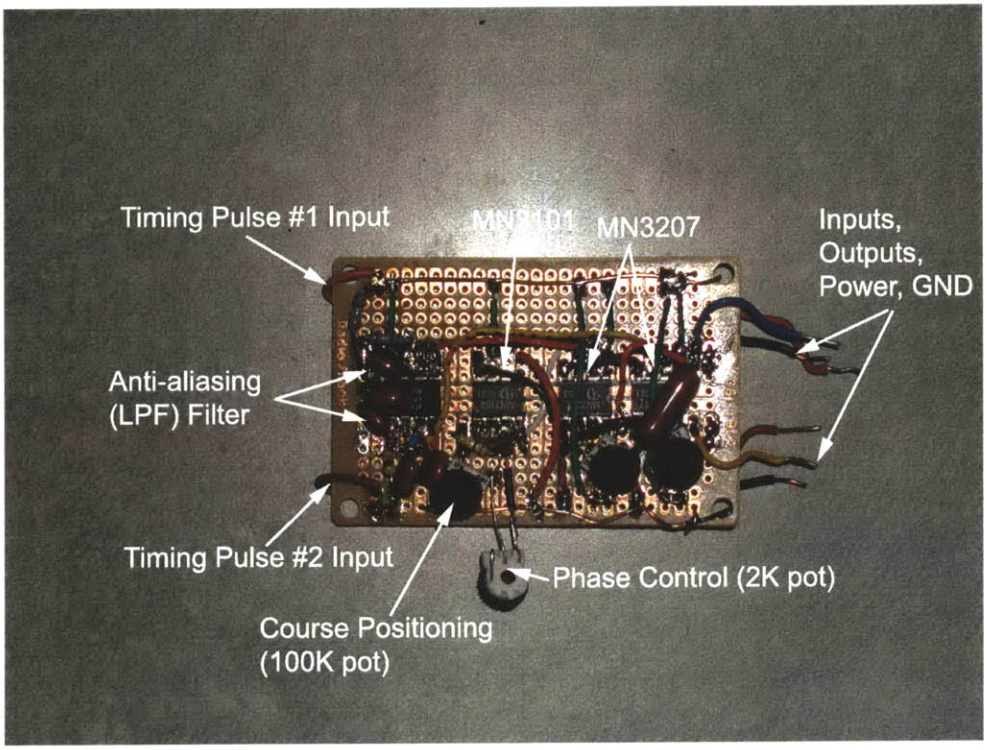

Figure 7-11: A picture of the time delay circuit used along with the input anti-aliasing filter.

chip generates the voltages needed to bias the transistor gates of the delay chip as well as the timing pulses that govern the opening and closing of transistors and gates to move the

signal through the chip. These timing signals are called CP1 and CP2, as explained in the Panasonic BBD manual.[25] These two clock signals, CP1 and CP2 are controllable from an RC network. By varying either the resistance or capacitance, the unmarked R and C at the bottom of the schematic of Figure 7-10, the amount of time delay can be adjusted continuously.

The problem with this method of tuning is the sensitivity of the clock chip to stray or parasitic capacitances. The capacitance used in this project is $C = 100\text{pF}$. The handbook suggests a value from 20pF to 200pF. When using a breadboard, the capacitances between two adjacent rails can be as high as 10pF and vary as objects such as wires, scope probes, one's hand, or a screwdriver pass around them. For this reason, the delay circuitry was mounted on a separate PC board that was inserted vertically above the breadboard. Furthermore, this electrostatic sensitivity limits the tuning to potentiometers. Attempts at using sliding rotary variable capacitors introduced jitter into the clock signals caused by capacitative coupling from the tuning screwdriver into the clock pins. The variable capacitors did not give as linear of a response in the time delay as the potentiometers.

The final design for R uses a 100KΩ fixed resistor, a 100KΩ potentiometer for coarse adjustments, and a 2KΩ potentiometer for the actual phase control. A plastic screwdriver is still used as a metal screwdriver still introduces some jitter into the clock signals through capacitative coupling. In a finished product, this time delay circuitry would be mounted in a shielded enclosure for adequate protection.

7.2.1 Anti-Aliasing and Low Pass Filtering Circuitry

The MN3207 time delay chips work by discretizing or chopping up a continuous analog signal and placing the discrete signal parts into buckets (capacitors) that hold the signal's charge until the clock signals arrive and the signal moves into the next bucket. This process is otherwise known as sampling and is exactly how some analog-to-digital converters work. Nyquist's theorem says for a given sampling rate, in this case bucket moving rate, the maximum frequency of the input signal must be at most half this sampling frequency for no distortion to occur.[39] For this reason, the input timing pulses, ideally square waves containing odd harmonic frequencies up to infinity, must be filtered to remove the high frequency signal content. This process is called anti-aliasing and it is accomplished here by using a second order, active low pass filter shown in Figure 7-12. If the signal is not

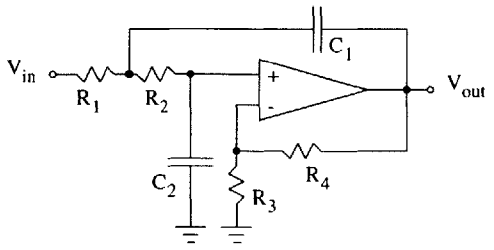

Figure 7-12: A second order active low pass filter (LPF). This variety is known as a Sallen-Key filter.

anti-aliased, the output will be discontinuous. This will show up as bumps in the output if the output is also low pass filtered.

This transfer function for this filter is:

$$H(s) = \frac{\frac{1}{R_1 R_2 C_1 C_2}(1 + \frac{R_4}{R_3})}{s^2 + (\frac{1}{R_2 C_1} + \frac{1}{R_1 C_1} - \frac{R_4}{R_2 R_3 C_2})s + \frac{1}{R_1 R_2 C_1 C_2}} \tag{7.3}$$

A thorough description of this circuit and how to set its gain, bandwidth, and quality factors are given by Payton's *Analog Electronics.*[26] This double pole filter is used as both the anti-aliasing filter before the time delay circuit and as the low pass filter after the time delay circuit. In both of these applications, a unity gain is desired. The gain, corner frequency, and quality factor of this filter are given by:

$$Gain = 1 + \frac{R_4}{R_3} \tag{7.4}$$

$$\omega_n = \frac{1}{\sqrt{R_1 R_2 C_1 C_2}} \tag{7.5}$$

$$Q = \frac{1}{\sqrt{\frac{R_2 C_2}{R_1 C_1}} + \sqrt{\frac{R_1 C_2}{R_2 C_1}} - \frac{R_4}{R_3}\sqrt{\frac{R_1 C_1}{R_2 C_2}}} \tag{7.6}$$

For a unity gain, R_4 is set to zero. This makes the value of R_3 irrelevant. C_1 is set to twice C_2 with $C_2 = 0.01\mu$F and C_1 realized by putting two capacitors identical to C_2 in parallel with one another. This reduces component variations such as temperature coefficients and tolerance. If two components are manufactured in the same process batch, they are generally more matched in their specifications than two components made in different batches or assembly lines. For this reason, R_1 and R_2 were chosen to be equal, in this case,

10KΩ. This gives a corner frequency of $\omega_n = 7.1 \cdot 10^3$ rad/sec or $f_n = 1.1$kHz. This value is well below the Nyquist value needed to satisfy the clock pulse timing. For completeness, the quality factor of this filter is: $Q = 0.707$, so there is minimal overshoot between the filter's input and output signals in the time domain. Figure 7-13 shows the ideal behavior of this filter in both the frequency domain and in the time domain while Figure 7-14 shows the measured response of the filter from the oscilloscope. Figure 7-15 is a picture of the constructed filters and remaining signal processing.

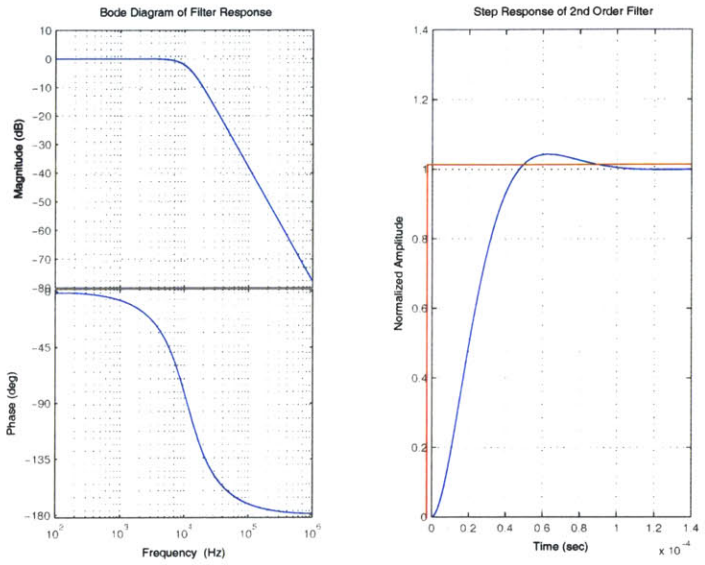

Figure 7-13: Ideal behavior of the 2^{nd} order LPF used in the time delay circuit.

The output of the time delay circuit also requires filtering to remove the high frequency switching ripple that is superimposed on the output signal. There is also some distortion due to drift caused by the capacitors used on the time delay chip. These capacitors have some decay time constant that manifests itself in some drift of the signal as it moves along from capacitor to capacitor in the time delay chip. The output low pass filter removes these higher frequency jitters and discontinuities and restores the original filtered signal. Figure 7-16 shows an oscilloscope waveform of the output of the time delay without any filtering. Figure 7-17 shows oscilloscope traces of the filtered waveform before and after a time delay.

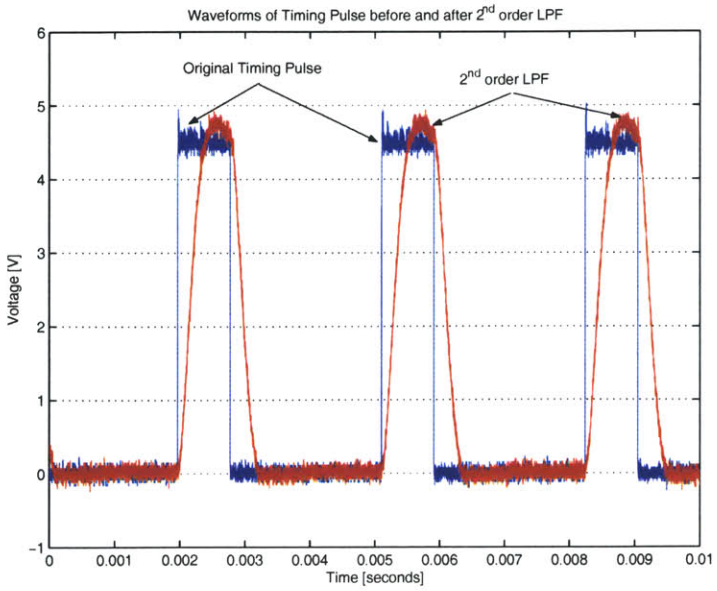

Figure 7-14: Waveform of timing pulse before and after passing through a 2^{nd} order LPF. $f_n = 1.1\text{kHz}$

7.2.2 Restoring the Square Wave Timing Pulses

Before these time delayed waveforms can be passed to the switches and gate drivers, they must be converted back into square wave pulses. To do this, two LM311 comparators are used to compare the filtered waveforms to a voltage reference. When the time delayed signal voltage crosses this threshold, the comparator output goes high. In this fashion, a square wave timing pulse is constructed. The input, hysteresis, and pull-up resistors are kept identical to those used in the previous comparator section, 51KΩ, 1MΩ, and 5.6KΩ, respectively. The only difference in component choices with these comparators is the voltage divider network used to generate a threshold voltage. In this case, a 33KΩ fixed resistor and a 10KΩ potentiometer are used. The potentiometers are used to adjust the duration of these timing pulses. For this project, these delayed timing pulses sent to the slave system were kept identical in duration to those of the master system. However, by adjusting these potentiometers, their durations could be changed. Figure 7-18 shows the schematic used to implement the circuit.

Figure 7-19 shows the oscilloscope waveforms for the low pass filtered original timing pulse, the low pass filtered, time delayed output, and the final pulse after going through the

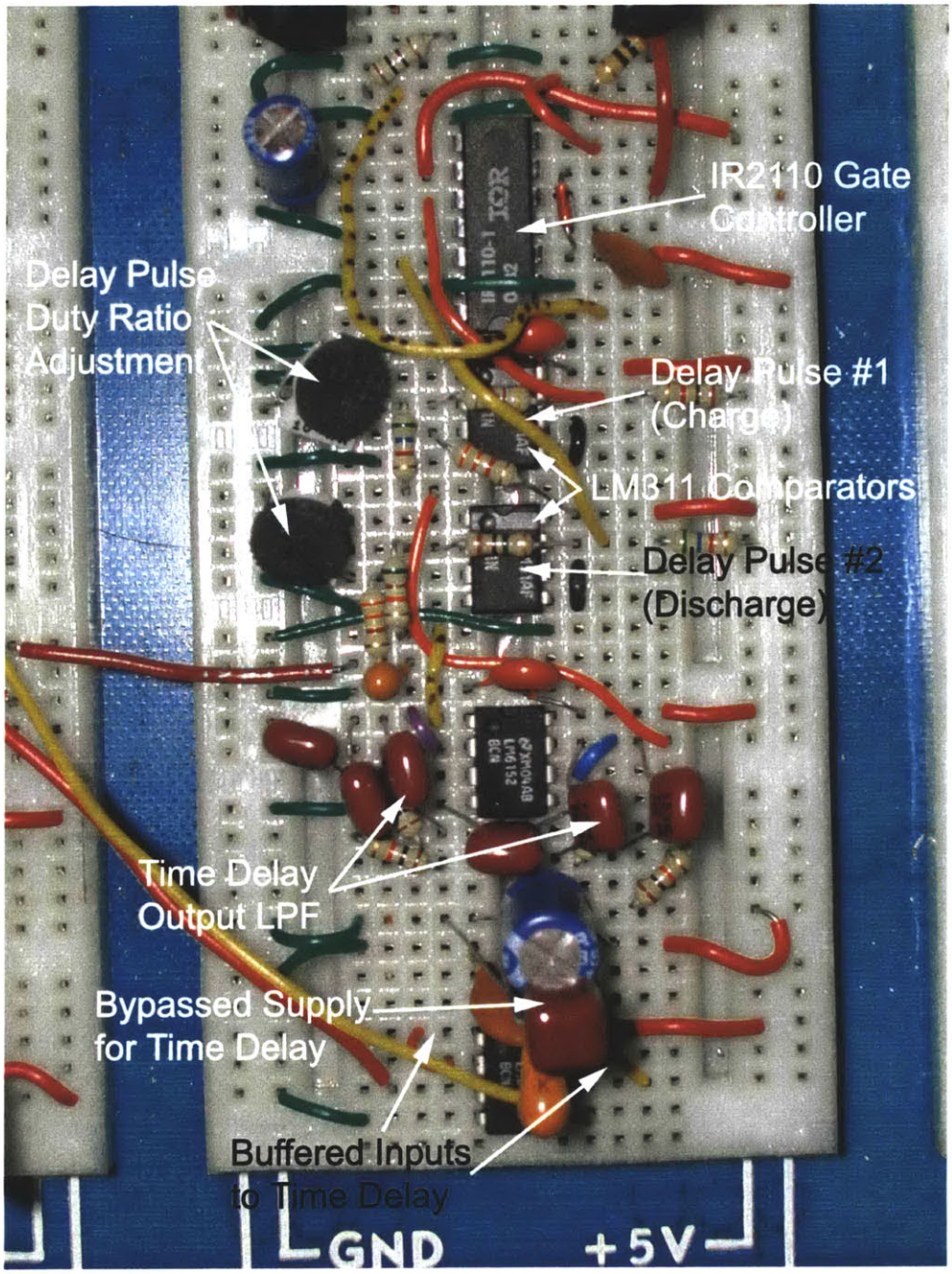

Figure 7-15: A picture of the output filtering needed by the time delay lines and the LM311 comparators needed to restore the filtered timing signals into square wave pulses.

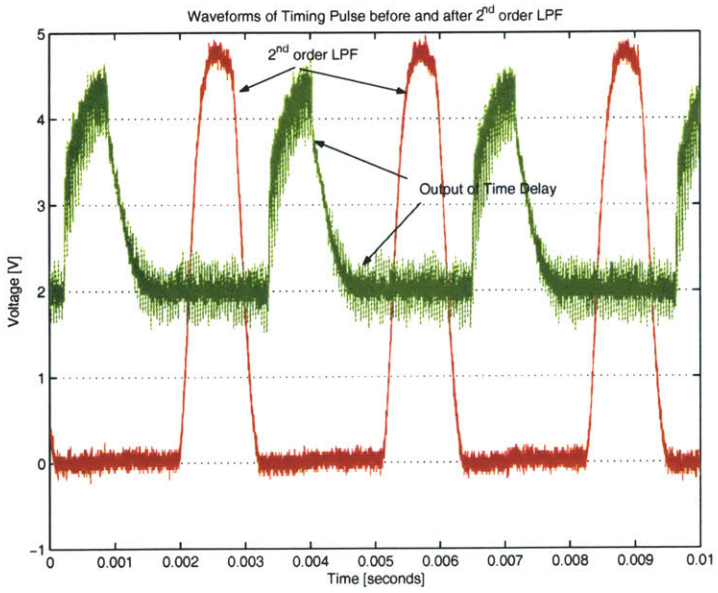

Figure 7-16: Waveforms showing the LPF input to the time delay circuit and the time delayed output. Notice that the signal is referenced to 2V. This is correct operation for this chip.

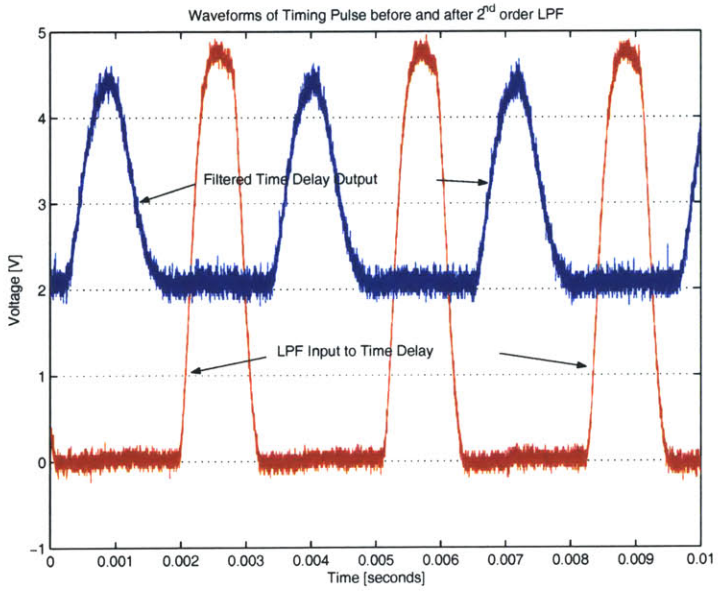

Figure 7-17: Waveform showing the time delay output after a second order LPF has removed the discontinuities and high frequency switching jitter.

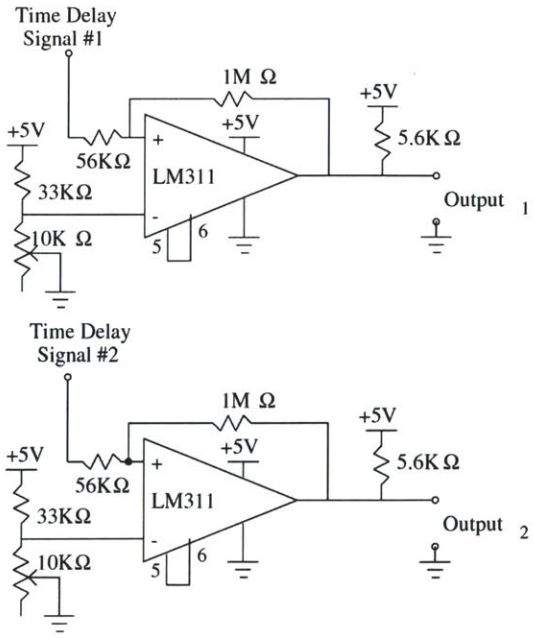

Figure 7-18: Schematic diagram of the LM311 comparators used to turn the filtered time delay output into square wave timing pulses.

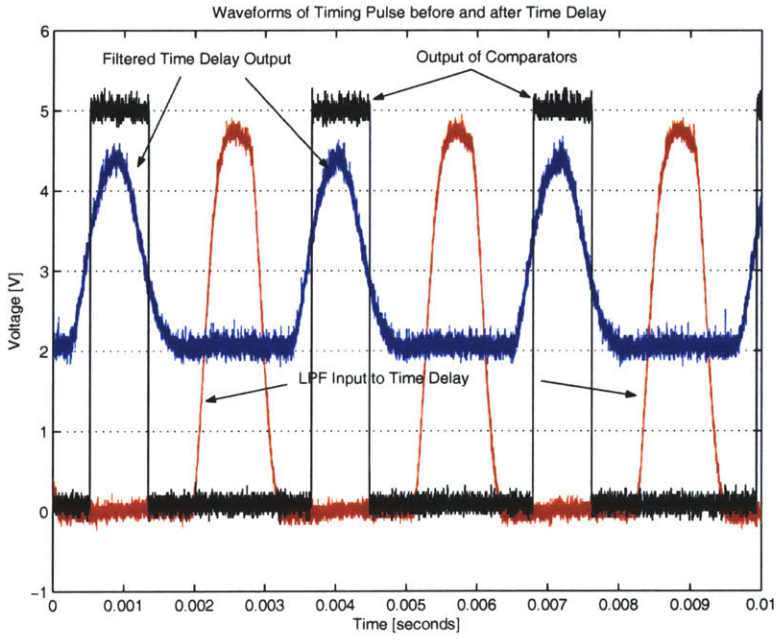

Figure 7-19: Waveforms showing the low pass filtered timing pulse before the time delay, after the filtering, and after going through the LM311.

comparator. This new timing pulse is sent to the gate drivers that control the transistor switches.

7.3 Switching Devices and Drivers

Three types of switches were used in this project: mechanical, relay, and electronic. Each type of switch was used as the discharge switch so that their performance in actuating the pulsed system could be evaluated. The circuit in which these switches were evaluated is presented.

7.3.1 Mechanical Switches

The mechanical switch used in this project is a double pole single throw switch as shown in Figure 7-20. The switch was physically 1.3 inches long, 0.25 inches wide, and had lever style actuator.

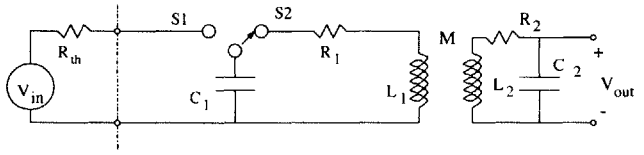

Figure 7-20: Equivalent schematic to setup used to generate coil waveforms.

This experimental setup was used to gather data on the individual resonant circuits which is presented in the next section. One of the recurring problems with the mechanical switch was that it "leaked" voltage during switch transitions. The details of this problem are presented along with the gathered data. Figure 7-21 shows the mechanical switch (on the left) and the wetted reed relay (right) used in this project.

7.3.2 Relay Switches

An important factor in choosing relays is their typically low on-resistance, R_{on}, typically much less than 0.01Ω. The downside of relays is bounce; a phenomenon whereby the switch does not completely turn on or turn off in a single instant. During a single transition, a relay will make several intermittent connections. Factors such as age, the chemical composition of the surface of the switch contacts, the inertia of the switching components, and other

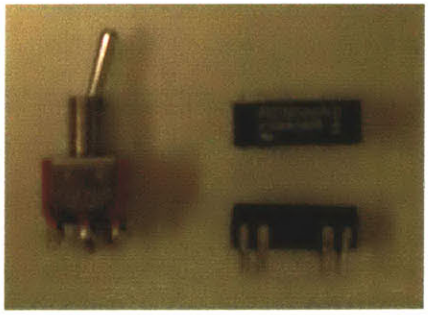

Figure 7-21: Picture showing the mechanical switch (left) and the wetted reed relay (right) used.

factors determine how the switch will behave when in transition. The important fact to remember is that *all* mechanical switches exhibit bounce. Figure 7-22 shows the effects of bounce on a waveform.

Even if bounce is not a factor when switching, if the dynamics of the switched system occur on a larger time scale than the bounce period, a poor switch contact can have larger than expected on resistance and degrade the quality factor of the output. When testing, the same coil and capacitor combination was used in both the secondary and primary circuits. Unfortunately, no result faster than a few hertz could be attained that did not exhibit switch bounce or have a faster decay rate than the waveforms obtained by mechanically actuating the switches. For reference, the relays used were REMtech wetted reed relay, model PRMA1A05. These relays claim to be operation in any orientation and up to 500Hz switching with a 150mΩ on-resistance. However, they list a time of 1.2ms for contact, including bounce and another 1ms for release, which is inconsistent.[16]

7.3.3 Electronic Switches

The switches used in the final version of this project were power MOSFETs that had very low on resistance; the switch used to discharge the capacitor, the International Rectifier

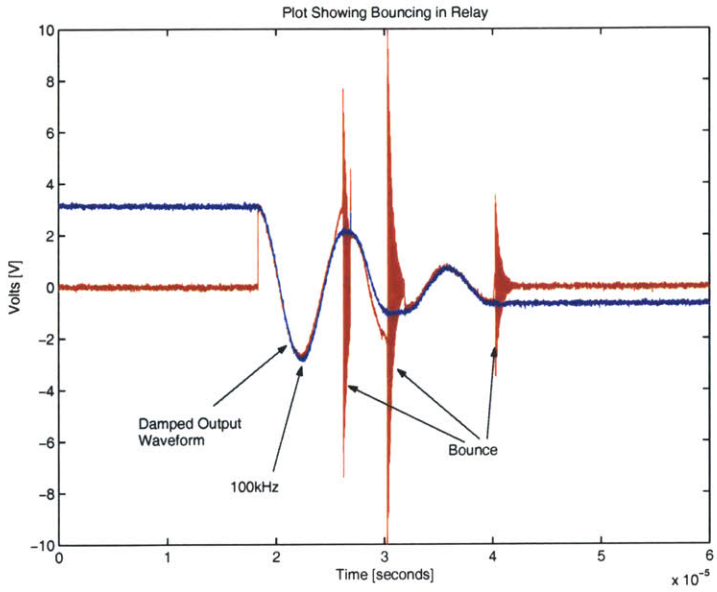

Figure 7-22: Scope waveform showing relay bouncing after initial contact. Operating frequency is 15Hz. Relay is an PRMA1A05 wetted reed relay.

IR3101-D1 had a maximum on resistance of $R_{on} = 0.019\Omega$. The maximum turn on and rise times are quoted as 90ns and 220ns respectively.[13] With the capability to handle a continuous current of 64A and block a charged capacitor voltage of 30V, this is an excellent switch for this application. International Rectifier makes power MOSFETs with still larger voltage and current ratings with similarly low on resistances.

The charging switch is a Fairchild Semiconductor FP3055LE transistor. It has a maximum on resistance of $R_{on} = 0.107\Omega$, meaning that it can bring to almost full charge a 0.4μF capacitor in $t_{charge} = 5RC = 220$ns which is excellent for the speed at which this system is operating. It can handle a current of 11A and has a 60V breakdown voltage.[30] With a cost less than a dollar, this transistor is ideal for the charging requirements. Both types of transistors used are in a TO-220 style packaging.

Figure 7-23 gives a schematic of the switching circuit used to control the primary of the resonant system while Figure 7-24 shows a picture of its implementation. Notice that the discharge switch is now between the inductor and ground instead of between the inductor and capacitor as shown previously. While the switch could be located in either location, the issue of how to turn the switch on and off becomes very important.

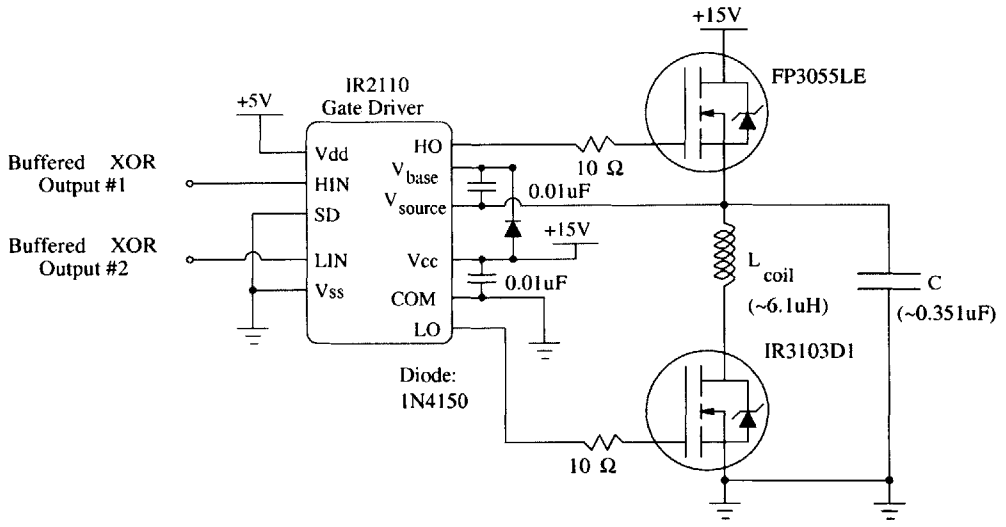

Figure 7-23: Schematic of gate driver and MOSFETs used to make switches.

To turn an N-channel MOSFET transistor on, such that it stops blocking voltage between its drain (typically the top for a schematic n-channel) and source (bottom) terminals, a positive voltage must be applied to the gate terminal relative to the source. However, the timing signals generated to control these switches range from zero to five volts; when the logic signal first turns on the charging transistor, the capacitor sits at ground potential, zero volts. As it's charging, it pushes the source of the transistor up to the voltage rail, 15 volts in this case. As soon as the source voltage goes over a few volts, the transistor turns off as $V_{gs} < 1V$, the minimum voltage necessary to keep the transistor on. While the bottom discharge MOSFET is referenced to ground thus allowing it to be kept active during operation, the top MOSFET requires a gate driver to keep it activated during charging. The IR2110 is the solution. It is a standard high side/low side gate driver used in power supply applications with this topology.

For reference, use of bipolar junction transistors was not considered because they require a current to keep them activated, not a voltage. As the gate driver used in this system is rated for voltage and not current, the switches were implemented as MOSFET transistors. Practically, the MOSFETs found meeting the drive requirements were cheaper than the BJTs of similar ratings.

International Rectifier makes a high and low side MOSFET driver, the IR2110 [12], that drives MOSFETs arranged in this configuration: the charging MOSFET referenced to the

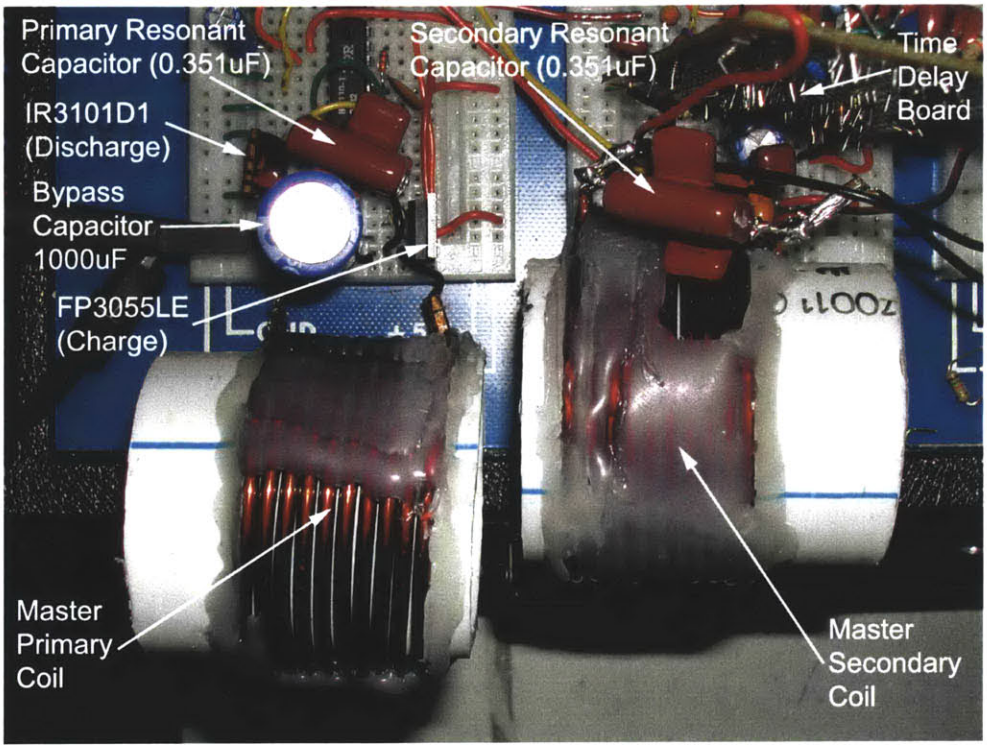

Figure 7-24: Picture of the Master system gate controls and transistor switches as well as coil and capacitor.

top supply rail, the discharge MOSFET referenced to the ground or negative supply rail, as previously shown in Figure 7-23. This chip uses TTL logic pulses as inputs to activate the gate driver pins, HO (high side gate output) and LO (low side gate output). By using an isolated high side voltage stage, it can handle high side voltage supplies of 600V. This voltage isolation is done by connecting to the source of the high side switch. The gate of the high side can be properly biased on when the source voltage is known, i.e. so that $V_{GS} > 0.7$V.

The 10Ω gate resistors are used to limit the current that can flow when the gate is turned on or off, as well as to make sure that the gate charge does flow out when turned off. Typically, the gate resistors vary from as little as 1Ω to as much as 100Ω, depending on the amount of current load the transistor is attempting to switch off. As the MOSFET is activated by having a charge (a voltage) in the gate, then the resistor can be thought of as a voltage to current converter that supplies the charge when turning the gate on and facilitates the charge being pulled away by the IR2110 when the gate is turned off. Furthermore, as the gate of the MOSFET can be modelled as a capacitance, then the constitutive relation $I = C\frac{dV_{gate}}{dt}$ applies. The resistor should make sure this transient current is limited to an acceptable value.

7.4 Resonant System Construction and Switching

The capacitors and inductors used in this project were kept small and operated at relatively low frequencies in order to minimize the effects of parasitics and to overcome the construction obstacles themselves instead of compounding them with design limitations. Furthermore, the primary and secondary of both the master and slave system were kept balanced and equal, meaning that instead of having the secondary be a single coil, it was built with a capacitor attached to observe the symmetry of the waveforms.

7.4.1 Coil Construction

There were three sets of coils built for measurements: the first set was built to determine the variability of inductance and to compare and perfect coil construction techniques, the second set of coils were used to test the relay and and mechanical switch techniques. A third set of four coils are more uniform in inductance and size and were used with the

transistor switching to measure the phase controlled outputs. Pictures of a coil from each set are shown in Figure 7-25:

All coils are constructed with enamel insulated wire, 10 AWG, with average diameter of 0.1019 inches (bare) and 0.1050 inches with enamel (2.59mm diameter bare, 2.67mm diameter coated). Its resistivity is 0.9989Ω per thousand feet at 20°C (0.00328Ω per meter).

Each coil has ten turns of wire and is formed on schedule 40 PVC. The length of the wire in the coils varies depending on how tightly the turns are wrapped. The two main differences between the three sets of coils are their diameters and the tightness of their coil wrappings. The electrical characteristics of each coil were measured on an Impedance Meter 252 from Electro Scientific Industries. The critical measurements of each coil are listed below in Table 7.4.1.

Coil	Diameter (in)	Length (in)	Inductance (H)	Resistance (1kHz)
Coil 1	2.373	1.341	7.1μH	1.48mΩ
Coil 2	2.375	1.371	7.0μH	1.75mΩ
Coil A	2.360	1.286	7.1μH	1.35mΩ
Coil B	2.369	1.327	7.4μH	1.84mΩ
Coil C	1.906	1.120	6.0μH	1.20mΩ
Coil D	1.902	1.129	5.8μH	1.23mΩ
Coil E	1.911	1.117	5.7μH	1.20mΩ
Coil F	1.910	1.094	5.6μH	1.14mΩ

Due to the relations of the dimension of the coils produced, that the diameter is not much smaller than the length, it is difficult to mathematically predict their inductance using the standard inductance formulas.

$$L_{solenoid} \approx \frac{a^2 N^2}{9a + 10b}\ \mu H \tag{7.7}$$

Using Wheeler's formula in equation 7.7, where a, the average coil radius, and b, the average coil length, are in inches, gives a value for inductance that is typically 20% larger than experimentally found. This is due to the assumption in the formula that *length* > 0.8 *radius*. Table 7.4.1 shows the comparisons of predicted and actual results for the inductance.

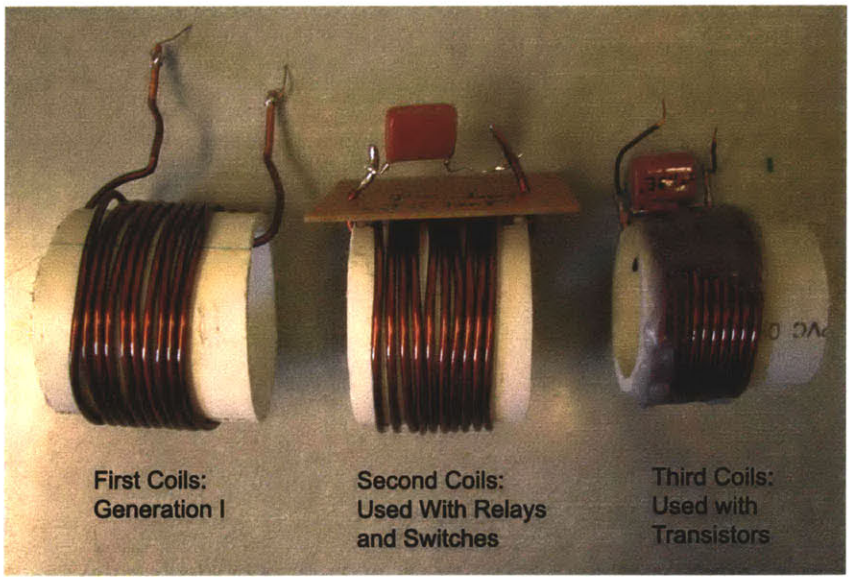

Figure 7-25: Picture of the three generations of inductor coils built to test the theory of this project. Each set had 10 turns, but construction techniques improved with each generation.

Coil	1	2	A	B	C	D	E	F
Predicted (μH)	5.84	5.85	5.93	5.86	4.59	4.56	4.62	4.67
Actual (μH)	7.1	7.0	7.1	7.4	6.0	5.8	5.7	5.6
% Error	18	16	16	21	24	21	19	17

The self resonant frequency of the resonant system was chosen to be approximately 100kHz so that the AC and proximity resistance multipliers were negligible, in other words so that the skin depth, δ is approximated as much less than the diameter of the wire. Furthermore, capacitors exhibit inductance above a certain frequency, depending on their construction. The capacitors used in this project are polypropylene. They have a critical transition frequency typically in the megahertz above which point they become more inductive than capacitive. The exact number is heavily dependent on the size and lead length of the individual capacitor. Polypropylene capacitors are high Q. A high Q capacitor is one that has a very low parasitic resistance in parallel with its dielectric or equivalently, a very large resistance in series with its dielectric. In other words, there is very little loss due to resistive dissipation and the capacitor could be modelled as an ideal capacitor in comparison to the inductor.

For coils A and B, a capacitance of $0.351\mu F$ is necessary to achieve resonance at $100kHz$ using the formula $\omega_n = \frac{1}{\sqrt{LC}}$. To achieve this, two capacitors of values 0.330μF and 0.022μF are wired in parallel. For coils C through F, to achieve resonance at approximately $100kHz$, a capacitance of 0.385μF was used, comprised of a 0.330μF, a 0.033μF, and a 0.022μF capacitor wired in parallel. These exact components give a calculated resonant frequency of 107kHz for a 5.8μH inductor.

This choice in capacitance represents a mistake made in the initial testing of the inductors. When measuring their values and recording initial responses, the inductors were resting on a metal surface. This groundplane gave an erroneous inductance reading on the order of 6.5μH instead of 5.8μH. When this mistake was discovered, instead of replacing the capacitors and rebuilding the system to achieve a 100kHz resonance, the old capacitors were kept.

When hooked up using a hand actuated switch, the coils still did not resonate at the frequencies predicted. This is due to the parasitic capacitance found between the windings of the inductor itself which has been neglected up to this point. Medhurst's formulas, from

a previous chapter, states that the capacitance of a coil is given by $C_{coil} = 2Ha$ where a is the radius in inches and H is a constant based on the ratio of coil length divided by diameter. The quoted value for coil A is 1.2pF, however, Medhurst stipulates that this formula is valid only for ground referenced coils. In these experiments, the coils were left floating on the return (ungrounded) plug of the power supply.

Table 7.4.1 shows the results of these switching experiments and the effective interwinding capacitance found in the coils. Remember that this parasitic capacitance is frequency dependent. The data is taken when the given coil is acting as the secondary such that there are no switches to add parasitic resistances to its waveforms. Note that coils 1 and 2 were not tested in this or in any following experiment. This data was taken at 21°C at 30% RH on a wooden bench away from a groundplane or magnetic material. The supplied voltage source was $+5V$ from a GW model GPS-1850 DC power supply. The value of Q is determined by counting the number of cycles that occur until the peak magnitude is less than 5% of the initial discharge magnitude. R_{eff} is computed from the dissipation factor measured on the Impedance Analyzer at 1kHz of the coil/capacitor combination.

Coil	A	B	C	D	E	F
L (Measured μH)	7.1	7.4	6.0	5.8	5.7	5.6
C (Measured μF)	0.351	0.350	0.380	0.383	0.382	0.384
f_n (kHz)	104	108	121	120	119	120
$C_{parasitic}$ (μF)	0.021	0.057	0.092	0.080	0.068	0.070
Q measured	57	59	65	70	64	61
R_{eff} (Ω)	0.081	0.085	0.012	0.01	0.011	0.011

Figure 7-26 and 7-27 show the oscilloscope waveforms taken with coils A and B, respectively, taken as primaries in a resonant system. The secondary coil was not included. Figure 7-28 shows the response of coils D and F with a 5V input. Figure 7-29 shows a 10V charge with the influence of a secondary coil. The method of collecting this data is presented in the next section.

7.4.2 Response Waveforms from Mechanically Switched Systems

The data in Table 7.4.1 was gathered from a relatively simple experimental setup whereby a timing pulse was generated by a mechanical double pole, single throw switch actuated by

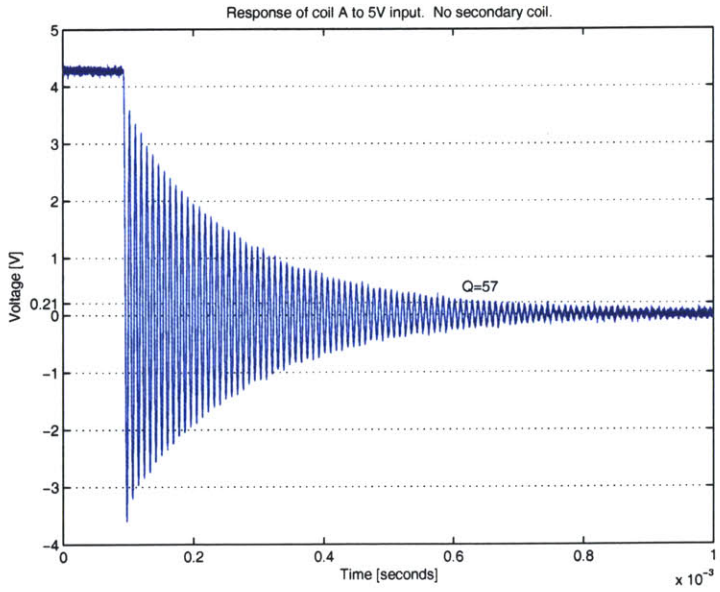

Figure 7-26: Response waveform of coil A with initial 5V charge. Q is evaluated at 5% of the initial value

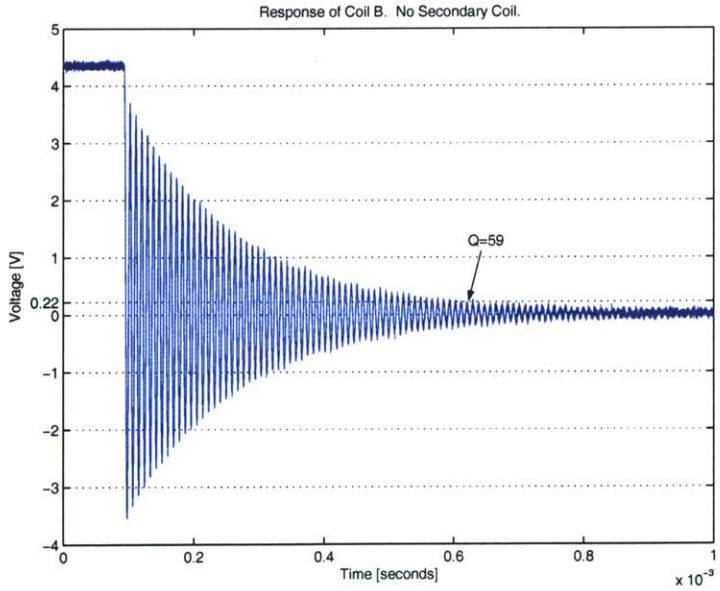

Figure 7-27: Response waveform of coil B with initial 5V charge. Q is evaluated at 5% of initial value.

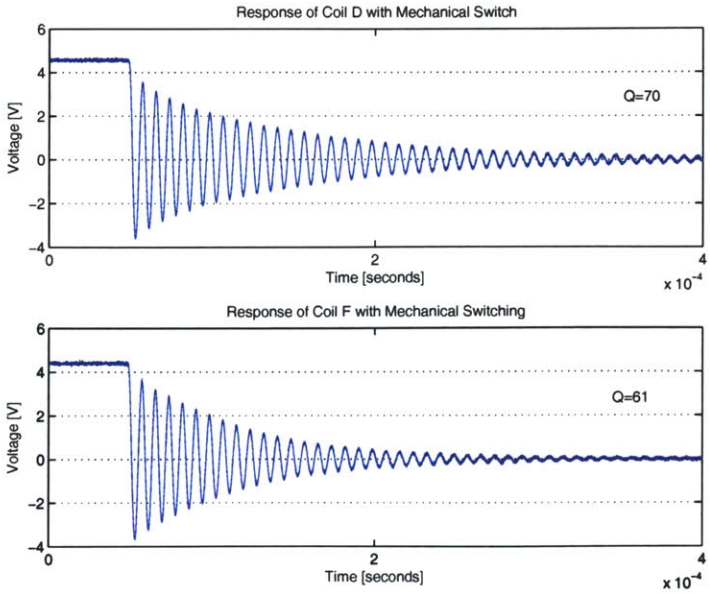

Figure 7-28: Response waveforms for coils D (top) and F (bottom) without a secondary coil. Q is not readable from plots due to scaling; 5% of 4.5V is not easily seen on these plots.

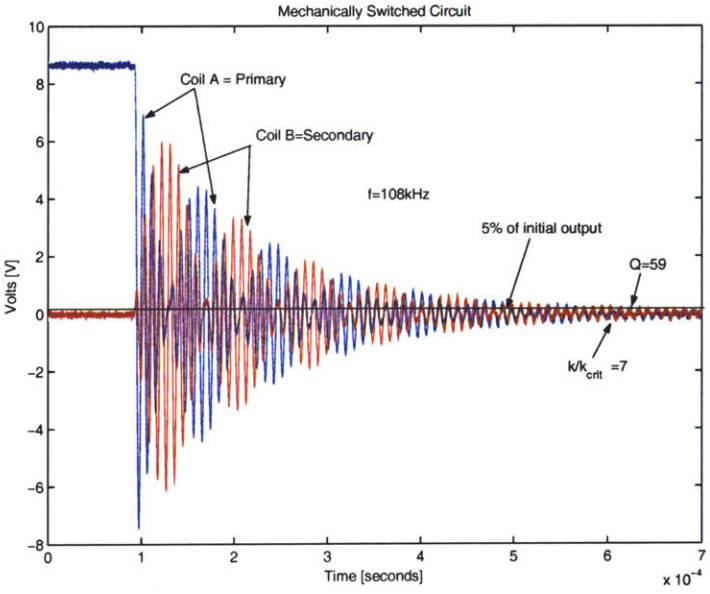

Figure 7-29: Oscilloscope waveform showing how the resonant frequency, the Q factor, and k are determinable from the output voltages. A charging voltage of 10V is used.

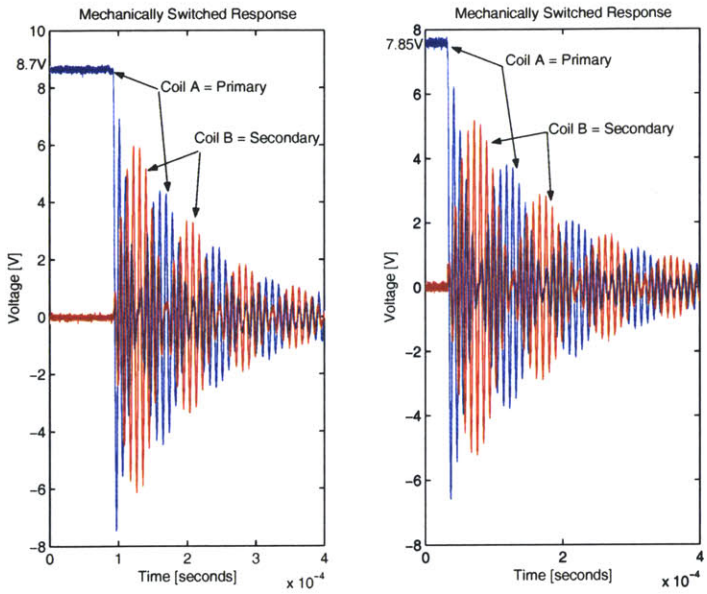

Figure 7-30: Oscilloscope output showing loss of charged voltage. Setup and initial conditions were identical in both cases. Applied voltage was 10V.

hand. The switch was actuated to charge the capacitor from a +5V supply, then rapidly turned to discharge the capacitor through the inductor coil. The experimental setup was shown in Figure 7-20.

There are two problems with the mechanical switch. The first is the bleeding of the power supply voltage from the capacitor. During the "rapid" actuation of the switch, the voltage across the capacitor would *sometimes* drop by as much as two volts. No suitable explanation could be found to explain this phenomenon. Figure 7-30 shows this drop in charged voltage. The setup and initial conditions for both scope outputs were identical.

The other problem is the repeatability of the measurements. When mechanically switching, measured waveforms would sometimes have larger decay rates, δ_{upper} and δ_{lower}, than previously recorded waveforms. The resistance of the switch would change between repetitions. This is a property of the switch contact surfaces. The characteristic impedance of coils A and B are $Z_o = \sqrt{\frac{L}{C}}$, which is 4.5Ω and 4.6Ω respectively. This gives a surge current from a 10V supply of 2.2A. This amount of current has the ability to pit and deposit metallic bits on the surface contacts of the physically small, inexpensive switch.

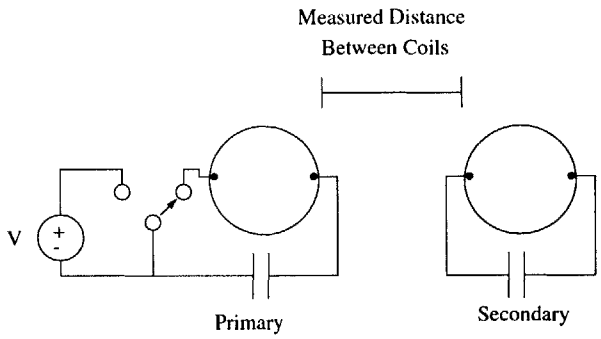

Figure 7-31: Top view of the experimental setup to measure k between primary and secondary coils.

7.4.3 The Effects of k

While measuring the output using the manually actuated mechanical switch, a determination of k was made by moving the A and B coils, with their associated capacitors, apart by a specified amount and recording the secondary's output waveform. This is the reason for the perforated boards attached to them, as seen in the picture of Figure 7-25. The edge of the boards slid along a wooden track with a ruler attached to its surface. The resulting waveforms showed the dependence of distance, and thereby mutual inductance and k, on the induced secondary voltage.

Figure 7-31 shows the experimental setup used to measure k between the primary and secondary coils. For these measurements, the primary coil was always coil A while the secondary coil was always B with the same capacitor used as previously stated. The distance between the coils is *not* between their centers, but between their closest surfaces. The voltage source is a 5V source, not the 10V used previously. Below approximately 6V, the changing resistive losses in the switch contacts was mitigated as the problem of spurious voltage spikes during switching was also eliminated. However, there was still a loss of approximately half a volt during the transition to discharge.

The recorded waveforms closely follow the patterns predicted in previous chapters. The oscilloscope waveforms shown in Figures 7-32, 7-33, 7-34, 7-35, 7-36, 7-37, and 7-38 are taken at increasing distances between the primary and secondary coil. From counting the number of beats on the secondary and the number of waveform cycles in each beat, values for k and k_{crit} can be estimated, as well as the resonant frequency and decay rate of the

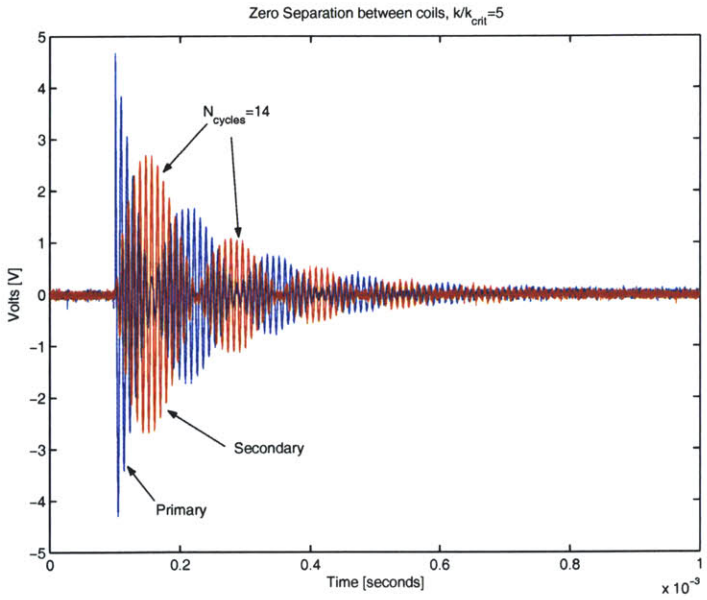

Figure 7-32: Zero separation between coils. $\frac{k}{k_{crit}} = 5$. $N_{cycles} = 14$. The measured waveforms are AC coupled

system. With this information, values for Q_1 and Q_2 can be ascertained.

Using relations presented in earlier chapters, it is easily shown that $N_{beats} = \gamma = \frac{k}{k_{crit}}$, $N_{cycles} \approx \frac{1}{k}$, and $k_{crit} = \frac{1}{\sqrt{Q_1 Q_2}}$. Rearranging these equations yields:

$$Q_1 Q_2 \approx (\gamma N_{cycles})^2 \tag{7.8}$$

Table 7.4.3 shows the experimentally derived values for the product $Q_1 Q_2$ for each of the separation oscilloscope plots. For reference, the Q of coil A is 57, while the Q for coil B is 59, yielding a product of 3363. The percentage error is taken from this value. The square root error shows approximately how far off the predicted average Q for each coil is from the experimentally found value above. Note that the Q found by counting the cycles of the primary and secondary was still greater than 50 for each distance, although counting the cycles on coil B, the secondary, proved very difficult owing to the small voltage induced. This table ultimately shows the error between the experimentally found values for Q and the approximate formulas derived in the previous chapters.

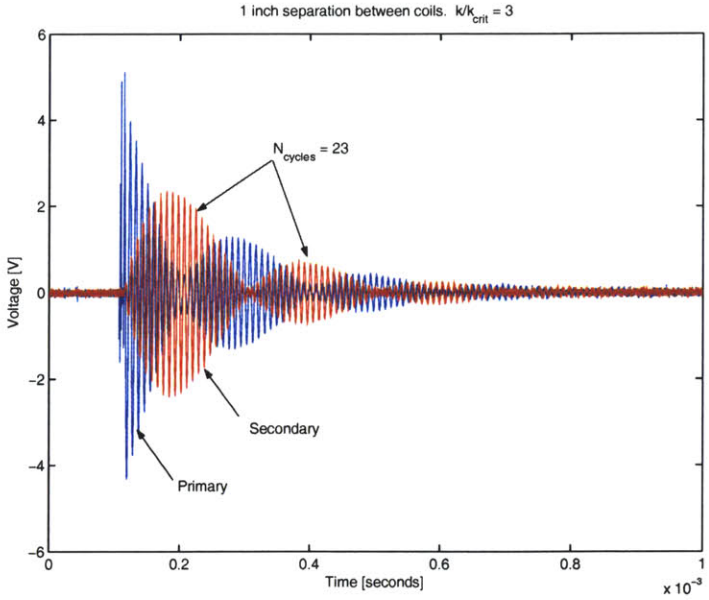

Figure 7-33: 1 inch separation between coils. $\frac{k}{k_{crit}} = 3$. $N_{cycles} = 23$

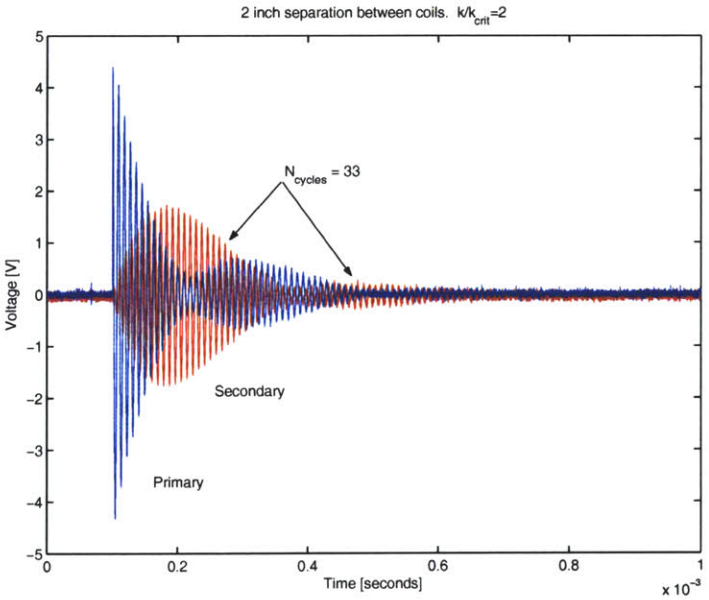

Figure 7-34: 2 inch separation between coils. $\frac{k}{k_{crit}} = 2$. $N_{cycles} = 33$

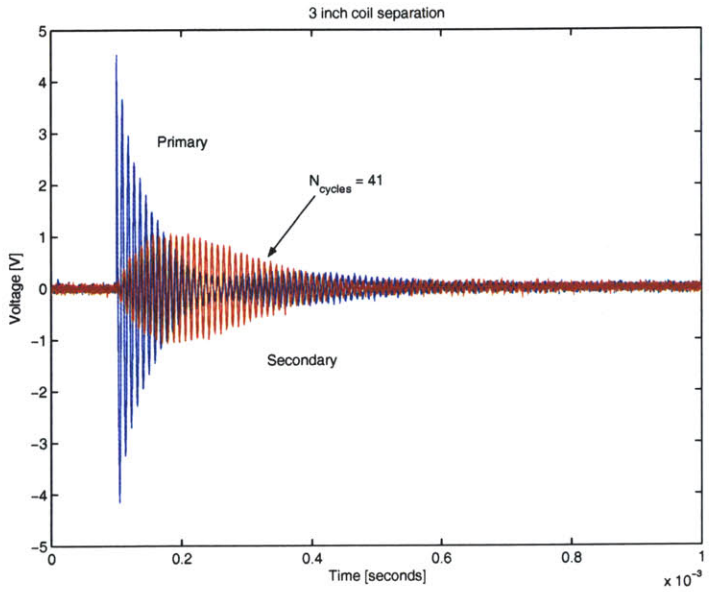

Figure 7-35: 3 inch separation between coils. $\frac{k}{k_{crit}} \approx 1$. $N_{cycles} = 41$

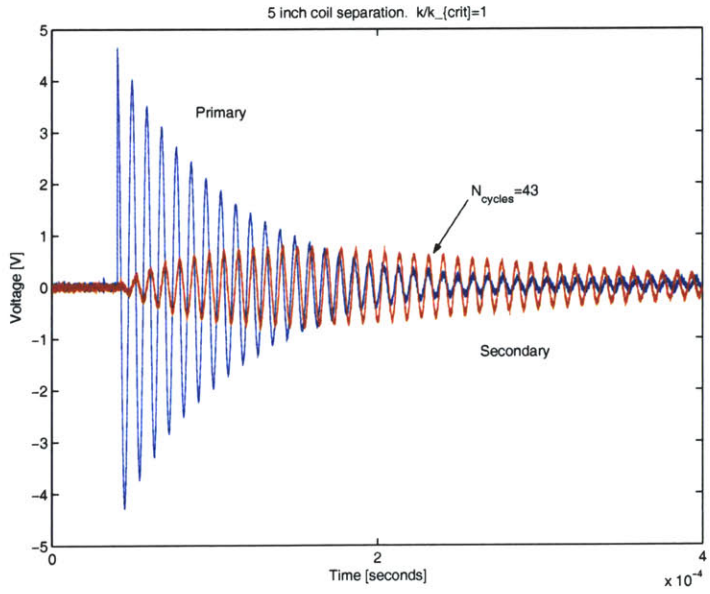

Figure 7-36: 5 inch separation between coils. $\frac{k}{k_{crit}} < 1$. $N_{cycles} = 43$. Note the change in time scale for this plot.

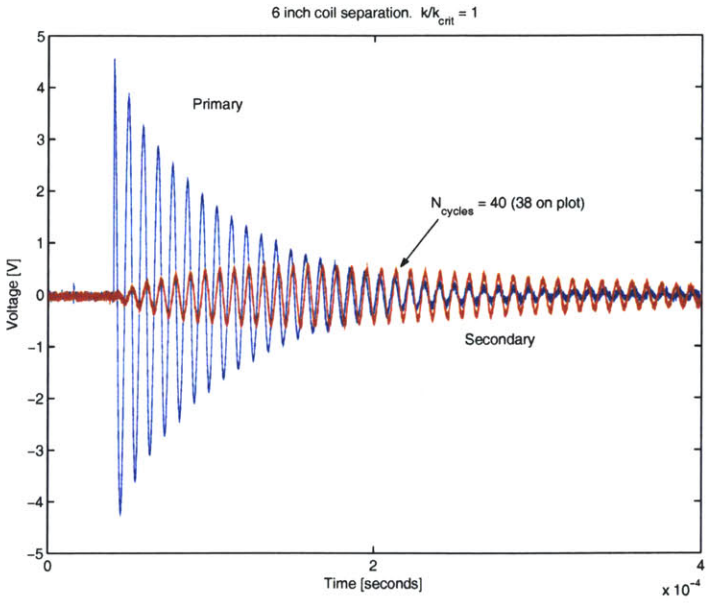

Figure 7-37: 6 inch separation between coils. $\frac{k}{k_{crit}} < 1$. $N_{cycles} = 40$

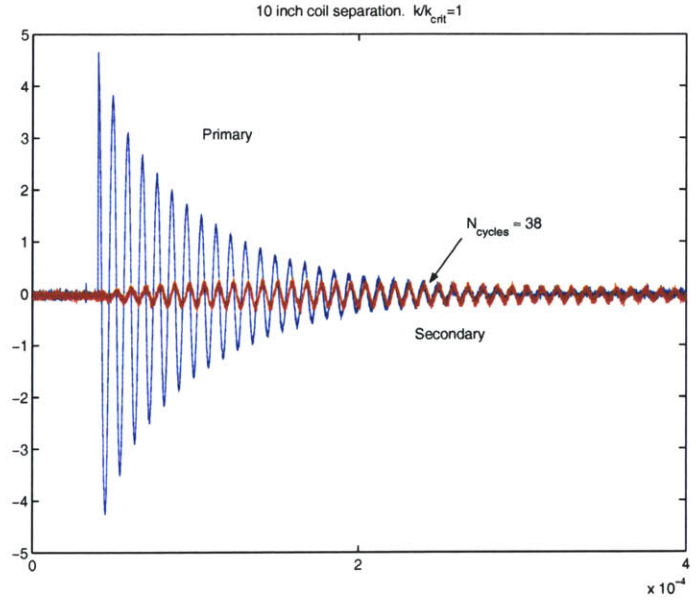

Figure 7-38: 10 inch separation between coils. $\frac{k}{k_{crit}} < 1$. $N_{cycles} = 38$

Separation	N_{cycles}	γ	Q_1Q_2	% error	Sqrt(Error)
0 inches	14	5	4900	46%	21%
1 inch	23	3	4761	42%	20%
2 inches	33	1	1089	68%	26%
3 inches	41	1	1681	50%	22%
5 inches	43	1	1849	45%	21%
6 inches	40	1	1600	52%	23%
10 inches	38	1	1444	57%	24%

Temperature Coefficients

To test the effects of temperature on the capacitor and coil performance, coils C, D, E, and F as well as their associated capacitors were placed in an oven at 50°C at 30% relative humidity for a one hour duration. Upon removal, the effects were measured as shown in Table 7.4.3. The comparison temperature is $21°C$ as stated previously.

Coils	C	D	E	F
Heated L (μH)	6.0	5.8	5.7	5.6
Δ ppm/C	0	0	0	0
Heated C (μH)	0.377	0.382	0.377	0.382
Δ ppm/C	272	90	451	180
R_{eff}	0.011	0.012	0.011	0.009

One interesting result is that while the capacitor values changed somewhat, the inductor values themselves did not appreciably change. However, the dissipation factors ($\tan(\delta)$) that determine the effective DC resistance for the inductors did change noticeably. Figure 7-39 shows the output of one of these heated sets of coils. The most significant alteration is the increased damping ratio dictating the decay rate of the waveforms.

The Master and Slave System

There are two identical sets of switches and drivers in this system, the Master the Slave system. Each systems takes the timing signals seen at the inputs to the IR2110 and charges and discharges the capacitor and coil resonant system accordingly. The only difference between the two systems is that the slave system secondary coil is connected to a varactor

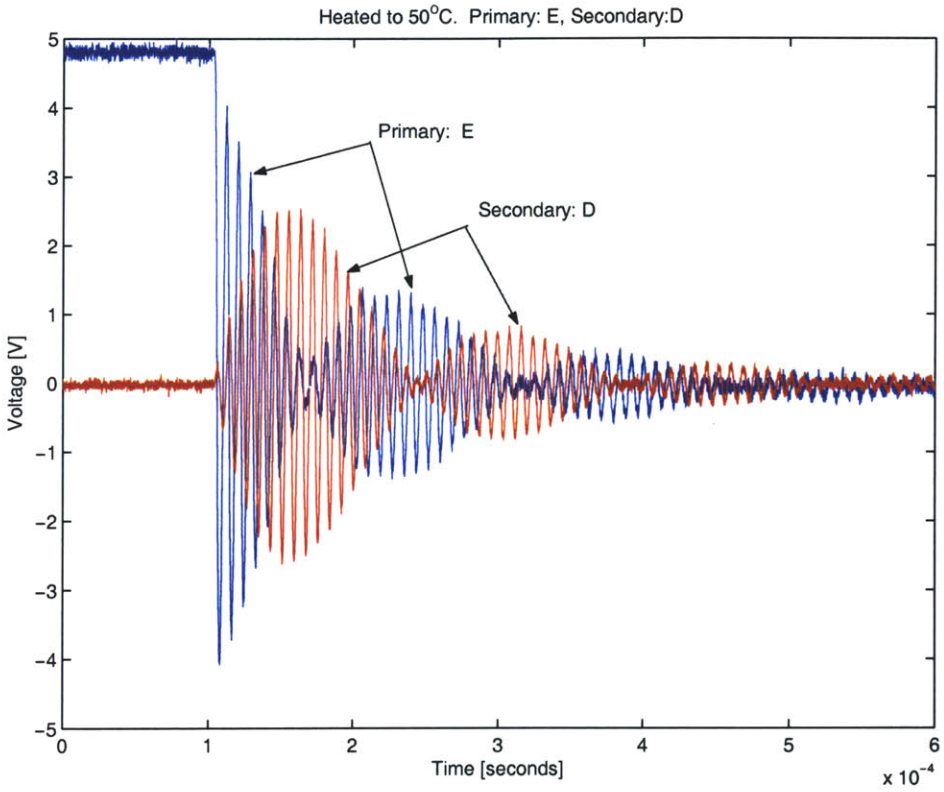

Figure 7-39: Output waveforms of heated coil and capacitor components. Operation at 50°C does not significantly affect operation.

diode that slightly changes its resonant frequency to match that of the master secondary coil. Not counting this, there are no differences in construction between the two systems. The reason the varactor diode is connected to the slave secondary and not to the master primary is because the two secondary coils are the antennae outputs of the system; for the phased array to transfer power, these two antennaes must be resonating at the same frequency.

Figure 7-40 shows all four coils used in this system. The two coils on the top of the picture comprise the slave system, while the bottom two are the master system. The leftmost coils are the primaries of each system while the rightmost coils are the secondaries. The distance between the two coils is 8 inches. While previous results suggest at least 10 inches between system for minimal linking of flux, the secondary outputs appear to be minimally affected by the proximity, especially since the secondaries are usually responding to the flux from their own primary coils when this cross coupling is an issue.

Figure 7-41 shows the slave switching system with all of its associated components.

System Operation

Figure 7-42 shows the operation of the system. The two square wave timing pulses are TTL logic, going from +5V to ground. When the discharge pulse goes high, the primary capacitor discharges through the inductor coil, resonating. There are no beats as the secondary coil has been removed. When the charging pulse goes high, the capacitor charges up to +15V within a few microseconds as the charging transistor has very little channel impedance. This operation is mirrored by the slave primary coil.

One important issue is power supply bypassing. When the transistors activate, there is either a large power draw on the voltage supply to fill the resonant capacitor up with charge or a draw on the ground return when the coil is resonating. When resonating, the inductor coil attempts to pull the ground to its potential, whether that be a positive or negative potential. If the power supply is not "stiff" enough, meaning that it cannot supply enough current to keep its output potentials fixed, then any other circuit connected to these rails will see its power supply fluctuate. For example, if a digital logic chip, such as the XOR gate shares a common ground line with the resonant system, when the system discharges, the XOR gate ground may be pulled up or down such that the chip fails to operate for some amount of time. The solution to this problem is to isolate the ground of the timing

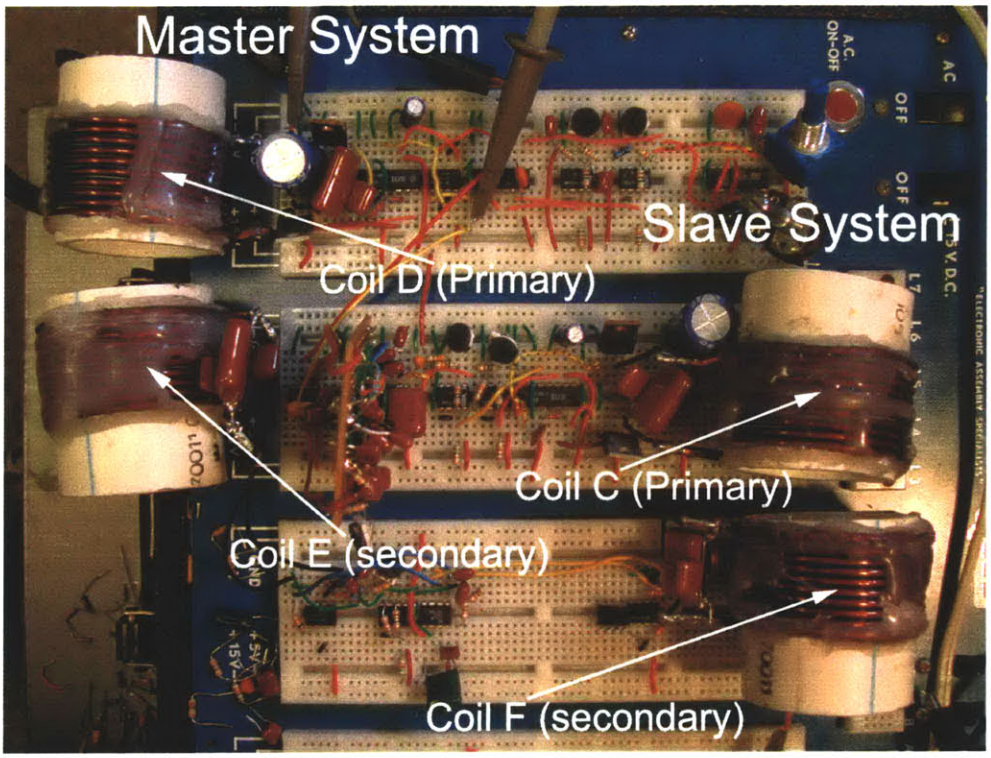

Figure 7-40: Picture showing the Master and Slave resonant systems. Separation between the two systems is important to avoid linking the magnetic flux between the two systems.

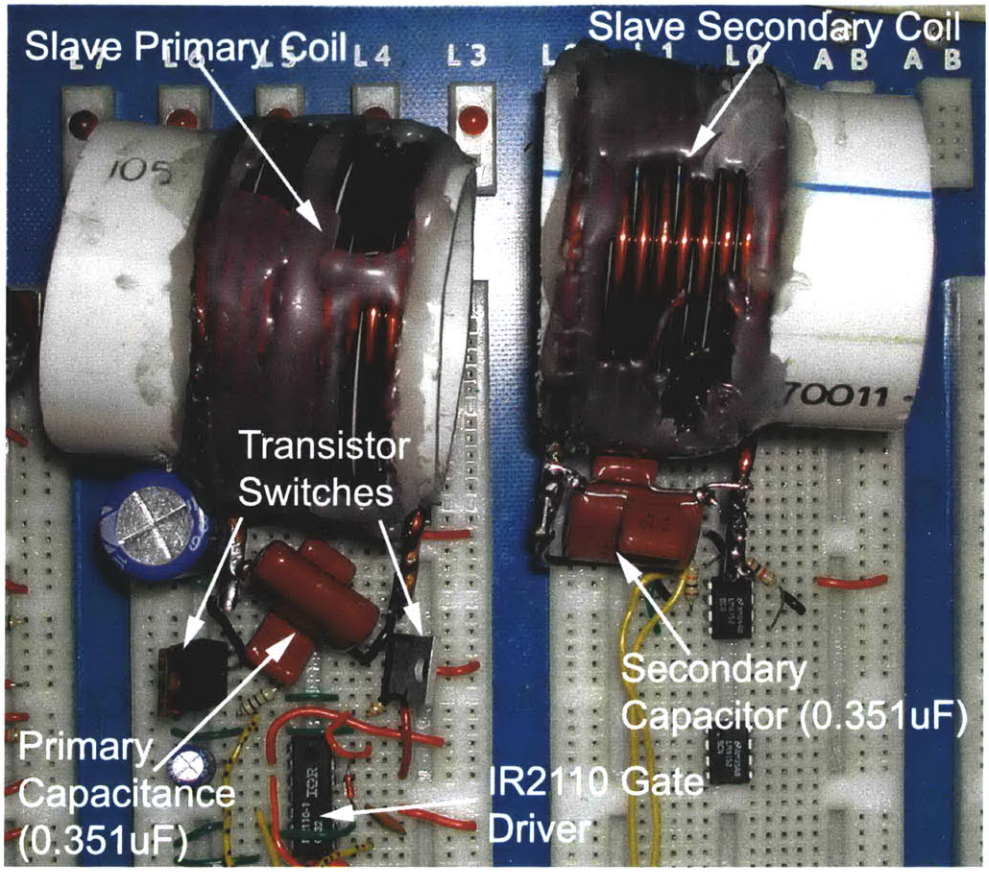

Figure 7-41: Picture of the slave resonant system.

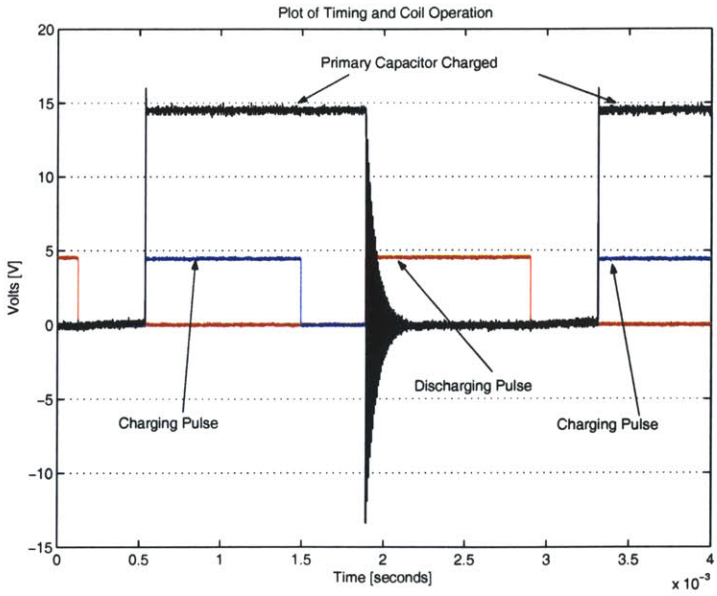

Figure 7-42: Oscilloscope waveform showing timing pulses and primary coil charging and discharging.

signal circuitry from the ground of the resonating system circuitry. This is facilitated by the IR2110 gate driver as it is designed for precisely this requirement.

Furthermore, if both resonant systems charge or discharge at approximately the same time, as they are normally supposed to do when operating as a dipole array, the power supply rails may not be able to supply enough power to keep the voltage seen by each system constant. Figure 7-43 shows a partial discharge in the slave capacitor when the master capacitor is charged. The waveform on the left is over a smaller time interval than the waveform on the right.

Bypassing is not only required for the resonant system, but is highly recommended for every IC on the breadboard. The LM311 specification sheet extols the necessity of power supply bypassing when engaged in high frequency operation. Most other chip specification sheets also mention some form of bypassing as important to the operation of the chip. In this project, most digital IC's are bypassed with either a 2.2nF ceramic capacitor or a 0.1μF polyester capacitor while the analog IC's are bypassed with 0.01μF ceramic and another capacitor. The resonant systems are bypassed with a 1000μF electrolytic capacitor and a 1μF polyester capacitor, and a tantalum capacitor. The time delay IC's are bypassed with a

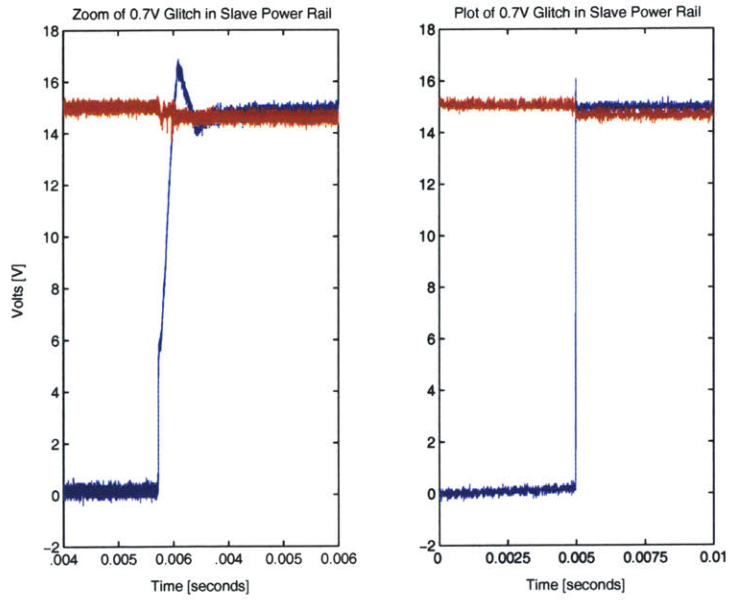

Figure 7-43: Oscilloscope waveform showing blip due to lack of power supply bypassing. Left hand waveform is zoomed in version of right hand waveform.

47μF electrolytic, a 10μF tantalum, and a 0.01μF ceramic capacitor. For systems handling greater voltages or currents than those used in this project, it is highly recommended to use separate power supplies for the timing circuitry and the resonant system circuitry. For more information, see Kent Lundberg's manual.[19]

The waveforms observed from the master and slave primary and secondary circuits are presented and analyzed in the following chapter.

7.5 Tuning and Frequency Feedback Control Circuitry

At this point, it remains to tune the four coils such that they are all resonating at the same frequency. Before any electronic feedback methods were used, it was useful to manually tune the coils using extra discrete capacitors. Note that coil E with a resonant frequency of $f_n = 119$kHz was selected to be the master secondary coil from which all other coils are tuned. Since it has the slowest resonant frequency of the four coils used, C, D, or F, it was assumed that capacitance could be added, instead of subtracted, to the other three coils as necessary to tune them to coil E's resonant frequency. Figure 7-44 shows the waveforms when the secondary coil is mismatched by by a set amount of capacitance. It should be

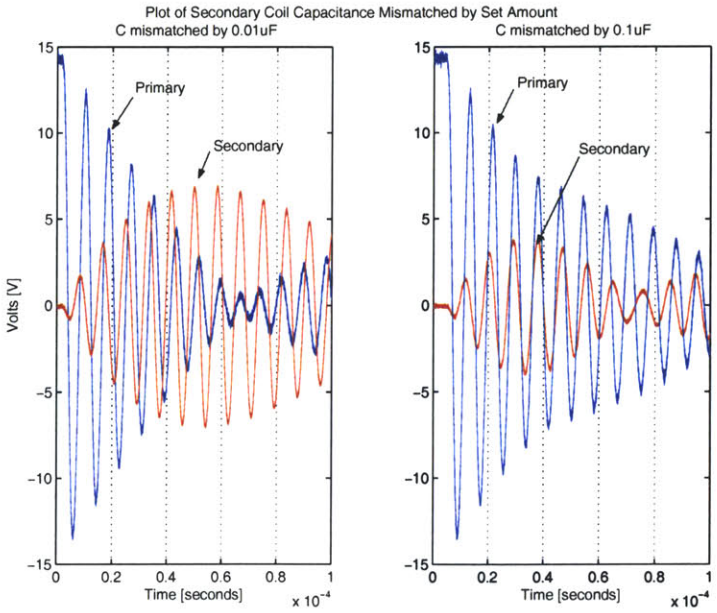

Figure 7-44: Primary and secondary waveforms when the secondary is mismatched by 0.01μF (left) or 0.1μF (right)

evident by inspection when there is a gross mismatch in resonant frequencies between the primary and secondary as there is not a uniform decay envelope around the waveform.

As the components are already closely matched, the output waveforms should not be as extreme as those in Figure 7-44. The output waveforms will probably resemble those of Figure 7-45. The first indication of a frequency mismatch is the mismatching of the beats. When properly tuned, the beats of the primary and secondary will alternate; the node of one waveform will be approximately the peak of the other and vice versa.

For the figure in question, the secondary reaches its peak a few cycles before the primary reaches its null. Upon closer inspection, the secondary, coil E, is resonating at 119kHz, as found in previous experiments, while the primary, coil D is resonating at 116kHz. This indicates that there is some capacitance, 0.025μF to be precise, due to the power supply bypass capacitors (over 1000μF), transistors, and the breadboard itself. However, 3kHz is actually very little variation in frequency considering the waveforms only exist for on average 600μs before decaying, giving a maximum frequency resolution of approximately 1.7kHz. Since these coils are being manually tuned, it is possible to place this capacitance in parallel with the secondary coil thus giving the two coils identical resonant frequencies.

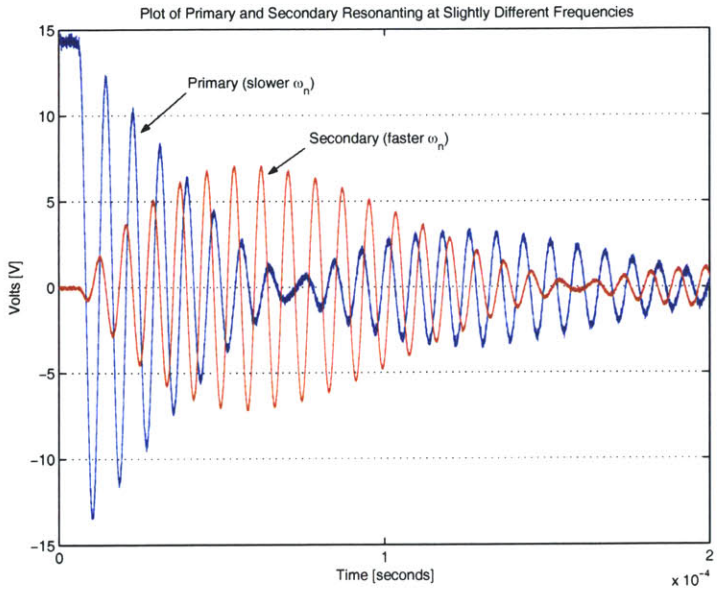

Figure 7-45: Waveform of slight frequency mismatch. When comparing beats, null of one does not correspond to peak of other.

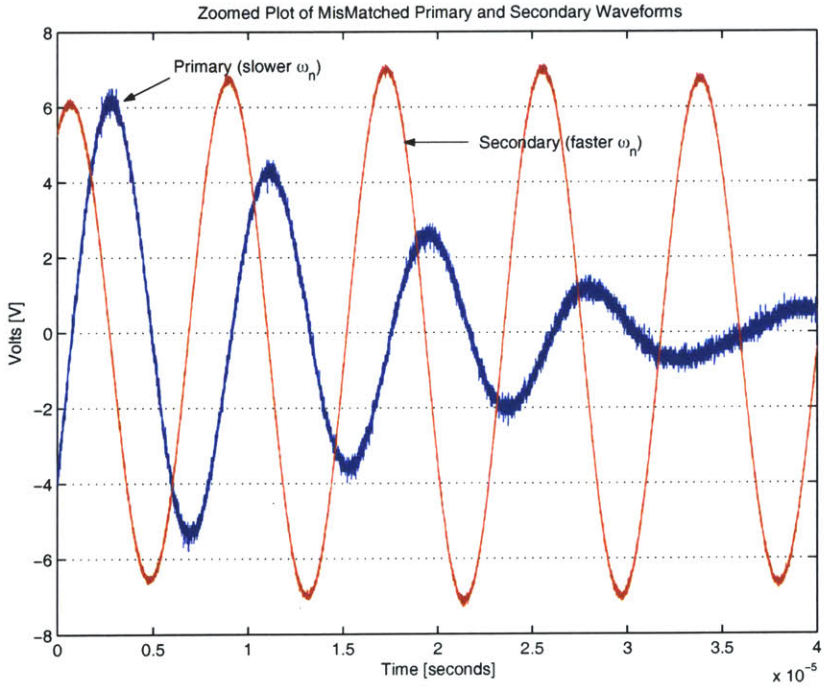

Figure 7-46: Zoomed scale to show how frequency mismatch affects the primary and secondary waveforms.

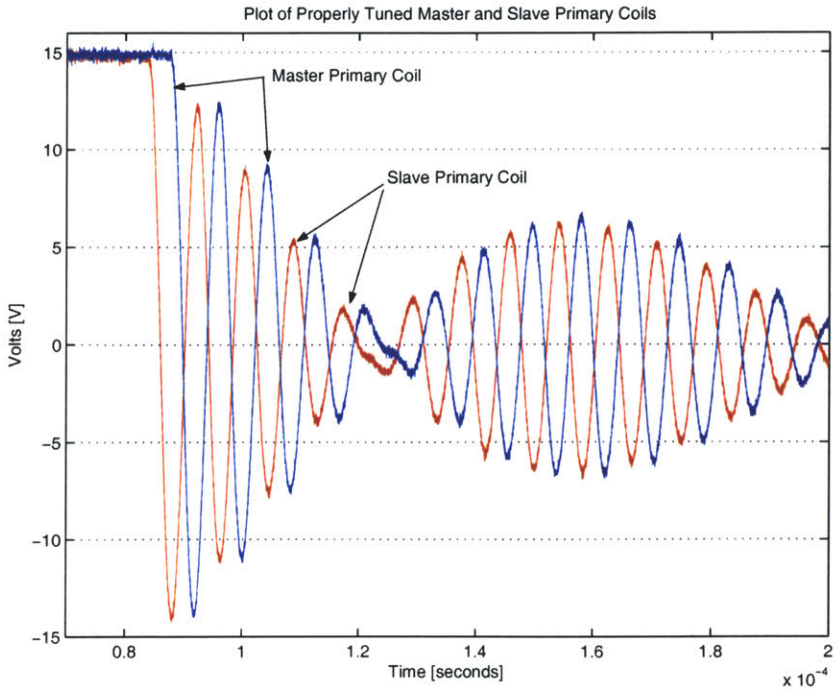

Figure 7-47: Waveforms of properly matched primary coils. Phase between master and slave primary is approximately 150^o.

Figure 7-46 shows a close up view of the frequency mismatched coils. Because these two coils were only slightly mismatched, the peaks of one the individual cycles closely corresponds to a zero crossing of the other. When the two coils are properly tuned, it is time to then match the slave system secondary to the master secondary. Finally, the slave primary coil should be matched to the slave secondary. When this is accomplished, and their coupling coefficients, k are equal, the output waveforms should be identical. Figure 7-47 shows properly tuned primary coil waveforms for the master and slave system. The relative phase shift between the two waveforms is 150^o. The secondary coil waveforms correspond in an identical fashion.

Adjusting the Relative Phase

As seen in Figure 7-47, precise phase control is possible with the 2KΩ potentiometer found in the time delay circuit. However, the system does not start out with the master and slave waveforms so close. Instead, the two output waveforms will probably be separated by a

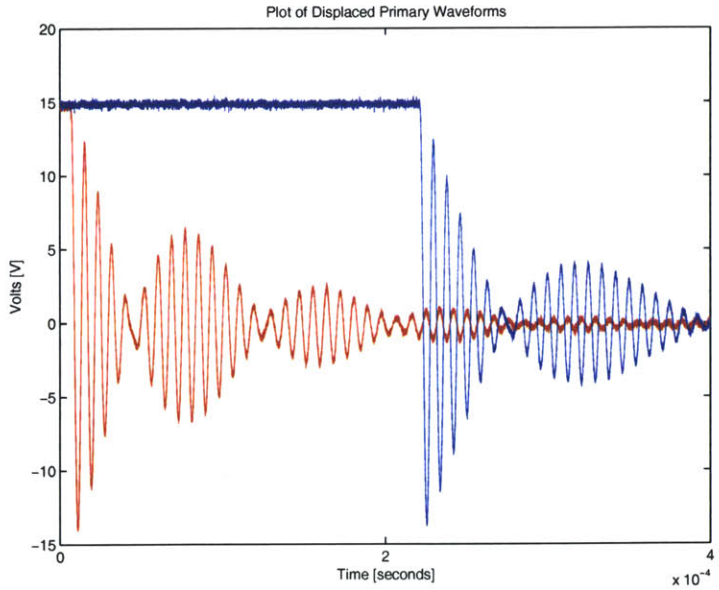

Figure 7-48: Waveform of grossly phase mismatched waveforms. Use the 100K potentiometer to adjust the slave primary back towards the master.

fair amount of time delay as shown in Figure 7-48. Only by having a 100KΩ potentiometer in series with the 2KΩ potentiometer can these waveforms be brought closer together such that the relative phase of the two systems is between -180^o and $+180^o$.

The underlying assumption behind phase control is that the frequency mismatch between the master and slave systems is never greater than than approximate 1.7kHz resolution. If the mismatch is greater than this, then the relative phase between the two systems will vary over the duration of the waveforms. The equations to determine the amount of phase drift are described in the previous chapter. However, for this system to work without periodic manual tuning, some form of feedback frequency control must exist.

Figures 7-49, 7-50, and 7-51 show more relative phase differences between the master and slave primary coils. Notice that the master primary coil has slightly greater losses than the slave primary. This is expected since the master primary circuit has the discharge transistor in its oscillation loop.

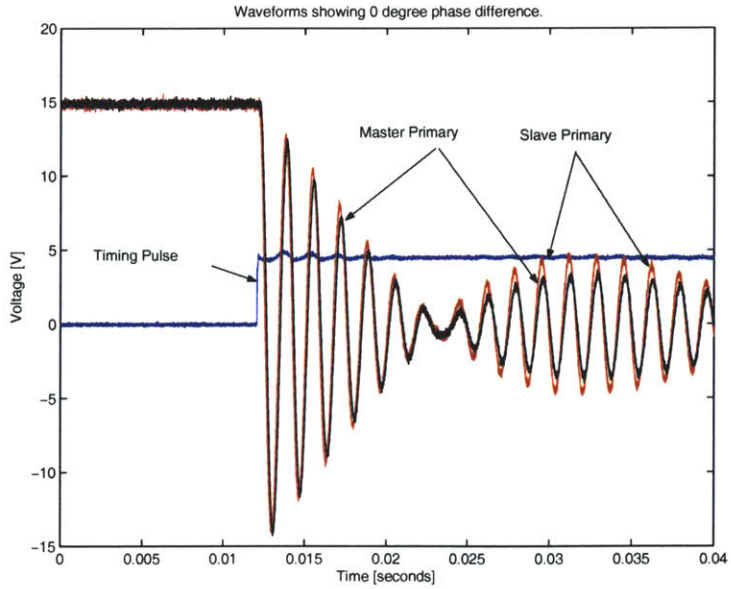

Figure 7-49: Waveforms showing 0 degrees phase separation. Notice that the Master primary has slightly greater losses than the Slave primary.

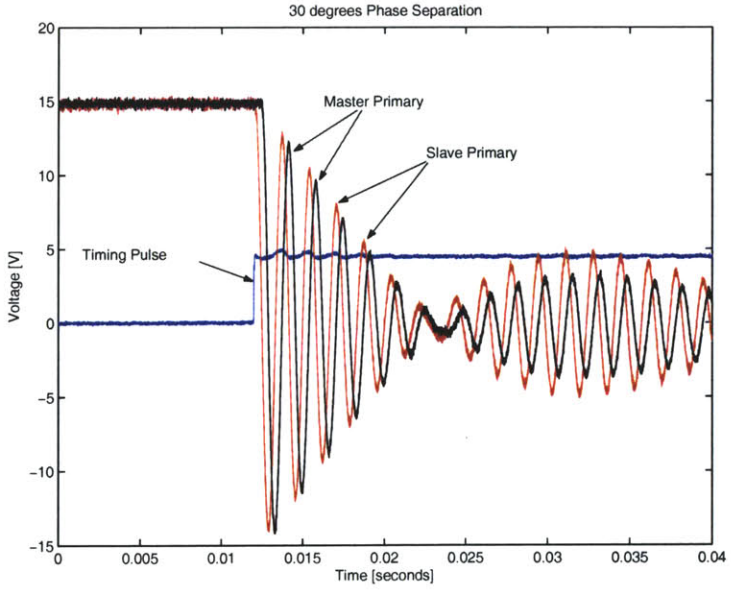

Figure 7-50: Waveforms showing 30 degrees of phase separation.

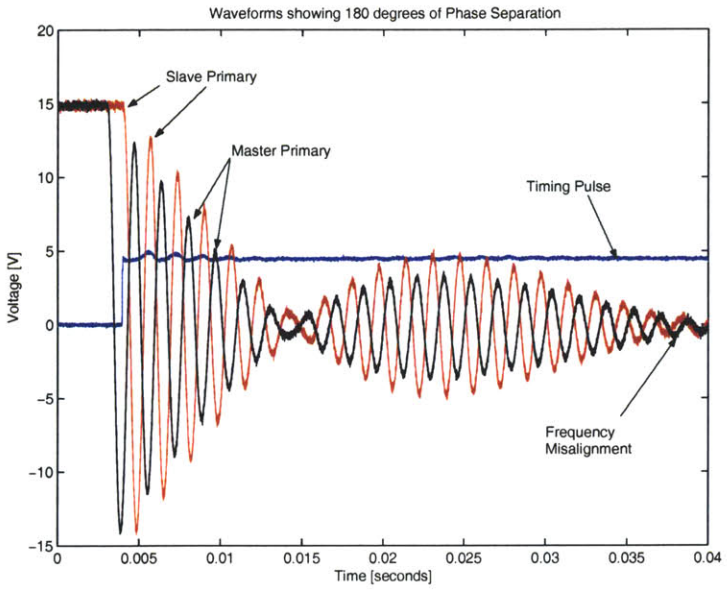

Figure 7-51: Waveforms showing approximately 180 degrees of phase separation. Notice the frequency misalignment at the end of the plots.

7.5.1 Feedback System for Frequency Matching

The frequency matching circuit is the most difficult portion of the project to construct. This is due to both the signal processing needed to do frequency matching as well as the more complicated nature of the integrated chips involved relative to those used previously. However, this system allows an initially tuned system to compensate for temperature effects and other gradual phenomenon that cause slight variations in the resonant frequency of a coil. While the method shown here only keeps the two secondary coils matched, all other coils could be arranged with feedback loops that keep them frequency matched to the master secondary coil.

Because this is a pulsed system, the two output waveforms are only present for a fraction of the total operating time of the circuit, approximately 25% for this project. In addition, the frequency output has beats, meaning that the amplitude of the signal is varying from zero to a nonconstant maximum until it decays away. A standard phase lock loop IC will have difficulty locking on to the desired frequency output because it is not a continuous carrier frequency. The output of the secondary coils, for this project, is zero for much of the time; there is no signal for which the PLL can achieve lock. Furthermore, the phase lock

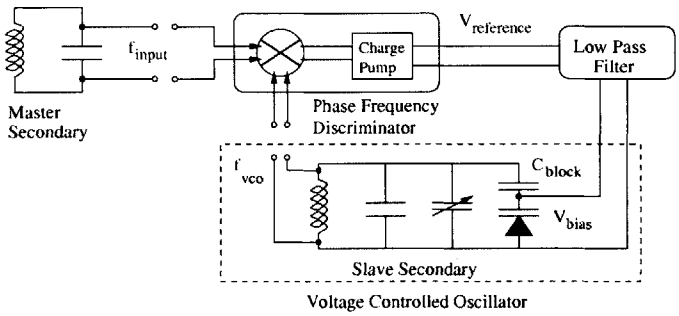

Figure 7-52: Block diagram showing one essential portion of the frequency matching system.

loop output will constantly vary as the input frequencies vary, due to the beats, and decay. This variation in the output of the PLL means that each time the resonant signal decays, the bias voltage output applied to the varactor diodes to tune the slave secondary to the master secondary is forgotten. If this system is to keep itself tuned between subsequent discharges, there must be some form of memory for the diodes between discharges.

There are essentially two parts to this circuit. The first, described in the previous chapter is the standard phase locked loop. The block diagram for its operation was shown previously, but is given again in Figure 7-52. The second essential component is the sample and hold for memory and the associated control circuitry. A block diagram is shown in Figure 7-53. Essentially, the secondary voltage waveform is AM demodulated to extract when the beats occur. The system converts the beats that are greater in magnitude than a specified voltage threshold into gate control pulses for the sample and hold. The PLL circuit, during these beats, compares and outputs a voltage that is proportional to the difference between the two resonant frequencies. This voltage is given to the sample and hold to continuously output during until the next discharge when the secondary waveform reaches a peak. Now, the difference between the two frequencies is minimized and a smaller correction voltage is feed into the sample and hold chip. This new correction voltage is added to the previous voltage, until the system reaches a steady state limited by the resolution of the discharge, a few kilohertz in this case.

The full schematic of this feedback circuit is shown in Figure 7-54. Figure 7-55 shows a photograph of the complete frequency feedback loop in action. The action of the phase locked loop circuitry and the sample and hold controls are explained below.

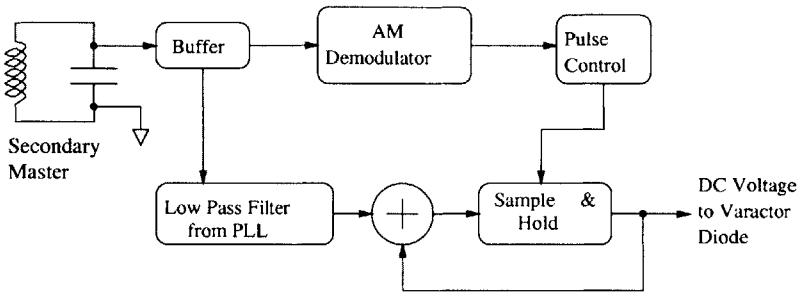

Figure 7-53: Block diagram showing essential parts of the control circuitry for the sample and hold circuitry.

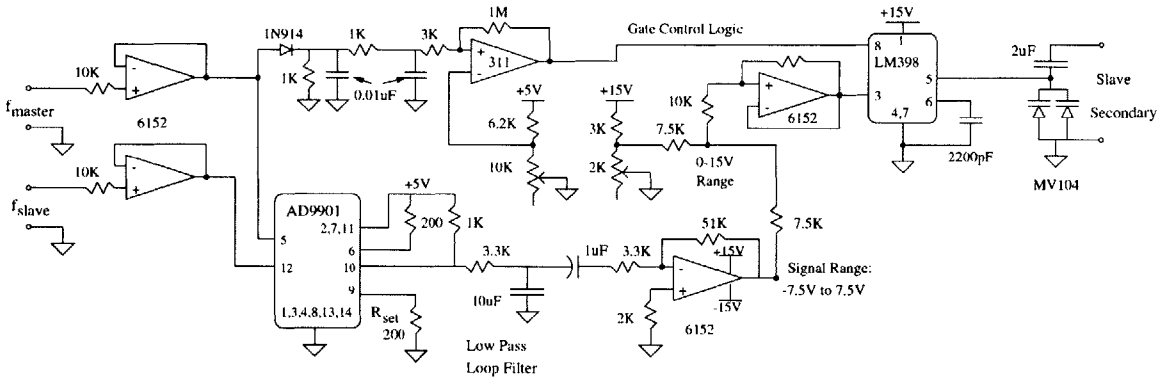

Figure 7-54: Schematic of frequency control feedback circuit. Note ground reference is to the master and slave secondary coil, which are tied together for a common reference.

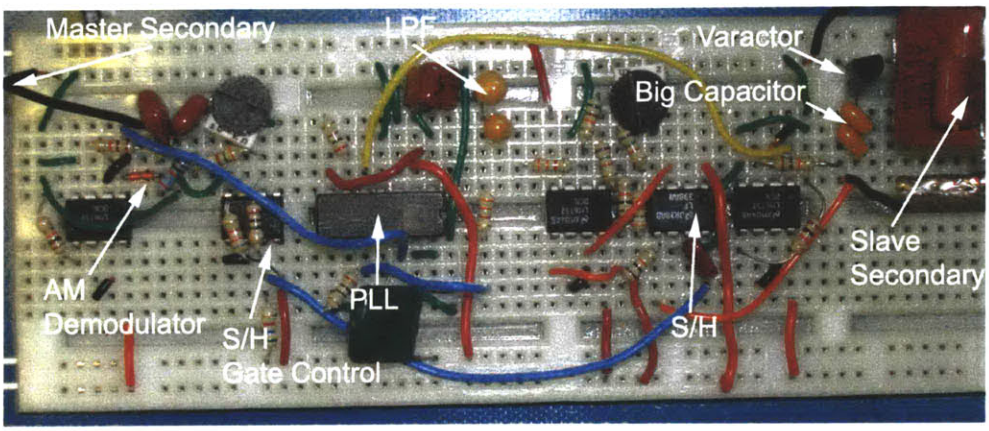

Figure 7-55: Photograph showing the frequency feedback circuitry. The master secondary and slave secondary are outside of the picture.

Phase Locked Loop

The heart of the phase locked loop is the Analog Devices AD9901.[3] It is a phase and frequency discriminator meaning that it detects the difference in frequency between two signals and outputs a signal whose DC value is proportional to the difference between the two input signals. If the two frequencies are equal, then its output is proportional to the phase difference between the two signals. For this project, only the input signal frequency differences are of concern. As there is an ambiguity of approximately 2 to 3kHz in tuning, depending on the length of the waveform decay, the two resonant frequencies will never be precisely matched enough for the AD9901 to revert to phase control mode. This is verified by comparing the oscilloscope waveforms with those listed in the data sheet.

In frequency discrimination mode, the chip functions identically to a four quadrant analog multiplier followed by a low pass filter and a frequency to voltage converter. While building the equivalent circuit would allow greater control over the output waveform, a four quadrant analog multiplier and frequency to voltage converter are an order of magnitude more expensive than a comparable PLL IC. For reference, Analog Devices makes excellent multipliers (AD633 or AD650) while National Semiconductor produces the least expensive frequency to voltage converters on the market (LM331).

Before discussing how the circuit in Figure 7-54 works, it is first important to note the grounding features of this circuit. Because this circuit operates on the waveforms of the secondary coils, it must be referenced to the common ground of the secondary coils. Because the secondary coils are electrically floating, in that they could be referenced to any other voltage available, there is no uniquely definable ground in this circuit. For this reason, the closest end loop of the secondary to the primary coil is designated common ground. The common grounds of the slave and master secondary coils are tied together. In this circuit, this common ground is then tied to the ground bus of the rest of the system, but this need not be done. As long as the supply voltages used in this circuit are referenced to the common of the two secondary coils, this system can be electrically isolated from that of the primary coils.

Getting back to the circuit's operation, the voltage waveform induced on the secondary coils are each sent through a unity gain non-inverting buffer, an LM6152 dual op amp in this case with its supply rails tied to the common and to +15V. Both the signals from the

primary and secondary are feed into the AD9901. Because this chip can operate in many different modes, there are two outputs and a current limiting resistor, R_{set} that need to be terminated with a suitable resistance. The data sheet explains the R_{set} resistor; it limits the output current via the relation: $I_{max} = \frac{0.47V}{R_{set}}$. It is set to 200Ω for a maximum output current of 2.4mA. The inverting output, pin 10, is tied to the +5V rail via a 1KΩ resistor while the non-inverting output, pin 6, is tied to the voltage rail with a 200Ω resistor. Note, however, that in standard TTL operation, there is no difference between the output of the inverting and non-inverting output. The AD9901 has its supply voltage, pin 2, bypassed with a 1μF and a 0.1μF capacitor.

The output of the AD9901 must be low pass filtered, a 3.3KΩ resistor followed by a shunting tantalum capacitor of 10μF are used. This gives a corner frequency of 4.8Hz which is slow enough to for the sample and hold circuit to capture the signal without putting high frequency signals on its output. Now, some creative circuitry is used to turn this output into a signal that can be used with the varactor diodes. The varactor diodes change their junction capacitance based on the applied DC voltage. However, the higher the DC bias, the lower the junction capacitance. For the MV104 varactors used in this project, a zero volt bias implies an 80pF junction capacitance while a 32 volt bias gives a 30pF capacitance. For this project, a +15 volt supply is used, so that will be the maximum bias voltage used. The problem is how to convert the 4Hz signal out of the low pass filter into a DC voltage between zero and 15 volts.

The solution used is to remove the DC offset from the low pass output signal. As the circuit does not know what the DC offset value of the PLL output is, it simply removes it. This signal is inverted and amplified to approximately an output range of ±7.5V. Then, a +7.5V bias is applied to this signal such that it spans from zero to +15 volts. This value is then sampled by the sample and hold chip.

To accomplish this, first, a 1μF tantalum capacitor is used to remove the DC offset. Next, an inverting op amp with a gain of $K = \frac{51K\Omega}{3.3K\Omega} = 15.5$ is used to take a signal that had a maximum measured spread of one volt (−0.5V to +0.5V) and convert it to one with the desired range. This signal is added to a resistive divider acting as a DC voltage source. The 7.5KΩ resistors ensure the voltage magnitudes are added correctly. Next, this slowly varying, 4Hz signal is added to the previous voltage being held by the sample and hold chip via the 10KΩ resistors. This new varactor offset voltage is sampled and held until the next

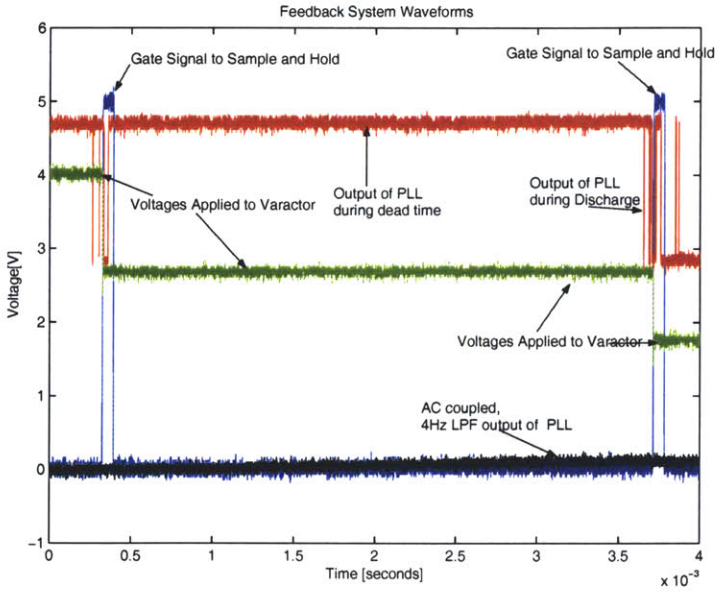

Figure 7-56: Oscilloscope waveforms of PLL feedback system. Notice that PLL output during discharge is a PWM signal whose DC value represents frequency difference.

discharge cycle. Figure 7-56 shows the oscilloscope waveforms taken to show this operation.

Sample and Hold

The sample and hold chip used in this project is the National Semiconductor LM398. The LM398 functions similarly to a unity gain buffer. However, instead of continuously operating, it requires a TTL logic signal to tell it when to sample its input. When the chip is sampling the input, it holds the signal on the output. When the TTL logic goes low, the chip stops responding to its input and holds the DC value of its output.

The LM398 requires a holding capacitor to hold a DC value. This capacitor cannot be too big, otherwise it takes too much time for it to charge. If the capacitor cannot charge to the needed output voltage before the gate control signal turns off, then the output is unstable. However, if the hold capacitor is too small, then it will not be able to hold the output voltage long enough without discharging or losing voltage to its load. To balance this tradeoff, a 2200pF polypropylene capacitor is used as the holding capacitor. As seen in Figure 7-56, there is little evidence of voltage droop. Even though a relatively small capacitor is used in this project, the 4Hz signal still has some higher frequency components

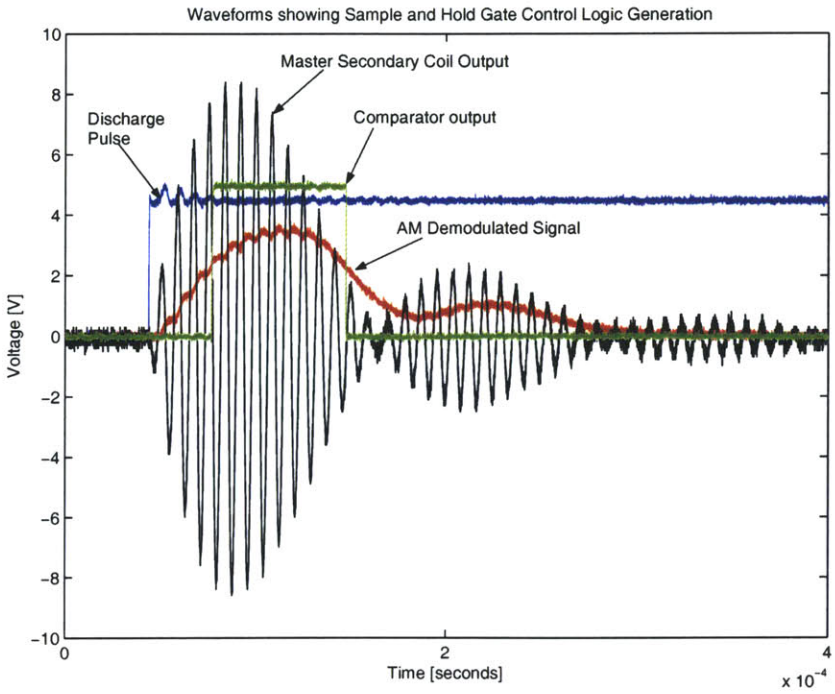

Figure 7-57: Oscilloscope waveforms showing the generation of the sample and hold gate control pulse. Note that the AM demodulated signal shown has already gone through the low pass filter.

that are included in the LM398 output. These higher frequency components give slight discontinuities on the output when the chip is transitioning from a sample to a holding mode. Since the slave secondary waveform is active during this transition, it is important to keep this high frequency output to a minimum as it adversely affects secondary coil performance.

To determine when the gate pulse should activate, an AM demodulator circuit was built. Realizing that the secondary waveform, with its amplitude beats is simply the superposition of two frequencies, one higher than the other, it is relatively simple to build a demodulator that gives only the beat waveform without the internal cycles. Figure 7-57 shows these waveforms.

This demodulator is built by taking an output from the master secondary coil directly from the input buffer. The demodulator itself consists of the 1N914 diode as well as the shunt 1KΩ resistor and 0.01μF polypropylene capacitor. The following 1KΩ and shunt 0.01μF capacitor are a low pass filter that removes some of higher frequency spikes from

the beat waveform. Next, an LM311 comparator is used to turn this waveform into a set of TTL logic pulses that turn the sample and hold gate on and off. The resistor values used for this comparator are identical to those used before except for the input impedance. A large value, on the order of 10KΩ or larger, resulted in a very small signal being extracted from the demodulator. At the reference terminal of the LM311, a resistive divider network of 6.2KΩ resistor and a 10KΩ potentiometer is used, proving a nominal bias of 2.2V. The output of this comparator goes directly to the LM398 gate control pin.

The DC voltage is blocked from affecting the secondary slave coil via two NPO ceramic 1μF capacitors wired in parallel. The voltage is supplied to four varactor diodes, of which there are two in each TO-92 package.[23] The capacitance supplied by the varactors totals from 320pF at zero volts bias to 160pF at 15V bias. This range of capacitances gives a 43Hz range of frequency variation, much less than the 2kHz needed for an effect on the slave's secondary voltage waveform to be noticed. To get 2kHz resolution requires a variable capacitance of 16nF. This would require 100 MV104 packages wired in parallel. Most varactor diodes cannot provide this degree of junction capacitance. If the resonant frequency of the system were increased by a factor or 10, then only four diodes, two TO-92 packages, would be required to achieve 3kHz resolution. Practically, this limitation requires that, for a resonant frequency of 100kHz, the slave secondary coil be tuned very closely to the master secondary.

Chapter 8

Comparisons and Analysis of Coupled Resonant Systems

The waveforms shown in the previous chapter closely resemble the theoretical models derived in previous chapters. This chapter aims to compare the experimentally measured waveforms with those derived from the theoretical coupled fourth order model. The uniquely defining parameters Q_1, Q_2, and k are found for each set of measured waveforms, i.e. each set of primary and secondary coils. These parameters are used to plot the theoretical voltage waveforms. The computer scripts used to generate these theoretical models and compare them to the measured data are included in the appendix under $tesla1.m$.

8.1 Comparisons of Waveforms

Figure 8-1 shows a comparison between the measured oscilloscope waveforms and the theoretical model that best fits the measured primary and secondary responses, specifically for the master primary and secondary coils, D and E, respectively. The parameters that define the waveform are: initial voltage: V_{in}, resonant frequency: ω_n, the quality factors: Q_1, Q_2, and the coupling coefficient: k. For all the waveforms dealt with in this chapter, the initial voltage, V_{in} is set to 15 volts. The resonant frequency is assumed to be matched between the primary and secondary waveforms. Although this assumption is not necessarily true, all the plots have a time scale between zero and 200μseconds. This gives a resolution of 5kHz. Thus, any frequency mismatch less than 5kHz will appear as a slight error between the theoretical and measured waveforms. As all the measured resonant frequencies for the

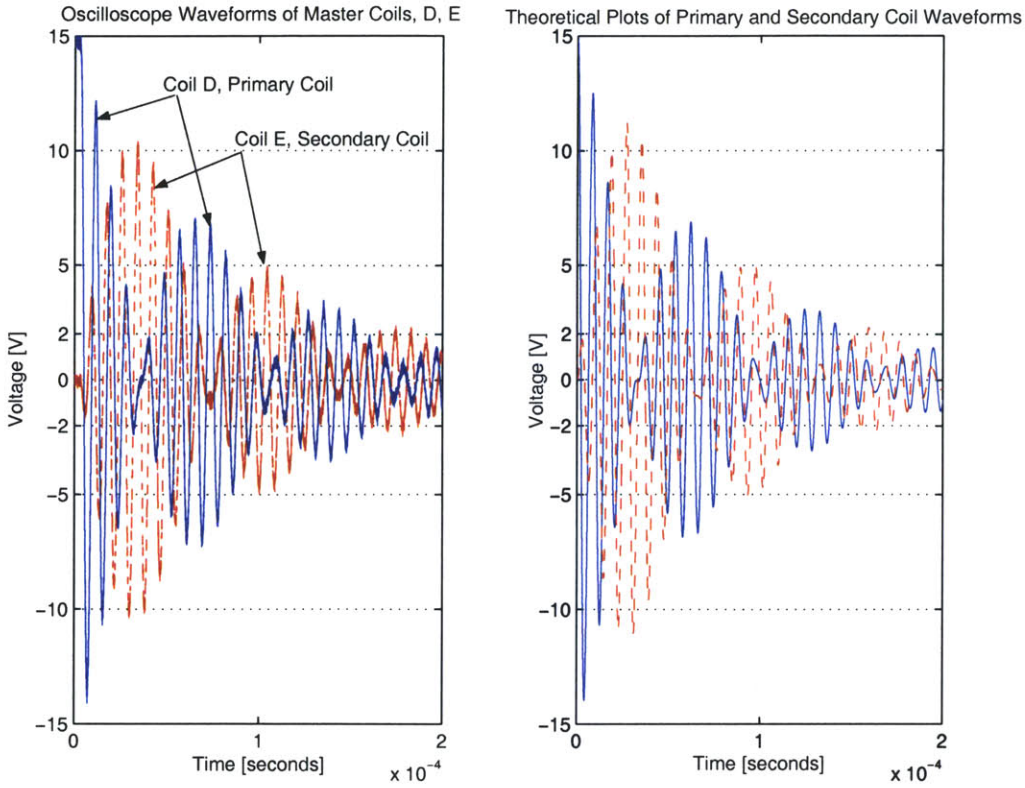

Figure 8-1: Comparison of coils D (primary) and E (secondary) (left side) to the theoretical model (right side). Parameters: $f_n = 118\text{kHz}$, $Q_1 = 32$, $Q_2 = 34$, and $k = \frac{1}{8.3}$

coils C, D, E, and F are between 116kHz and 120kHz, supposing a resonant frequency of $f_n = 118\text{kHz}$ for all the coils should introduce negligible errors.

This comparison shows a generally good agreement between the measured data and theoretical model. The parameters used are: $V_{in} = 15\text{V}$, $f_n = 118\text{kHz}$, $Q_1 = 32$, $Q_2 = 34$, and $k = \frac{1}{8.3}$. The general factors to look for when comparing these waveforms are the number of cycles in each beat and the shape of the decay formed by the peaks of the waveform cycles. However, with five parameters being used to determine the shape of the theoretical waveform, it is necessary to find a process by which these factors can be determined. Again, the resonant frequency is assumed equal for all coils to $f_n = 118\text{kHz}$ and $V_{in} = 15$ volts, but the values of Q_1, Q_2, and k are interrelated and thus are difficult to determine purely through guesswork.

8.1.1 Method of Determining Parameters

There is a straightforward procedure for finding the parameters Q_1, Q_2, and k that best fit the system. The concept is to match the envelope waveforms introduced in previous chapters to get approximate values for Q_1, Q_2, and k. Then, a complete model of the output waveform can be generated, compared with the measured data, and altered accordingly.

The procedure begins with counting the approximate number of complete cycles in the first beat of the secondary waveform. This number is the inverse the coupling coefficient, k to within 0.5. Next, the number of beats in the waveform is known to be $N_{beats} = \frac{k}{k_{crit}}$ where $k_{crit} = \frac{1}{\sqrt{Q_1 Q_2}}$. Knowing N_{beats} and k sets the value for the geometric mean of the quality factors. Assume that the quality factors are equal and plot the envelope waveforms. The envelope waveforms are given in equations 8.1 and 8.2. Their derivation is found in chapter 3.

$$V_{decay}(t) = V_{in}\sqrt{\frac{L_2}{L_1}}e^{-\frac{\omega_n}{4}\frac{Q_1+Q_2}{Q_1Q_2}t} \tag{8.1}$$

$$V_{env}(t) = V_{in}\sqrt{\frac{L_2}{L_1}}e^{-\frac{\omega_n}{4}\frac{Q_1+Q_2}{Q_1Q_2}t}\sin(\frac{\omega_{upper}-\omega_{lower}}{2}t) \tag{8.2}$$

Equation 8.1 gives the theoretically idealized decay rate of the system while equation 8.2 dictates the envelope waveform for the beats for the secondary coil. The equation governing the envelope of the primary coil beats replaces the *sine* with a *cosine* as the primary and secondary are almost exactly 90^o out of phase. The values of Q may need to be varied by an amount, usually less than a factor of 2 or 3, so the sinusoidal envelope curves better fit the measured data.

With the envelope equations set, a complete waveform can be generated according to the equations 8.3 and 8.4:

$$V_{pri}(t) = \frac{V_{in}}{2}\left(e^{(-\delta_{upper}t)}\cos(\omega_{upper}t) + e^{(-\delta_{lower}t)}\cos(\omega_{lower}t)\right) \tag{8.3}$$

$$V_{sec}(t) = \frac{V_{in}}{2}\sqrt{\frac{L_2}{L_1}}\left(e^{(-\delta_{lower}t)}\cos(\omega_{lower}t) - e^{(-\delta_{upper}t)}\cos(\omega_{upper}t)\right) \tag{8.4}$$

Figure 8-2 shows the results for the primary waveform thus far. The parameters used to generate these envelope conditions are $Q_1 = 32$, $Q_2 = 34$, and $k = \frac{1}{8}$. This was arrived at

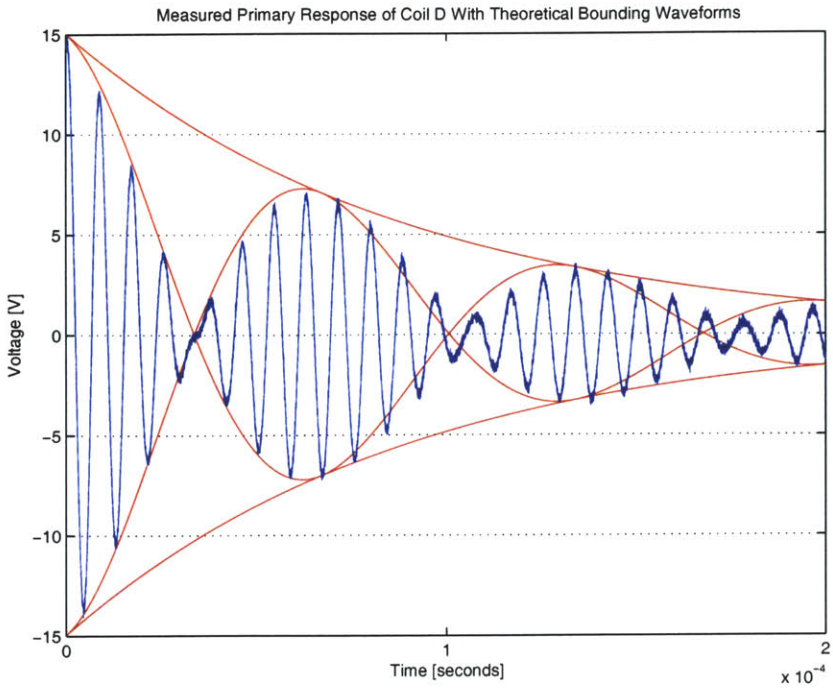

Figure 8-2: Plot of primary coil response with theoretical envelope waveforms. Parameters: $Q_1 = 32$, $Q_2 = 34$, and $k = \frac{1}{8}$.

because 8 cycles were counted in each beat. There are four beats of the secondary waveform, or three primary beats plus the beat during its initial discharge. Thus, the primary can be said to have four beats. This gives the equation $\frac{k}{k_{crit}} = k\sqrt{Q_1 Q_2} = 4$ which leads to $\sqrt{Q_1 Q_2} = 32$. As the values of the quality factors are assumed approximately equal, then starting values of $Q_1 = Q_2 = 32$ were assumed. Now, the envelope lines are removed and replaced with the complete model using equations 8.3 and 8.4 for the primary and secondary waveforms respectively.

Figure 8-3 shows a comparison between the measured primary response of coil D and a theoretical model (left side) while the rightmost plot shows the comparison between the secondary response of coil E and its theoretical model. Again, the parameters used were $Q_1 = 32$, $Q_2 = 34$, and $k = \frac{1}{8}$. The largest problem with this response is the error at the beat nulls, when the waveform changes from one beat to another and there is a zero crossing of the envelope sinusoid of equation 8.2. This is solved by changing the value of k slightly. By using a value of $k = \frac{1}{8.3}$ while keeping $Q_1 = 32$ and $Q_2 = 34$ gives improved matching

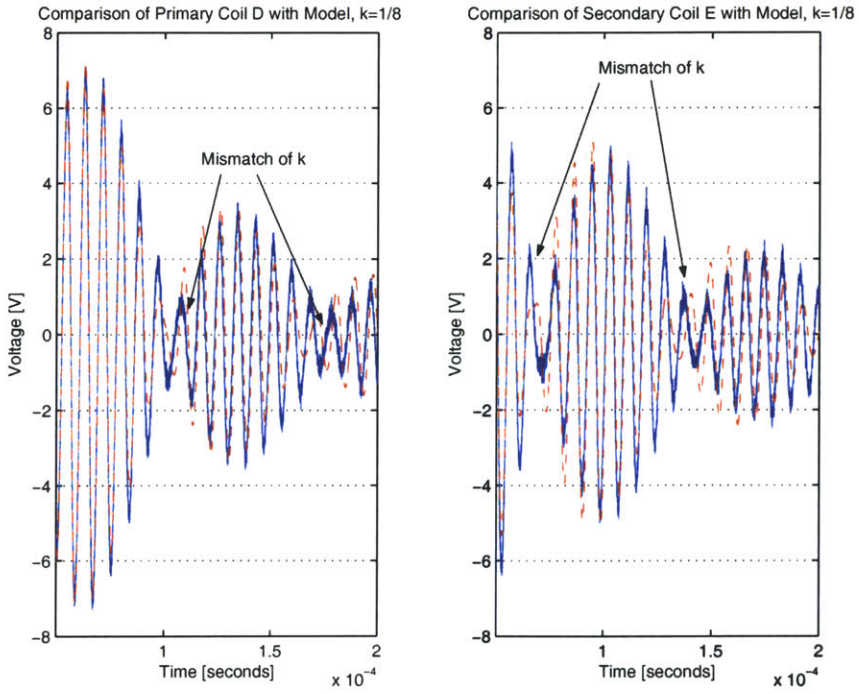

Figure 8-3: Plot of primary coil response (solid) with theoretical response (dashed) waveform. Parameters: $Q_1 = 32$, $Q_2 = 34$, and $k = \frac{1}{8}$.

between the measured and predicted response.

Figures 8-4 and 8-5 show the recomputed envelope curves for the above coil D and E waveforms. The envelope curves agree more closely with the measured voltage waveform during the nulls between beats.

To observe the accuracy of the theoretical prediction, the theoretical waveforms are overlaid with the measured waveforms using the new value for k. Figure 8-6 shows the waveform recorded from the master primary coil D plotted with the the revised theoretical predication for its behavior. Figure 8-7 shows a comparison for the master secondary coil E. The behavior of the primary coil is remarkably accurate while that of the secondary is less conforming, but still quite accurate.

The delay observed in Figure 8-6 (and later plots) between the theoretical and measured response waveforms is *intentional* as it allows important features between the two plots to be better compared. The measured waveform has a fixed delay of 3μs. This delay is the same for all future delayed plots.

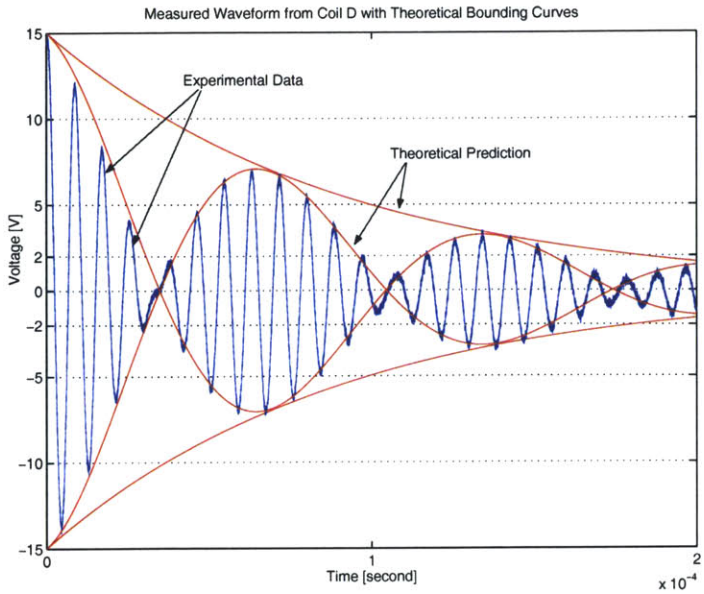

Figure 8-4: The measured primary coil response from D with the theoretical envelope curves overlaid. Parameters: $Q_1 = 32$, $Q_2 = 34$, and $k = \frac{1}{8.3}$.

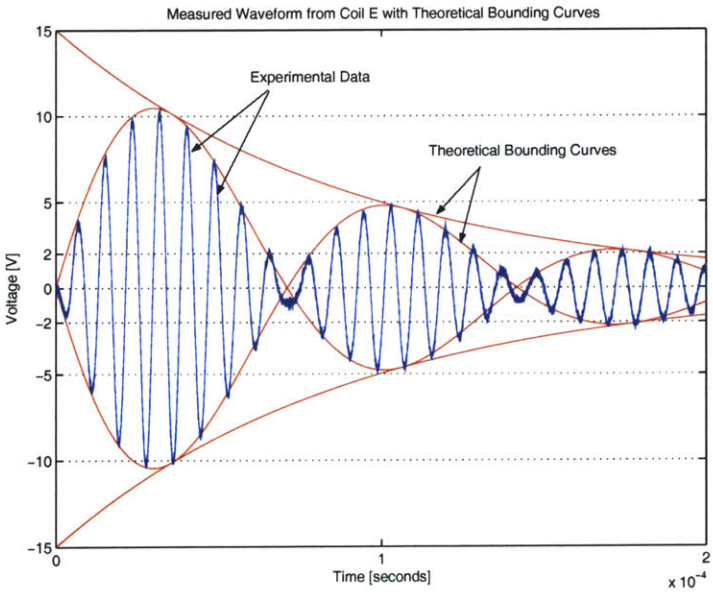

Figure 8-5: The measured secondary coil response from E with theoretical envelope curves overlaid. Parameters: $Q_1 = 32$, $Q_2 = 34$, and $k = \frac{1}{8.3}$.

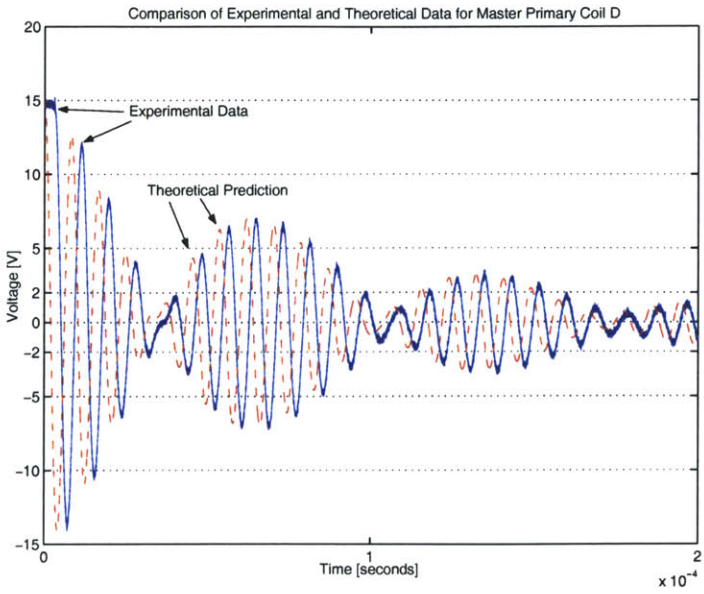

Figure 8-6: Plot of measured primary coil data (solid) overlaid with revised theoretical waveform (dashed). Note that the experimental data is intentionally time delayed. Parameters: $Q_1 = 32$, $Q_2 = 34$, and $k = \frac{1}{8.3}$.

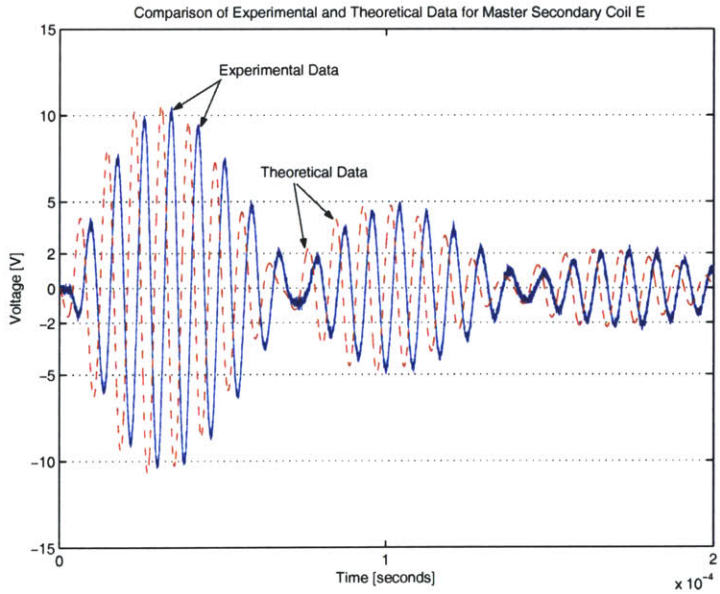

Figure 8-7: Plot of measured secondary coil data overlaid with revised theoretical waveform. Again, note that the experimental data is time delayed. Parameters: $Q_1 = 32$, $Q_2 = 34$, and $k = \frac{1}{8.3}$.

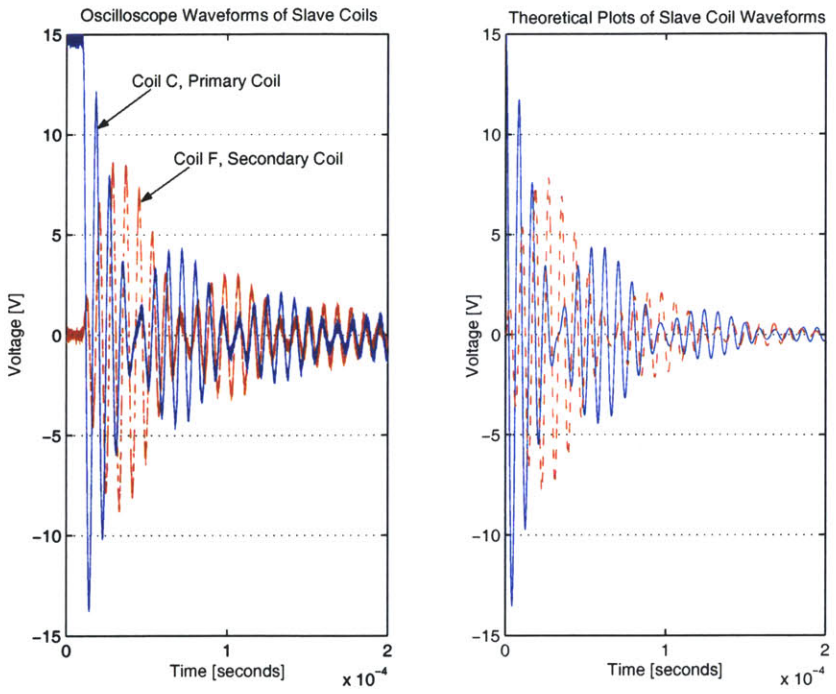

Figure 8-8: Comparison of measured waveforms for the slave system (left) to the theoretical waveforms computed (right). Parameters: $Q_1 = 23$, $Q_2 = 22$, and $k = \frac{1}{7.5}$

Figure 8-8 shows a comparison of the measured slave primary and secondary coils on the left with the computed theoretical waveforms on the right. Again, they appear to agree. For a better comparison, the measured waveform for the slave primary coil, coil C,is delayed and overlaid with the theoretical waveform using the parameters $Q_1 = 23$, $Q_2 = 22$, and $k = \frac{1}{7.5}$. This is consistent with the presence of 3 secondary beats and 7 cycles per beat. While there were discrepancies in the beat nulls with the secondary E coil before, they are now found in the primary C coil. This is due to the choice of k. If k is reduced to $\frac{1}{7.3}$, then the secondary coil F, will have a slight discrepancy. Figure 8-9 shows the side by side comparison of the primary C coil results with this discrepancy while Figure 8-10 shows the comparison for the secondary coil F. The maximum error during the beats between the coil C waveforms is approximately $\frac{5.1-4.7}{4.7} = 8.5\%$ during a negative peak in the middle of the second beat.

For comparison, another set of measured data with only two beats is shown in Figure 8-11. The purpose in this is to determine if the quality factors found with this data are

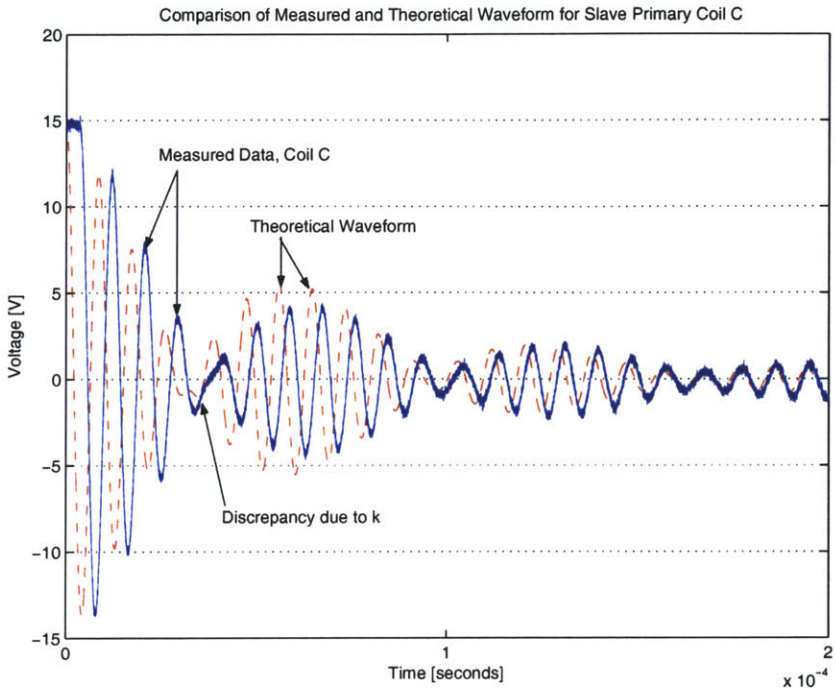

Figure 8-9: Comparison of slave primary coil C measured results to theoretical waveform. Parameters: $Q_1 = 23$, $Q_2 = 22$, and $k = \frac{1}{7.5}$. The measured data has been time delayed for clarity.

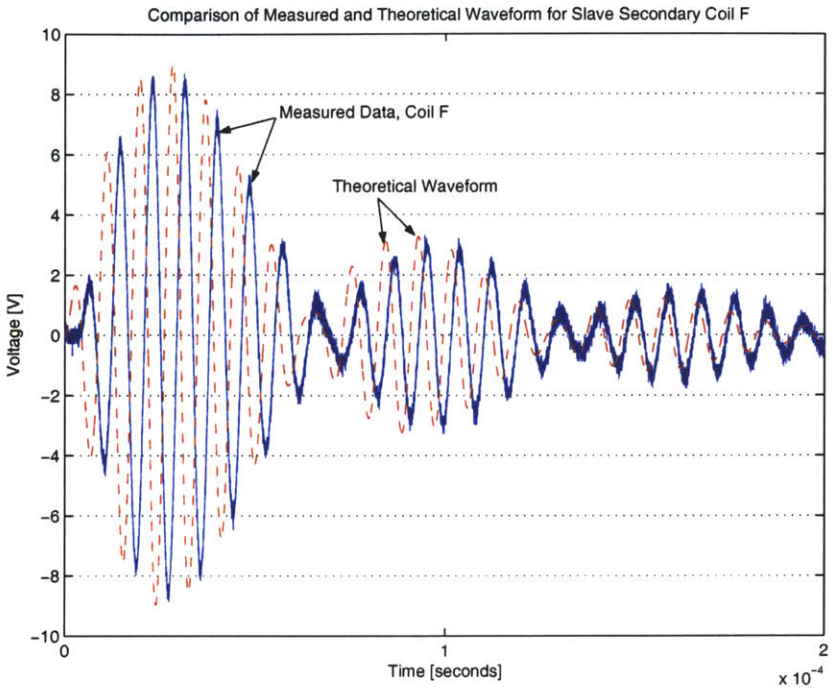

Figure 8-10: Comparison of slave secondary coil F measured results to theoretical waveform. Parameters: $Q_1 = 23$, $Q_2 = 22$, and $k = \frac{1}{7.5}$. The measured data has been time delayed for clarity.

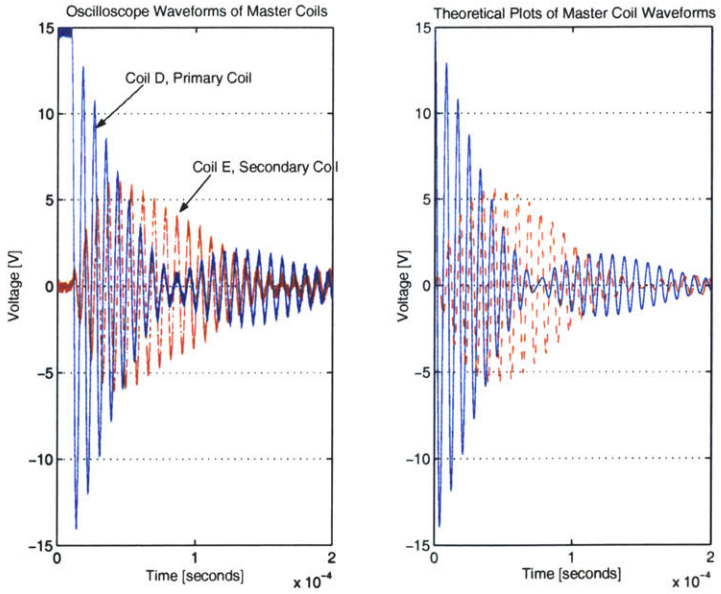

Figure 8-11: Comparison of measured data (left) and plot of theoretical data that closely matches it (right). Parameters: $Q_1 = 29$, $Q_2 = 26$, and $k = \frac{1}{18}$.

identical to those found in the previous three beat analysis.

Figure 8-12 shows a comparison of the measured primary coil D waveform with its theoretical counterpart. The match between the two is excellent, with less than a 4% difference in the magnitudes between corresponding peaks, except at the first beat null. The quality factors have changed however to $Q_1 = 29$ and $Q_2 = 26$ with $k = \frac{1}{18}$. Surprisingly, the product of the waveform cycles per beat and the number of beats, $18 \cdot 2 = 36$ predicts a quality factor of 36. However, the quality factors were approximately 25% less than predicted. The difference between the accurate prediction of the three beat system and the two beat system now considered is the small value of the coupling coefficient, k. The ideal model from which the theoretical model is derived does not consider parasitic losses due to a low coupling coefficient. Instead, a small k implies less energy being coupled between the primary and secondary and a longer time for each beat to occur. It does not consider losses to other magnetic objects or parasitics.

Figure 8-13 shows the side by side comparison for the master secondary coil E. The match is less accurate than for the primary coil, with more overshoot in the middle of the beat. However, it very accurately models the beginning and end of the first beat waveform

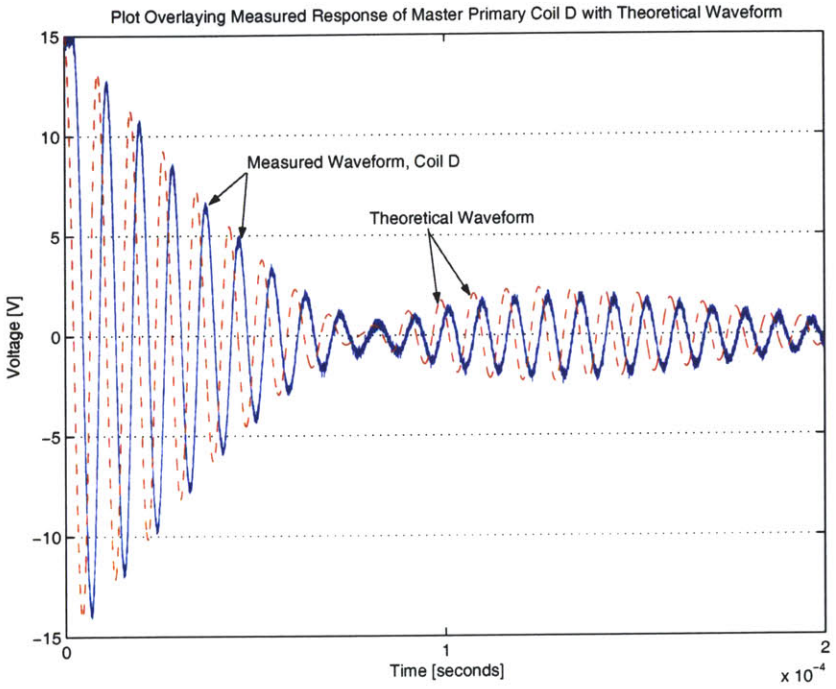

Figure 8-12: Comparison of master primary coil D measured results with theoretical waveform. Parameters: $Q_1 = 29$, $Q_2 = 26$, and $k = \frac{1}{18}$. The measured data has been time delayed for clarity.

and the beginning of the second beat well. That the peak of the first beat is less than expected implies that the envelope exponential governing the decay of the waveform is slightly larger than predicted. The results for coils C and F are very similar. Note that for $Q_1 = 29$ and $Q_2 = 26$, k_{crit} is computed to be $k_{crit} = 0.036$. This gives $\frac{k}{k_{crit}} = 1.53$.

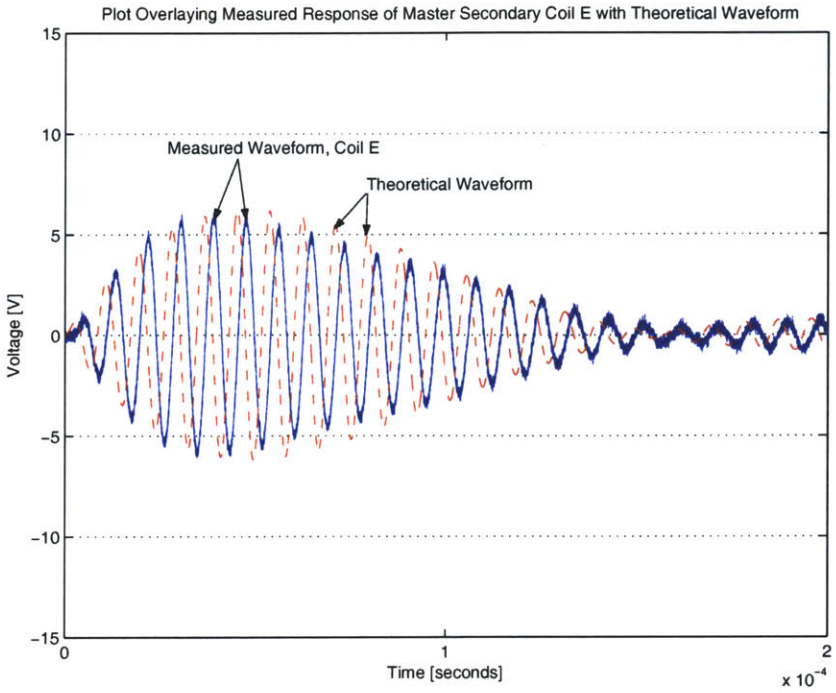

Figure 8-13: Comparison of master secondary coil E measured results with theoretical waveform. Parameters: $Q_1 = 29$, $Q_2 = 26$, and $k = \frac{1}{18}$. The measured data has been time delayed for clarity.

8.2 Analysis of Quality Factors

The first question after performing this analysis is to ask why the quality factors for these four coils, C, D, E, and F, were measured between 61 and 70 when they were actuated with a mechanical switch while they are only between 20 and 34 now. While the primary circuit has the addition of the discharge transistor which adds non-negligible losses to the system, the secondary coil is identical to the coil used in the mechanically switched system. The reason why the Q of the secondary dropped by an approximate factor of 3 is precisely because the Q of the primary dropped by a factor of 3. This is due to of Faraday's law

of electromagnetic induction. When the voltage applied to the primary coil produces a magnetic field, there is a voltage induced on the secondary coil due to the flux linked to it by the primary coil. When the voltage waveform across the primary coil decays after 20 to 34 cycles, there is no voltage across the primary to induce a voltage in the secondary. This is why the measured Q of the secondary coil is almost always less than that of the primary. The Q measurements of the secondary coil, when it is coupled to the primary, give an *effective* Q for the coupled, switched system. Whereas the Q of unswitched and uncoupled primary or secondary circuit may be large, this effective Q found when the primary and secondary are switched and coupled takes into account the losses due to these two phenomenon.

While these differences in quality factor values for various beat responses is significant, it is important to convert these differences into the resistive losses seen by the system. These losses can be compared to the results found for the mechanically switched systems (Previous Q). Table 8.2 shows these values with resistance computed in ohms along with the damping coefficients δ_{upper} and δ_{lower}. These damping ratios govern the decay rate of the envelope curves shown previously.

Coil:	D	E	C	F
Previous Q	70	64	65	61
$N_{beats} = 3$	$Q_1 = 32$	$Q_2 = 34$	$Q_1 = 23$	$Q_2 = 22$
	$R_1 = .13\Omega$	$R_2 = .12\Omega$	$R_1 = .19\Omega$	$R_2 = .19\Omega$
	$\delta_{upper} = 1.3e4$	$\delta_{lower} = 1.0e4$	$\delta_{upper} = 1.9e4$	$\delta_{lower} = 1.5e4$
$N_{beats} = 2$	$Q_1 = 29$	$Q_2 = 26$	$Q_1 = 20$	$Q_2 = 20$
	$R_1 = .15\Omega$	$R_2 = .16\Omega$	$R_1 = .22\Omega$	$R_2 = .21\Omega$
	$\delta_{upper} = 1.4e4$	$\delta_{lower} = 1.3e4$	$\delta_{upper} = 2.0e4$	$\delta_{lower} = 1.8e4$

Evidently, ohmic variation on the order of 0.01Ω can cause 10% variations in the quality factor. One explanation is the increase in resistance and capacitance in the channel of the switching MOSFET, the IR3103, at lower voltages and currents. These factors would both increase conduction losses. However, the answer is more likely due to a fundamental loss of energy through the coupling of flux. The greater the value of k, the tighter the primary and secondary coils are coupled. However, for any k less than unity, there is flux that is not linked between the coils. This is called leakage flux. Ideally, it is assumed that there are no other magnetic sources in the vicinity, so by Gauss' law, this leakage flux couples back to

its source resulting in no net loss. However, there are losses present in any real system. For example, the power supply powering this circuit with its own inductors and transformers was located below the breadboard on which the circuit was built. As k goes from $\frac{1}{8} = .125$ to $\frac{1}{18} = .0556$, only 5.6% of the total magnetic flux generated by the primary is linked to the secondary and inducing the secondary voltage waveform.

While the exact reasoning for any energy loss is debatable, it represents a small fraction of deviance of the measured primary and secondary waveforms from their predicted shapes. The agreement between the measured and predicted waveforms is at worst 8.5% during the beats of the waveforms, while during the beat nulls, when the waveform transitions from one beat to another, the shape is strongly influenced by the value of k used to model the system. This sensitivity was shown during the derivation of these modelling formulas. However, most of the modelled waveforms fit the data to within a 5% tolerance. Overall, the level of accuracy to which these measured waveforms can be predicted demonstrates the applicability of the fourth order model and the approximations used to represent this coupled resonant system.

Chapter 9

Project Conclusion

9.1 Wireless Power Transmission

Having built a unit that can control two separate coupled resonant systems, it remains to transmit power from these secondary coils linked in a linear phased array. This, however, is a solved problem. Radio transmitters and radar systems used frequency locked, dipole antennaes to focus electromagnetic energy on specific targets.[31, chapter 9] In the case of radar, the electromagnetic energy is focused at a very specific spatial target, often at sizable distances. For this project, the secondary coils themselves are used as the radiating antennae. If designed to resonate at a higher frequency in the RF band, these secondary coils would radiate electromagnetic energy in a manner like that of a radio station transmitting antennae. While the power extracted from radio and radar systems is quite limited, there are differences between the signal driven radio and radar systems and the pulsed system in this project that allow for greater power densities to be delivered via electromagnetic radiation.

One difference between this pulsed system and the standard radar and radio applications in that the system is not driven by an input signal oscillating at a specific carrier frequency but rather allowed to oscillate at its own natural resonant frequency. For example, instead of each radio station having to generate its own carrier frequency and then tune its amplifiers and antennae to this carrier frequency, the pulsed system only has its resonator coils tuned to a specific resonant frequency. There is no carrier signal nor is there a requirement for any control electronics to resonate at the desired output resonant frequency. The only portion of this circuit required to operate at the resonant frequency are the coupled resonators

themselves, not their timing circuitry. The feedback circuitry used to lock the coils sees this resonant frequency, but this need not be the case. If the resonant frequency were too high for the electronics to measure, a method of sampling the secondary output waveform could be used to determine if the two were operating at the same frequency. This sampling principle is identical to using a strobe at 100 flashes per seconds to watch an event that occurs at 200 or 400 times per second.

Another difference between this pulsed system and traditional radio systems is the need for a high gain, high speed amplifier to power the transmitting antennae. These amplifier designs limit the amount of output power that can be delivered because they must have enough bandwidth as to not attenuate the signal carrier frequency.[19] With a pulsed self resonant system, there is no high speed, high gain amplifier. Instead, there is a DC power supply that charges part of the system while a switch decouples the energy storage elements of the resonator. Arguably, it is easier to construct higher voltage DC power supplies than it is to construct amplifiers with higher gain-bandwidth products. The limiting factor for many high voltage DC supplies is the breakdown potential of its surrounding media while the limiting factors for amplifier design are the gain-bandwidth products of the transistors themselves and the topology of the amplifier circuit.

Thus, the classic limitations associated with radio frequency technology are decoupled by using a pulsed system. Instead of requiring an amplifier to both oscillate at the carrier frequency and power the antennae, the pulsed system utilizes a DC power supply to achieve the desired output power or gain while utilizing the resonant structure of the antennae itself, in the form of the secondary coil, to produce an output resonant frequency. Utilizing a pulsed system allows the realization of higher frequency, higher output power systems.

One tradeoff is that there must be switches present in the primary to control the charging and discharging. The conduction path for the discharge switch is exposed to the resonant frequency and DC voltage of the primary itself while the charging switch must be able to withstand the DC voltage. Furthermore, the discharge switch must be able to actuate itself in an amount of time that does not adversely affect the primary voltage waveform, as the relays did with its bouncing glitches. Because the discharge switch must decouple to energy storage elements of the resonator to keep them from resonating, the form of this switch is heavily influenced by the nature of the resonant system itself.

While there are limitations on how fast a transistor can turn on and the amount of DC

voltage is can block, there is a generalization that may present another switching solution. The primary and secondary coils used in this project were inductors and capacitors wired in parallel to make a resonator with a frequency $\omega_n = \frac{1}{\sqrt{LC}}$. However, the resonator can be any structure that resonates at a fixed frequency, such as a cavity resonator or an antennae structure. It is not unreasonable to attain resonance modes in excess of 100GHz using enclosed cavity resonators while to build a traditional radio transmitter that operated at such a high frequency would be near impossible with current electronics technology and manufacturing techniques.[31, page 347] While it is not conceptually simple to explain how the voltage gain possible from a primary to secondary coil is duplicated in cavity resonators, such gains are possible. With cavity resonators, there is no need for transistors. The switching methodology could utilize separate electromagnetic or quantum phenomenon to actuate the charging and discharging of the resonators. Further discussion on this topic is beyond the scope of this thesis.

Despite these conceptual differences in generating an output signal, both the pulsed system and the standard radio and radar systems seen today utilize a phased array network to focus the output radiation on a specific point and thus transmit their electromagnetic energy to a target location or locations. The system presented here does so in a nearly identical manner. By operating the phased array in an identical manner, the wireless transmission of high frequency, high voltage power is indeed possible.

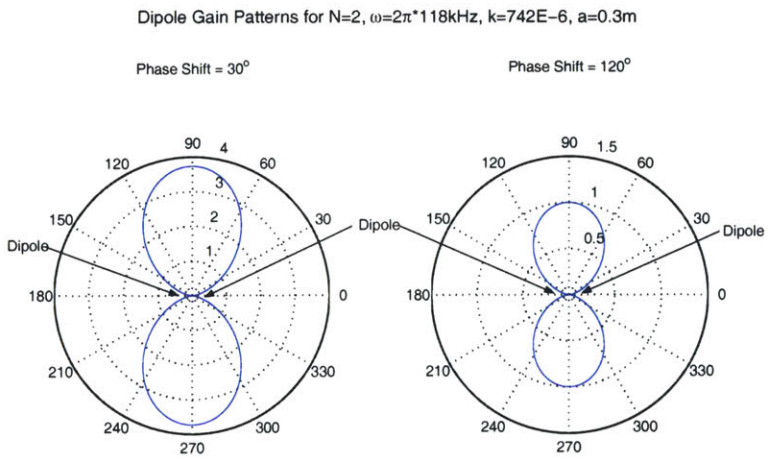

Figure 9-1: Plot of the dipole gain for the constructed system for relative phase shifts of $\Phi = 30^o$ and $\Phi = 120^o$. Parameters are: $N = 2$, $k = 742 \cdot 10^{-6}$[rad/m], and $a = 0.3$[m]

The dipole array constructed for this project has an idealized gain pattern shown in Figure 9-1. Using the dipole gain equation stated in chapter 6, with the parameters $N = 2$, $k = 741 \cdot 10^{-6}$[rad/m] (taking $\omega = 2\pi \cdot 118$kHz), and $a = 0.3$[meters], it plots the gain for a relative phase shift Φ equal to 30^o (left) and 120^o (right). The gain equation is restated below:

$$Gain(\theta, \phi = 0) \sim \sin^2(\theta) \frac{\sin^2(\frac{N}{2}(\Phi + ka\sin(\theta)))}{\sin^2(\frac{1}{2}(\Phi + ka\sin(\theta)))}$$

Increasing the number of dipole antennaes in the array increases the user's ability to control the gain pattern.

9.2 Future Work

This project only begins to explore the possibilities for pulsed power systems and wireless power transmission. While this project did not attempt to build a receiver coil to measure the transmitted power of the system, there are several important considerations before doing so that must be addressed.

The first concern with wireless power transmission is the safety of biological tissue in the vicinity of the transmitter coils. Recent scares with cell phone usage and high voltage power lines causing cancer have prompted more research into the hazards of prolonged exposure of biological tissue to electromagnetic fields. There have been many studies finding that these sources of electromagnetic fields are reasonably safe, but there are defined limits for exposure.[4] The US Food and Drug Administration cites an exposure level of 1.6 W/kg in any one gram of tissue at 800MHz as the threshold for cancer causing levels.[6] Exposure levels for higher frequencies are pending review. This implies a limit to the power densities that can be transmitted if any biological organisms are present. However, if the system is operating at frequencies much higher than 800MHz, there is reason to suspect that the exposure level would be higher.

Before any amount of power could be transmitted, it would be necessary to measure the electromagnetic radiation at all points around the resonant coils to ensure that the power is being transmitted correctly and to the proper spatial location. Furthermore, it would be necessary to ensure that in the event of failure, the system would not radiate excessively.

The second concern is electromagnetic interference with other systems. While the res-

onant frequency of the system, ω_n may not interfere with neighboring systems, there are harmonics that may be large enough in magnitude to adversely interfere with other equipment. These harmonics include second, third, etc. harmonics of the resonant frequency, ω_n as well as any high frequency resonant modes of the physical resonator structure itself. Another possible source of harmonics is from the timing pulses.

Most electronic devices today must undergo an electromagnetic emissions test to ensure they do not output excessive radiation. The pulsed system would need to undergo some form of this test to ensure that the radiated output waveform did not contain harmonics or contain other frequency content that would interfere with the receiving unit circuitry, communication systems, and other nearby systems.

9.3 Project Conclusion

This project started as an attempt to design a Tesla coil. While there are many guides offering step-by-step advice to building Tesla coils of various sizes and power levels, there is a noticeable lack of information regarding their design, specifically how to design a coil such that it meets a certain criteria, not just "produces long sparks and streamers". There is a curious lack of Tesla coil technology present in modern power supply equipment, a task to which it would appear well suited. By deriving a generalized theory of operation that did not depend on any specific components, it is hoped that designers and engineers will utilize concepts Nikola Tesla experimented with over 50 years ago.

To reinforce the scientific nature of this work, the term Tesla coil was used interchangeably with coupled resonant system. As the common conception when thinking of Tesla coils is a physically large solenoidal coil supporting a metallic structure, the term coupled resonant system is used with greater preference as the general theory derived in this thesis describes *any* two resonant systems coupled by an electrostatic or magnetostatic phenomenon, not only ones realized with an inductor and capacitor.

To the effect of wireless power transmission, it is certainly possible with proper engineering. While the concept of radiating a concentrated electromagnetic field on a specific location in space is identical to that of radar systems, the use of a pulsed system to store the power and then radiate it as opposed to continuously radiating allows for a decoupling of the power supply requirements and high frequency resonance. By both driving the coupled

resonant system with pulses and linking multiple units together via a phase difference for focusing the radiated power, wireless power transmission is a reality.

Appendix A

Appendix A: Derivation of Time and Frequency Domain Relations

The following derivations and caveats are from the relations in chapters 2 and 3 describing second order and coupled second order systems. The derivations are shown in the order in which they are referenced in the thesis.

A.1 Necessary Requirements of the Laplace Transforms

While the Laplace transform is a powerful tool for analyzing electrical circuits, there are some very restrictive conditions on its use. These conditions are linearity, time invariance, and causality. The linearity conditions states that the original function relating an input signal $x(t)$ to its output signal $y(t)$ must be able to satisfy the following condition:

$$\mathcal{L}[a \cdot f(t) + b \cdot g(t)] = a \cdot F(s) + b \cdot G(s) \tag{A.1}$$

where a, b are constants, and $\mathcal{L}[\cdot]$ specifies the Laplace transform of a function.

In addition, the function must be time invariant. This means that the function must be able to slide on the time axis while keeping its output fixed relative to the sliding time axis. For example, if for an input function $x(t)$ and its output $y(t)$, then the following relation should also hold: $y(t - t_0) = f[x(t - t_0)]$ where $f[\cdot]$ is the function relating $x(t)$ and $y(t)$.

Finally, causality states that the input function must not depend on future values for its present value. For example, $y(t) = x(t+1)$ is noncausal because the value of the output,

$y(t)$ at $t = 5$ depends on the value of the input function $x(t)$ at time $t = 6$.

While these conditions seem fairly standard, they restrict many types of input functions. There are more general transforms that do not require such restrictions on its inputs, but their descriptions are beyond the scope of this thesis.

A.2 Why k is Between 0 And 1

Chapter 3 discusses the coupling coefficient, k, and its relationship to the flux coupled between the two inductors. To see why k is bounded, consider a transformer composed of two inductive elements that can be isolated electromagnetically from one another. The energy stored between them is given by the expression:

$$U = \frac{1}{2}L_1 i_1^2 + M i_1 i_2 + \frac{1}{2}L_2 i_2^2 \tag{A.2}$$

where M is the mutual inductance between the two coils. As the energy between the coils, U can never be negative (its minimum value is zero), then by expressing the ratio of the currents as $r = \frac{i_1}{i_2}$, an equation and a boundary condition, respectively, are obtained:

$$\begin{cases} \frac{2U}{i_1^2} = L_1 + 2Mr + L_2 r^2 \\ 0 \leq L_1 + 2Mr + L_2 r^2 \end{cases}$$

The minimum value of r is found by taking a derivative, $\frac{dU}{dr}$, and setting it equal to zero. The result is $r = \frac{-M}{L_2}$. Substituting this value back for r gives a minimum value of energy greater than or equal to the following:

$$L_1 + 2Mr + L_2 r^2 \geq 0 \tag{A.3}$$

which directly implies that:

$$M^2 \leq L_1 L_2 \tag{A.4}$$

Equality can be expressed by inserting a unitless coupling coefficient, k in the following manner:

$$M = k\sqrt{L_1 L_2} \tag{A.5}$$

where the coupling coefficient is bounded by $0 \leq k \leq 1$ for the above analysis to hold.[24,

A.3 Derivation of Perturbation Analysis

This results of this derivation are presented in Chapter 3, section 2. The derivation of the relation between the two system resonant frequencies, ω_{upper} and ω_{lower} in terms of the independent natural frequency ω_n and a perturbation δ requires using the solutions to the general characteristic fourth order polynomial:

$$\omega_{upper} = \sqrt{\frac{(\omega_1^2+\omega_2^2) + \sqrt{(\omega_1^2+\omega_2^2)^2 - 4(1-k^2)\omega_1^2\omega_2^2}}{2(1-k^2)}} \tag{A.6}$$

$$\omega_{lower} = \sqrt{\frac{(\omega_1^2+\omega_2^2) - \sqrt{(\omega_1^2+\omega_2^2)^2 - 4(1-k^2)\omega_1^2\omega_2^2}}{2(1-k^2)}} \tag{A.7}$$

Now, as ω_1 and ω_2 are related by the perturbation $\omega_2 = \omega_1 + \delta$, this is inserted into the above equations and simplified.

$$\omega_{upper} = \sqrt{\frac{(2\omega_1^2+2\omega_1\delta+\delta^2) + \sqrt{(2\omega_1^2+2\omega_1\delta+\delta^2)^2 - 4(1-k^2)\omega_1^4 + 2\omega_1^3\delta + \omega_1^2\delta^2}}{2(1-k^2)}} \tag{A.8}$$

Now, in order to simplify this expression it is necessary to make an assumption: that $\frac{\delta}{\omega_1} \ll 1$. By factoring an ω_1^2 out of the numerator, which yields an ω_1 outside of the primary square root, there are now terms of $\frac{\delta}{\omega_1}$ and $(\frac{\delta}{\omega_1})^2$. Ignoring the second order term in both the first several terms and inside the internal square root yields:

$$\omega_{upper} = \omega_1\sqrt{\frac{1+\frac{\delta}{\omega_1}+(\frac{\delta}{\omega_1})^2 + \sqrt{k^2(1+2\frac{\delta}{\omega_1}+(\frac{\delta}{\omega_1})^2)}}{(1-k^2)}} \tag{A.9}$$

To further simplify the result, it is necessary to take a Taylor expansion of the internal square root. Simplifying $\sqrt{1+x}$ as $1+\frac{1}{2}x$, the new result is:

$$\omega_{upper} \approx \omega_1\sqrt{\frac{1+\frac{\delta}{\omega_1}+k+k\frac{\delta}{\omega_1}}{1-k^2}} \tag{A.10}$$

Factoring and cancelling yields:

$$\omega_{upper} \approx \sqrt{\frac{1+\frac{\delta}{\omega_1}}{1-k}} \tag{A.11}$$

This is the result presented. The solution for ω_{lower} follows exactly as above, with the reversal of one sign.

$$\omega_{lower} \approx \sqrt{\frac{1-\frac{\delta}{\omega_1}}{1-k}} \tag{A.12}$$

A.4 Efficiency Integration

In chapter 4, section 2, an integral of the secondary current is computed and an approximate result given to find the secondary voltage. The voltage across the secondary capacitor is found by integrating the current in the secondary coil over time from zero to infinity. The resultant solution is of the form:

$$V_{cap} = \frac{Q_1 Q_2}{(Q_1+Q_2)\omega_n}(2+A+B+C+D) \tag{A.13}$$

where

$$A = \frac{(1-k)(Q_1+Q_2)^2}{(Q_1+Q_2)^2+16(1-k)Q_1^2Q_2^2} \tag{A.14}$$

$$B = \frac{(1+k)(Q_1+Q_2)^2}{(Q_1+Q_2)^2+16(1+k)Q_1^2Q_2^2} \tag{A.15}$$

$$C = -\frac{2(1-k^2)(Q_1+Q_2)^2}{(Q_1+Q_2)^2+4(1-k^2)(\sqrt{1-k}+\sqrt{1+k})^2Q_1^2Q_2^2} \tag{A.16}$$

$$D = -\frac{2(1-k^2)(Q_1+Q_2)^2}{(Q_1+Q_2)^2+8(1-k^2)(1-\sqrt{1-k^2})Q_1^2Q_2^2} \tag{A.17}$$

The dominant term when k is small and Q_2 large is the term D. The analysis is continued in the chapter for the expression V_{cap} with the A, B, and C terms neglected. They would have the effect of raising the output voltage slightly. Thus, the efficiency stated in chapter 4, section 2 is slightly conservative.

Another approximation used in the chapter is the expression for Z_{out}. The imaginary term is neglected as it is supposed that the real part in the numerator, Q_2 is much greater than the imaginary part, $j(1+k^2Q_1Q_2)$. This holds for k small ($k \sim k_{crit}$) and Q_2 large.

Appendix B

Appendix B: Compilations of Scripts

The following scripts were used in generating the theoretical waveforms for all aspects of design: the output voltages and currents, efficiencies, frequency domain plots, to list a few. The scripts were all written using MATLAB's M-file editor.

The first script is very useful in that it was designed to include most of the waveform equations needed to generate the output time domain waveforms. The user selects which output to graph by uncommenting the appropriate plot commands.

```
% Calculates voltages, currents, and energies across primary and secondary
% circuits

Vi = 1;         %Initial Voltage, usually normalized to unity
wn = 1;   % self-resonant frequency normalized to unity
Q1=50;                % USER sets Q1 and Q2
Q2=50;
R1=1;
R2=1;   % Set to be unity so that L2/L1=Q2/Q1
    %the value of k that splits the FD into two peaks
k_s = sqrt(1/2*(1/Q1^2+1/Q2^2)); % k_s is K_split
k_c=1/sqrt(Q1*Q2);  % Calculating vale of k_crit
```

```
k=3*k_c;       % USER changes desired k in terms of k_crit multiples
                 % 3 in this case

    tau_eff = (4*Q1*Q2)/(wn*(Q1+Q2));   % the time constant of the decay
    t = linspace(0,5*tau_eff,10000);    % response dies after 5 time constants
    %t=linspace(0,0.0002,10000);        % for plotting in real time
    x = 1/(2*pi)*wn*t;                  % normalized time i.e. 2pi x = wn*t
    x_eff = tau_eff*wn/(2*pi);

if (k>k_s)  %k_s is k_split usually just greater than k_crit
    fprintf('Peaks! Beats! k/k_c=%g',k/k_c)
        % Calculating peak frequencies and decay rates
    wu = wn/sqrt(1-k);
    wl = wn/sqrt(1+k);
    deltaL = wn/4*(1/Q1+1/Q2)*(wl^2-wn^2)/(wl^2-wn^2-k^2*wl^2);
    deltaU = wn/4*(1/Q1+1/Q2)*(wu^2-wn^2)/(wu^2-wn^2-k^2*wu^2);

else
    fprintf('No Peaks (Beats).  Need k/k_c>%g',k_s*1/k_c)
    % Compute numerical solution to charpoly
    p=roots([(1-k^2) wn*(1/Q1+1/Q2) wn^2*(2+1/(Q1*Q2)) wn^3*(1/Q1+1/Q2) wn^4]);
        deltaU = -1*real(p(1));
        deltaL=-1*real(p(3));
        wu = abs(imag(p(1)));
        wl = abs(imag(p(3)));

        if (wu<wl)
            deltaU=-1*real(p(3));
            deltaL=-1*real(p(1));
            wu = abs(imag(p(3)));
            wl = abs(imag(p(1)));
```

```
        end

end

fprintf('\r')
fprintf('Q2/Q1 = %g', Q2/Q1)
figure

% Current waveforms
i1=-0.5*1/(wn*Q1*R1)*(wl*exp(-deltaL*t).*sin(wl*t)+
    ...wu*exp(-deltaU*t).*sin(wu*t));
i2=1/(2*wn*sqrt(Q1*R1*Q2*R2))*(wu*exp(-deltaU*t).*sin(wu*t)-
    ...wl*exp(-deltaL*t).*sin(wl*t));

% voltages across the inductors
vL1 = -0.5/wn^2*(wl^2*exp(-deltaL*t).*cos(wl*t)+
    ...wu^2*exp(-deltaU*t).*cos(wu*t));
vL2 = -0.5/wn^2*(wl^2*exp(-deltaL*t).*cos(wl*t)-
    ...wu^2*exp(-deltaU*t).*cos(wu*t))*sqrt(Q2*R2/(Q1*R1));

% voltage across the primary capacitor
v1_1=0.5*(exp(-deltaU*t).*(cos(wu*t))+exp(-deltaL*t).*(cos(wl*t)));
v1_2=0.5*(exp(-deltaU*t).*sin(wu*t)*deltaU/wu+
    ...exp(-deltaL*t).*sin(wl*t)*deltaL/wl);
v1=Vi*(v1_1+v1_2);

% voltage across the secondary capacitor
v2_1 = 0.5*sqrt(Q2*R2/(Q1*R1))*(exp(-deltaL*t).*cos(wl*t) -
exp(-deltaU*t).*cos(wu*t)); v2_2 =
0.5*sqrt(Q2*R2/(Q1*R1))*(exp(-deltaL*t).*sin(wl*t)*deltaL/wl -
exp(-deltaU*t).*sin(wu*t)*deltaU/wu); v2 = Vi*(v2_1+v2_2);
```

```
% power dissipated in the two resonators
Pdiss1=R1*i1.^2;
Pdiss2=R2*i2.^2;

% energy dissipated in the two resonators
E1=(v1.^2+wn*Q1*R1*i1.^2);
E2=(v2.^2+(wn*Q2*R2)*i2.^2);

plot(t,v1)
%plot(x,vL1)
%plot(x,Pdiss1)
hold on
%plot(x,Pdiss2,'r')
%plot(x,vL2,'r')
plot(t,v2,'r')
%plot(x,E2)

%title(['k/k_{crit} = ',num2str(k/k_c),', k_{crit} = ',num2str(k_c),'
    ...Q1= ',num2str(Q1),'  Q2= ',num2str(Q2),' \delta_U=',
    ...num2str(deltaU),' \delta_L=',num2str(deltaL)])
%ylabel('Output Voltage Gain')
ylabel('Normalized Dissipated Power, [Watts/V_{in}^2]')
xlabel('Normalized Time, x') hold on
%end

% Bounding envelope equations
    % bounding exponential/sinusoid
%plot(x,sqrt(Q2*R2/Q1/R1)*exp(-0.25*(Q1+Q2)*wn/(Q1*Q2)*t).*sin((wu-wl)/2*t),'r')
%plot(x,-1*exp(-0.25*(Q1+Q2)*wn/(Q1*Q2)*t).*sin((wu-wl)/2*t),'r')

    % bounding exponential
%plot(x,sqrt(Q2*R2/Q1/R1)*exp(-0.25*(Q1+Q2)*wn/(Q1*Q2)*t), 'c')
```

```
%plot(x,1/sqrt(1-k^2)*exp(-wn/4*(1/Q1+1/Q2)*1/(1-k)*t),'c')
```

The remainder of the scripts presented below follow the order in which they were used to generate figures in this document. The next script was adapted from Terman's book[33] although he gives an equation, not an actual script.

```
% Script to show relative output voltage versus max output voltage over k
figure

x=linspace(0,5,10000);
relvolt = 2*x./(x.^2 + 1);

plot(x,relvolt) xlabel('k/k_{crit}')
ylabel('Relative Output
Voltage at w=w_n') title('Plot of Relative Output Voltage to
Maximized Output Voltage over k')
```

This script calculates the frequency domain plots showing the magnitude of the current when the system is driven off resonance. It is not a good script for theoretical work as it contains too many changing parameters to gain much insight.

```
% Plot of normalized current magnitudes when the system is driven at a
% frequency w.  Illustrates the advantages of driving system near
% resonance.

% w takes the place of the frequency operator s here
w=linspace(0,4,100e3);  % As w_natural = 1/sqrt(LC) = 1, center it

C1=1;  % unit value components
C2=1; L1=1; L2=1; R1=1; R2=1;
M = 0.1*L1*L2;  % A k=0.1 value, does not affect magnitude plot

X1 = L1*w-1./(C1*w);
X2 = L2*w-1./(C2*w);
```

```
% Plotting the impedances of the primary and secondary via parts

% I don't need abs(Z1) for this
Z2 = sqrt(R2^2 + X1.^2);

Z1p = sqrt((R1+M^2*w.^2./(Z2.^2)).^2 + (X1-M^2*w.^2./(Z2.^2)).^2);

Z2Z1p =
sqrt((R1^2+X1.^2).*(R2^2+X2.^2)+2*M^2*w.^2.*(R1*R2-X1.*X2));

i1 = 1./Z1p;  % Working out current magnitudes
i2 = M*w./(Z2Z1p); norm2=max(i2);

figure
subplot(1,2,1), plot(w,i1)
grid on
hold on
plot(w,i2/norm2,'r')
xlabel('Frequency, w')
ylabel('Normalized
Current Magnitudes')
title('Plot of Normalized Current Magnitudes
over Driving Frequency')

%%% Now working for k>k_split

C1=1;  % unit value components
C2=1; L1=1; L2=1; R1=0.1; R2=0.1;
M = 0.2*L1*L2;  % A k=0.2 value, linearly scales magnitude plot

X1 = L1*w-1./(C1*w);
```

```
X2 = L2*w-1./(C2*w);

% I don't need abs(Z1) for this
Z2 = sqrt(R2^2 + X1.^2);

Z1p = sqrt((R1+M^2*w.^2./(Z2.^2)).^2 + (X1-M^2*w.^2./(Z2.^2)).^2);

Z2Z1p =
sqrt((R1^2+X1.^2).*(R2^2+X2.^2)+2*M^2*w.^2.*(R1*R2-X1.*X2));

i1 = 1./Z1p;  % Working out current magnitudes
i2 = M*w./(Z2Z1p);
norm1=max(i1); % for normalizing it
norm2=max(i2);

subplot(1,2,2), plot(w,i1/norm1)
grid on
hold on
plot(w,i2/norm2,'r')
xlabel('Frequency, w')
ylabel('Normalized
Current Magnitudes')
title('Plot of Normalized Current Magnitudes
over Driving Frequency')
```

This script builds the root locus plots found at the end of the frequency domain section of chapter 3. The script is simple in that each sets of poles and zeros must be plotted by hand. This was found to be easier than having the computer plot poles for a range of k and these poles were often hard to find and distinguish for various changes in parameters.

```
% Quick script for building a root locus plot of voltage gain!
s=tf('s'); wn=1;
```

```
Q1=50; Q2=200;
k_c=1/sqrt(Q1*Q2);

figure
hold on

for n=.1:.2:2.1,
    k=n*k_c;
    Vgain = k*wn^2/((1-k^2)*s^4+wn*(1/Q1+1/Q2)*s^3+wn^2*(2+1/(Q1*Q2))*s^2 +
    ...wn^3*(1/Q1+1/Q2)*s+wn^4);
    pzmap(Vgain)    % the two zeros (s^2) at zero are taken out to help
                    %the autoplotter get the axes tighter
end

% Uncomment the remainder of the code to start plots, otherwise, leave out
%k=0;
%s=tf('s');
%wn = 1;

%for j=1:4,

    %for i=2:3,
 %       Q1=10^i;
 %       Q2=Q1;
 %       k(2) = 1/sqrt(Q1*Q2);   % critcal coupling k
 %       k(3) =  k(2)+0.01;  % above critical
 %       k(4) = k(2) +0.02;
 %       k(1) = k(2) /2;  % below critical

 %       cp = (1-k(j)^2)*s^4+wn*(1/Q1+1/Q2)*s^3+wn^2*(2+1/(Q1*Q2))*s^2 +
 %           ...wn^3*(1/Q1+1/Q2)*s+wn^4;
 %       mine = 1/cp;
```

```
%      figure(i+2)

%       subplot(4,1,j)
%       impulse(mine)
%       title([' k=',num2str(k(j))])
%       ylabel(['Q= ',num2str(Q1)])

%   end
%end
   % figure
   % subplot 211
   % pzmap(mine)
   % title(['Q1 = ',num2str(Q1)])

   % subplot 212
   % rlocus(mine)

   % figure
   bode(mine)
   title(['Q1 = ',num2str(Q1)])
```

This next script begins the time domain section of chapter 3. It shows how changes in k and ω_2 affect the frequencies ω_{upper} and ω_{lower}. Note that the variable kp is the coupling coefficient, k.

```
% When w1 /= w2, this script plots how the two system resonant
% frequencies are affected by a change in w2.

w1=1;
w2=logspace(-2,1, 10000);   % a range of frequencies
kp=[0.01 0.1 0.3];          % a range of coupling coefficients
```

```
figure
for i=1:length(kp),
    term = (w1^2+w2.^2).^2-4*(1-kp(i)^2)*w1^2*w2.^2);
    wu=sqrt(((w1^2+w2.^2)+sqrt(term)/(2*(1-kp(i)^2)));
    wl=sqrt(((w1^2+w2.^2)-sqrt(term)/(2*(1-kp(i)^2)));
    plot(w2,wu,'r')
    hold on
    grid on
    plot(w2,wl)
    xlabel('Normalized Frequency, w2/w1')
    ylabel('Operating Frequency, rad/sec')
    title('Plot of Resonant System Frequencies over frequency ratio w2/w1')
end
```

This script plots the inductor voltages of both the primary and secondary when the two second order systems are tuned to different frequencies.

```
% Plot of Inductor voltage vs. w2

t=linspace(0,50*2*pi,100000);
w1=1;
w2=1+.1; %Change the addend here to see the effect on the voltages
kp=[0.1 0.2];   % Add various coupling coefficients here

figure for i=1:length(kp),
    term=(w1^2+w2.^2).^2-4*(1-kp(i)^2)*w1^2*w2.^2);
    wu=sqrt(((w1^2+w2.^2)+sqrt(term)/(2*(1-kp(i)^2)));
    wl=sqrt(((w1^2+w2.^2)-sqrt(term)/(2*(1-kp(i)^2)));

    % The inductor voltages
    v1n= 0.5*(cos(wl*t) + cos(wu*t));
    v2n= 0.5*(cos(wl*t) - cos(wu*t));
```

```
    % the inductor currents
    i1n= 0.5*(wl.*sin(wl*t) + wu.*sin(wu*t));
    i2n= 0.5*(wl.*sin(wl*t) - wu.*sin(wu*t));

    subplot(1,2,i), plot(t,v2n,'r')
    hold on
    grid on
    %plot(t,0.5*(i2n).^2)
    plot(t,v1n)
    xlabel('Time [sec]')
    ylabel('Normalized Voltage and Energy (dashed)')
    title('Plot of Normalized Inductor Voltages, w1=1, w2=2 rad/sec,
        ...k=0.01 (left) k=0.3(right)')
end
```

The following script plots the damping ratios δ_{upper} and δ_{lower} versus a range of coupling values.

```
% Plotting damping ratios over range of k

wn = 1;              % self-resonant frequency normalized
%Q1=20;                % USER sets Q1 and Q2
%Q2=200;
k_c=1/sqrt(Q1*Q2);  % Calculating vale of k_crit
k=linspace(0.001,5*k_c,5000);

% Calculating peak frequencies
    wu = wn./sqrt(1-k.*sqrt(1-k_c^2./(2*k.^2)*(Q1/Q2+Q2/Q1)));
    wl = wn./sqrt(1+k.*sqrt(1-k_c^2./(2*k.^2)*(Q1/Q2+Q2/Q1)));

    delta1 = wn/4*(1/Q1+1/Q2)*(wl.^2-wn^2)./(wl.^2-wn^2-k.^2.*wl.^2);
    delta2 = wn/4*(1/Q1+1/Q2)*(wu.^2-wn^2)./(wu.^2-wn^2-k.^2.*wu.^2);
```

```
%figure
title(['k_{crit} = ',num2str(k_c),'  Q1= ',num2str(Q1),'  Q2=
',num2str(Q2)])
ylabel('Damping Coefficient')
xlabel('Normalized
Coupling Coefficient, k/k_{crit}')
hold on

plot(k/k_c,delta1) plot(k/k_c,delta2,'r')
```

This next script is interesting as it plots waveforms that are perturbed in secondary resonant frequency from the primary resonant frequency.

```
% Script to determine the effect of perturbation on system

w1=1; k=0.1;
del = [0.1, 0.05, 0]; % where del = delta/w1 = 10% perturbation!
t=linspace(0,2*pi/(w1*k), 100000);  % Normalized time, GIVES ONE PERIOD
x=w1.*t/(2*pi);  % Normalizes time to beat frequency, counts beats!

figure for i=1:length(del),
    wl = w1/sqrt(1+k)*sqrt(1+del(i));
    wu = w1/sqrt(1-k)*sqrt(1+del(i));

    i1n= 0.5*(sin(wl*t)./sqrt(1+k) + sin(wu*t)./sqrt(1-k));
    i2n= 0.5*(sin(wl*t)./sqrt(1+k) - sin(wu*t)./sqrt(1-k));
    v1n= 0.5*(cos(wl*t)./(1+k) + cos(wu*t)./(1-k));
    v2n= 0.5*(cos(wl*t)./(1+k) - cos(wu*t)./(1-k));
    % standard to measure relative phase shift
    %    plot(x,v1n,'r')

    plot(x,v2n)
```

```
    hold on
    grid on
end xlabel('Normalized Time, x') ylabel('Normalized Voltage
Magnitude')
title('Measure of Variation of Secondary Voltage by Perturbation,
    ...\delta=0, 5%, 10%')
```

The next script is used in chapter 4 for calculating the efficiencies of the system. It computes and generates the power efficiency over time.

```
% Plotting the power efficiencies over Q's for time t=tau_eff
% Goal here is to find an optimum Q ratio to expend power across system

wn = 1;              % self-resonant frequency normalized
Q1=10;                % USER sets Q1 and Q2
%Q2=10;
fact = logspace(-2,2,10000); %Or a range of Q2
Q2= fact*Q1;

k_c=1./sqrt(Q1*Q2);  % Calculating vale of k_crit
k=2*k_c;      % USER changes desired k in terms of k_crit multiples
tau_eff = 4*Q1.*Q2./(wn*(Q1+Q2));
%t = 0:tau_eff/10000:5*tau_eff;
t=tau_eff;

    wl = wn./sqrt(1+k.*sqrt(1-k_c.^2./(2*k.^2).*(Q1./Q2+Q2/Q1)));
    wu = wn./sqrt(1-k.*sqrt(1-k_c.^2./(2*k.^2).*(Q1./Q2+Q2/Q1)));

    delta1 = wn/4*(1./Q1+1./Q2).*(wl.^2-wn^2)./(wl.^2-wn^2-k.^2.*wl.^2);
    delta2 = wn/4*(1./Q1+1./Q2).*(wu.^2-wn^2)./(wu.^2-wn^2-k.^2.*wu.^2);

%Computing power efficiency
nu_m=(1-2*(delta2+delta1)./((delta2+delta1).^2+(wu-wl).^2));
```

```
plot(k,nu_m,'r') hold on xlabel('Coupling Coefficient, k')
ylabel('Efficiency')

figure
%semilogy(wn*t/(2*pi),(1+k^2*Q1*Q2)/(4*Q2)*nu2)
semilogx(Q2,nu2)
xlabel('Q2/Q1 ratio')
%xlabel('Normalized time (0 to 5\tau_{eff})')
ylabel('Loaded Power Efficiency') title('Plot of Loaded efficiency
over Q at time t=\tau_{eff}')
```

Bibliography

[1] *Reference Data for Radio Engineers.* International Telephone and Telegraph Corporation, New York, NY, 4th edition, 1956.

[2] C. B. Aiken. Two-mesh tuned coupled circuit filters. *Proc. of the I.R.E.*, 25:230/672, February/June 1937.

[3] Inc. Analog Devices. Ad9901 specification sheet. website. http://www.analog.com.

[4] U.S. Army, 2001. http://chppm-www.apgea.army.mil/rfup/website/cellular.htm; accessed September, 10, 2003.

[5] Roland E. Best. *Phase-Locked Loops.* McGraw-Hill, NY, 2003.

[6] IEEE C95. Ieee standard for safety levels with respect to human exposure to radio frequency electromagnetic fields, 3khz to 300ghz. pages 1–1991. IEEE, Apr 27 1992.

[7] Chathan M. Cooke. Time-domain response of circuits, decay, and resonance from sudden inputs, April 2001. unpublished.

[8] Robert W. Erickson. *Fundamentals of Power Electronics.* Kluwer Academic Publishers, MA, 2001.

[9] Floyd Martin Gardner. *Phase-lock Techniques.* Wiley, NY, 1979.

[10] G. R. M. Garratt. *The Early History of Radio: From Faraday to Marconi.* Number 20 in IEE History of Technology. IEE Publishing, December 1994.

[11] Henry Guerlac. *Radar in World War II.* Number 8 in History of Modern Physics. American Institute of Physics, NY, 1987.

[12] International Rectifer Inc. Ir2110 high and low side driver. website. http://www.irf.com.

[13] International Rectifer Inc. Irl3101d1 power mosfet. website. http://www.irf.com.

[14] National Semiconductor Inc. Lm311 specification sheet. website. http://www.national.com.

[15] National Semiconductor Inc. Lm556 specification sheet. website. http://www.national.com.

[16] SRC Devices Inc. Dip 14 series reed relays. website. http://www.srcdevices.com.

[17] Dr. Gary L. Johnson. Solid state tesla coil. 2001.

[18] A. K. Jonscher. *Dielectric Response in Solids.* Chelsea Dielectrics Press, London, UK, 1983.

[19] Kent Lundberg. Become one with the transistor. Booklet, February 5. 2003.

[20] Richard Lundin. A handbook formula for the inductance of a single-layer circular coil. *Proc. of the IEEE*, 73(9):1428–1429, Sept. 1985.

[21] R. G. Medhurst. High frequency resistance and self-capacitance of single-layer solenoids. *Wireless Engineer*, 24(281):35–43, Feb. 1947.

[22] Ryan Myers. Pwm fan controllers. website. http://casemods.pointofnoreturn.org /pwm/circuit2.html.

[23] Semiconductor Components Industries LLC ON Semiconductor. Mv104 specification sheet. website. http://www.onsemi.com.

[24] Leigh Page and Norman Adams. *Principles of Electricity.* D. Van Nostrand Co., 4th edition, 1969.

[25] Panasonic. *Audio Signal Delay BBD Series.* Reprinted by Digikey Corp.

[26] Walsh V. Payton, A.J. *Analog Electronics with Op Amps.* Cambridge University Press, NY, 2nd edition, 1993.

[27] Bob Pease. Understand capacitor soakage to optimize analog systems. *EDN Magazine*, Oct. 13 1982. http://www.national.com/rap.

[28] E. S. Purington. Single and coupled-circuit systems. *Proc. of the I.R.E.*, 18:938, June 1930.

[29] Rahul Sarpeshkar and George Efthivoulidis. A new geometry for two-pole underdamped transfer functions, Fall 2000. unpublished.

[30] Fairchild Semiconductor. Rfd3055le n-channel power mosfet. website. http://www.fairchildsemi.com.

[31] David H. Staelin. *Electromagnetic Waves.* Prentice Hall, NJ, 1998.

[32] F. E. Terman. *Radio Engineers' Handbook.* McGraw-Hill Book Company, Inc., York, PA, 1st edition, 1943.

[33] F. E. Terman. *Radio Engineering.* McGraw-Hill Book Company, Inc., New York, NY, 3rd edition, 1947.

[34] Nikola Tesla. *Experiments with Alternate Currents of High Potential and High Frequency.* Fredonia Books, Amsterdam, The Netherlands, 2002.

[35] Nikola Tesla. *Nikola Tesla on his Work with Alternating Currents and Their Application to Wireless Telegraphy, Telephony, and Transmission of Power.* Twenty First Century Books, Breckenridge, CO, 2002.

[36] M. E. Van Valkenburg. *Analog Filter Design.* Holt, Reinhart, and Winston, New York, NY, 1982.

[37] Charles S. Walker. *Capacitance, Inductance, and Crosstalk Analysis.* Artech House Inc., Norwood MA, 1990.

[38] H. A. Wheeler. Simple inductance formulas for radio coils. *Proc. IRE*, 16:1398–1400, 1928.

[39] Alan S. Wilsky and Alan V. Oppenheim. *Signals and Systems.* Pretence Hall, 1983.

[40] Xicor. X90100 specification sheet. website. http://www.xicor.com.